# PREDICTION OF POWER LOSSES IN AN AUTOMOTIVE GEARBOX INCORPORATING A THERMALLY COUPLED LUBRICATION MODEL

**by**

**Athanasios Christodoulias**

**This dissertation is submitted in fulfilment of the requirements for the degree of**

**Doctor of Philosophy (PhD) and Diploma of Imperial College (DIC)**

**in the Tribology group**

**Department of Mechanical Engineering**

**Imperial College London**

**June 2017**

# ABSTRACT

The continuous tightening of environmental standards, and in particular the stricter vehicle CO2 emission regulations, have put increased pressure on passenger vehicle manufacturers to develop more efficient components. One way of improving fuel consumption and reducing emissions in a vehicle is by reducing the friction-related power loss in major components such as the engine and the transmission.

Between 5% and 6% of the total fuel energy that the car converts is lost through friction in the transmission and ends up as heat being absorbed by the transmission lubricant. The principal aim of this project was developing a method to accurately predict power losses in the gearbox -the main transmission component- while at the same time having the ability to assess the influence of lubricant properties on the gearbox efficiency. For this purpose, a thermally coupled numerical model was developed, incorporating lubricant parameters extracted from rheological tests. The model calculates the friction coefficient in gear elastohydrodynamic (EHL) contacts and then uses it in an iterative scheme to predict in-contact and bulk temperatures as well as power losses. Finally, the model's predictions for gears are coupled to current experimentally derived models for bearing and churning losses.

The method has been applied to a single speed gearbox and a manual six speed automotive gearbox. Two fully formulated lubricants of nominally same specification were tested and comparisons were made for different input conditions and gear geometry changes. In the second case, a light duty truck fitted with the simulated gearbox has been instrumented and tested under different conditions. Temperature predictions from experimental drive cycles have been compared to model predictions and standardised drive cycles have also been simulated.

Results show that the overall gear power loss is heavily dependent on the input torque and that the lambda ratio of the contact affects each component differently. In addition, the distribution of losses between gear friction, bearings and gear churning is not constant but depends on the selected components, the gear geometry, the surface roughness and the specific lubricant rheology. Furthermore, significant power loss differences of up to 11.7% and sump temperature differences of up to 3.1 °C respectively have been predicted between the two oils. Simulations of the six speed gearbox have shown that the model is able to predict bulk oil sump temperatures within 5-10% of measured values and can effectively be used to compare and rank different lubricants in terms of overall efficiency for a given gearbox.

# ACKNOWLEDGMENTS

First and foremost, I would like to thank Professor Andy Olver for giving me the opportunity to embark on this journey and helping me in every way possible throughout my first year. I will always be grateful.

I would like to thank Dr Amir Kadiric for his supervision and his valuable and continuous support throughout the remainder of this project.

A special thanks to all the people at Valvoline USA, who sponsored this work, for providing me with their support and technical expertise.

I would like to acknowledge all my colleagues in the Tribology Group, and all of my friends and family for their support, be it professional or personal.

Finally, a very special thanks to my parents; simply put, I wouldn't have done this without their support. This thesis is dedicated to them.

# DECLARATION OF AUTHORSHIP

I, Athanasios Christodoulias, declare that this thesis titled, 'PREDICTION OF POWER LOSSES IN AN AUTOMOTIVE GEARBOX INCORPORATING A THERMALLY COUPLED LUBRICATION MODEL' and the work presented in it are my own. I confirm that:

- This work was done wholly or mainly while in candidature for a research degree at the Imperial College of London.
- Where I have consulted the published work of others, this is always clearly attributed.
- Where I have quoted from the work of others, the source is always given. With the exception of such quotations, this thesis is entirely my own work.
- I have acknowledged all main sources of help.
- Where the thesis is based on work done by myself jointly with others, I have made clear exactly what was done by others and what I have contributed myself.

Signed: ATHANASIOS CHRISTODOULIAS

Date: 26th June 2017

# COPYRIGHT DECLARATION

The copyright of this thesis rests with the author and is made available under a Creative Commons Attribution Non-Commercial No Derivatives licence. Researchers are free to copy, distribute or transmit the thesis on the condition that they attribute it, that they do not use it for commercial purposes and that they do not alter, transform or build upon it. For any reuse or redistribution, researchers must make clear to others the licence terms of this work.

# CONTENTS

**ABSTRACT** ..... **II**

**ACKNOWLEDGMENTS** ..... **III**

**DECLARATION OF AUTHORSHIP** ..... **IV**

**COPYRIGHT DECLARATION** ..... **V**

**CONTENTS** ..... **VI**

**LIST OF FIGURES** ..... **X**

**NOMENCLATURE** ..... **XVII**

**1. INTRODUCTION** ..... **1**

1.1 BACKGROUND ..... 2

1.2 RESEARCH GOALS ..... 6

1.3 THESIS OUTLINE ..... 8

**2. LITERATURE REVIEW** ..... **10**

2.1 INTRODUCTION ..... 11

2.2 BACKGROUND ..... 11

*2.2.1 Automotive drivetrain* ..... *11*

*2.2.2 Gearboxes* ..... *12*

*2.2.3 Gears* ..... *13*

*2.2.4 Bearings* ..... *16*

2.3 LUBRICATION ..... 17

*2.3.1 The importance of lubrication* ..... *17*

*2.3.2 Lubricant composition* ..... *18*

*2.3.3 Lubrication methods* ..... *19*

*2.3.4 Lubricant viscosity and rheology* ..... *21*

*2.3.5 Film thickness and lubrication regimes* ..... *25*

2.4 LOSSES IN TRANSMISSION SYSTEMS ..... 30

*2.4.1 Gear EHL losses* ..... *30*

*2.4.2 Churning losses* ..... *34*
*2.4.3 Bearing and seal losses* ..... *35*
*2.4.4 Other losses* ..... *38*
*2.4.5 Lubricant selection in transmission systems* ..... *39*
*2.4.6 Gearbox efficiency* ..... *40*

**3. METHODOLOGY FOR THE PREDICTION OF POWER LOSSES IN A GEARBOX ..... 44**

3.1 INTRODUCTION ..... 45
3.2 EHL LOSS PREDICTION ..... 45
*3.2.1 General approach* ..... *45*
*3.2.2 EHL film thickness and traction prediction* ..... *47*
*3.2.3 EHL contact temperatures* ..... *50*
*3.2.4 EHL numerical calculation scheme for gears* ..... *54*
*3.2.5 EHL friction model validation* ..... *58*
3.3 CHURNING LOSS PREDICTION ..... 62
*3.3.1 Model description* ..... *62*
*3.3.2 Churning model validation* ..... *65*
3.4 BEARING LOSS PREDICTION ..... 70
*3.4.1 Model description* ..... *70*
*3.4.2 Bearing model validation* ..... *71*
3.5 SUMMARY ..... 72

**4. CHARACTERISATION OF LUBRICANTS ..... 74**

4.1 INTRODUCTION ..... 75
4.2 STUDIED LUBRICANTS ..... 75
4.3 BALL-ON-DISC TESTS ..... 76
*4.3.1 Test apparatus* ..... *76*
*4.3.2 Friction coefficient and film thickness results and their treatment to obtain rheological constants for oils A and B* ..... *79*
*4.3.3 Boundary friction measurements and its role in predicting the gear teeth contact friction* ..... *90*
4.4 SUMMARY ..... 92

**5. MODELLING RESULTS: SINGLE STAGE GEARBOX ..... 94**

5.1 Introduction ..... 95
5.2 Modelling of gear teeth contact losses in an example spur gear pair ..... 95
5.3 Gear teeth contact calculations ..... 97
5.4 Effect of roughness on gear contact losses ..... 100
5.5 Modelling of additional losses ..... 101
*5.5.1 Bearing and seal losses ..... 101*
*5.5.2 Gear churning losses ..... 103*
5.6 Lubricant comparison ..... 104
*5.6.1 Comparison of fully formulated oils ..... 104*
*5.6.2 Parametric study on the influence of lubricant properties on gear friction ..... 108*
*5.6.3 The influence of lubricant viscosity on losses breakdown ..... 113*
5.7 Parametric studies on the influence of selected parameters on gearbox power losses ..... 116
*5.7.1 Losses breakdown and the influence of bearing selection ..... 116*
*5.7.2 The influence of face-width ratio on losses breakdown ..... 121*
*5.7.3 The influence of the tooth number on losses breakdown ..... 123*
*5.7.4 The influence of gear ratio on losses breakdown ..... 125*
5.8 Summary ..... 126

**6. PREDICTING LOSSES UNDER REAL ROAD CONDITIONS IN A 6 SPEED AUTOMOTIVE GEARBOX ..... 128**

6.1 Introduction ..... 129
6.2 Simulation ..... 129
*6.2.1 Experimental drive cycle, vehicle details and model inputs ..... 129*
*6.2.2 Thermal model of the full gearbox ..... 137*
*6.2.3 Comparison of model predictions to measurements ..... 139*
*6.2.4 Model predictions in standardised drive cycles ..... 144*
6.3 SUMMARY ..... 155

**7. DISCUSSION ..... 156**

*7.1 Introduction ..... 157*
*7.2 Advantages and limitations of the proposed gearbox efficiency model ..... 157*
*7.3 Main results ..... 159*

**8. CONCLUSIONS ..... 164**

8.1 SUMMARY ..... 165
8.2 MAIN ACHIEVEMENTS ..... 165
8.3 FUTURE WORK ..... 167
**9. APPENDIX: FEA GEARBOX SIMULATION ..... 170**
**REFERENCES ..... A**

# LIST OF FIGURES

*Figure 1.1: Monthly average Brent crude oil barrel prices 1987-2015*[1] ..... 2
*Figure 1.2: The global CO2 regulations applied to passenger cars* ..... 3
*Figure 1.3: Energy use in an average passenger car* ..... 4
*Figure 2.1: Typical configurations of an automotive drivetrain* ..... 12
*Figure 2.2: A typical 5-speed constant-mesh manual automotive gearbox (Getrag)* ..... 13
*Figure 2.3: Classification of gears* ..... 14
*Figure 2.4: The geometry of a pinion and gear pair in mesh* ..... 15
*Figure 2.5: Single row deep groove ball bearing -DGBB- (right) and tapered roller bearing -TRB- (left) (SKF)* ..... 17
*Figure 2.6: Dip lubrication (left) and jet lubrication (right)* ..... 20
*Figure 2.7: Newtonian fluid (left) vs. non-Newtonian, shear thinning fluid (right)* ..... 22
*Figure 2.8: The effect of shear rate on viscosity for different lubricants* ..... 22
*Figure 2.9: An interferometry image of an EHL point contact (a) and an EHL line contact (b)* ..... 28
*Figure 2.10: A typical Stribeck curve and the lubrication regions.* ..... 29
*Figure 2.11: Losses in a typical gearbox* ..... 31
*Figure 2.12: Bearing losses for different bearing designs (Adapted from )* ..... 36
*Figure 2.13: The components of the total frictional moment shown for an open spherical roller bearing operating in a high viscosity oil bath* ..... 38
*Figure 3.1: The temperatures in the EHL contact* ..... 45
*Figure 3.2: Determination of lubrication regime for EHL traction prediction in Olver and Spikes model* ..... 49
*Figure 3.3: The constantly variable radius of contact in a gear pair.* ..... 55
*Figure 3.4: The load profile as modelled in the gear pair (W is the maximum value of the normal load, F)* ..... 56
*Figure 3.5: Flowchart of the EHL model algorithm* ..... 57
*Figure 3.6: The effect of slide roll ratio on the temperatures and the friction coefficient when the slower disc rotates at 4000 rpm (Max contact pressure = 2.11 GPa)* ..... 61
*Figure 3.7: The effect of slide roll ratio on the temperatures and the friction coefficient when the slower disc rotates at 20000 rpm (Max contact pressure = 2.11 GPa)* ..... 61

*Figure 3.8: The effect of slide roll ratio on the temperatures and the friction coefficient when the slower disc rotates at 100 rpm (Max contact pressure = 1.29 GPa) ..... 62*
*Figure 3.9: The swell effect in a gear pair ..... 64*
*Figure 3.10: Comparison of the high and low speed formulae to predict churning power loss (Gear 7, Oil no. 1, h/Rp=0.55) ..... 67*
*Figure 3.11: Churning power loss results for two different single spur gears rotating in the oil sump (h/Rp=0.5, oil no. 1) ..... 67*
*Figure 3.12: The additional churning power loss due to "counter-clockwise" rotation (h/Rp=0.5, oil no. 1) ..... 68*
*Figure 3.13: Total churning power loss for a pinion-gear pair of mn = 1.5 (mm), (h/Rp=0.5, oil no. 1) ..... 69*
*Figure 3.14: The influence of oil properties on churning power losses and equilibrium sump temperatures (Gear 7, h/Rp=0.55, N=1000 rpm) ..... 69*
*Figure 3.15: The basic geometry and principal dimensions of the 32210 J2/Q bearing (SKF) ..... 71*
*Figure 3.16: The components of the frictional moment for the 32210 bearing (inputs: radial load, Fr = 5 kN, axial load, Fa = 3 kN, T = 50 °C) using online calculator tools based on the Morales-Espejel model (calculator) and the current implementation of the model (rolling/sliding/drag/total) ..... 72*
*Figure 4.1: The MTM2 rig used to measure friction with the studied gearbox oils and subsequently obtain the shear stress-strain rate relationships of for the oils ..... 77*
*Figure 4.2: The EHD2 rig used to measure lubricant film thickness ..... 78*
*Figure 4.3: The traction coefficient vs SRR ..... 80*
*Figure 4.4: The shear stress vs shear rate curves ..... 81*
*Figure 4.5: The measured friction coefficient vs SRR at constant entrainment speed of 2.75 m/s over a range of loads ..... 82*
*Figure 4.6: The shear stress vs shear rate curves at constant entrainment speed of 2.75 m/s for oil A over a range of loads obtained using the measured data shown in Figure 4.5 above.... 82*
*Figure 4.7: The repeatability of the friction measurements at 40 °C ..... 83*
*Figure 4.8: The film thickness variation with SRR at 40 °C ..... 84*
*Figure 4.9: The measured film thickness for oil A at 50% SRR ..... 85*
*Figure 4.10: The fit of the Eyring equation to the measured traction data for oil A at 145 °C and 20 N ..... 86*

*Figure 4.11: Variation of Eyring stress with temperature (Oil A)* ..... *87*
*Figure 4.12: Variation of Eyring stress with pressure (Oil A)* ..... *87*
*Figure 4.13: Variation of Eyring stress with temperature (Oil B)* ..... *88*
*Figure 4.14: Variation of Eyring stress with pressure (Oil B)* ..... *88*
*Figure 4.15: Stribeck curves of the two lubricants using rough specimens at 40 °C, 0.86 GPa, 50% SRR* ..... *92*
*Figure 5.1: The components and layout of the simulated single stage gearbox* ..... *97*
*Figure 5.2: The load and calculated Hertzian maximum contact pressure and slide roll ratio along the path of contact for the specified gear pair and loading* ..... *98*
*Figure 5.3: The coefficient of friction, lambda ratio and mean film temperature along the path of contact* ..... *99*
*Figure 5.4: The efficiency of the gear pair along the contact path* ..... *99*
*Figure 5.5: Predicted gear friction losses variation with rotational speed for ground and polished surface finishing at 65 °C and 640 Nm* ..... *101*
*Figure 5.6: Predicted gear frictional losses variation with input torque for ground and polished surface finishing at 65 °C and 2000 rpm* ..... *101*
*Figure 5.7: The basic geometry of the 6307 RS1 bearing (SKF)* ..... *102*
*Figure 5.8: The predicted churning losses of the modelled gear pair (i.e. combined loss for both gears) at 65 $^{0}$C for both lubricants at two different immersion depths.* ..... *104*
*Figure 5.9: The power loss of the gear pair for lubricants A and B when only gear friction is considered (the quoted percentages indicate the increase in losses with oil B relative to oil A) for a sump temperature of 65 °C and ground surface roughness (430 nm)* ..... *105*
*Figure 5.10: The efficiency of the gear pair for lubricants A and B when only gear friction is considered (the quoted percentages indicate the drop in efficiency with oil B relative to oil A) for a sump temperature of 65 °C and ground surface roughness (430 nm)* ..... *106*
*Figure 5.11: The power loss of the gear pair for lubricants A and B when gear friction, bearing, seal and churning losses are included (the quoted percentages indicate the increase in losses with oil B relative to oil A) for a sump temperature of 65 °C and ground surface roughness (430 nm)* ..... *107*
*Figure 5.12: The efficiency of the gear pair for lubricants A and B when gear friction, bearing, seal and churning losses are included (the quoted percentages indicate the drop in efficiency with oil B relative to oil A) for a sump temperature of 65 °C and ground surface roughness (430 nm)* ..... *108*

*Figure 5.13: The power loss of the gear pair for lubricants A, A1, A2 and A3 when only gear friction is considered for a sump temperature of 65 °C and ground surface roughness (430 nm)* ..... *109*
*Figure 5.14: The efficiency of the gear pair for lubricants A, A1, A2 and A3 when only gear friction is considered for a sump temperature of 65 °C and ground surface roughness (430 nm)* ..... *110*
*Figure 5.15: The gear friction losses variation with rotational speed for lubricants A, A1, A2 and A3 (Input torque = 640 Nm)* ..... *112*
*Figure 5.16: The gear friction losses variation with input torque for lubricants A, A1, A2 and A3 (Input speed = 2000 rpm)* ..... *113*
*Figure 5.17: The effect of lubricant viscosity on the losses breakdown for an input torque of 300 Nm (1250 rpm, 65 C°, 1:1, fixed module, immersion depth 6mn)* ..... *114*
*Figure 5.18: The effect of lubricant viscosity on the losses breakdown for an input torque of 640 Nm (1250 rpm, 65 C°, 1:1, fixed module, immersion depth 6mn)* ..... *114*
*Figure 5.19: The effect of lubricant viscosity on the losses breakdown for an input torque of 300 Nm (3000 rpm, 65 C°, 1:1, fixed module, immersion depth 6mn)* ..... *115*
*Figure 5.20: The effect of lubricant viscosity on the losses breakdown for an input torque of 640 Nm (3000 rpm, 65 C°, 1:1, fixed module, immersion depth 6mn)* ..... *115*
*Figure 5.21: The cumulative losses in the gearbox when the 6307 RS1 DGBB is used* ..... *117*
*Figure 5.22: The cumulative losses in the gearbox when the 32210 J2/Q TRB is used (no axial load)* ..... *118*
*Figure 5.23: The cumulative losses in the gearbox when the 32210 J2/Q TRB is used (axial load/radial load = 1/3)* ..... *119*
*Figure 5.24: The power loss of the gear pair for lubricants A and B when TRBs are used (no axial load)* ..... *121*
*Figure 5.25: The efficiency of the gear pair for lubricants A and B when TRBs are used (no axial load)* ..... *121*
*Figure 5.26: The losses breakdown for the gear pair as the face-width ratio of the pair is increased at an input torque of 300 Nm (1250 rpm, 65 C°, 1:1, immersion depth 6mn, variable module, variable dref)* ..... *123*
*Figure 5.27: The losses breakdown for the gear pair as the face-width ratio of the pair is increased at an input torque of 640 Nm (1250 rpm, 65 C°, 1:1, immersion depth 6mn, variable module, variable dref)* ..... *123*

*Figure 5.28: The losses breakdown for the gear pair as the number of teeth is increased at an input torque of 300 Nm (1250 rpm, 65 C°, 1:1, immersion depth 6mn, fixed module, variable dref)* ..... *124*
*Figure 5.29: The losses breakdown for the gear pair as the number of teeth is increased at an input torque of 640 Nm (1250 rpm, 65 C°, 1:1, immersion depth 6mn, variable module, variable dref)* ..... *124*
*Figure 5.30: The losses breakdown of the gear pair for six different gear ratios and an input torque of 300 Nm (1250 rpm, 65 C°, gear immersion depth 6mn, fixed module, variable gear dref)* ..... *126*
*Figure 5.31: The losses breakdown of the gear pair for six different gear ratios and an input torque of 640 Nm (1250 rpm, 65 C°, gear immersion depth 6mn, fixed module, variable gear dref)* ..... *126*
*Figure 6.1: Engine power and torque curves at wide open throttle for the 6.7L Cummins turbodiesel engine installed in the vehicle considered (data supplied by Valvoline)* ..... *131*
*Figure 6.2: The vehicle that was used for the experimental drive cycle* ..... *131*
*Figure 6.3: The G56 six speed full synchromesh automotive gearbox* ..... *132*
*Figure 6.4: The speed profile for the experimental drive cycle 1* ..... *133*
*Figure 6.5: The speed profile for the experimental drive cycle 2* ..... *133*
*Figure 6.6: The speed profile for the experimental drive cycle 3* ..... *134*
*Figure 6.7: Surface roughness measurement of the 6th gear* ..... *136*
*Figure 6.8: The temperature readings from the thermocouples mounted inside and around the gearbox as well as the ambient temperature reading (ch8) for the first experimental drive cycle shown in Figure 6.4* ..... *137*
*Figure 6.9: Predicted vs experimental sump temperature for lubricants A and B (experimental drive cycle 1)* ..... *140*
*Figure 6.10: Predicted vs experimental sump temperature for lubricants A and B (experimental drive cycle 2)* ..... *140*
*Figure 6.11: Predicted vs experimental sump temperature for lubricants A and B (experimental drive cycle 3)* ..... *141*
*Figure 6.12: The losses breakdown in the G56 gearbox (experimental cycle 1)* ..... *142*
*Figure 6.13: The losses breakdown in the G56 gearbox (experimental cycle 2)* ..... *142*
*Figure 6.14: The losses breakdown in the G56 gearbox (experimental cycle 3)* ..... *143*

*Figure 6.15: The losses breakdown per bearing in the G56 gearbox for Oil A (experimental cycle 1)* ..... *144*
*Figure 6.16: The New European Drive Cycle (NEDC) including an initial 40 s idle period* *145*
*Figure 6.17: The Artemis URM150 drive cycle* ..... *145*
*Figure 6.18: A comparison between the two shift strategies and the effect of gradient resistance on the NEDC drive cycle (Oil A)* ..... *148*
*Figure 6.19: The predicted sump temperatures for oils A and B for the NEDC drive cycle (Shift 1)* ..... *149*
*Figure 6.20: The losses breakdown in the gearbox for the NEDC drive cycle (Shift 1). For clarity, only total losses are shown for oil B.* ..... *149*
*Figure 6.21: The predicted sump temperatures for oils A and B for the NEDC drive cycle (Shift 2 + gradient)* ..... *150*
*Figure 6.22: The losses breakdown in the gearbox for the NEDC drive cycle (Shift 2 + gradient). For clarity, only total losses are shown for oil B* ..... *151*
*Figure 6.23: The predicted sump temperatures for oils A and B for the Artemis URM 150 drive cycle (Shift 1)* ..... *151*
*Figure 6.24: The losses breakdown in the gearbox for the Artemis URM 150 drive cycle (Shift 1)* ..... *152*
*Figure 6.25: The losses breakdown for the experimental and standardised drive cycles (Oil A)* ..... *153*
*Figure 6.26: The difference in maximum predicted temperature between oils A and B for each of the simulated drive cycles (predicted temperature for oil B is always higher)* ..... *154*
*Figure 6.27: The difference in overall efficiency between oils A and B* ..... *154*
*Figure 9.1: The FEA method flowchart* ..... *172*
*Figure 9.2: A sample FEA model of a single stage gearbox with a lump mass representing the mass of the vehicle* ..... *172*
*Figure 9.3: Coarse (80000 elements) vs finest (800000 elements) mesh setting* ..... *173*
*Figure 9.4: The velocity profile of the airflow around the sample gearbox* ..... *174*
*Figure 9.5: The flow of the oil and air created by the friction due to the rotational motion of the bearings and the discs inside the gearbox. There is constant heat exchange between the air and oil domain however the two fluids are separated by a thin boundary layer as simulation of a two phase flow in 3D was computationally demanding (there is no mixing of the two phases and the CFD model is single phase)* ..... *174*

*Figure 9.6: A sample FEA model of the commercial automotive gearbox when 6$^{th}$ gear is engaged*.....176

# NOMENCLATURE

$A$ : EHL contact area ($m^2$)

$A_{gbox}$ : Surface area of the gearbox ($m^2$)

$b$ : Tooth face width (m)

$B_1/B_1$ : Transient thermal resistance of contacting body

$C_{ch}$ : Churning torque (Nm)

$C_m$ : Dimensionless torque

$D_p$: Gear pitch diameter (m)

$D_0$ : Deborah number

$E'$ : Reduced modulus of Elasticity (Pa)

$E^*$ : Contact modulus (Pa)

$F$ : Normal load (N)

$Fr = \Omega^2 R_p/g$ : Froude number dependant on the gear parameters

$g$ : Gravitational acceleration ($m/s^2$)

$h$ : Gear immersion depth (m)

$h_0/h_c$ : Minimum/central EHL film thickness (m)

$h_t/h_s$ : Convective heat transfer coefficient for the gear track/sides

$k_{oil}$ : Thermal conductivity of the oil (W/m-K)

$L$ : Length of EHL contact (m)

$m$ : Mass (kg)

$M$ : Bearing frictional moment (Nm) (subscripts explained in text)

$M_{total}/M_{track}/M_{sides}$ : Total/track/sides thermal resistance of the gear

$M_1/M_2$ : Steady state thermal resistance of contacting body

$m_n$ : Normal module (m)

$N$ : Rotational speed (r/m)

$Nu$ : Nusselt number

$P$ : Power loss (W) (subscripts explained in text)

$Pr$ : Prandtl number

$\dot{q}$ : Generated heat (W)

$R$ : Gear ratio

$R_p$ : Gear pitch radius (m)

$R_{qc}$ : Combined/composite surface roughness

$R_{q1}/R_{q2}$ : RMS surface roughness of contacting body

$R'x$ : Reduced radius of contact (m)

$Re/Re_c$ : Reynolds number / Critical Reynolds number

$R_a/R_g/R_r$ : Aerodynamic/Gradient/Rolling resistance force (N)

$r_w$ : Wheel radius (m)

$S$ : Non dimensional strain rate

$S_0$ : Atmospheric slope index (Roelands equation)

$S_m$ : Submerged surface area ($m^2$)

$SRR$: Slide roll ratio

$t/t_s$ : Time/time spent in the oil sump (s)

$T_A$ / $T_B$ / $T_F$ : Ambient/Boundary/Flash temperature (K)

$\overline{T}$ : Mean film temperature (K)

$U$ : Entrainment velocity (m/s)

$U_s$: Sliding velocity (m/s)

$v$ : Velocity (m/s)

$V_0$ : Oil volume ($m^3$)

$VI$ : Viscosity index

$W$ : Total (maximum) contact load (N)

$\alpha$ : Pressure-viscosity coefficient

$\alpha_h$ : Heat partition

$\alpha_0$ : EHL semi contact width (m)

$\dot{\gamma}$ : Shear rate ($s^{-1}$)

$(\Delta T_f)_{av}$ : Average flash temperature rise (K)

$(\Delta T_{oil})_{av}$ : Average oil temperature rise (K)

$\Delta_t$ : Time step duration (s)

$\eta$ : Dynamic viscosity (Pa.s) (subscripts – 0: inlet at atmospheric pressure / P: in-contact)

$\eta_\infty$ : Roelands viscosity constant (=0.0000631 Pa.s)

$\lambda$ : Lambda ratio

$\mu$ : Friction coefficient (subscripts - eff: effective or mixed / b: boundary / f: fluid)

$\nu$ : Kinematic viscosity ($m^2/s$) / Poisson's ratio

$\tau$ : Shear stress (Pa) (subscripts - c: critical/limiting superscript *: non-dimensional)

$\chi$ : Thermal diffusivity of material ($m^2/s$)

$\Omega$ : Rotational speed (r/m)

# 1. INTRODUCTION

## 1.1 Background

During the last decade, worldwide energy demand has risen significantly, as a result of an increasing global population and rapid economic growth in major developing economies[1]. In turn, this leads to an increased demand in fuel and a subsequent rise in crude oil prices[2] as shown in Figure 1.1. A recent price drop due to oversupply is already being reversed after the Organization of the Petroleum Exporting Countries (OPEC) agreed to cap the oil output to as low as 32.5 million barrels a day[3].

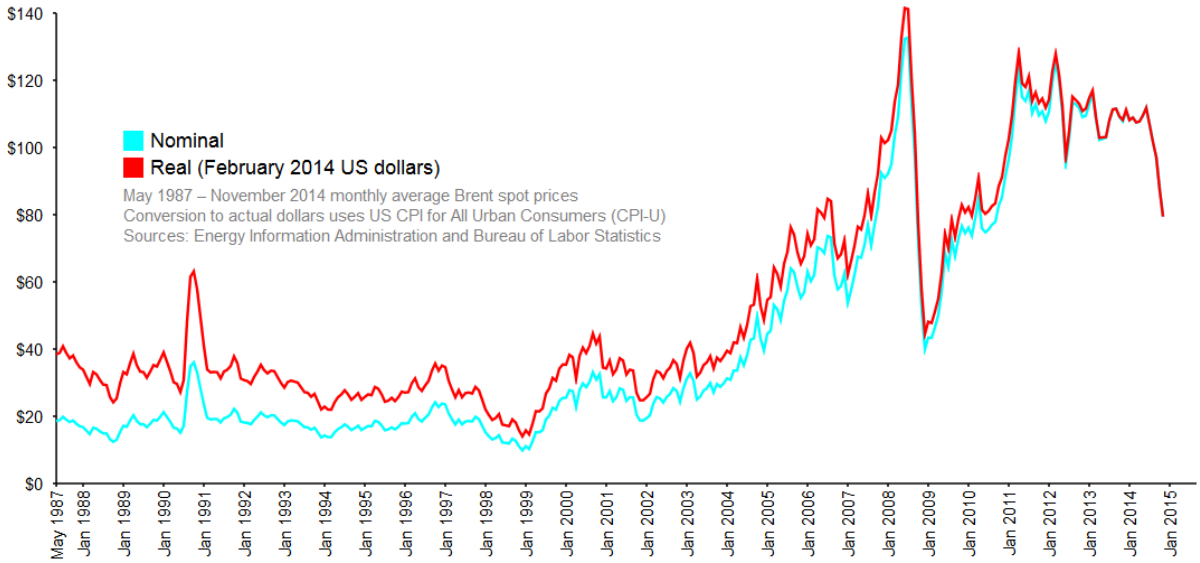



**Figure 1.1: Monthly average Brent crude oil barrel prices 1987-2015[1]**

Furthermore, the global warming concerns amongst the scientific community are well established and governments are under rising pressure to take action. These concerns led to international treaties the most significant of which was the Kyoto Protocol[4] which aims to set binding targets for man-made CO2 emissions. So far, the protocol has been ratified by 192 State Parties. During the last UN conference for climate change, COP 21, a landmark new agreement was reached, setting the foundations for an ambitious target of limiting global temperature rise to 1.5 °C compared to pre-industrial levels[5].

As a result of these agreements, automotive manufacturers are under pressure to reduce the CO2 emissions of the vehicles they are producing. In the EU, light duty vehicles produce about 15% of the total CO2 in the EU with heavy duty vehicles being responsible for an additional 6%[6]. The regulators have set specific objectives for vehicle manufacturers for the average emissions of their fleet[7], while a similar set of measures was also introduced in the US[8] and elsewhere. Figure 1.2 shows the current global restrictions for passenger cars as well as the

projected targets. These figures are based on the NEDC (New European Driving Cycle) emissions.

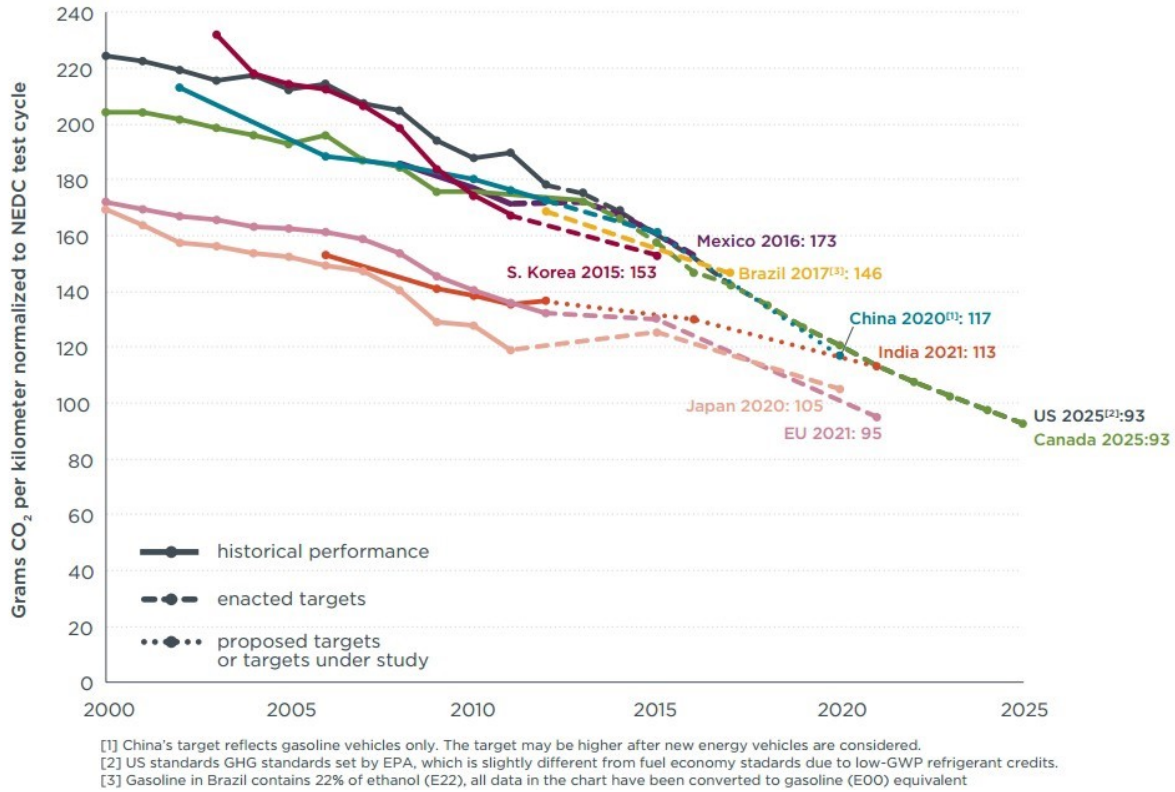



**Figure 1.2: The global CO2 regulations applied to passenger cars[9]**

In order to meet these conditions, automotive manufacturers engaged in a quest to improve the efficiency of the internal combustion engine as well as the rest of the components connected to it. Turbocharging of the engine as well as downsizing were among the solutions that slowly started to find their way into mass production. Engines of smaller capacity with equally small, electronically regulated turbochargers proved to be a winning recipe for meeting the stringent emission goals, and in recent years almost all of the manufacturers have implemented this approach. Nevertheless, the efficiency of the Internal Combustion Engine (ICE) is already at a very high level and is proving harder and harder to further improve on that.

In conjunction with the aforementioned measures, manufacturers introduced the use of lighter materials and manufacturing processes in order to reduce the weight of the vehicles themselves as this has a direct impact on the overall energy required to move the vehicle and is consequently beneficial when it comes to fuel consumption and emissions. In addition to this, numerous techniques were incorporated to save energy such as reduced rolling resistance, alternative fuels and regenerative braking. The latter became easier with the introduction of

hybrid vehicles which incorporate an electric motor working together with the ICE[10]. Zero emission vehicles which are solely battery powered are gaining ground fast but they are still significantly more expensive and have limited range compared to ICE powered vehicles.

Consequently, with the ICE still being dominant, the efficiency needs to be further improved in order to meet the increasing demand for lower emissions. The next logical step to achieve this is to improve efficiency of the numerous components that complete the powertrain of the vehicle, namely the differentials, the shafts, the clutch assembly and the transmission. Recent studies[11] [12] showed that the drivetrain of an average passenger car absorbs around five to six per cent of the total fuel energy in an average everyday situation of combined urban and extra-urban use. The breakdown of the fuel energy is shown in the Figure 1.3.

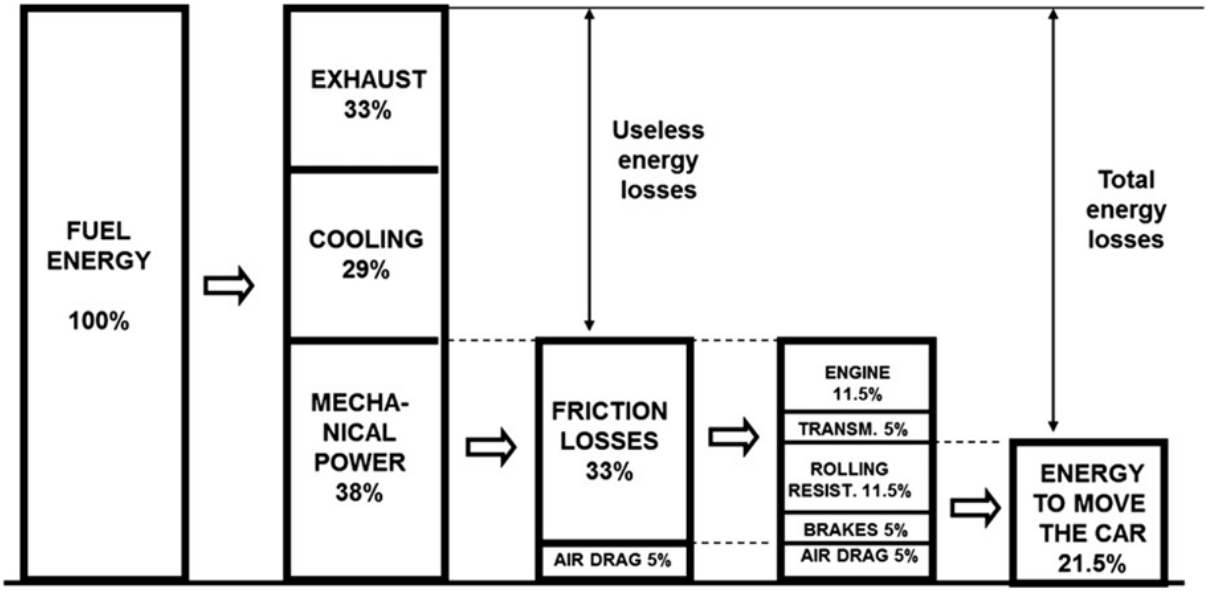



**Figure 1.3: Energy use in an average passenger car[11]**

With exhaust and cooling taking up 62% of the energy, the remaining 38% is the mechanical power. The actual energy that is used to move the car, overcoming rolling resistance, brake losses and air drag comprises 21.5% of the total, with 16.5% lost due to friction in the ICE and the transmission. It is therefore evident that transmission losses represent a significant proportion of overall friction losses or about 23% of the energy required to move the car. Most of this energy loss is in the form of heat resulting from friction and churning and it is absorbed by the transmission lubricant reducing the overall efficiency of the system. Although the figure of 5% is not significantly increased in heavy duty vehicles, which use complex multi-stage gearboxes, the absolute value of energy loss is much higher[13], making transmission efficiency in such vehicles even more significant. As an indication of the energy use through the life of a

medium family car transmission losses would roughly amount to 26 GJ of energy for a 100 kW engine output and 157 GJ when considering a medium duty commercial vehicle with an engine output of 400 kW. In the case of a Class 8 heavy duty vehicle this figure is expected to be significantly larger.

As a result, drivetrain and transmission efficiency has become a hot research topic during the last decade with manufacturers of both components and lubricants pursuing more efficient products. Most automotive lubricants advertise benefits such as reduced fuel consumption and improved efficiency, factors that would ultimately lead to financial benefits for the consumer. In conjunction with improving the energy density of batteries, limiting friction losses would be even more important for electric vehicles, as a reduction in friction power losses would result in extended range. The accurate efficiency prediction for complex components such as gearboxes remains challenging, not least due to complex influences of numerous lubricant parameters and the mutual dependency of various loss sources. Consequently, the reduction of lubricant related losses as a result of friction has become the main research target for manufacturers of both OEM and aftermarket lubricants.

Transmission losses are generally divided into two categories; load dependent and load independent losses. The first group is the result of Elastohydrodynamic (EHD) friction in gear teeth contacts and bearings while the load independent losses consist of churning losses, cage friction and drag in bearings as well as seal losses and auxiliary losses[14].

The ability to accurately assess different lubricants by knowing their EHD friction characteristics is crucial, as will be shown in this thesis. These friction characteristics are not only important because they directly affect power losses but are also difficult to predict and simulate without actually testing the lubricant. Existing numerical gear efficiency studies fail to sufficiently incorporate lubricant rheology and are limited to describing the lubricants in terms of “bulk” properties such as viscosity at atmospheric pressure, density and thermal conductivity, often not appropriately dealing with the rheological behaviour of the lubricant inside the EHD contact. It will be shown that even when the lubricants are of similar specification and carry exactly the same label, a significant difference in power losses can be observed due to differences in high shear rate viscosity characteristics and boundary friction behaviour.

There are well established experimental rig setups created specifically to measure power losses in gears such as the FZG-type gearbox. However, the process of experimentally testing

transmission lubricants using rig setups can be very expensive and time consuming. Measuring temperatures or viscosity in the extreme contact pressures encountered in non-conformal contacts such as gears can prove particularly challenging if not impossible. Furthermore, these rigs are of a specific back-to-back type, as will be described in the following chapter, meaning that their geometry is predefined rather than modular. As a result, there is no guarantee that any numbers obtained on a single-speed back to back gearbox will reflect the results obtained on an actual multi-speed or multi-stage gearbox. This study will show that the breakdown of losses can be different on an actual automotive gearbox compared to a single stage single speed rig. Finally, a very broad range of input conditions and possibly different components should be tested in order to sufficiently assess and experimentally compare lubricants in terms of efficiency.

For this reason, there is a need to develop a new modular approach that will combine experimental oil characterisation with power loss predictions in simulated gear contacts. Starting from the all-important friction characteristics of the lubricant and including the modelling of bearing and churning losses, such an approach would also require the individual modules to be interconnected and thermally coupled. In this thesis, a complete thermally coupled model able to calculate the individual component losses in a gearbox based on experimentally characterised lubricant rheology will attempt to address the aforementioned limitations of current methods and provide further insight into the effect of lubricant properties on temperatures and efficiency under variable duty. As the model is modular, it can adapt for an infinite number of lubricant and component combinations can be tested providing near 100% repeatability and significantly reducing the time needed to test a new lubricant during the design phase.

## 1.2 Research goals

The main goals of this project are summarised below

- The main goal of this research is to develop a method that can be used to predict the efficiency of a gearbox under real life operating conditions and account for the effect of specific lubricant properties on the overall efficiency. This allows for system optimisation and aids in the formulation and selection of the most efficient lubricant for a given transmission and operation cycle. The model is expected to account for variable duty cycles, lubricant rheological and boundary friction properties as well as gearbox

design and external conditions. Finally, the model should be able to differentiate between different lubricants in terms of friction behaviour under high contact pressures and overall efficiency for a given gearbox.

- The developed thermally coupled model should account for EHL friction losses in gear teeth contacts as well as bearing, seal and churning losses. The loss predictions will be coupled to a lump mass model of a six speed gearbox which, given the lubricant, vehicle and transmission input parameters can predict the power loss of the components and the oil sump temperature. Ultimately, measured lubricant temperatures from the gearbox will be compared to model predictions.

- Lubricant characterisation is also a very important part of the study. Ball-on-disc tribometer tests will be conducted to assess the rheological behaviour of the lubricants and the results will be incorporated in the model. This will allow for a more precise description of the lubricants' specific properties such as the viscosity dependence on temperature and pressure, and the boundary friction behaviour. The importance of the characterisation process will be demonstrated through lubricant comparison in the following chapters. It will be proven that lubricants of nominally the same specification can result in different power loss predictions due to the effect of different additive packages and combinations of base oil groups.

- As the accurate prediction of operating temperatures in a gearbox is crucial, this method should be able to predict the bulk operating temperatures in a given gearbox when the duty cycle is known.

- In addition to accuracy, flexibility and adaptability of the method will be important considerations for its design. The constructed model will be modular and as such, it should be possible to account for variations in gearbox geometry, component selection and lubricant properties as well as external conditions. Additional lubricants have been simulated based on the measured lubricant properties, confirming the capability of the model to be used as a robust lubricant comparison platform even when there is no time for experimental oil characterisation.

## 1.3 Thesis outline

This thesis is structured in ten chapters, and a brief description of each is given below;

The current chapter serves as an introduction to the work undertaken, provides the related background and outlines the main aims of the thesis.

Chapter 2 contains the relevant literature in the field of automotive drivetrain, with focus on published research in the field of transmission efficiency and lubrication that is relevant to present work.

Chapter 3 presents the modelling methodology which was followed in this project in order to predict EHL traction as well as contact and tooth flank temperatures - of importance in gear lubrication and friction. The overall numerical algorithm for gear friction calculations is also presented in addition to the adapted models for the prediction of bearing and churning loss. Finally, the model is validated for each of the individual loss sources, namely gear friction, bearings and churning, by comparing the outputs to appropriate published data.

Chapter 4 describes the experimental methodology which was followed in order to characterise the studied lubricants and extract the necessary lubricant parameters to be used in the overall gearbox efficiency model.

Chapter 5 presents a parametric study on the influence of various parameters on the overall gearbox efficiency. A single stage spur gearbox is used for this parametric study and the influence of gearbox design as well as lubricant parameters is assessed.

Chapter 6 uses the model to simulate a commercial 6 speed automotive gearbox in order to predict the losses under real road conditions. Results comprising efficiency, loss and temperature predictions are presented for both standardised and experimental drive cycles, while the measured temperature data are compared to the model predictions.

Chapter 7 provides an overall discussion on the results presented in this thesis as well as advantages and disadvantages of the presented model in relation to other gearbox efficiency studies.

Chapter 8 summarizes the present work, presents the main conclusions and provides suggestions for possible future work based on this study.

Chapter 9 (Appendix) contains a description of additional work that was conducted on multiphysics modelling of thermal flows in a gearbox.

# 2. LITERATURE REVIEW

## 2.1 Introduction

This chapter will explain the fundamental aspects of gearbox operation and describe the various components that are found in transmission systems. The work undertaken in this thesis and the described modelling methodology is applicable to any geared transmission including industrial and heavy duty gearboxes however the focus in this study will be on an automotive gearbox. Subsequently, a review of relevant literature on drivetrain efficiency will be presented, including existing numerical and experimental treatments of individual loss sources encountered in transmission systems. Current approaches to predict the overall gearbox efficiency will be reviewed and their limitations will be discussed. Finally, the theory behind elastohydrodynamic lubrication (EHL) will be summarised, particularly in relation to EHL traction and relevant lubricant properties as this underpins the approach of the current model to gear EHL losses as presented later in the thesis.

## 2.2 Background

### 2.2.1 Automotive drivetrain

The automotive drivetrain is the group of components that deliver power to the driving wheels of the vehicle[15]. It includes a clutch assembly, a gearbox, a differential and a number of drive shafts depending on the specific layout of the vehicle and the set or sets of wheels where the power is transmitted to. Typical configurations for an automotive drivetrain for the rear-wheel drive, front-wheel drive and four-wheel drive layouts are shown in Figure 2.1[16]. In each case, the transmission is connected to the ICE, the torque of the latter multiplied by the gearbox before being transmitted through a series of axles and shafts to a differential; from there it rotates the drive shafts before ending up propelling the vehicle through the wheels.

In the case of a four wheel drive vehicle, additional units called transfer cases are used in order to split the power between the two axles, introducing an additional element of power loss as well as increasing the overall vehicle weight. In the case of a front engine, front wheel drive vehicle there is no need for additional axles to transmit the power so that the gearbox and differential are commonly placed within the same housing. The efficiency, simplicity and cost of this design is superior compared to alternative layouts, thus it has found use in the majority of city cars.

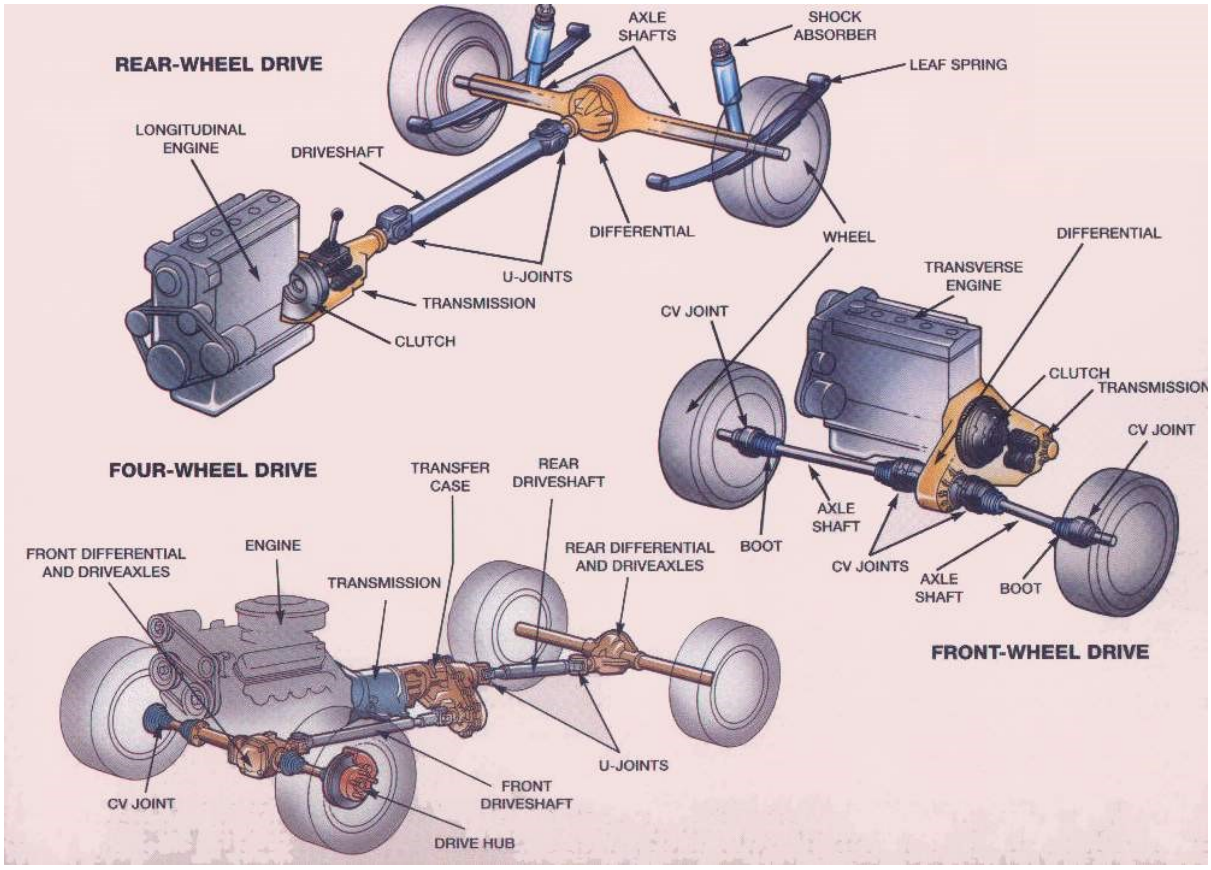



**Figure 2.1: Typical configurations of an automotive drivetrain[16]**

### 2.2.2 Gearboxes

The gearbox or transmission is the main and largest component of the drivetrain and is essentially a torque multiplication unit connecting the ICE to the differential or the axle, depending on the layout, through a clutch assembly[17 18]. The clutch assembly usually consists of a flywheel which stores kinetic energy converted by the engine, and one or more friction plates. In its simplest form, the gearbox consists of a set of gear pairs, each one providing a different gear ratio or torque multiplication factor.

The function of a vehicle transmission is to adapt the power and speed available from the engine to that required by the road conditions and the driver. An internal combustion engine develops the optimum torque, power and efficiency over a very narrow range of engine speeds and the job of the transmission is essentially to match the torque and speed of the engine to a much wider range of characteristics required of the driven vehicle while allowing the engine to operate as near to its peak efficiency point as possible. There are four distinguishable types of transmissions; geared mechanical multi-speed, geared semi-automatic multi-speed, geared

conventional hydrodynamic/mechanical automatic and mechanical, hydrodynamic, hydrostatic or electric continuously variable transmission (CVT) [19].

In their most common and simplest form, mechanical multi-speed gearboxes typically consist of three shafts, the input shaft the intermediate shaft and the output shaft. The intermediate and output shafts carry a set number of gears, spur or helical which, in the case of constant-mesh gearboxes are in mesh at all times. The input shaft is usually connected directly to the intermediate shaft and the two share the same input load while the output shaft carries the mating gears of the internal ratios[20]. A typical 5-speed constant-mesh manual gearbox is shown in Figure 2.2[21].

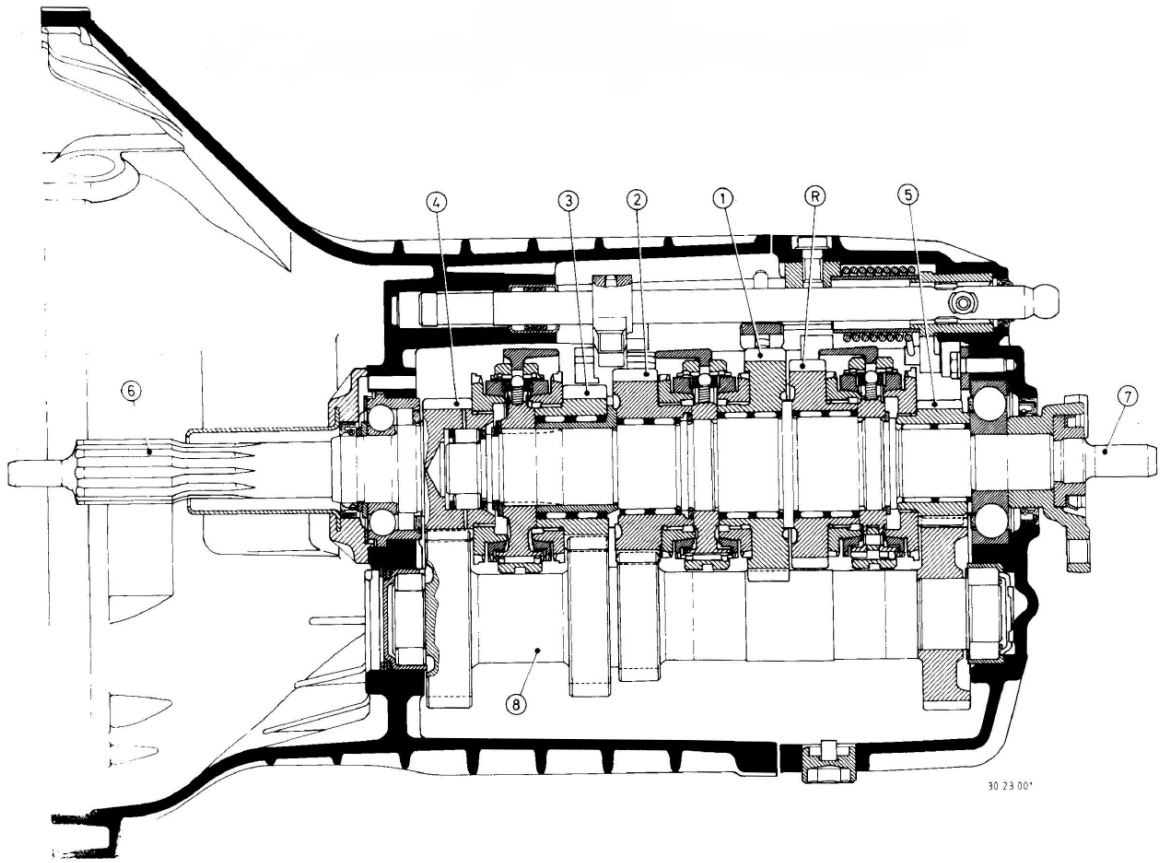



**Figure 2.2: A typical 5-speed constant-mesh manual automotive gearbox (Getrag)[21]**

### 2.2.3 Gears

A gear is a machine element containing teeth which mesh with the teeth of another gear, with the purpose of transmitting torque[22]. In most cases, gears mesh with rotating parts i.e. other

gears but a gear can also mesh with a rack converting rotational motion to linear motion. The torque and speed multiplication factor of a gear pair is a function of the number of teeth that each individual gear carries and the ratio of driven teeth to driver teeth is called gear ratio[23].

$$R = \frac{N_B}{N_A} = \frac{\omega_A}{\omega_B} = \frac{T_B}{T_A} \quad (1)$$

Where R is the gear ratio NA, NB is the number of teeth of the driven (B) and driver (A) gear respectively, ωA, ωB are their angular velocities and TB, TA are the torques on gears A and B respectively.

There are three main groups of gears[24] depending on the application; gears used to connect parallel shafts (spur, helical and rack and pinion), gears used to connect intersecting shafts (straight and spiral bevel gears) and gears used to connect non-parallel, non-intersecting shafts (hypoid and worm gears). Spur gears have teeth cut parallel to the gear axis and the contact path is also parallel to the gear axis. Helical gears on the other hand have teeth that are cut at an angle to the face of the gear. Spur and helical gears are extensively used in gearbox applications both industrial and automotive. Figure 2.3 shows a general classification of gears.

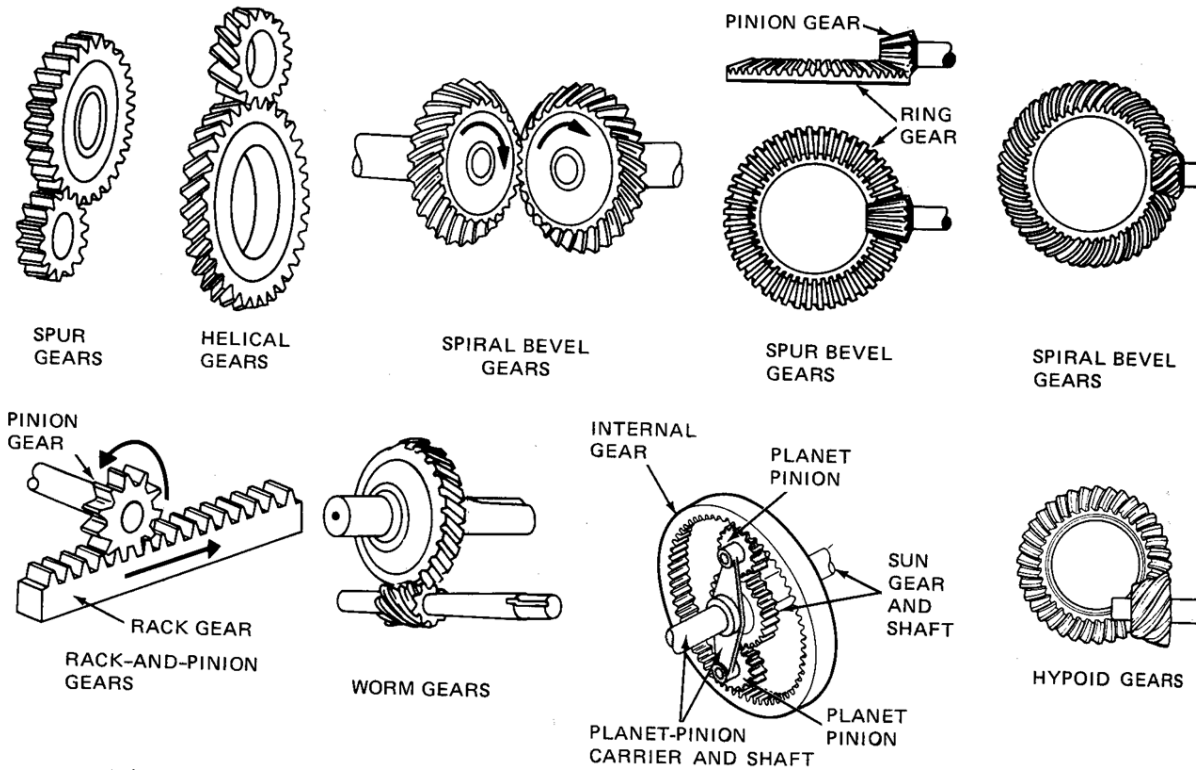



**Figure 2.3: Classification of gears**

Bevel and hypoid gears are used to connect shafts which are intersecting each other at an angle of 90̊ (vertical). Hypoid gears differ from bevel gears because of the off-centre positioning of the pinion in relation to the gear centre hence the need to classify them in a separate group. Worm gears are also used when the shafts are vertically aligned; however they are not commonly used in automotive applications as a result of very high sliding which decreases their efficiency. On the other hand, hypoid and bevel gears are very commonly used in differential units. The efficiency of spur and helical gears can be as high as 99.8%[25] whereas values of up to 99% can be achieved for bevel gears. On the contrary hypoid gears have a slightly lower efficiency at around 96% due to increased sliding[26] and worm gears are significantly less efficient, rarely exceeding 90%[27]. Automotive gearboxes predominantly use spur and helical gears; the geometry and basic definitions of a meshing spur gear pair is shown in Figure 2.4[28].

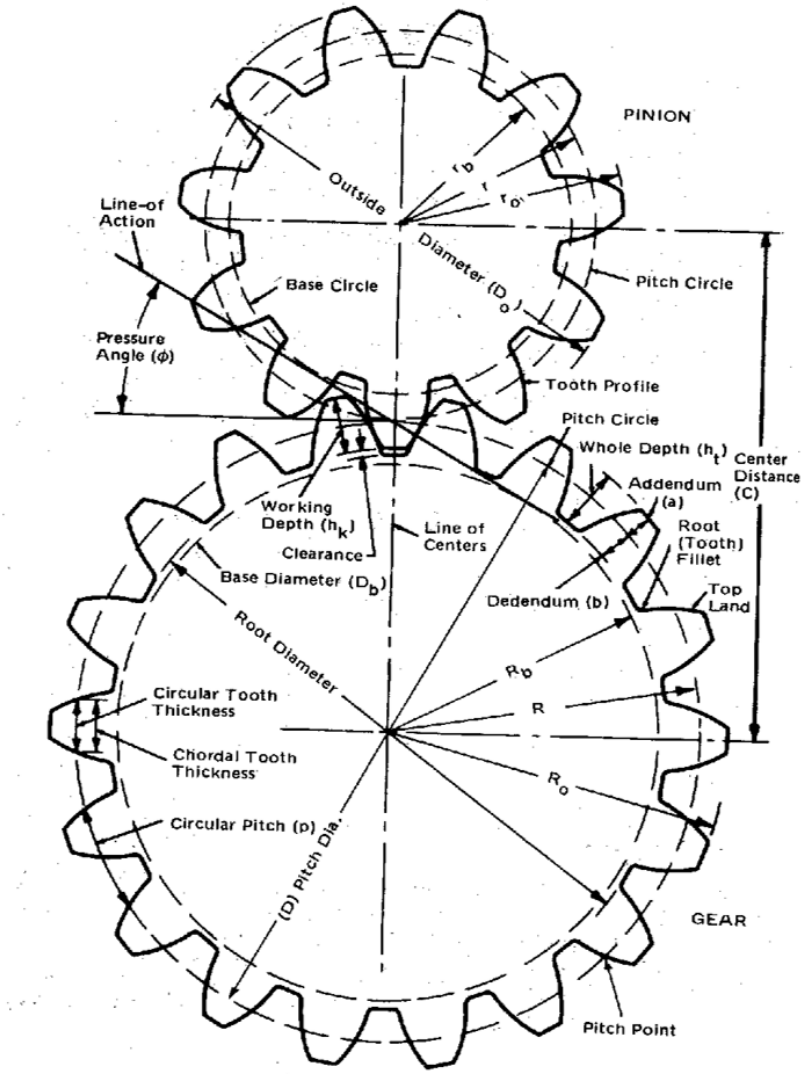



**Figure 2.4: The geometry of a pinion and gear pair in mesh**

### 2.2.4 Bearings

Bearings are machine elements that allow shafts to rotate freely, with minimum friction, while supporting axial and/or radial shaft loads[29]. Bearings come in many shapes and forms and can be categorised differently according to their shape, load support or geometry; however they are usually divided into rolling element bearings and plain or fluid film bearings[30].

Fluid film bearings use the force generated by a hydrodynamic or hydrostatic film to support the load while rubbing bearings are simply a layer of material separating the two surfaces. In transmission applications rolling element bearings are by far the most common type used. These bearings consist of a set of rolling elements which can be either of spherical, cylindrical roller (very thin cylinders called needles are also used) or spherical roller shape. These elements are located between the inner and outer raceways of the bearing and the element-raceway contact operates close to pure rolling conditions, thus reducing the contact friction. Rolling element bearings exhibit great reliability, smooth operation and high efficiency.

In most gearboxes, the shaft loads that need to be supported at each location are either radial, axial or a combination of the two. Deep groove ball bearings are generally used to support radial loads, although they can carry some axial loads too. They are efficient and cheap and come in many standard sizes. When support of significant axial loads in conjunction to the radial load is necessary in a typical transmission, tapered roller bearings are commonly used. Taper roller bearings involve a fair amount of sliding and their efficiency is generally lower than that of equivalent deep groove ball bearings. Both of these types commonly appear in single row or double row variations with the latter featuring an additional row of rolling elements. Figure 2.5 shows a typical ball bearing as well as a tapered roller bearing.



**Figure 2.5: Single row deep groove ball bearing -DGBB- (right) and tapered roller bearing -TRB- (left) (SKF)**

## 2.3 Lubrication

### 2.3.1 The importance of lubrication

The primary function of the lubricant is to provide a protective, lubricating film between the contacting surfaces, such as two gear teeth or the rolling element and raceway in a rolling bearing. In transmissions, the lubricant also provides cooling of the contacting components which is essential for their adequate performance. The composition and properties of a lubricant play a crucial role in any geared transmission. Properties such as viscosity greatly affect power losses as the thickness of film and the amount of shear in the film directly affect the temperature within the EHL contact. As mentioned before, most of the heat produced by the transmission components ends up being absorbed by the transmission lubricant. A significant amount of research has been undertaken to produce more efficient lubricants because even a numerically small difference in efficiency translates to important energy and fuel savings on a larger scale. In order to assess the effect of lubricant properties on transmission efficiency, it is imperative to get a solid grasp of the composition and properties of the lubricant and understand the role and behaviour of additives, especially those active in the high contact pressures and temperatures of a mixed-regime non-conformal contact.

Adequate lubrication must be ensured at all times in order to maintain smooth operation and prevent the seizure of moving parts, increase the operational life of the component and reduce the possibility of wear. Bearings usually operate in full film elastohydrodynamic lubrication (EHL) regime due to the very high surface finish of their components. However, this is not usually the case with gears as the surface roughness is significantly higher and superfinishing is not commonly used due to the increased production cost. As a result, gears usually operate in the mixed lubrication regime which means that the asperities on the surface of the teeth come into contact.

### 2.3.2 Lubricant composition

Lubricants are generally either grease or oils but in transmissions, oils are by far the most common lubricant. Lubricating oils usually consist of two components; the base fluid or base oil, which typically comprises 95% of the lubricant, and added chemicals called additives which take up the remaining 5%[31]. The base oil is what determines some of the physical properties of the lubricant (viscosity, density, full film EHL traction properties, thermal conductivity, pour point, volatility, biodegradability etc.) while the additives' purpose is to enhance specific properties of the lubricant such as reducing wear and friction in boundary regime, where fluid film thickness is insufficient to separate the surfaces, or providing corrosion protection[32].

According to their base fluid, lubricating base oils are divided in two main groups; mineral and synthetic. Mineral base oils are obtained through the distillation and treatment of crude petroleum and they are still the most widely used type of base oil mainly because of their low cost and high versatility. They can be categorised based on their chemical forms, their sulphur content and their viscosity. Synthetic base oils are derived by processing of petroleum or other products. They are very versatile and generally have superior heat resistance and oxidation properties and higher viscosity index (VI) compared to mineral oils however they are significantly more expensive although the price gap between the two is steadily closing. The use of synthetic base oils is necessary in some specialised or critical applications where the properties of mineral oils make them unsuitable such as very high operating temperatures. The main synthetic base fluid types are synthetic hydrocarbons (PAO, esters) which are usually products of the breaking down of complex petroleum molecules[33], silicon analogues (silicones) and organohalogens (such as PFPEs)[34]. Furthermore, biodegradable synthetic ester base stocks comprise a new generation of products with the aim of replacing traditional mineral oils. This

area is gaining increasing attention as a result of the global trend towards sustainability. These eco-friendly products could potentially be used to replace existing lubricants in automotive, metal working, cold rolling and other industrial applications[35].

Another commonly used lubricant is grease which is essentially the combination of a base oil and a substance called thickener, such as a metal soap for example, which creates a web of miniature fibres to trap the oil; greases commonly also include additives and fillers[36]. Greases are mostly used in permanently lubricated components or where extended lubrication intervals are allowed. They have good sealant properties but are less effective in conducting the heat away and are unsuitable for use at higher speeds.

As mentioned above, additives are chemical particles, designed to enhance the lubricant properties in one or more directions[37]. Some of the most important and common additives include: friction modifiers, whose main purpose is to reduce friction in mixed and boundary regimes; antiwear additives, which reduce wear where the fluid film thickness is critically low; extreme pressure (ep) additives, which are commonly used in gear oils to protect the components from scuffing damage by forming metal salts on the surfaces when there is insufficient EHD oil film and significant metal-to-metal contact occurs; detergents which prevent the formation of varnish on the engine parts and neutralise sulphuric and nitric acids; dispersants which act against coagulation of carbon particles resulting from, for example, incomplete combustion in IC engines and prevent the formation of soot; viscosity index (VI) improvers which increase the VI of the lubricant; general inhibitors which prevent corrosion, oxidation, rust and the formation of foam.

### 2.3.3 Lubrication methods

In order to provide the necessary level of lubrication, a lubrication system needs to be in place to feed the oil to the relevant contacts. In the case of a gearbox, there are two main methods of lubrication; splash or dip lubrication and jet lubrication[38]. In the first case, the gearbox casing is filled with oil up to a pre-defined level and lubrication of components that are completely or partially above that level is achieved by means of churning i.e. the gears are immersed in the lubricant and during their operation they pick up the lubricant and splash it around the casing. The lubricant can then reach the components that are not immersed, before flowing back to the oil sump. A design that allows enough clearance for picking up the oil and passages to lubricate the bearings should be implemented. This method of lubrication is simple and very cost

effective as no additional components are required. However, there is a limitation on the maximum peripheral speed of the gears which should not exceed 13-15 m/s[38] . The immersion depth should also be carefully selected to balance insufficient oil feed and excessive churning losses. Usually, the immersion depth is no more than six times the gear module. The oil cannot be filtered so there is an increased risk of oil contamination from debris and any oil cooling that may be necessary is also more difficult to achieve. Nevertheless, this lubrication method is by far the most commonly employed one in automotive gearboxes.

The other method of lubrication is forced or jet lubrication and is necessary when the peripheral speeds are in excess of 15 m/s. In this case, a high pressure pump and a circulation system is incorporated in the design which feeds the lubricant directly on to the components via nozzles in the form of a high speed jet. This method provides an additional cooling effect as the jet of oil comes into contact with the component and is therefore more suitable for high power applications where high rates of heat dissipation are needed. The application of this method is more expensive, makes the use of hydrodynamic bearings mandatory and requires careful nozzle positioning to ensure that all the components are adequately lubricated at all times and oil starvation, which can significantly reduce their operational life, is avoided. The schematics of splash and jet lubrication are shown in Figure 2.6.

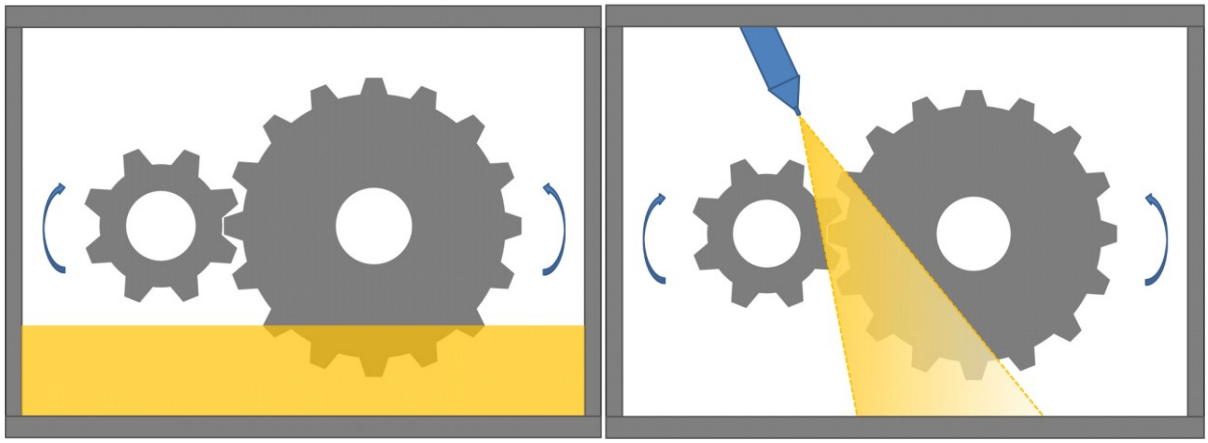


**Figure 2.6: Dip lubrication (left) and jet lubrication (right)**

Rolling bearings can be lubricated by grease (in case of sealed bearings) when the product of the bearing mean diameter $D_m$ and the rotational speed of the bearing $N$ in rpm is less than about 500000[39]. For high temperature and high speed applications jet lubrication is commonly applied which should take into consideration the position and number of nozzles, the flow rate of the lubricant and the jet velocity[40].

### 2.3.4 Lubricant viscosity and rheology

#### 2.3.4.1 Definition

The viscosity of a fluid is the tendency of the fluid to resist deformation by shear stress or flow[41]. It is perhaps the single most important property of the lubricant as it largely defines the thickness of the lubricating film that is formed between two surfaces. Low viscosity could lead to thin films and elevated wear due to the contact and rubbing of asperities, whereas too high a viscosity could lead to higher losses due to increased resistance to shear as well as increased churning loss in a dip-lubricated system. Viscosity is categorised in two forms; the dynamic and the kinematic viscosity[31].

Dynamic viscosity is depicted by the symbol $\eta$, and is the ratio of the shear stress $\tau$ applied to the lubricant to the strain rate (shear rate) $\dot{\gamma}$ of the lubricant;

$$\eta = \frac{shear\ stress}{strain\ rate} = \frac{\tau}{\dot{\gamma}} \quad (2)$$

The strain rate is analogous to the velocity gradient which is equal to the velocity in the direction of shear divided by the width of the shear zone or $u_s/h$ where $u_s$ is the sliding speed and h is the lubricant film thickness.

In the SI system of units, dynamic viscosity is measured in Pascal seconds (Pas), but the unit of Poise (P) or more commonly the Centipoise (cP) is widely used. The viscosity of a lubricant can be measured with devices called viscometers which come in many variants like capillary, rotational and high shear rate viscometers.

Kinematic viscosity, depicted by the symbol $\nu$, is a composite property which is equal to the ratio of the dynamic viscosity over the density $\rho$ of the fluid;

$$\nu = \frac{dynamic\ viscosity}{density} = \frac{\eta}{\rho} \quad (3)$$

In the metric system, kinematic viscosity is measured in $m^2/s$ the Stoke (S) or Centistoke (cS) (equal to 1 $mm^2/s$) are commonly employed

#### 2.3.4.2 Viscosity dependence on shear rate

When a fluid is Newtonian, the relationship between shear stress and strain rate is linear[42]. When this relationship breaks down and the viscosity of the fluid depends on the shear rate, shear duration or the rate at which the shear is applied, the fluid is classified as non-Newtonian.

Fluids which are non-Newtonian can either exhibit a shear thinning (or pseudoplastic) behaviour or a thixotropic behaviour. In the first case, the effective viscosity is reduced at high shear rates whereas in the second case viscosity reduces steadily while shearing is applied. The former behaviour is typical of multigrade oils while the latter is commonly encountered in greases. A graphical representation of Newtonian vs. shear thinning (non-Newtonian) behaviour and the effect of shear thinning behaviour on the viscosity for different lubricant grades [43] is shown in Figures 2.7 and 2.8 respectively.

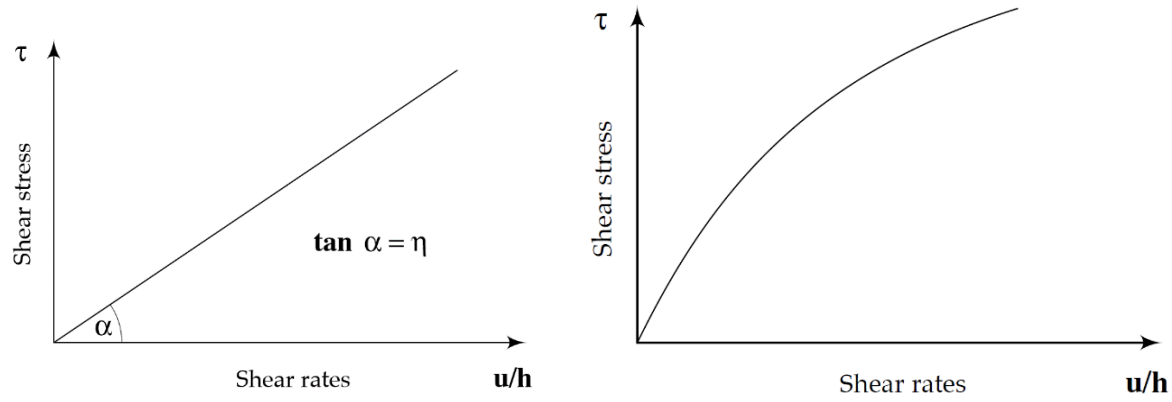



**Figure 2.7: Newtonian fluid (left) vs. non-Newtonian, shear thinning fluid (right)[43]**

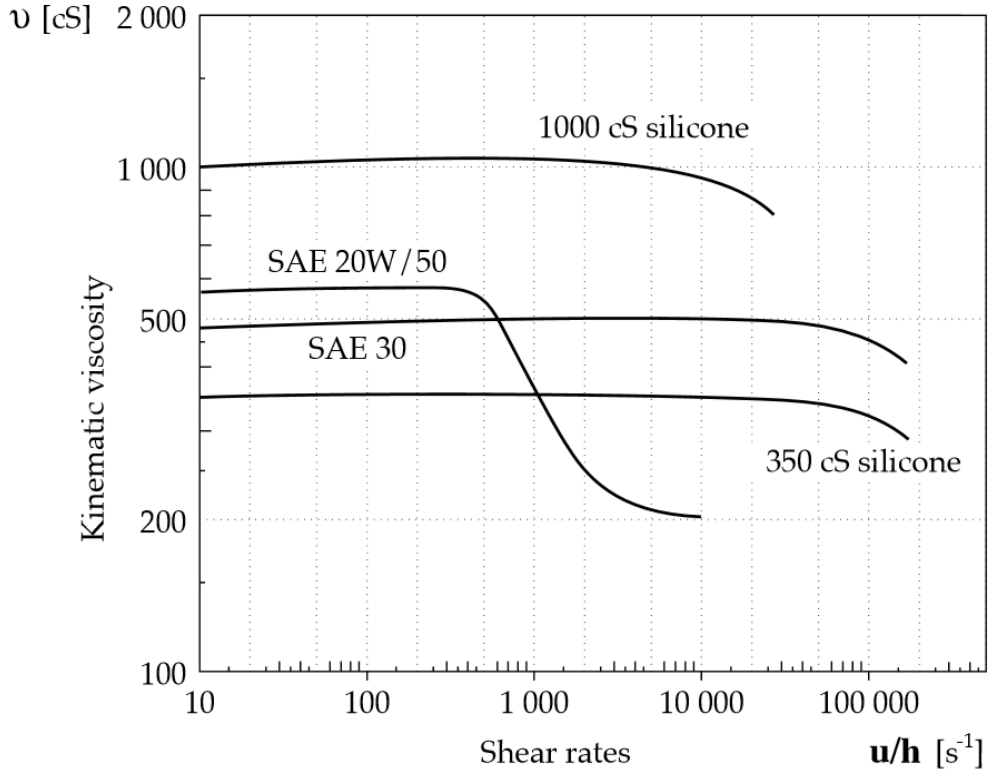



**Figure 2.8: The effect of shear rate on viscosity for different lubricants[43]**

All fluids are likely to shear thin if the shear rate is very high i.e. above $10^9$. In a typical high pressure EHD contact, the shear rate which would cause the lubricant to shear thin is usually not high enough to cause the phenomenon on its own however in most cases shear thinning can be observed due to high shear stress[31]. When considering such highly loaded contacts, such as those between gear teeth, where high shear stress can occur[44], this must be taken into account.

#### 2.3.4.3 Viscosity dependence on temperature

The viscosity of a viscous liquid reduces radically with temperature. Therefore the viscosity dependence on temperature is crucial for any calculations. Over the past century, numerous equations to describe the viscosity-temperature relationship were derived either empirically or model-based.

The earliest was developed by Reynolds[45] but is very inaccurate;

$$\eta = be^{aT} \quad (4)$$

A more accurate equation is given by Vogel[46], which includes three constants and is best used at lower temperatures;

$$\eta = \alpha e^{\frac{b}{T-c}} \quad (5)$$

A very important step to standardise the viscosity variation with temperature was the Walther equation[47];

$$\nu = a + bd^{\frac{1}{T^c}} \quad (6)$$

This equation formed the basis for the ASTM (American Society for Testing Materials) standard for the description of viscosity variation with temperature (ASTM D341-722[48]);

$$loglog(\nu + 0.7) = b - clogT \quad (7)$$

With the base of the logarithm being 10 and the units for $\nu$ and $T$ being centistokes (cSt) and Kelvin respectively. This equation is very useful because it forms the basis of the ASTM chart which can be used to find the viscosity of a given fluid when the viscosities at two other temperatures are known however the equation should not be used to extrapolate to very low temperatures. The ASTM equation is designed to work with kinematic viscosity but produces satisfactory results when used with dynamic viscosity[49].

The Viscosity Index of a lubricant is a measure of the kinematic viscosity dependence on temperature and the higher this number is the less viscosity is affected by temperature variations[50]. It is based on comparing the viscosity of the lubricant at 40℃ with the viscosity of two standard lubricants, the first having a VI of 0 and the second a VI of 100, while the standard lubricants and the test lubricant share the same viscosity at 100℃. When the value of the viscosity index is less than 100, it is calculated by the equation;

$$VI = \frac{\nu L - \nu U}{\nu L - \nu H} * 100 \quad (8)$$

With L being the oil with VI=0, H the oil with VI=100 and U being the lubricant the viscosity of which is unknown.

#### 2.3.4.4 Viscosity dependence on pressure

The viscosity of a lubricant increases significantly with pressure; in the case of a lubricated gear pair the viscosity of the lubricating oil typically increases by more than $10^4$ when the lubricant gets squeezed in the high-pressure section of the EHL contact formed by the mating gear teeth[51]. For this reason an equation accurately relating the increase of viscosity to the increase in pressure is vital for any EHL treatment of gear teeth contacts.

The most commonly used equation to describe the variation of viscosity with pressure is the one given by Barus[52];

$$\eta_p = \eta_0 e^{\alpha p} \quad (9)$$

Where the viscosity of the lubricant at pressure $p$ is $\eta_p$, the viscosity at zero pressure is $\eta_0$ and the alpha value α is a coefficient called pressure-viscosity coefficient which is approximately constant up to a pressure of about $10^8$ Pa.

When the pressure is higher than that there are two equations which can be used; the first of which is the Roelands equation which was proposed in both temperature corrected form (including the temperature variation) and in pressure corrected form (simpler). The equation below is the complete temperature corrected form[49];

$$\eta_p = \eta_\infty e^{\left(log_e\left(\frac{\eta_r}{\eta_\infty}\right)\left(1+\frac{p}{p_r}\right)^z\left(\frac{T_r+135}{T+135}\right)^{S_0}\right)} \quad (10)$$

In this equation, $\eta_\infty$ is a viscosity constant (=0.0000631 Pas), z is a lubricant specific constant, 135℃ is a temperature constant where the viscosity becomes infinitely high (actually -135℃),

and $\eta_r$ is the viscosity at atmospheric pressure and a reference temperature $Tr$. $S_0$ is the atmospheric slope index which is calculated using a chart derived from the ASTM chart.

The second equation that can be used is given by Cameron[53];

$$\eta_p = \eta_0(1 + cp)^n \quad (11)$$

Where $n$ and $c$ are constants with n=16.

### 2.3.5 Film thickness and lubrication regimes

The thickness of the lubricant film formed between two surfaces is crucial for the operation of any lubricated component. Achieving lubricating films that are just sufficiently thick can significantly reduce friction and subsequently increase the efficiency of the component without sacrificing durability[54]. The thickness of the film compared to the surface roughness is what determines the lubrication regime in which the contact operates. In conformal contacts, where the pressures are relatively low and no significant elastic deformation of the bodies occurs, the prevalent lubrication regime is hydrodynamic (HD) lubrication. A common application is journal bearings.

However, when the contact pressure is very high (order of GPa[55]) which usually happens when the surfaces are non-conformal (gears, bearings, cams), the lubricant is subjected to such extreme conditions that the viscosity increases dramatically, as described in the previous section (piezoviscous effect), and the force that the lubricant exerts to the surfaces is such that it causes elastic deformation (elastic effect). This lubrication regime is called Elastohydrodynamic Lubrication (EHL)[56].

The first equation that could be used to calculate lubricant parameters in a non-conformal hydrodynamic contact was suggested by Reynolds[45] and is derived by appropriately simplifying the full Navier Stokes equation. The equation is a description of the pressure field between two surfaces when the surfaces are pushed against each other;

$$\frac{\partial}{\partial x}\left\{\frac{h^3}{\eta}\frac{\partial p}{\partial x}\right\} + \frac{\partial}{\partial y}\left\{\frac{h^3}{\eta}\frac{\partial p}{\partial y}\right\} = 6\left\{U\frac{\partial h}{\partial x} + V\frac{\partial h}{\partial y} + 2(w_2 - w_1)\right\} \quad (12)$$

This equation can be solved to calculate crucial lubrication parameters such as the pressure distribution, the load, the friction force and hence the coefficient of friction as well as the flow. It can be applied in convergent wedges and therefore to model thrust pad bearings as well as journal bearings.

When the surfaces are non-conformal (counterformal) and the contact operates in EHL regime, the lubricant parameters are much harder to calculate as the combination of sliding (characteristic of non-conformal contacts), elastic deformation and dramatic viscosity increase has to be taken into account. For this reason, when these contacts were approached by Gumbel[57] and Martin[58] using the traditional Reynolds equation, the predicted film thickness was too small. Meldahl[59] incorporated the elastic deformation into his calculations, however, the predicted oil film thickness was still unreasonably small.

The first solution to predict reasonable values for the film thickness in line contacts was introduced by Grubin[60] and Ertel[61] with the assumption that the surfaces under EHL would deform according to the Hertzian theory for dry contacts. Their approach included piezoviscous effects and accounted for the material properties, the speed and the load in the contact using three non-dimensional parameters;

$$\overline{U} = \frac{U\eta_0}{E'R'_x} \quad (13)$$

$$\overline{G} = \alpha E' \quad (14)$$

$$\overline{W} = \overline{W_L} = \frac{W}{E'R'_x L} \quad (15)$$

referred to as the speed, material and load (in this case for a line contact) parameter respectively. U is the entrainment velocity, $\eta_0$ is the viscosity at zero pressure, E' is the reduced modulus of elasticity, derived from the Young's modulus, $R'_x$ is the combined radius of curvature, α is the pressure viscosity coefficient, W is the total normal load acting over the width of the contact L. Grubin's EHL film thicnkess equation is;

$$\frac{h_c}{R'x} = 1.95\,\overline{U}^{\frac{8}{11}}\overline{G}^{\frac{8}{11}}\overline{W}^{-\frac{1}{11}} \quad (16)$$

Dowson and Higginson[62] [63] introduced a coupled approach by incorporating both the piezoviscous and the elastic effect and produced a numerically derived solution to calculate the central film thickness $h_c$ and the minimum film thickness $h_0$;

$$\frac{h_0}{R'x} = 2.65\,\overline{U}^{0.7}\overline{G}^{0.54}\overline{W}^{-0.13} \quad (17)$$

$$\frac{h_c}{R'x} = 3.11\,\overline{U}^{0.69}\overline{G}^{0.56}\overline{W}^{-0.1} \quad (18)$$

This work was further developed by Hamrock and Dowson[64 65 66 67]who produced the most commonly used equations for point and elliptical contacts;

$$\frac{h_0}{R'x} = 3.63\,\overline{U}^{0.68}\overline{G}^{0.49}\overline{W}^{-0.073}\left(1 - \mathrm{e}^{-0.70\left(\frac{R'y}{R'x}\right)^{0.64}}\right) (19)$$

$$\frac{h_0}{R'x} = 3.63\,\overline{U}^{0.67}\overline{G}^{0.53}\overline{W}^{-0.067}\left(1 - 0.61\mathrm{e}^{-0.75\left(\frac{R'y}{R'x}\right)^{0.64}}\right) (20)$$

Finally, Chittenden[68 69] proposed a new formula for film thickness calculation, taking into account the effect of entrainment speed direction in an elliptical contact;

$$\frac{h_0}{R'x} = 3.00\,\overline{U}^{0.68}\overline{G}^{0.49}\overline{W}^{-0.073}\left(1 - \mathrm{e}^{-0.96\left(\frac{R'y}{R'x}\right)}\right) (21)$$

$$\frac{h_c}{R'x} = 3.06\,\overline{U}^{0.68}\overline{G}^{0.49}\overline{W}^{-0.073}\left(1 - \mathrm{e}^{-3.36\left(\frac{R'y}{R'x}\right)}\right) (22)$$

For $R'x \geq R'y$

$$\frac{h_0}{R'x} = 3.63\,\overline{U}^{0.68}\overline{G}^{0.49}\overline{W}^{-0.073}\left(1 - \mathrm{e}^{-0.67\left(\frac{R'y}{R'x}\right)^{\frac{2}{3}}}\right) (23)$$

$$\frac{h_c}{R'x} = 4.30\,\overline{U}^{0.68}\overline{G}^{0.49}\overline{W}^{-0.073}\left(1 - \mathrm{e}^{-1.30\left(\frac{R'y}{R'x}\right)^{\frac{2}{3}}}\right) (24)$$

For $R'x \leq R'y$

In the above equations there are two values to predict film thickness, $h_0$ and $h_c$, the first referring to the minimum film thickness while the second refers to the central film thickness. This is because in actual EHL contacts, the film does not have a constant thickness across the area of the contact, i.e. the contact is not completely conformal. The thickness of the film varies in the contact and can generally be divided into an area where it is relatively constant and a constriction area which has the shape of a horseshoe where the film thickness is lower; the central film thickness is commonly considered to be relevant to EHL traction while the minimum film thickness determines the amount of metal-to-metal contact and hence the

potential for damage accumulation. In addition, the above formulae are only applicable where the contact operates in EHL regime where both the piezoviscous and the elastic effect occur simultaneously.

In reality, a contact might operate in four different regimes depending on the occurrence of each of these effects namely the rigid-isoviscous, the rigid piezoviscous, the elastic-isoviscous (soft EHL) and the elastic-piezoviscous (EHL).

Therefore, the regime must first be identified and the appropriate regression equations must be employed to evaluate the point or line contact[70] [71]. Images of a point and a line contact operating in EHL regime obtained using a technique called optical interferometry can be seen in Figure 2.9[72]. This technique employs the use of a light source and a transparent solid coated with a semi-reflective coating to produce images of the EHL contact in operation usually between a sapphire disc and a steel ball[73].

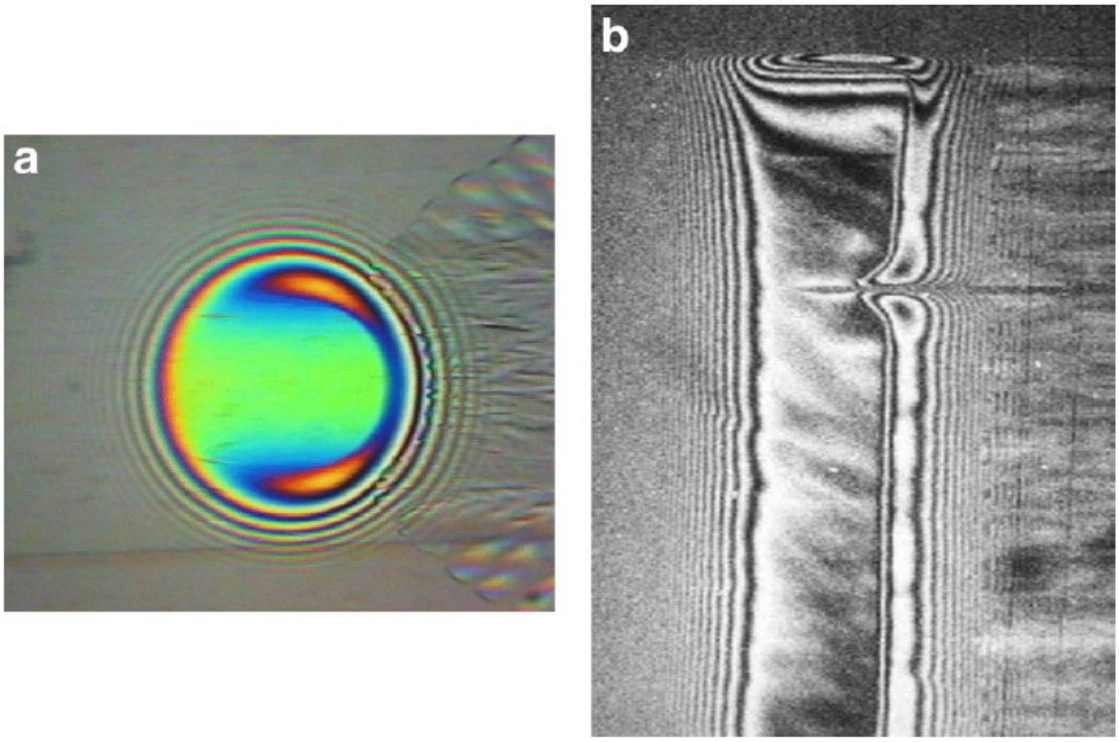



**Figure 2.9: An interferometry image of an EHL point contact (a) and an EHL line contact (b)[72]**

When the thickness of the lubricant film that separates the two surfaces becomes very low then surface asperities start to interact. Under these conditions, the load is only partially carried by the lubricant film with the asperities carrying the reminder through solid-to-solid contact. This

lubrication region is called mixed lubrication. When the pressure becomes so high that the lubricant cannot separate the two surfaces anymore and it practically gets trapped between the contact asperities then the asperities carry all the load; this region is called boundary lubrication. These two regimes are very important because they are commonly encountered in highly loaded components such as gears, cams and tappets but also in heated, misaligned or otherwise poorly setup components which would otherwise be expected to operate in full film conditions. Many damage mechanisms like seizure and wear originate in these regions and therefore understanding their operating principle is crucial for reliability and durability.

The concept of mixed and boundary lubrication regimes was largely based on the work of Stribeck[74] which dates back to the nineteenth century. This work resulted in one the most widely used tools to describe the regime in which the contact operates in terms of film thickness and friction coefficient, the Stribeck curve. This curve shows the variation of friction with a combined parameter of viscosity, load and speed demonstrating how the friction coefficient changes from a very high value when the lubricant film is non-existent (boundary) to a lower value obtained in fully separated contacts operating in EHL or HD. The transitional area between boundary and EHL is not clearly defined and it is a representation of the mixed lubrication regime. A typical Stribeck curve explaining the different regimes is shown in Figure 2.10[43].

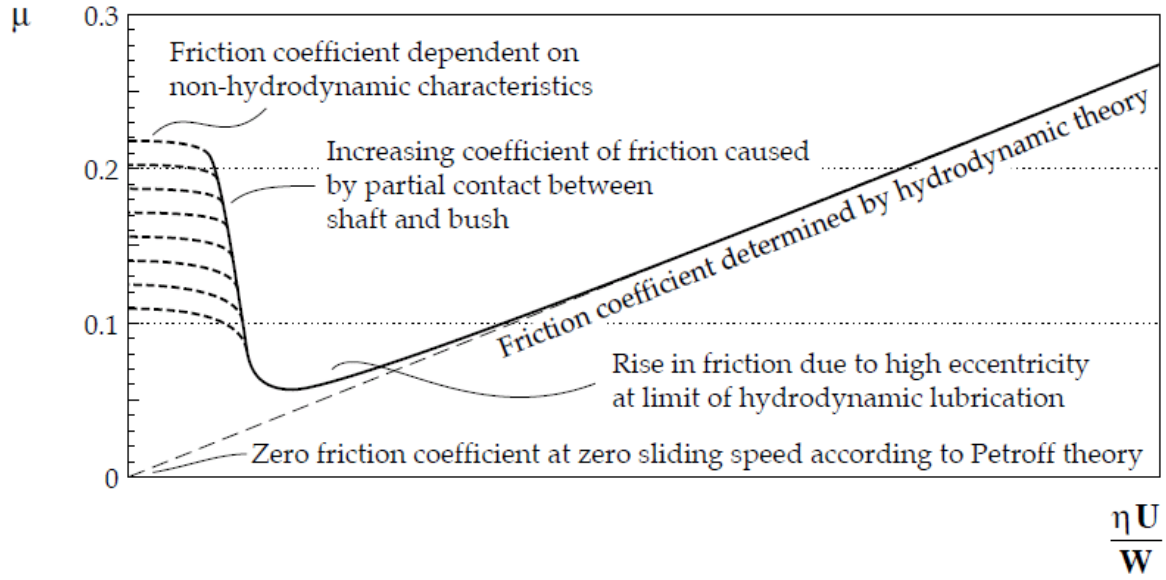



**Figure 2.10: A typical Stribeck curve and the lubrication regions[43].**

As mentioned earlier in this chapter, the critical balance that must be achieved for optimal efficiency without sacrificing durability and reducing operational life is related to the film thickness. A value that is very low can cause the component to operate in boundary and mixed lubrication regimes, with resulting increase in surface damage. On the other hand if the film is excessively thick then the friction will rise as a result of the lubricant's resistance to shear. A parameter that is commonly associated to the Stribeck curve and is used as a rough indicator of the operating regime is the lambda ratio;

$$\lambda = \frac{h_0}{R_{qc}} (25)$$

Where

$$R_{qc} = \sqrt{R_{q1}^2 + R_{q2}^2} (26)$$

And $R_{q1}$ $R_{q2}$ is the RMS roughness of surface 1 and surface 2 respectively. Generally, when the component operates at a lambda ratio significantly above 1 (usually between 2 and 4) a satisfactory life is to be expected[75]. On the other hand when the component operates for an extensive period of time at lambda ratios below 1 the operational life can be expected to reduce[76].

## 2.4 Losses in transmission systems

### 2.4.1 Gear EHL losses

When a gearbox is in operation, the power losses, usually in the form of heat can originate from gears, bearings and seals, as well as auxiliary components[14]. Regarding gear and bearing losses, they can be separated in no load losses, which are present regardless of a load being applied, and load-dependent losses whose magnitude depends on the applied load. The no-load losses depend mainly on lubricant parameters such as density and viscosity whereas the load losses depend on the load, the sliding velocity and the friction coefficient. A breakdown of these losses is shown in Figure 2.11; the efficiency of a gearbox is highly dependent both on the magnitude and the relative proportion of these losses.

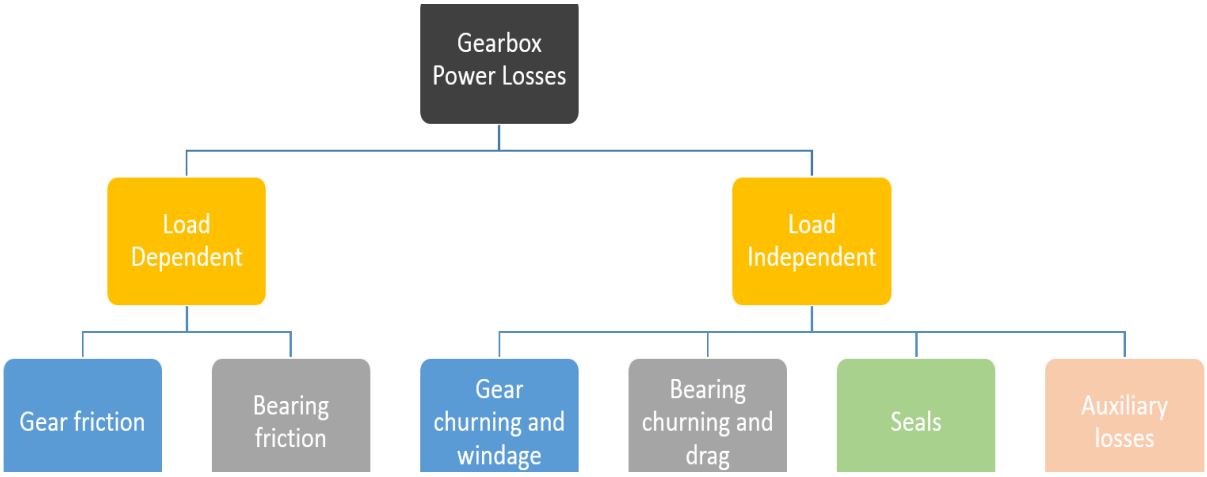



**Figure 2.11: Losses in a typical gearbox**

The source of gear EHL losses is the friction generated in the path of contact formed between the mating surfaces of the gear teeth. This loss depends on the value of the friction coefficient, the normal load applied to the contact and the sliding velocity. There are numerous published theoretical models to evaluate the friction-based mechanical efficiency both for spur and helical gears with the main difference owing to the way the friction coefficient is evaluated. A group of models[77 78 79 80] use an average value for the friction coefficient, μ, which is constant along the path of contact while other models[81 82 83 84 85 86] differ in terms of allowing the friction coefficient to vary at each point of the contact path. These models have commonly used the results obtained from a two disc machine, originally developed by Merritt[87], to offer a simplified approach to model a gear teeth contact, to form empirical formulae. Some of the most widely used empirical formulae for traction prediction have been developed based on a similar two disc machine concept such as those from Benedict and Kelley[88] and Cameron and O'Donoghue[89]. Finally, models have been developed[90 91 92 93 94 95] which negate the use of empirical equations and are based on physics to calculate the coefficient of friction.

In order to extract representative and accurate Elastohydrodynamic traction predictions, one must consider two main factors. The first is the extremely complex rheological behaviour of the lubricant under the severe conditions that are encountered in a typical EHD contact. Rheological equations have been developed to account for this complex in-contact behaviour such as the Maxwell-limiting-shear-stress model which will be used in this study. The second effect that must be taken into account is the strong coupling between temperature and traction which is encountered in all EHD systems which mix rolling and sliding. In a gear contact, the

slide to roll ratio varies drastically along the contact path and its effect on traction prediction must be taken into account accordingly.

The friction coefficient affects the temperature of the lubricant inside the contact and the amount of heat generated within the contact. The amount of heat generated in the contact will directly affect the temperature of the surrounding bodies and, in turn, heat up the lubricant that will be fed back into the contact and change the EHD film thickness. In conjunction with the lubricant rheology which will be different at the elevated temperature, the lambda ratio will be affected and consequently the friction until the system reaches thermal equilibrium. In addition, the temperature of the lubricant at the inlet will also be determined by the temperature of the bodies. In turn, temperature strongly affects the rheological properties of the lubricant and therefore the friction coefficient.

Therefore, the combination of lubricant parameters, surface roughness, film thickness and thermal effects must be taken into account and the interaction between them should be continuously evaluated using an iterative process as they are strongly coupled. Most existing models fail to account for one or more of the above. Furthermore, the friction coefficient in gear teeth contacts should be calculated along the contact path and average values or empirical models should be avoided. As the friction varies drastically along the contact path, models based on empirical equations are limited to a specific range of conditions and cannot account, for example, for the low slide roll ratios which are observed close to the pitch point. Moreover, experimentally derived models fail to account for the thermal coupling, the specific lubricant rheology and the different surface characteristics. As a result, they fail to be flexible when the setup, the lubricant or the geometry change. The latter is very important as friction behaviour is drastically different depending on surface texture and roughness.

Ideally, the friction coefficient should be calculated using an iterative approach that simultaneously takes into account all of the aforementioned transient effects in the most accurate way possible while at the same time making some necessary simplifications to avoid excessive computational demand. Surface roughness is crucial and should also be taken into account in the calculations especially so because gears tend to operate in the mixed and boundary lubrication regime. Olver and Spikes[96] have published a comprehensive model based on Eyring theory to predict the friction and temperatures in an EHL contact which can be readily modified and adapted for gear applications, as is done later in this thesis. Their model uses the approach developed by Johnson and co-workers[97 98 99] to predict traction and combines

this with an analysis of the heat transfer between the contact and the surroundings to predict the temperature rise within the EHL film. The film thickness is calculated using the EHL regression equations and the variation of lubricant parameters with pressure and temperature is taken into account through measured data[100].

In the model, the operating regime of the contact is determined through the use of several non-dimensional parameters as described previously and then the mean shear stress in the contact can be evaluated using a suitable equation. Once the mean shear stress is known, the fluid friction coefficient can be evaluated as the value of the mean shear stress over the value of the mean contact pressure;

$$\mu = \frac{\bar{\tau}}{\bar{p}} \quad (27)$$

The strain rate can then be calculated as the sliding velocity of the contact over the film thickness obtained through regression equations;

$$\dot{\gamma} = \frac{U_s}{h_c} \quad (28)$$

The approach by Johnson includes the assumption of a limiting shear stress which is a maximum value that the shear stress carried by the lubricant cannot exceed. Therefore the shear stress is capped at this limiting value when the calculated value is higher. When the fluid friction coefficient is calculated, it can be modified to incorporate the surface roughness. The temperature rise in the surface of the contacting solids, at the inlet and in the centre of the EHL contact can then be calculated and the film thickness and shear stress can be re-evaluated using the new temperatures until convergence is achieved and a final value of the friction coefficient is calculated.

Finally the gear power loss can be evaluated as;

$$P_{loss} = \mu_{eff} W U_s \quad (29)$$

Where $\mu_{eff}$ is the effective friction coefficient incorporating the surface roughness, $W$ is the total normal load and $U_s$ is the sliding speed. This approach will be presented in detail in the next chapter.

### 2.4.2 Churning losses

When a component is rotating inside a fluid, churning loss is equal to the energy required to overcome the inertial and shear resistance of the fluid and subsequently displace it so the component can move. Churning is mostly dependent on the fluid properties, viscosity being the most crucial; a high viscosity fluid will resist movement more than a lower viscosity fluid. In the case of gearboxes, the immersion depth of the gears will strongly affect churning losses as it determines the quantity of the lubricant that must be moved in order for the gear to rotate. The drag torque of discs rotating in a fluid has been the subject of several studies[101 102 103]. Gears however exhibit a different behaviour compared to discs due to the difference in geometry and thermal response. Gear churning has been experimentally investigated in studies by Terekhov[104], Boness[105] and Lauster and Boos[106] taking into account the lubricant rheology, the rotational speed of the gears as well as the gear geometry and the immersion depth. Boness's experimental study included gear and discs submerged in oil and water and resulted in a formula which includes a fit of a non-dimensional churning torque;

$$C_{ch} = \frac{\rho}{2}\Omega^2 S_m R_p^3 C_m \quad (30)$$

Where $C_{ch}$ is the dimensionless churning torque, $\rho$ is the lubricant density, $\Omega$ is the rotational speed of the gear, $S_m$ is the immersed surface area of the pinion, $R_p$ is the pitch radius of the gear and $C_m$ is the dimensionless drag torque which depends on the Reynolds number. The proposed equation results in the drag torque increasing when a lower viscosity fluid is used, an observation not in agreement with available experimental data.

Terekhov expanded on this work by changing the definition of the churning torque to include the effect of the oil immersion depth, the gear geometry and the Froude (Fr) and Reynolds (Re) numbers correlating their use to the experimental results;

$$C_{ch} = \rho\Omega^2 R_p^4 b C_m \quad (31)$$

With

$$C_m = \psi_1 \left(\frac{h}{R_o}\right)^{\psi_2} \left(\frac{V_i}{v_m}\right)^{\psi_3} \left(\frac{V_g}{v_m}\right)^{\psi_4} \left(\frac{b}{R_o}\right)^{\psi_5} Re^{\psi_6} Fr^{\psi_7} \quad (32)$$

Where $h$ is the immersion depth, $V_i$ and $V_g$ is the volume of the gear and the oil respectively, $R_o$ is the tip diameter of the gear and b is the face width of the gear.

Another formula for the calculation of churning losses has been suggested by Hohn[107] while Olver[108] observed a reduced effect of viscosity when the rotational speeds are high by comparing existing empirical models with new experimental data, obtained using a purpose-built churning rig to test single and meshed gears immersed in various liquids. The study observed large discrepancies between Boness's and Terekhov's empirical models and the measured churning loss while it concluded that simply correlating the churning torque to a viscosity based Reynolds number may be flawed. This assumption was recently validated by Kolekar et al, who pointed out that the churning loss is controlled by the balance of inertial and gravitational forces[109].

Recent experimental studies by Changenet and Velex[110 111] also confirmed the aforementioned assumptions and further improved the churning torque calculations by introducing several additional parameters and producing more accurate equations for the prediction of churning losses. While the basic structure of Boness's equation remains, many parameters that led to the latter having discrepancies compared to experiments have been adjusted. Their method uses a critical Reynolds number to differentiate between a low-medium speed regime and a high speed regime, with viscous effects included in the Reynolds number at low speeds giving way to inertia effects at higher speeds. This two-regime method gives much improved predictions compared to older models. Their model includes the sense of rotation of the gears, as it has been proven to significantly affect churning loss through the creation of a "swell effect" where the larger gear changes the effective immersion depth of the pinion or vice versa. In addition, they expanded on the core churning model by studying the effects of enclosure and deflectors on the losses.

The model by Changenet and Velex[110] was implemented to predict the churning results included in this thesis as it provides the most robust way of calculating losses, taking into account not only the lubricant and material properties but also the arrangement of the gears and the kinematics. Furthermore, it has been validated by experiments. A detailed description of the model, including a direct comparison and validation of the implementation employed in the present study, will be given in the next chapter.

### 2.4.3 Bearing and seal losses

Load independent losses in bearings depend on the geometry of the bearing, the way the bearings are arranged as well as the lubricant properties, mainly viscosity. Cylindrical roller

bearings usually have low churning losses as do tapered roller bearings however for the latter, the pre-load applied to the bearings can significantly increase the load-independent losses[112].

Bearings losses that are load dependent, largely follow the same mechanism as gear losses. Therefore, they also depend on the bearing geometry and size as well as the magnitude of the load and the amount of sliding in the bearing elements. Figure 2.12 shows the losses in different types of bearings and highlights the dependency of losses on the geometry.

The arrangement, pre-loading and temperature strongly influence the bearing frictional losses, with the elevated temperature significantly reducing the lubricant viscosity and therefore leading to reduced losses, provided that no increase of solid-to-solid contact occurs. Experimental studies conducted on a manual 6 speed gearbox have shown that alternative bearing arrangements (i.e. cross-locating tapered roller bearings vs. locating contact ball bearings and non-locating cylindrical roller bearings) and designs can lead to a reduction of losses of 50% at 40 $^0$C and that the reduction persists at 90 $^0$C, being 20%[113].

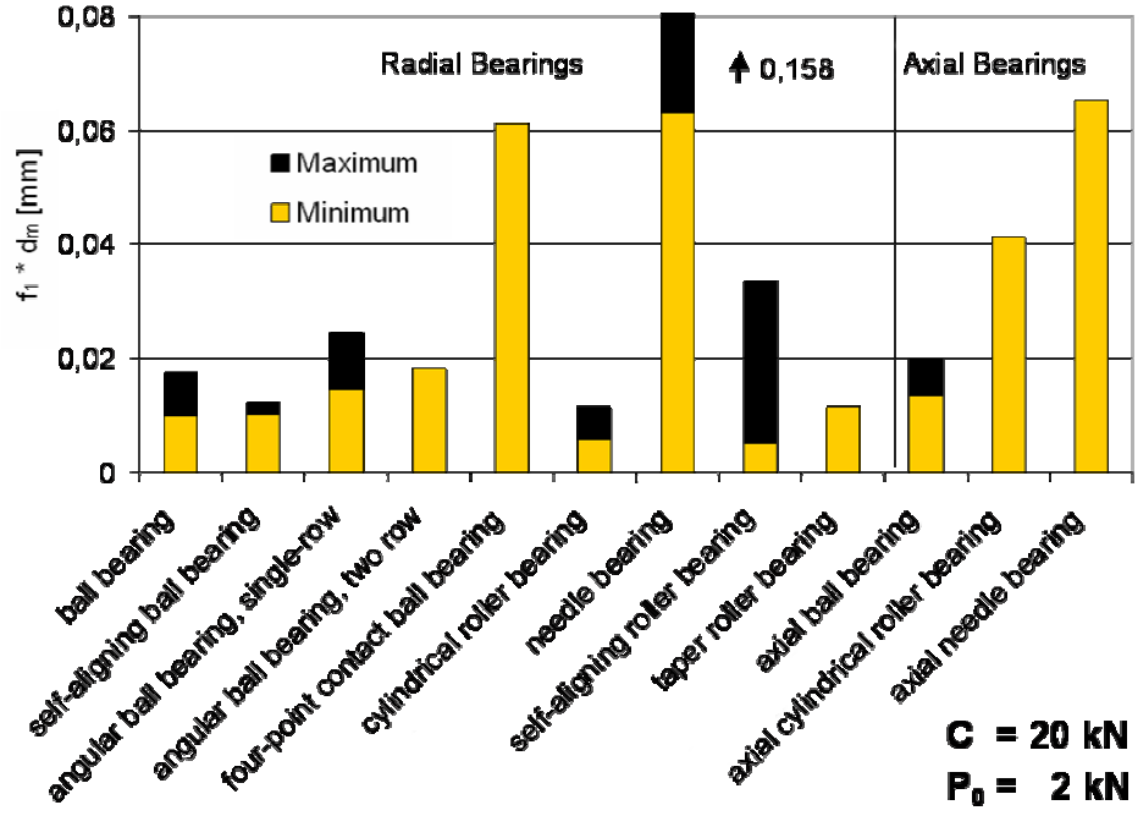



**Figure 2.12: Bearing losses for different bearing designs (Adapted from [14])**

Some studies have used empirical formulae to calculate the load dependent bearing friction torque. One example can be found in Khonsari et al[114] however there is a general lack of recent

bearing friction models in literature and a full treatment of historical models is beyond the scope of this thesis. A comprehensive model for the prediction of bearing losses has been developed by Morales-Espejel[115]. This model is unique in the sense that it separates the physical sources of friction in a rolling bearing and individually accounts for each one before adding them together to predict the overall frictional moment. The model takes into account all the losses present in a rolling bearing, namely rolling friction, sliding friction, and drag. This model is referred to as the "Four Sources Model"[116]. The model is experimentally validated and widely accepted in the bearing industry. For this reason, it will be used in the current study for bearing and seal loss prediction.

The equation to predict the total frictional moment in the bearing is given as;

$$M = \varphi_{ish}\varphi_{rs}M_{rr} + M_{sl} + M_{seal} + M_{drag} \quad (33)$$

Where $\varphi_{ish}$ is the rolling friction factor, $\varphi_{rs}$ is the multiplication factor, $M_{rr}$ is the total rolling frictional moment, $M_{sl}$ is the total sliding frictional moment, $M_{seal}$ is the frictional moment of the seals and $M_{drag}$ is the frictional moment due to lubricant drag. The model is able to accurately reproduce Stribeck curves as the rotational speed increases, showing the transition from high friction at low speeds to lower friction due to film build up at higher speeds, and the reduction of film thickness due to starvation and shear heating at the contact inlet. The four different sources of loss in a bearing according to the model are shown in Figure 2.13 (not including seals). A more detailed description, including an explanation of the frictional moment components and a validation of the current implementation will be given in the next chapter.

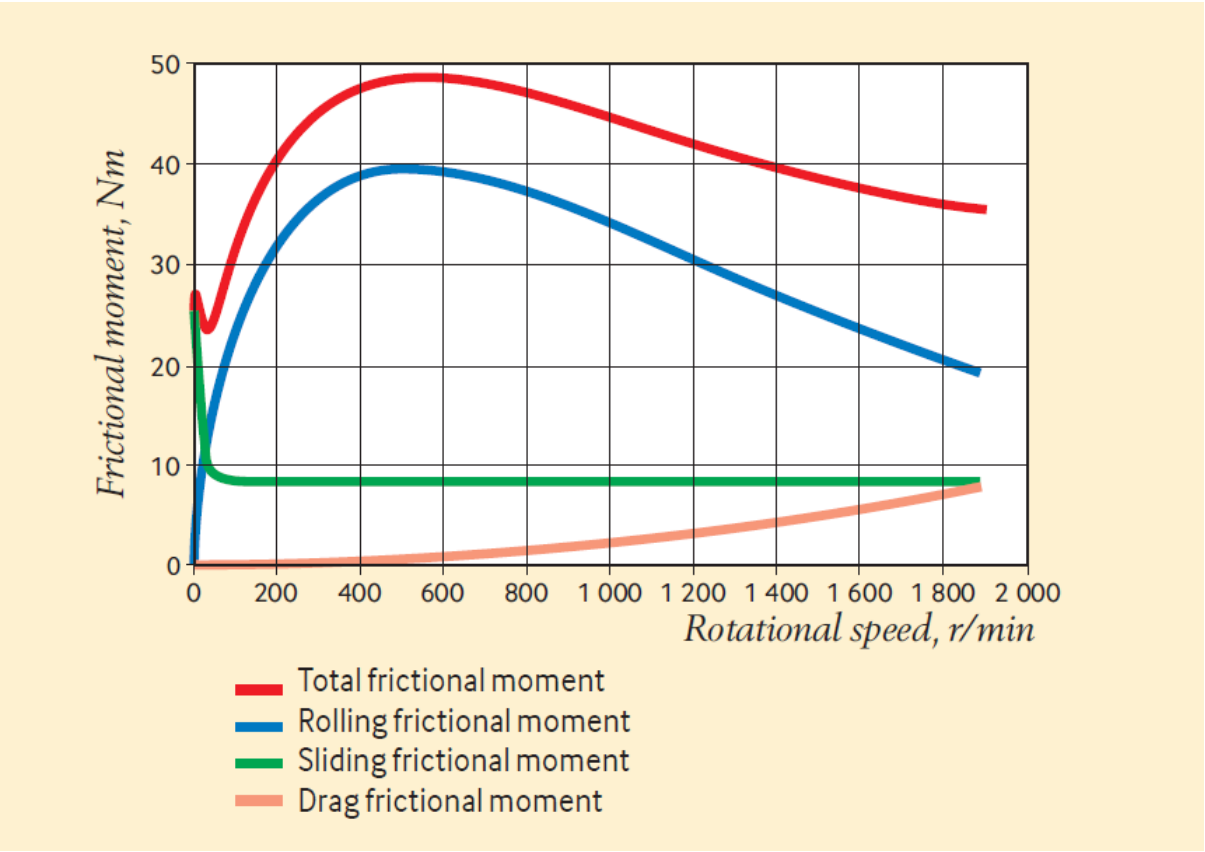



**Figure 2.13: The components of the total frictional moment shown for an open spherical roller bearing operating in a high viscosity oil bath[115]**

### 2.4.4 Other losses

Other losses that are commonly encountered in transmission systems include windage and pumping or pocketing losses as well as losses stemming from the use of auxiliary systems such as pumps and circulation systems.

Windage losses arise from the resistance that the air poses to the movement of the gears and as such the loss mechanism is similar to churning losses. These losses have been investigated by several authors such as Loewenthal and Anderson[117 118] whose work points out that the contribution of windage losses to the overall loss is relatively small but they can become important in very high speed applications. The same authors have published an equation for the prediction of windage losses in a gear pair which shows that gear geometry ($R_i$, $b_i$) and rotational speed ($N_i$) as well as the air viscosity ($\mu_i$) are the main parameters to influence windage losses;

$$P_{windage} = C_1(1 + 2.3\left(\frac{b_i}{R_i}\right)N_i^{2.8}R_i^{4.6}(0.028\mu_i + C_2)^{0.2} \quad (34)$$

Another study conducted by Dawson[119] showed that windage in spur and helical gears is mostly affected by geometry and it includes a formula based on result fitting;

$$P_{windage} = N^{2.9}(0.16D^{3.9} + D^{2.9}F^{0.75}M^{1.15})10 - 20\varphi\lambda \quad (35)$$

Where $F$ is the face width, $M$ is the module, $D$ is the root diameter of the gear, $\varphi$ is a parameter and $\lambda$ is a constant.

Diab, Changenet and Velex[120] also studied windage losses in spur gears and their results show good correlation with experiments. Generally, although windage losses have been extensively studied, their overall contribution in practical gear applications is low.

### 2.4.5 Lubricant selection in transmission systems

The selection of lubricant is a crucial factor for reliable operation of a gearing application. However, its significance on efficient operation commonly does not receive sufficient attention, partly due to the lack of available understanding – this is one of the more important factors which this thesis attempts to address. The selection of lubricant additives is also very important and they should be used only when they are necessary. Usually, the procedure to test a lubricant involves load carrying tests to evaluate failure mechanisms such as scuffing and scoring. Some of the most commonly used tests are disc tests[121], gear tests[122 123], the test using a four-ball setup[124] and the Timken test[125]. Lubricant thermal response has been studied by Olver[126], who used a disc machine to point out that the response is strongly influenced by the skin temperature of the component, something that is expected to be the case when additives are operating. It is also important that the skin temperature is calculated or measured at all points of the regime where the component operates, therefore the chosen method should cover the expected operating temperature range.

Despite the significance of the specific lubricant rheology, there are not many studies to account for the effect of different lubricants on the predicted efficiency and the ability to pinpoint differences between lubricants in terms of fuel economy is currently limited. Petry Johnson et al. [127] have tested multiple lubricants in order to study this effect with their results showing that the overall efficiency is indeed affected by the lubricant type and the difference between lubricants can be very pronounced. Moreover, the automotive axle efficiency study of Kolekar et al[128] has showed that the ranking order of lubricants can change according to the specified duty cycle with high viscosity friction modified oils being more efficient in severe

conditions and lower viscosity oils being better for city driving or low duty driving conditions for axle applications considered.

In this study, an attempt to experimentally characterise the lubricants will be made by means of ball on disc tests. This will allow for a more accurate modelling of the lubricant's properties under varying temperature and pressure conditions. Extracting specific coefficients and parameters directly from high contact pressure friction tests is an indirect way to measure the properties that cannot be measured normally. A wide range of contact pressures and temperatures will be used to create a database of lubricant rheological properties that can then be incorporated in any gear efficiency study to improve the accuracy of the predictions. As there are no published studies that include lubricant rheology in this detailed way, this is expected to improve the current understanding of trends and the behaviour of the lubricant under variable duty cycles. Ultimately the aim of this work is to develop a method not only for accurate efficiency and temperature predictions in a gearbox but also aid in the formulation of bespoke, application-specific lubricants.

### 2.4.6 Gearbox efficiency

The subject of gear-related efficiency has received increasing attention since the 1980's with field pioneers Anderson and co-authors[129 130]. They calculated efficiency of simple spur gears and incorporated bearing and churning losses. Their predictions generally showed good agreement with experimental results from spur gear test rigs however the range of conditions was relatively limited as the experimental data available at the time was not very accurate at part load. The studies used empirical formulae for the calculation of friction and the prediction of bearing loss which have much improved since and there was no provision to predict in-contact temperatures, which had to be estimated from the experimental oil supply temperature. Nevertheless, these studies were of significant importance, as they approached the efficiency problem in an integrated way taking into account auxiliary losses and also studying the breakdown of different losses within the system.

Interest in gear efficiency has become even more significant in recent years aided by more stringent regulations and the need to prevent environmental damage. The experimental study of Petry Johnson and co-authors[127] involved an integrated multi-loss approach studying multiple lubricants. They used a jet lubricated FZG-type back to back test rig and studied the breakdown of losses under full load, part load and no load using three different lubricants at a

constant temperature. They also accounted for different values of surface roughness (chemically polished and ground gears) and different teeth number. Their results showed that gear efficiency remains relatively constant when the speed and torque increases, that the normal module and the surface roughness significantly affect gear power loss and that lubricant viscosity is the most influential factor for churning losses. Finally, they stressed the importance of lubricant selection at the design stage in order to maximise efficiency. Many of the findings from this study are compared to their results and the modelled gear pair in chapter 6 has the same geometry as the 23T gear pair that was used in that study. One drawback is that all the tests were performed under steady state temperature conditions and subsequently fail to account for temperature variation. Also, in a dip lubricated gearbox, the loss distribution could be different compared to the jet lubricated FZG test rig.

Li & Kahraman[131] and more recently Chang & Jeng[132] focused on a single spur gear pair. In the first case, the focus was on gear load-dependent losses and the study also included transient effects. The predictions were compared to experimental results from Petry Johnson et al[127] and they were in good agreement. The second study uses Eyring's equation to connect shear stress and shear rate and also uses the well-established Barus equation to describe the viscosity variation inside the EHL contact. It goes on to study the effects of gear geometry and lubricant properties on the efficiency of the gear and compares results to Petry Johnson's study with good accuracy.

Michaelis et al.[14] also published a comprehensive study involving an FZG type gearbox and including additional losses due to churning as well as bearings and seals while more authors[133] [134] have also considered applications to industrial gearboxes in their models. As mentioned previously, all the methods and techniques for gear modelling and efficiency predictions do not apply only on automotive gearboxes but practically on any geared transmission including industrial and other heavy duty applications. In Michaelis' study the focus was on optimising gearbox efficiency using high loss wind turbine gearboxes as an example of potential energy savings through the use of low viscosity oils (for no-load losses), more efficient bearing arrangements as well as low-loss gears (short-teethed wider helical gears) for reducing load dependent losses.

In addition to gear friction, no-load losses, mostly due to churning of the lubricant, are of particular importance for the efficiency of dip lubricated components. Since the use of dip lubrication is very common in all kinds of gearboxes, the accurate prediction of these losses is

crucial for gearbox efficiency. As mentioned earlier, authors such as Changenet & Velex[110 111] extensively studied the role of this type of losses and pursued the most accurate way of modelling their complex nature taking into account the specific geometry of components as well as the design of the casing and deflectors. Their study also focuses on the significant added loss in a system where the gears rotate anti-clockwise (i.e. the oil is being splashed upwards) and new empirical formulae are proposed which incorporate the sense of rotation.

In the quest of augmented efficiency, the thermal behaviour of components is key. Several flows are created by the various heat sources acting simultaneously inside an operating gearbox which are particularly challenging to study using analytical equations mainly because of the complex component geometry. Authors like Long & Lord[135] and Taburdagitan[136] used a finite element approach to model spur gear pairs and predict surface temperatures under specific conditions. These studies produce mixed results as sometimes they overpredict surface temperatures, unless the boundary conditions are experimentally derived, while generally they fail to accurately account for the coefficient of friction, using average values instead.

Another way to include thermal effects and get close to a coupled efficiency model is through the use of thermal networks. Changenet and Velex[137] modelled a six speed gearbox using a thermal network approach which included the use of interconnected lump thermal elements and was based on analytical equations. This is the only efficiency study which relies on existing models to simulate a six speed gearbox and includes comparisons to experimentally derived results using a bench test of an automotive gearbox. It considers gear friction as well as bearings and churning. The results are in good agreement with the measured data for that gearbox when a combination of bulk temperature predictions and power loss calculations is considered. Nevertheless, the model is steady state and uses a least accurate prediction for the coefficient of friction and fails to account for the specific lubricant rheology. Moreover, a moving vehicle would be exposed to additional heat loss to the environment which is important for temperature and therefore efficiency predictions and there is no comparison between lubricants.

All of the aforementioned studies have produced useful results for gear efficiency predictions however, there is no published study to date that goes beyond describing the lubricants using the basic variables such as viscosity, density and thermal conductivity at atmospheric pressure. There is no doubt that viscosity is indeed very influential for power losses and there is a lot of research aimed towards accurately describing the way viscosity and the other lubricant properties vary inside the EHL contact. Further lubricant testing is needed in that direction as

two lubricants with different formulation but similar viscosity ratings could behave very differently under high contact pressures, as will be proven in this thesis.

Another important consideration is that FZG test rigs are not fully representative of a multi stage gearbox. The losses breakdown can be significantly different depending on the application and the conditions. There is usually a very broad range of conditions that a gearbox operates in and a good model should be able to readily adapt to these conditions - it is much easier to change input conditions in a simulator than building a test rig. Most studies fail to make provision for transient conditions and focus on steady state predictions instead. However, pseudo-steady state conditions are not commonly encountered in practice, especially in automotive applications where a car or heavy goods vehicle (HGV) is subjected to a highly transient drive cycle.

Finally, it has to be noted that there are two degrees of thermal coupling that must be taken into account when considering a real life gearbox. The first is the coupling between the EHL contact, bulk and inlet temperatures, friction coefficient and lambda ratio, and the second is the coupling of the components to the environment. There is currently a need for a comprehensive method to accurately predict in-contact traction and power loss at every point of the gear contact path, using experimentally characterised lubricant rheology. The method should take into account the additional loss sources using the most up to date models and predict losses for an entire gearbox under different duty cycles. Most importantly, it should be applicable to any geared application and the predicted values should compare well to experiments, preferably to a real life application where there are many additional and unpredictable parameters to take into account. In this thesis, an attempt will be made to develop a model that can be easily adapted and used by manufacturers for testing purposes in the design phase of a component.

# 3. METHODOLOGY FOR THE PREDICTION OF POWER LOSSES IN A GEARBOX

## 3.1 Introduction

In this section, the modelling methodology to predict friction losses in EHL contacts between gear teeth contacts, including the adopted approach for prediction of tooth flank and contact temperatures, will be presented. This core model will later be incorporated in the overall efficiency model for an automotive gearbox. First the individual parts of the model are described and then the overall model algorithm for gear teeth contacts is presented. Each module, namely the EHL friction model, the churning and the bearing model will be validated against published experimental and analytical predictions. These separate modules will then be coupled and the complete model will be used to simulate a single stage spur gearbox and a six speed commercial automotive gearbox, the results of which are presented in chapters 5 and 6 respectively.

## 3.2 EHL loss prediction

### 3.2.1 General approach

Perhaps the most important consideration for accurate EHL traction prediction is the thermal coupling within and around the contact. As mentioned above, empirical models for EHL prediction such as the Benedict and Kelley model[88], might give a satisfactory prediction for quick calculations however they fail to capture the complicated coupling of the temperatures inside and outside the EHL contact. A typical EHL contact between two rotating non-conformal bodies is shown in Figure 3.1.

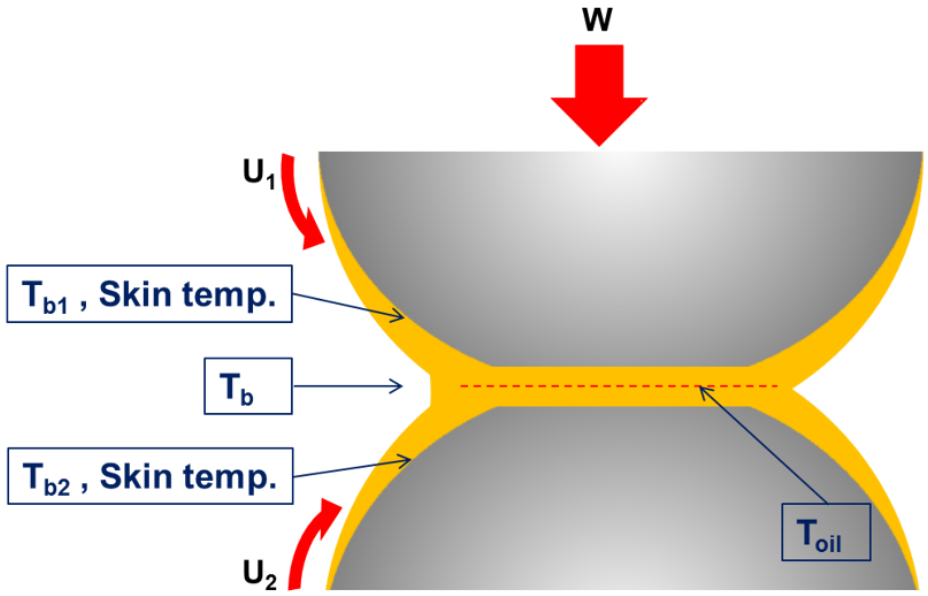



**Figure 3.1: The temperatures in the EHL contact**

There are two temperatures that are crucial in the calculations; the first is the temperature of the film (Toil), which affects traction; all the lubricant properties used to calculate traction have to be evaluated at that temperature. However, the thickness of the lubricant film depends on the viscosity at the inlet which in turn is strongly dependant on the inlet temperature. The assumption here is that the temperature of the lubricant immediately before it enters the contact is determined by the temperature at the surface of the two bodies (Tb1, Tb2). Since the bodies have higher temperature than the surroundings, a weighted average of the two temperatures (Tb) is used to define the inlet temperature. This will be detailed in the next section.

Inside the EHL contact, heat is generated because of the rubbing of asperities and also because of shearing of the lubricant film, as the two bodies move through the contact. This heat will be conducted through the lubricant film and the two bodies and will therefore affect their surface temperature. In order to calculate the amount of heat entering each body, the use of a heat partition is necessary because the two bodies will not always have the same surface temperatures as the two bodies can have different geometry (in the case of gears, they are usually of different size). Finally, the mean film temperature which ultimately defines traction can be estimated by adding the temperature rise due to asperity contact and shear heating (shear is assumed along the central plane) to the bulk temperature, Tb.

In the case of a gear contact, where the radii of curvature of the contacting bodies change continuously along the contact path, it is necessary to perform these coupled calculations at every point along the contact path hence an iterative scheme has to be employed to account for this transient behaviour. Furthermore, any prediction of the friction coefficient needs to take into account the surface roughness since gears operate mostly in the mixed lubrication regime.

In this study, an iterative numerical calculation scheme to account for the transient variation of contact conditions will be developed, based on the methodology of Olver and Spikes[96], which will be expanded and adapted to calculate traction in gear contacts. Gear surface roughness will be incorporated in the scheme through the use of an effective friction coefficient. Once the friction coefficient in the contact path is known, the instantaneous power loss and therefore the efficiency of the pair can be found. Finally, existing models will be used to account for churning and bearing losses. All of the core models used will be validated against published results.

### 3.2.2 EHL film thickness and traction prediction

The model used to calculate friction and predict temperatures within the EHL contact adopts the approach of Olver and Spikes[96] for predicting contact temperatures in a dip lubricated disc pair. The EHL regression equations developed by Chittenden[68] [69], presented earlier, are used to calculate the minimum and central film thickness. For a line contact, where $R'y = 0$, these equations become:

$$\frac{h_0}{R'x} = 3.63\,\overline{U}^{0.68}\overline{G}^{0.49}\overline{W}^{-0.073} \quad (36)$$

$$\frac{h_c}{R'x} = 4.30\,\overline{U}^{0.68}\overline{G}^{0.49}\overline{W}^{-0.073} \quad (37)$$

Where the non-dimensional parameters

$$\overline{U} = \frac{U\eta_0}{E'R'_x} \quad (38)$$

$$\overline{G} = \alpha_0 E' \quad (39)$$

$$\overline{W} = \overline{W_L} = \frac{W}{E'R'_x L} \quad (40)$$

are the speed, load and material parameter respectively.Once the film thickness is calculated, the strain rate can be evaluated using the equation:

$$\dot{\gamma} = \frac{U_s}{h_c} \quad (41)$$

This assumes a constant velocity gradient in the central film area where the film thickness is equal to $h_c$. In the film thickness calculation, the viscosity should be evaluated at the temperature and pressure of the lubricant immediately before it enters the EHL contact (contact inlet). Therefore, the viscosity of the lubricant at 40 $^0$C and 100 $^0$C has been used in conjunction with the ASTM equation to evaluate the viscosity at the temperature of the contact inlet. Initially the actual temperature is not known and therefore the starting temperature of the oil sump is used in the calculation.

To evaluate the friction coefficient in a high pressure EHL contact, the relationship between the strain rate $\dot{\gamma}$ and the shear stress $\tau$, is needed. The most appropriate way of describing this relationship for a lubricant has been a subject of a heated debate recently. There are generally two approaches; the first[138] [139] uses the traction results from tribometers to derive the

rheological properties of the lubricant and the second [140] [141] involves the use of high pressure rheometers to evaluate the behaviour of the lubricant under high stresses and strains. Both methods have limitations but they can both be successfully applied to predict EHL traction as shown by Spikes[7272].

This work adopts the first of the above approaches, using traction coefficients obtained in a ball-on-disc tribometer in combination with the Eyring rheology model, to describe shear stress – shear rate relationship for the chosen lubricants. In the Eyring model[142], the shear rate and shear stress are connected through the equation:

$$\dot{\gamma} = \frac{\tau_0}{\eta} sinh\left(\frac{\tau}{\tau_0}\right) \quad (42)$$

In order to apply this equation, the viscosity must be evaluated at the temperature and pressure inside the EHL contact. To achieve this, the temperature and pressure-corrected Roelands equation is used.

$$\frac{\eta_P}{\eta_\infty} = e^{\left(log_e\left(\frac{\eta_r}{\eta_\infty}\right)\left(1+\frac{p}{p_r}\right)^z\left(\frac{T_r+135}{T+135}\right)^{S_0}\right)} \quad (43)$$

The mean shear stress in the contact is calculated using the Ree-Eyring approach, as adapted by Johnson and co-workers[143] [144] [145] however other methods can also be applied just as well[146]. Evans's[147] assumption that the basic lubricant properties remain constant within the EHL contact is utilised in the model. In order to define the regime where the contact operates, Olver and Spikes[96] use three non-dimensional parameters:

$$S = \frac{\dot{\gamma}\eta_0}{\tau_0} \quad (44)$$

$$D_0 = \frac{\eta_0 U}{2\alpha_0 G_e} \quad (45)$$

$$\tau_c^* = \frac{\tau_c}{\tau_o} \quad (46)$$

Where $S$ is the non-dimensional strain rate, $D_0$ is the Deborah number, $U$ is the entrainment speed, $\alpha_0$ is the Hertzian contact half-width in the entrainment direction, $G_e$ is the effective elastic shear modulus, $\tau_c$ is the limiting (or critical) shear stress and $\tau_o$ is the Eyring stress. After these parameters are calculated then the mean shear stress in the contact can be evaluated with a suitable equation for the identified regime as shown in Figure 3.2;

| Question | Criterion | Mean shear stress formula |
|---|---|---|
| Stage 1 | | |
| Is the response viscoelastic? | i.e. $D_0 > 1$ | |
| Is there shear thinning? | i.e. $S > \sinh 1$ | |
| Stage 2 | | |
| If the response is *not* viscoelastic *and* there is *no* shear thinning, then | | $\bar{\tau}^* = S$ |
| If there is shear thinning *but* the response is *not* viscoelastic, then | | $\bar{\tau}^* = \sinh^{-1} S$ |
| If the response is viscoelastic *but* there is *no* shear thinning, then | | $\bar{\tau}^* = S[1 - D_0(1 - e^{-1/D_0})]$ |
| If the response is viscoelastic *and* there is shear thinning with $\tau^* > 2$, then | | $\tau^* \approx \ln(2S) - \ln(1 + 2\lvert S - \frac{1}{2}\rvert e^{-S^*/(2D_0)})$ (see text) |
| Stage 3 | | |
| Is the plastic limit reached? | i.e. $\bar{\tau}^* > \tau_c^*$ | |
| If so, then discard previous value and put | | $\bar{\tau}^* = \tau_c^*$ |

**Figure 3.2: Determination of lubrication regime for EHL traction prediction in Olver and Spikes model[96]**

When the predicted mean shear stress exceeds the critical value of the limiting shear stress then the value is capped. In this study the operating regime for the gear pair has been almost exclusively in the shear thinning non-viscoelastic regime where the non-dimensional shear stress can be expressed as the reverse hyperbolic sinus of S.

Once the shear stress is known, the fluid friction coefficient $\mu_f$ can be calculated as;

$$\mu_f = \frac{\bar{\tau}}{\bar{p}} \quad (47)$$

The mean pressure in the EHL contact is calculated using the Hertz equation as follows;

$$\bar{p} = \frac{\pi}{4}\sqrt{\frac{FE^*}{\pi L R'_x}} \quad (48)$$

$$E^* = \left(\frac{1-\nu_1^2}{E_1} + \frac{1-\nu_2^2}{E_2}\right)^{-1} \quad (49)$$

$$R'_x = \left(\frac{1}{R_{x1}} + \frac{1}{R_{x2}}\right) \quad (50)$$

Where $F$ is the normal load, $E^*$ is the contact modulus, $L$ is the contact length and $R_x$ is the reduced radius of contact.

Since gears routinely operate in the mixed lubrication regime, surface roughness needs to be taken into account in the friction calculations. This can be achieved by means of the lambda

ratio as described in the previous chapter and a formula has been suggested by Smeeth and Spikes[148] to incorporate surface roughness;

$$\mu = \mu_f + \frac{\mu_b - \mu_f}{(1+\lambda)^m} \quad (51)$$

Where $\mu_f$ is the fluid friction coefficient, $\mu_b$ is the boundary friction coefficient, $\lambda$ is the lambda ratio and m is a coefficient with a value of 2. This way of incorporating the surface roughness represents an interpolation between the full film conditions where the friction coefficient is equal to $\mu_f$ and the boundary regime where the friction coefficient has the value of $\mu_b$. This approach is supported by some recent experimental evidence by Bair et al.[76] and Guegan et al.[149] who pointed out that the lambda ratio is representative of mixed lubrication in rough contacts.

### 3.2.3 EHL contact temperatures

As pointed out above, the EHL traction has to be evaluated using the viscosity, and hence the temperature and pressure, within the EHL contact, whereas the film thickness is determined by the lubricant viscosity, and temperature, at the contact inlet. Therefore, there is a need to predict both the inlet and the contact temperatures. Commonly these two temperatures can be treated individually, but in case of gears there is a strong connection between them as the heat that is generated in the gear teeth contacts, which is dependent on contact temperature and traction, increases the temperature of the rotating gear as a whole, which in turn affects the inlet temperature since this is equal to gear tooth flank temperature. An additional complication occurs due to the two gears potentially rotating at different speeds and hence having different tooth flank temperatures, necessitating the introduction of some means of accounting for this difference when calculating the oil inlet temperature.

The heat flow from the contact to the surroundings can be described as follows; initially, the temperature of the lubricant is equal to the temperature of the oil bath, $T_{sump}$. This is assumed to be constant and equal to the ambient temperature, $T_a$ when just the EHL contact and the gear contact is considered – no coupling to the environment. As a result of contact friction there is a contact flash temperature rise $(\Delta T_f)_{av}$ which for a line contact can be calculated as[96];

$$(\Delta T_f)_{av} = \frac{1.06 a_h \dot{q}}{Ak}\left(\frac{\chi_1 \alpha_0}{U_1}\right)^{1/2} = 1.06 B_1 \alpha_h \dot{q} \quad (52)$$

Where $A$ is the total contact surface area, $k$ is the thermal conductivity of the material, $\dot{q}$ is the total heat generated in the contact due to sliding, $\chi_1$ is the thermal diffusivity of body 1, $\alpha_0$ is the contact half-width, $U_1$ is the speed of body 1 and $a_h$ is the heat partition which is a measure of the proportion of the total generated heat entering body 1;

$$\alpha_h = \frac{1.06B_2 + \frac{h_c}{2k_{oil}A} + M_2}{1.06(B_1 + B_2) + \frac{h_c}{k_{oil}A} + (M_1 + M_2)} \quad (53)$$

Where $B_1$, $B_2$ is the transient thermal resistance of the two surfaces, $M_1$, $M_2$ is the total steady state thermal resistance for bodies 1 and 2 respectively (equation 59), calculated using the thin disc approximation from Olver[126], and $k_{oil}$ is the thermal conductivity of the lubricant. It has to be noted that the flash temperature rise equation is written for body 1 however the result would be the same for body 2 except $1 - \alpha_h$ would have to be used instead.

In nominally dry contacts, the above is sufficient to predict contact temperatures. However, in the case of an EHL contact where the lubricant film has a non-negligible thickness, there will be heat generated through shearing and the heat division happens somewhere within the lubricant film itself. The assumption that the lubricant shears across the centre of the contact has been suggested and experimentally validated[150]. Therefore the temperature rise of the lubricant over that of the contacting surfaces, $(\Delta T_{oil})_{av}$ can be evaluated;

$$(\Delta T_{oil})_{av} = \frac{\mu W U_s h_c}{8Ak_{oil}} = \frac{U_s \bar{\tau} h_c}{8k_{oil}} \quad (54)$$

Where $W$ is the total normal load and $U_s$ is the sliding velocity.

The heat that is generated in the contact is conducted through the solid surfaces. As a result of this phenomenon, the surface temperature of each body will rise and when the surfaces enter the contact again, their elevated temperature will cause an increase of the inlet temperature which will be higher than $T_{sump}$ and equal to the weighted average of each body's skin temperature rise. The inlet temperature will then be;

$$T_B = \frac{U_1 T_{B1} + U_2 T_{B2}}{U_1 + U_2} \quad (55)$$

Where

$$T_{B1} = T_{sump} + a_h \dot{q} M_1 \quad (56)$$

$$T_{B2} = T_{sump} + (1 - a_h)\dot{q}M_2 (57)$$

is the skin temperature rise and $U_1$, $U_2$ are the velocities of the two bodies respectively.

Finally, to calculate the mean temperature of the film itself the three components must be added together so that;

$$\overline{T} = T_{oil} = T_B + (\Delta T_f)_{av} + (\Delta T_{oil})_{av} (58)$$

### 3.2.3.1 General approach

### 3.2.3.2 Heat transfer coefficients and gear thermal resistance

The method described above, which forms the basis of the Olver and Spikes model[96] can be directly applied to discs operating in fully flooded conditions without any modifications. For gears operating in a lubricant sump however there are additional complications that need to be taken into account.

As shown above, in order to evaluate the heat partition, one needs to calculate the steady state thermal resistance of the two bodies, $M_1$ and $M_2$ respectively. For each of the bodies, the total thermal resistance consists of two elements; the thermal resistance of the track and the thermal resistance of the sides. If these are known, then the total thermal resistance for each body can be found as follows;

$$M_{total} = \frac{1}{1/M_{track} + 1/M_{sides}} (59)$$

In order to calculate the thermal resistance for the track, the assumption of a cylinder of infinite length is made where the face width is much larger than the radius i.e. $b >> R$ so that heat is lost only through the track. Then the thermal resistance of the gear track can be calculated as[151]

$$M_{track} = \frac{1}{2\pi R b h_t} (60)$$

Where $h_t$ is the convective heat transfer coefficient of the gear track.

To calculate the sides steady state thermal resistance, another assumption has to be made, the "thin disc approximation". This essentially treats the disc (gear) as a very thin disc where the face width is much smaller than the radius i.e. $b << R$. Furthermore, the thermal gradient is

assumed to be in the radial dimension only. Then the standard solution for a circular cooling fin can be applied and the sides steady state thermal resistance can be calculated as[152]

$$M_{sides} = \left(8.88(h_s kb)^{1/2} R \frac{I_1[R(2h_s/kb)^{1/2}]}{I_0[R(2h_s/kb)^{1/2}]}\right)^{-1} (61)$$

Where $h_s$ is the convective heat transfer coefficient of the gear sides, $k$ is the thermal conductivity and $I_1[R(2h_s/kb)^{1/2}]$ $I_0[R(2h_s/kb)^{1/2}]$ are modified Bessel functions of the first kind – first and zero order respectively.

To calculate the heat transfer coefficient for the gear sides the standard solution for forced convection over a flat plate of length L in laminar flow can be used

$$Nu = \frac{h_s L}{k_{oil}} = 0.664 Re^{1/2} Pr^{1/3} \ (62)$$

Where $Nu$ is the average Nusselt number for a plate of length L, representing the ratio of total heat transfer to conductive heat transfer, $Re$ is the average Reynolds number and $Pr$ is the Prandtl number. For a disc, one can set $L = 2\pi R$, which is equivalent to assuming that the cooling lubricant is expelled once per revolution and then the average heat transfer coefficient for the sides can be estimated as:

$$h_s = 0.265 R^{-1/2} U^{1/2} \rho^{1/3} C_p{}^{1/3} k^{2/3} v^{-1/6} (63)$$

Where $U$ is the entrainment speed of the lubricant. This shows that the heat transfer coefficient for the gear sides is largely independent of temperature as the exponent of the lubricant viscosity is weak.

When it comes to the gear track a different approach was followed to improve the calculations by including factors that are not taken into account in the equations above. The assumption here was that a pocket of oil rests on the gear tooth which absorbs all the heat generated in the contact. That pocket of oil is trapped between the gear teeth, heat is conducted from the (hotter) gear and then the oil is expelled during meshing. While the oil is in contact with the tooth, the problem becomes that of 1-dimensional transient conduction from the metallic body to the oil. Following the standard solution from literature

$$\dot{q}_i = \frac{k\Delta T}{\sqrt{\pi \chi t}} (64)$$

One can find the average rate of heat flow over a specific period of time. This can be assumed to be the duration of one rotation or the amount of time that the gear spends in the oil sump. The second approach was chosen as more realistic and therefore the immersion depth of the gear now affects the heat transfer coefficient directly

$$\bar{\dot{q}}_i = \frac{1}{t_s}\int_0^{t_s} \frac{k\Delta T}{\sqrt{\pi\chi t}}\,dt = \frac{1}{t_s}\frac{k\Delta T}{\sqrt{\pi\chi}}\frac{t_s^{1/2}}{1/2} \quad (65)$$

Where $\chi$ is the thermal diffusivity. The heat transfer coefficient for the gear track can be calculated as follows

$$h_t = \frac{\bar{\dot{q}}_i}{\Delta T} = 0.2582(\cos^{-1}(1-h/R))^{-1/2}k^{1/2}d^{1/2}\rho^{1/2}C_p{}^{1/2}N^{1/2} \quad (66)$$

Where $N$ is the rotational speed of the gear in revolutions per minute and $h$ is the immersion depth.

### 3.2.4 EHL numerical calculation scheme for gears

The EHL traction and temperature prediction model described above is now applied to real gear teeth contacts. This presents additional complexities since the conditions, including pressure, slide-roll ratio, entrainment speeds, film thickness and friction all vary along the contact path. Furthermore, the inlet and contact temperatures are interdependent, linked through contact traction coefficient and resulting frictional heat flowing into the gear bodies. To deal with these complexities, an iterative numerical calculation scheme was developed and implemented in Matlab. Two spur gears are modelled here, although the approach is just as valid for helical gears provided the appropriate changes in geometry are implemented.

The specifics of this approach as the contact point X moves from A to B are shown in Figure 3.3. The base radii of the gears, as shown in the figure, are equal to $O_1T_1$ and $O_2T_2$ or $d_{b1}$ and $d_{b2}$ respectively, the tip circles have a diameter of $d_{a1}$ and $d_{a2}$ while the pitch (or working) circles of the gears have a diameter of $d_{w1}$ and $d_{w2}$. The latter are equal to the reference diameters if the addendum modification coefficients are equal to zero. Along the path of contact, P is the pitch point where no sliding occurs (and hence the predicted friction coefficient should be zero – something that is not captured by empirical equations). Finally, when considering a gear pair, one must calculate the working transverse pressure angle, $\alpha_{tw}$, which is the angle between the line of action (common tangent to the base circles) and the line of

centres. In order to evaluate the transverse pressure angle, the centre distance of the pair needs to be known. As mentioned previously, for the single speed gearbox, the 23T gears from Petry Johnson et al[127] were used. Therefore, the geometry of the gear pair is known a priori and it is used to work out the position along the path of contact and the appropriate contact radii.

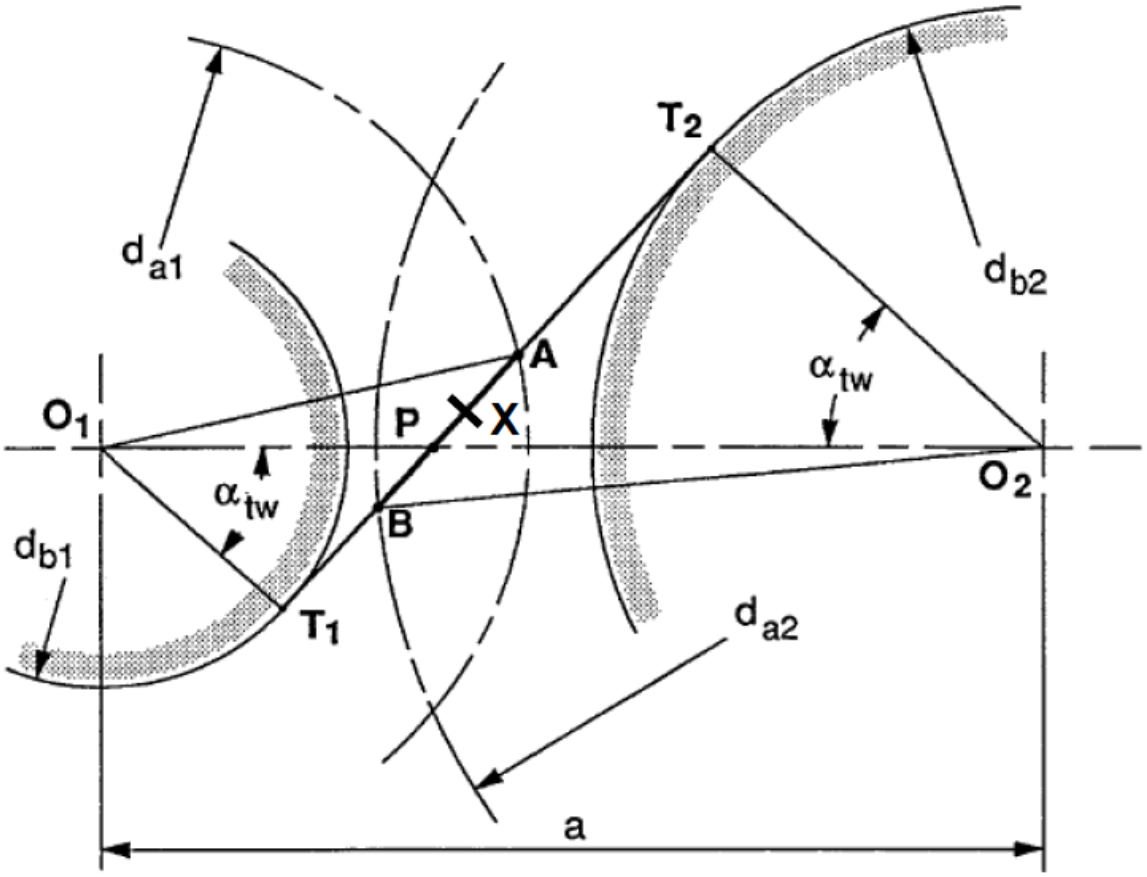



**Figure 3.3: The constantly variable radius of contact in a gear pair**

In addition, the load sharing between gear teeth pairs needs to be accounted for. For the usual contact ratio of between 1 and 2, the applied loading resulting from transmitted torque is either carried by a single pair of teeth or shared between two pairs of teeth. For the variation in tooth load during the double pair contact, the load was modelled as a linear interpolation between zero and maximum value (that which is applicable in the single pair region). For simplicity gears were assumed not to have any profile reliefs. The schematics of the load variation on a gear tooth along the path of contact are shown in Figure 3.4, where the lengths AB and CD represent the double pair contact while the length BC is where only one pair of teeth is in mesh.

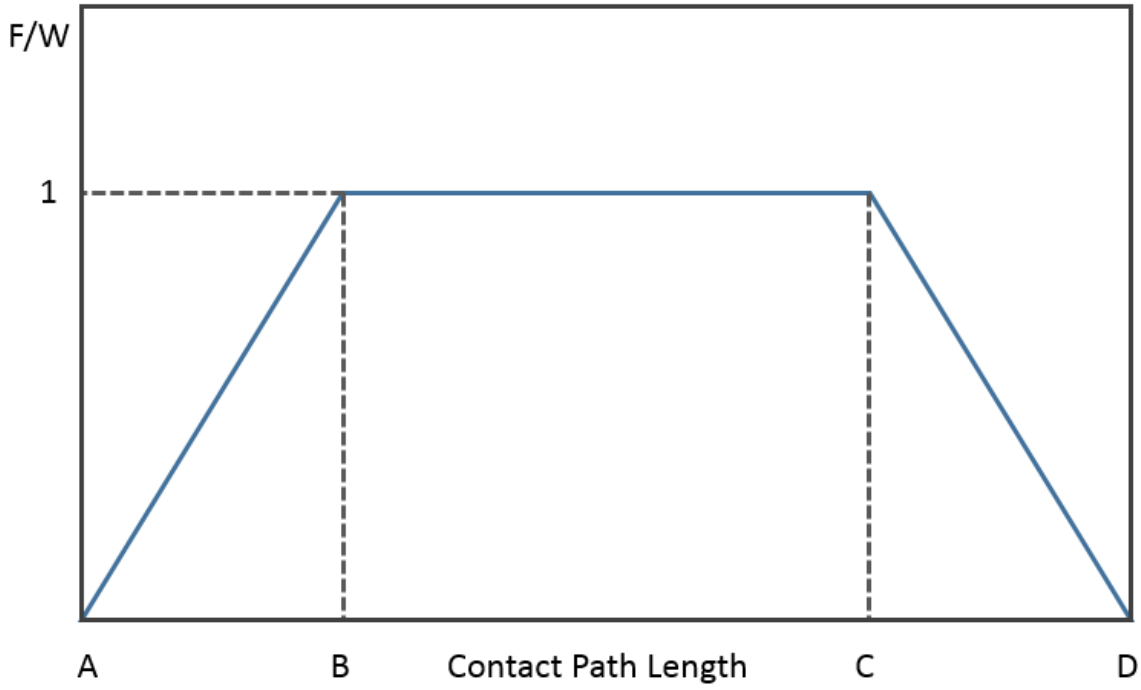



**Figure 3.4: The load profile as modelled in the gear pair (W is the maximum value of the normal load, F)**

In order to apply the EHL model to a gear contact, the scheme has to include an outer loop which calculates the friction along the gear contact path. The geometry of an involute spur gear tooth flank dictates that the tooth's radius of curvature is continuously changing as the gears mesh. Therefore, a time interval is used to progress along the path of contact. All necessary parameters for friction prediction are worked out at each time interval. It is important to understand that there are two loops in the scheme; the first (inner) loop, which is repeated twice to account for the average bulk temperature (explained below) calculates the traction inside the EHD contact for a specific point in the contact path. The second (outer) loop is used to progress along the contact path and repeats the first loop at each consecutive point. When the traction and power loss is calculated at each of the 400 points in the contact path, the results are extracted and saved. A flowchart of the overall computation algorithm is shown in Figure 3.5.

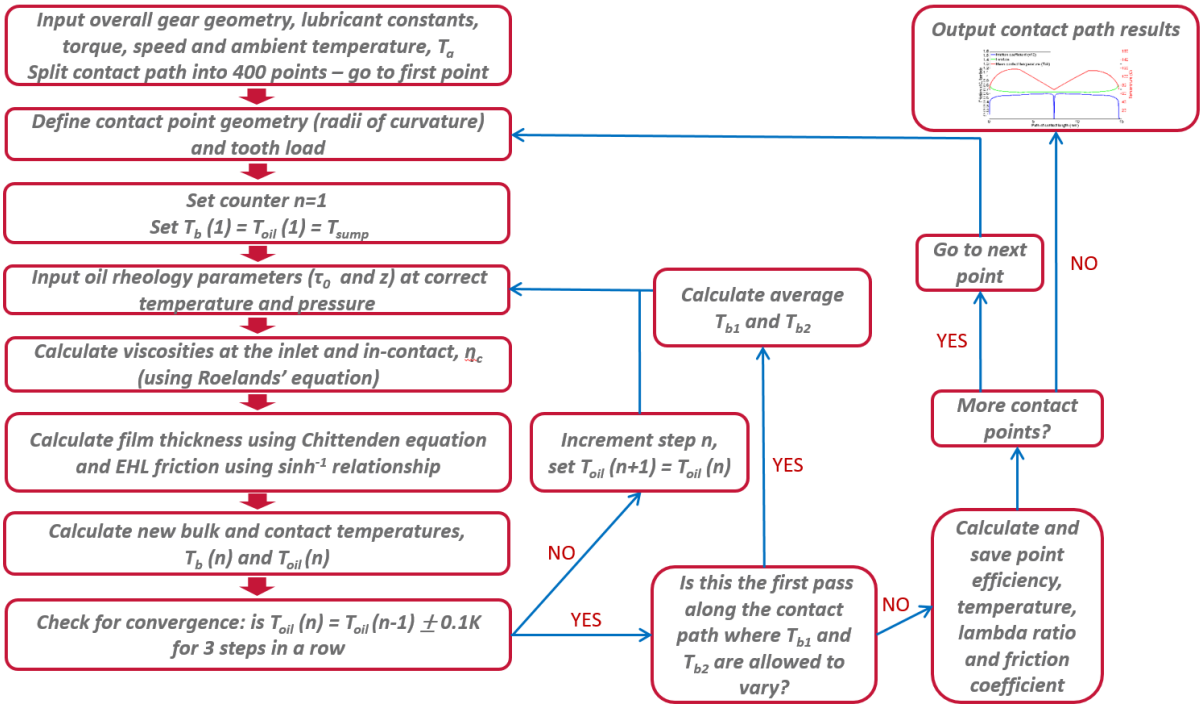



**Figure 3.5: Flowchart of the EHL model algorithm**

The loop is initiated by assuming a value for the friction coefficient so that the calculation of the EHL contact temperature rise is possible and all temperatures are set to be equal to $T_{sump}$. The torque and speed inputs are set and the rheological parameters of the lubricant are evaluated at the correct temperature and pressure. The viscosities are then calculated at the inlet using the ASTM equation and inside the contact using Roelands equation. In the next step, the film thickness is calculated from the Chittenden equation and the EHL friction is evaluated using the non-dimensional parameters to decide the operating regime. All three new contact temperatures can then be evaluated and compared to the initial temperatures; if the convergence criterion of 0.1 $^0$C is met, the instantaneous frictional power loss for that point can be found simply by multiplying the load with the converged friction coefficient and the sliding speed. Once all parameters converge, the steady state friction coefficient, contact temperatures and dissipated heat are output by the scheme and the temperatures are coupled to the inputs of the next point. The process is repeated until the friction, temperatures and losses are calculated at each point along the contact path.

In the case of a gear contact, there are additional complexities that need to be accounted for. Due to the cyclic variation of the contact conditions in the mesh, the heat input varies across the contact path, resulting in different contact and tooth flank temperature predictions for each time interval. However, given the speed with which the contact path is traversed, such fast

temperature variations of the gear bulk temperature (tooth flank temperature) are unrealistic. Therefore, the skin temperature used in the film calculations is the average of bulk temperatures calculated for each time interval, which provides a more realistic approach as long as the bulk temperature of the individual bodies is allowed to vary in order to account for size differences between the mating gears. To implement this in the code, the full loop of the algorithm is run once to calculate this average bulk temperature and then the loop is re-run, including temperature at each time interval, using the average bulk temperature calculated on the first loop as the oil inlet temperature.

As far as computational efficiency is concerned, the most significant factor that affects calculation time is the number of points the contact path is split into, which in turn determines the number of iterations for the internal loop (Figure 3.5). Using a personal computer with 16 GB of RAM and a Core i7 CPU, a simulation can be completed in under 2 minutes when the contact path is split into 125 points. This number provides the best compromise between accuracy and speed, and there is less than 2% deviation compared to the power loss predictions obtained using 400 points, which take around 7 minutes. The results which will be presented in chapter 5 were obtained using 400 points however the number of points was decreased to 125 for the six speed gearbox which will be presented in chapter 6. As the deviation of the power loss prediction. Increasing the number of points beyond 500, where simulations of the single speed gearbox take around 8 minutes, gives no further accuracy benefits even if larger gears with longer contact paths are simulated.

Later on, this two loop scheme will be further expanded to take into account the multiple components and the change of input conditions (torque, speed, ambient temperature and air velocity) in order to calculate the losses in a multi speed gearbox under different drive cycles. The mass of the individual components of the gearbox (including the lubricant) will be included in the calculations through the use of a lump mass model. This will complete the thermal coupling and allow for temperature and efficiency predictions from the multi speed gearbox to be compared to the results of road tests. The results of this comparison will be presented in chapter 6.

### 3.2.5 EHL friction model validation

There are no detailed treatments of film, traction and temperature of a gear tooth contact, so for the purpose of validating the predictions of the current gear EHL loss model, its predictions

were compared to published results of Olver and Spikes[96] for a disc-on-disc example. To achieve this, the present model was run in a simplified form and with identical conditions to those considered by Olver and Spikes. The relevant inputs for the model can be seen in Table 1. It should be noted that they do not provide the relevant lubricant properties at all temperatures encountered in the presented validation examples, and hence it was necessary to extrapolate between given values in order to cover the complete temperature range considered here.

An important issue that has to be taken into account in this case is the fit used to interpolate and extrapolate the values that the parameters have at various temperatures. As illustrated in the next figures, the predicted temperature in the film can theoretically reach up to 200 °C, provided that the lubricant is able to reach these temperatures without boiling. Therefore there is a need to find an appropriate fit to extrapolate to these higher temperatures. The fits that have been used in this case are exponential fits between the values at 40 °C and 100 °C. The exponential fit was found to better match the results and it was therefore applied as there was no information in the published study on the fits used.

**Table 1: Lubricant properties and disc geometry of system under consideration**

| **Lubricant properties (ISO VG220)** | | | **Disc Geometry** | |
|---|---|---|---|---|
| Property | 40 °C | 100 °C | Property | Value |
| Kinematic viscosity, ν (cSt) | 220 | 17 | Diameter (mm) | 50 |
| Density, ρ (kg/m$^3$) | 890 | 876 | Width (mm) | 5 |
| Pressure-viscosity exponent, α (GPa$^{-1}$) | 17.4 | 14.6 | Max contact pressure (GPa) | 1.29,2.11 |
| Shear modulus, G (MPa) | 110 | 12 | Slower disc speed (rpm) | 100,4000, 20000 |
| Eyring stress, $\tau_E$ (MPa) | 7 | 9 | Material | AISI 4340 steel |
| Thermal conductivity, $k_{oil}$ (W/m K) | 0.14 | 0.14 | | |

The figures below show a comparison between the current model and Olver and Spikes results for a range of different conditions. They show the effect of different slide roll ratios on a two disc system. The Slide Roll ratio (SRR) is the ratio of the difference of the velocities of disc 1, $U_{d1}$, and disc 2, $U_{d2}$, (sliding speed) to the mean value of the velocities (entrainment speed).

$$SRR = \frac{Sliding\ speed}{Entrainment\ speed} = \frac{|U_{d1} - U_{d2}|}{\frac{U_{d1} + U_{d2}}{2}} \quad (67)$$

The behaviour of the disc-on-disc example system used here is very dependent on the rotational speed of the discs and the contact pressures. This may intuitively be expected since the slide roll ratio and the rotational speed affect both the friction coefficient and the predicted temperatures as well as the point where the limiting shear stress will be reached, as described in Chapter 3 of this thesis.

In the first case (Figure 3.6) where the speed of the slower disc is 4000 rpm, the system reaches the limiting shear stress but as the predicted temperature increases due to the higher slide roll ratios, the shear modulus drops and the system reverts back to the viscoelastic shear thinning regime. In the second simulation (Figure 3.7), the disc speeds are very high which results in very low friction coefficients, characteristic of such systems due to the dominance of elastic effects. While the total heat input is similar to the first case, the film thickness is much higher and the thicker film insulating the two surfaces results in lower surface temperatures. Finally, Figure 3.8 shows the behaviour of the system examined at very low speeds and lower contact pressure where the limiting shear stress is reached very quickly resulting in a flat friction coefficient while, due to the low speeds, shear is limited resulting in very slight temperature rise. The published values were interpreted from the paper and the values calculated by the current model fall within 2% of the interpretations in all cases.

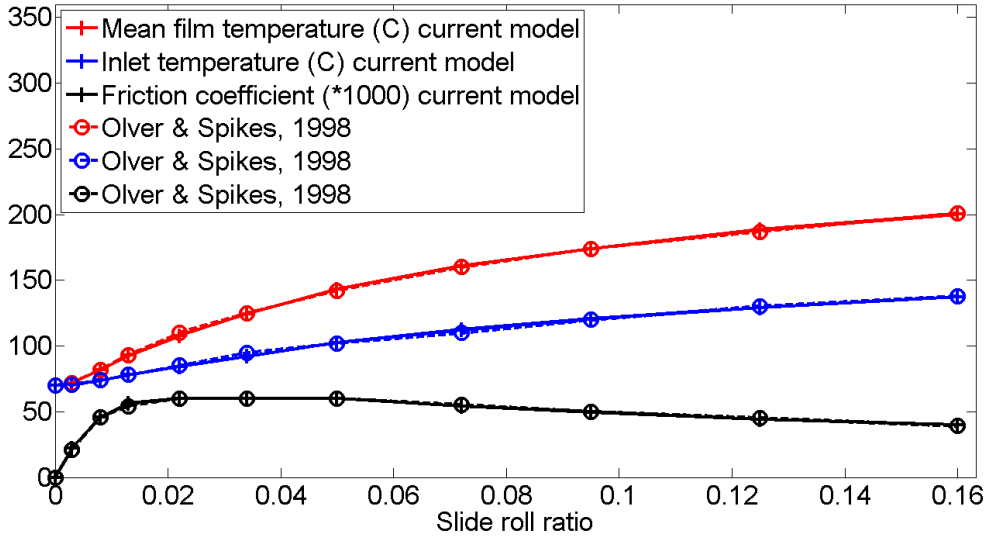



**Figure 3.6: The effect of slide roll ratio on the temperatures and the friction coefficient when the slower disc rotates at 4000 rpm (Max contact pressure = 2.11 GPa)**

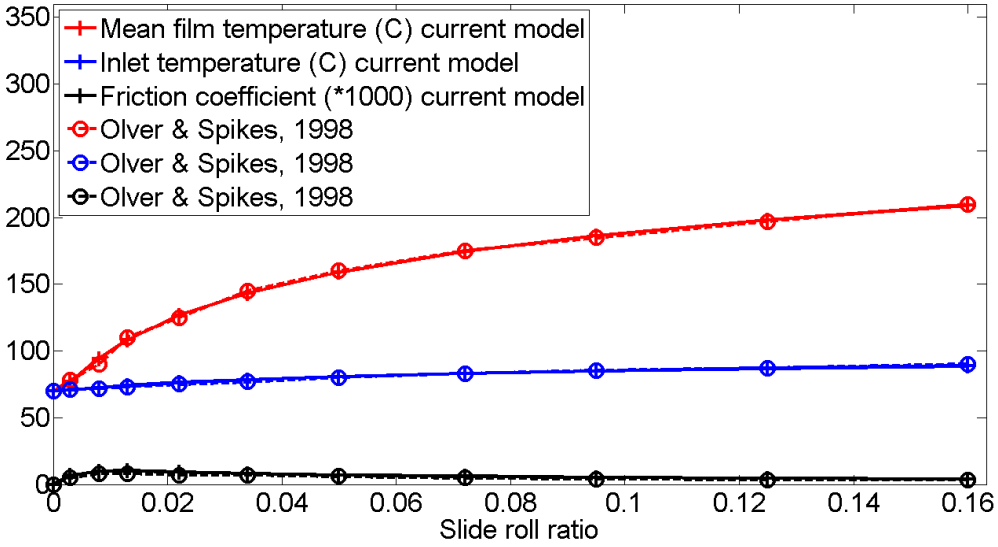



**Figure 3.7: The effect of slide roll ratio on the temperatures and the friction coefficient when the slower disc rotates at 20000 rpm (Max contact pressure = 2.11 GPa)**

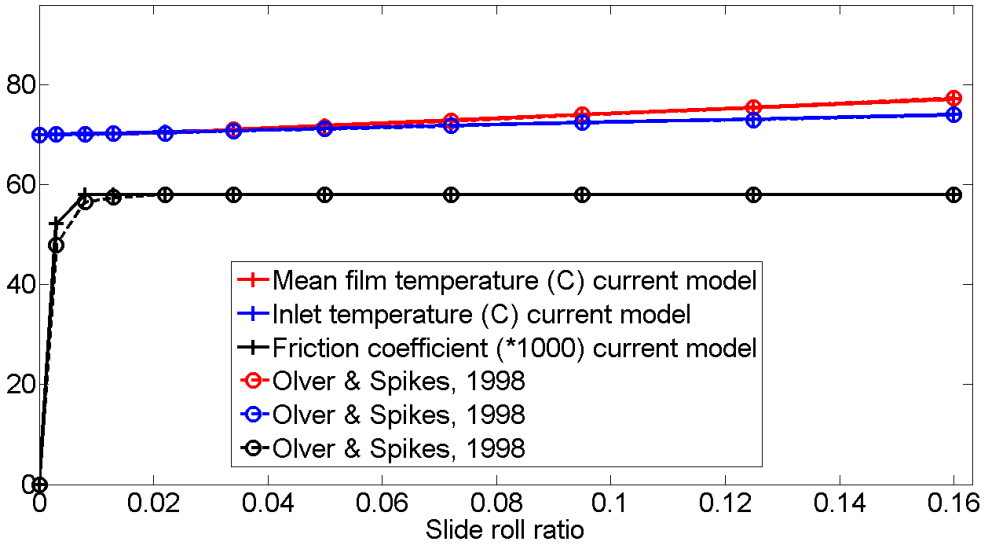



**Figure 3.8: The effect of slide roll ratio on the temperatures and the friction coefficient when the slower disc rotates at 100 rpm (Max contact pressure = 1.29 GPa)**

## 3.3 Churning loss prediction

### 3.3.1 Model description

Churning losses in the gearbox efficiency model were taken into account by means of incorporating an experimentally derived model by Changenet et al[110 111]. This model has been chosen in the current study because it includes several additional considerations which makes the predictions under specific conditions more accurate compared to older models. The most important consideration that was taken into account was the sense of rotation of the gears. Changenet et al have proven experimentally that, when calculating churning losses for a gear pair, simply adding the individual losses of the pinion and gear produces erroneous results for a counterclockwise sense of rotation (when pinion and gear rotate in a way that the lubricant is splashed upwards). This can be attributed to the occurrence of a "swell effect" where the larger gear changes the effective immersion depth of the pinion or vice versa.

It has to be noted that the effect of air and lubricant trapping by the gear teeth has not been directly incorporated in the aforementioned churning study, however, these additional losses have been experimentally proven to be negligible with the swell effect being prominent. The reason for this is that when the gear ratio is equal to one, the experimentally measured churning power loss was found to be almost equal to adding the individual power loss of the two gears thus proving that air-lubricant trapping related losses are relatively insignificant. At higher

speeds or when lubricant is sprayed directly into the mesh, it is possible that these losses represent a non-negligible proportion of the overall loss.

The model uses the expression for the calculation of churning torque in the form described by equation

$$C_{ch} = \frac{\rho}{2}\Omega^2 S_m R_p^3 C_m \quad (68)$$

With $\Omega$ being the rotational speed of the gear and $R_p$ is the pitch radius of the gear. Then the speed regime that the gears operate in is found using the critical Reynolds number:

$$Re_c = \frac{\Omega R_p b}{\nu} \quad (69)$$

Where $b$ and $\nu$ the tooth face width and kinematic viscosity respectively. This critical Reynolds number is employed to signify the transition from a low speed region to a high speed region. This is necessary as it was found that it is impossible to develop a single equation for the calculation of churning losses. The reason for this is that at lower rotational speeds, the gear geometry's influence is limited to the submerged surface area of the gear while the face width and the tooth number can be neglected. On the other hand, when the speed is high, the viscosity of the lubricant appears to be less influential, as the inertia forces become more significant compared to the viscous forces. For this reason, a different formula is employed for the high speed region, replacing the Reynolds number with the ratio of the face width over the pitch diameter of the gear. The two formula method has been experimentally proven in a test rig developed by Changenet et al and the results are in very good agreement with experiments, as will be shown in the next section.

The expression for the calculation of the churning torque used in Changenet et al.[110] model is;

$$C_m = 1.366\left(\frac{h}{D_p}\right)^{0.45}\left(\frac{V_0}{D_p^3}\right)^{0.1} Fr^{-0.6} Re^{-0.21} \quad (70)$$

When $Re_c < 6000$

$$C_m = 3.644\left(\frac{h}{D_p}\right)^{0.1}\left(\frac{V_0}{D_p^3}\right)^{-0.35} Fr^{-0.88}\left(\frac{b}{D_p}\right)^{0.85} \quad (71)$$

When $Re_c > 9000$

And a linear interpolation between the two formulae is employed when $6000 \leq Re_c \leq 9000$

Finally, the overall churning power loss for each of the gears can be calculated:

$$P_{ch} = C_{ch}\,\Omega \quad (72)$$

An additional power loss that takes into account the rotation of the gears relative to each other which under the circumstances described previously can create the "swell effect" is[110];

$$\Delta P = \frac{1}{2}\rho\Omega^3 S_m R_p^3 \Delta C_m \quad (73)$$

With

$$\Delta C_m = 17.7 Fr^{0.67} \frac{u-1}{u^8}\left[1 - \left(\frac{h}{R_p}\right)_{GEAR}\right] \quad (74)$$

Being the additional churning torque and $u$ being the gear ratio. When the gear ratio is equal to 1, the swell effect is negligible and there is no variation in the oil level under steady-state conditions; under this condition, the additional power loss is zero. On the other hand, when the gears' rotation is clockwise (i.e. the gears have a tendency to splash the oil upwards) and there is a difference between the gear and pinion diameters, the larger gear tends to elevate the operating oil level of the smaller gear, causing an increase in the independent churning loss for that gear. A schematic representation of this phenomenon is shown in Figure 3.9.

In the next section, the current implementation of the model will be compared to the published results.

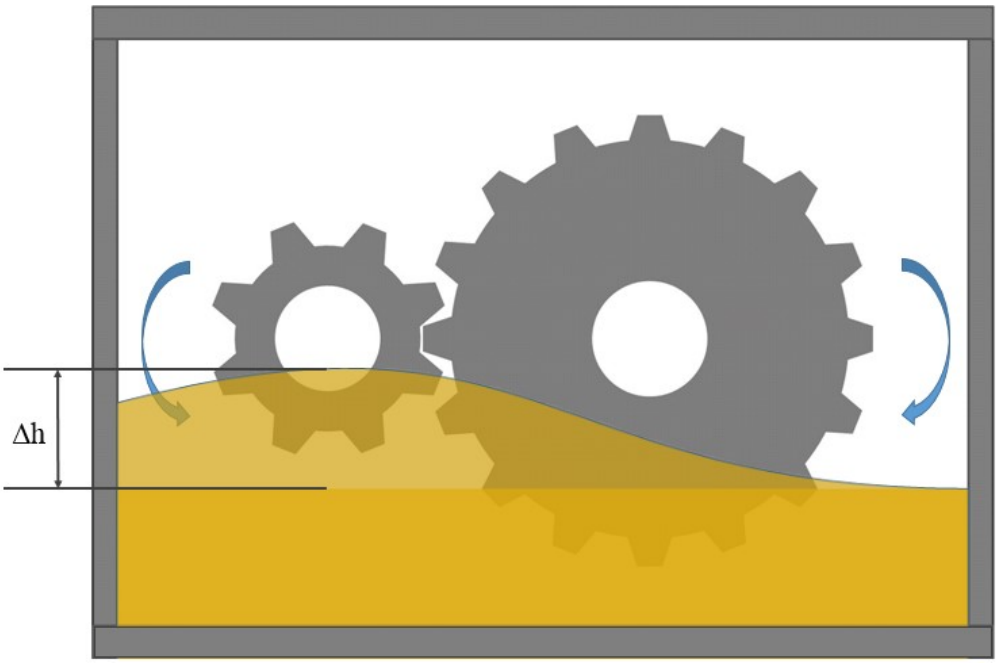



**Figure 3.9: The swell effect in a gear pair**

### 3.3.2 Churning model validation

For the purpose of validation of the present implementation of Changenet et al model[110], the predictions obtained with the current code were compared to those reported by Changenet et al. The results of this comparison are presented in this section.

The system considered by Changenet et al was a purpose built churning test rig, which comprises an electric powered single gear pair which is dip lubricated. The level of the oil can be adjusted and different gear pairs were tested. For the purpose of this comparison, all lubricant properties, geometry and dimensions were identical to those used in Changenet et al. There were four different gear pairs and three different lubricants that were modelled according to the information reported by Changenet et al. Table 2 shows the most important parameters of the system modelled. The only case when enough information was available to create exact comparisons of the published model and the implementation included in the current thesis is shown in Figure 3.10, which shows a graphic representation of the churning torque equations. The critical Reynolds number determines which of the two equations will be used for the calculation with the first used for lower values and the second used for higher values. The numerical average of the two equations is used in the transition regime.

Figures 3.10-3.14 show like for like comparisons of the model and the previously reported results. To reproduce this figure, the equilibrium temperatures had to be known for all rotational speeds. The values for 1000 and 2000 rpm could be derived from the paper with a temperature of 28 degrees for the first point and a value of 41 degrees for the second point, resulting in exact predictions. For the 3 remaining rotational speeds, since the equilibrium temperatures were not quoted in the experimental study, they were selected to match the results, with an assumption of higher temperatures for higher speeds as a result of higher churning power loss. This assumption is realistic given the very high rotational speeds and the relatively small size of the churning rig. The temperatures that were used for the five rotational speeds were 28 °C, 41 °C, 50 °C, 60 °C and 70 °C respectively, values that led to very good agreement with the published results. It has to be noted that churning losses in the model are also quite sensitive to the volume of the oil in the sump, Vo. This was also not quoted in the paper and a value that fits most results in the best way and is realistic for the size of the gearbox was found to be Vo = 2.5 litres. Other minor adjustments such as the way density is modelled (i.e. used as a single value or used as a fit), rounding and graphs interpretation are likely responsible for the small (less than 2%) discrepancies observed.

**Table 2: The lubricant parameters and the geometry of the system as reported by Changenet et al.[110] [111] in their churning study and used here to validate the present implementation of their model**

| **Lubricant properties** | | | |
|---|---|---|---|
| Oil No. | Kinematic viscosity, ν (cSt) at 40 °C | Kinematic viscosity, ν (cSt) at 100 °C | Density, ρ (kg/m$^3$) at 15 °C |
| 1 | 48 | 8.3 | 873 |
| 2 | 73.5 | 10.4 | 896 |
| 3 | 320 | 24 | 898 |

| **Gear properties** | | | | | |
|---|---|---|---|---|---|
| | Gear 1 | Gear 2 | Gear 3 | Gear 4 | Gear 7 |
| Module (mm) | 1.5 | 1.5 | 3 | 3 | 5 |
| Face width (mm) | 14 | 14 | 24 | 24 | 24 |
| Pitch diameter (mm) | 96 | 153 | 90 | 159 | 150 |
| Outside diameter (mm) | 97.5 | 154.5 | 93 | 162 | 155 |
| Base diameter (mm) | 94.125 | 151.125 | 86.25 | 155.25 | 143.75 |
| Number of teeth | 64 | 102 | 30 | 53 | 30 |
| Pressure angle (deg) | 20 | 20 | 20 | 20 | 20 |

For the conditions reproduced in the remaining figures, the equilibrium temperatures were not quoted by Changenet et al[110] and for this reason, a constant temperature was selected to verify the trends of the current implementation. Figure 3.11 shows how churning losses are affected by rotational speed - the most influential factor for churning losses. The most important thing to note here is the transition region which is clearly visible between 2000 rpm and 4000 rpm. The point where the transition occurs is very important as it affects the shape of the curves. As the critical Reynolds number goes above 6000, the churning torque is calculated using a linear interpolation of two formulae (see Chapter 3). This subsequently affects the losses because as rotational speed increases, the gear geometry and the viscosity which is more influential at low speeds give way to an increased influence of inertia forces and therefore the Reynolds number is not included in the high speed formula, employed for critical Reynolds numbers above 9000.

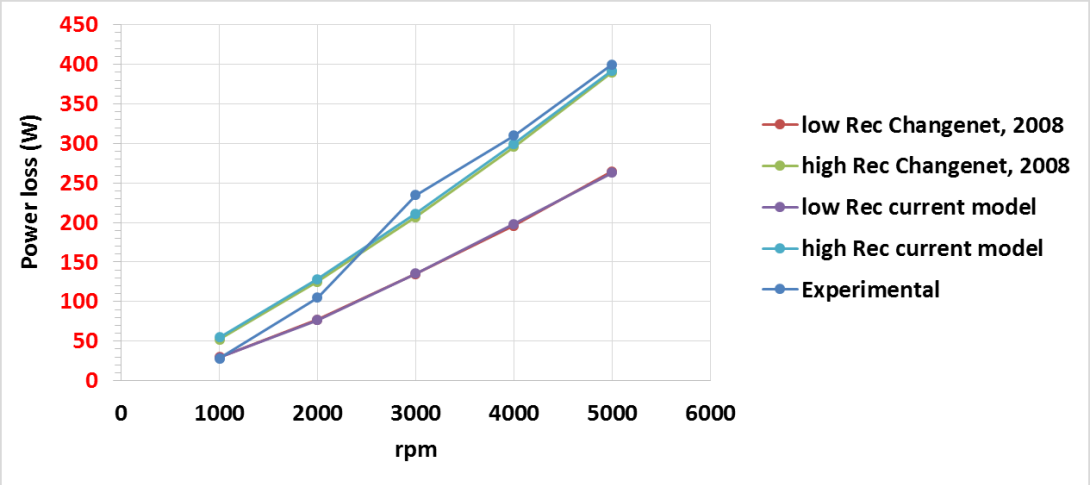



**Figure 3.10: Comparison of the high and low speed formulae to predict churning power loss (Gear 7, Oil no. 1, h/Rp=0.55)**

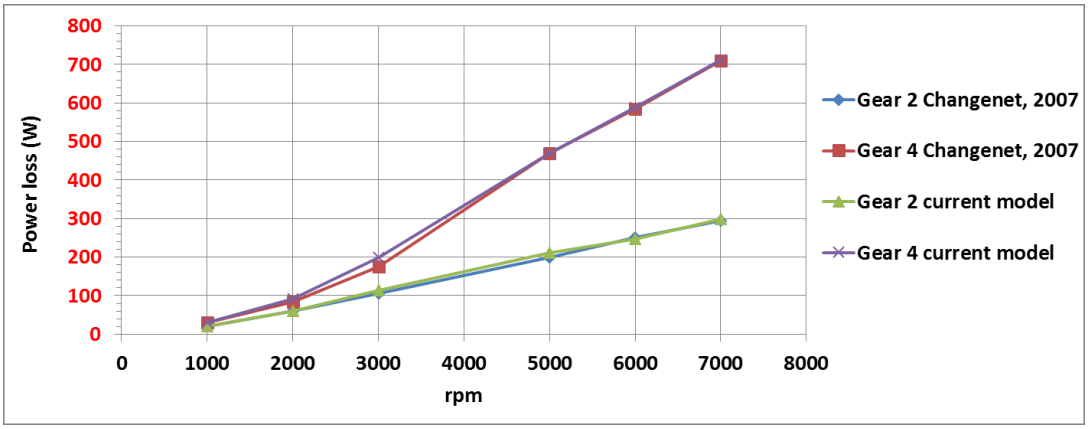



**Figure 3.11: Churning power loss results for two different single spur gears rotating in the oil sump (h/Rp=0.5, oil no. 1)**

It should be noted that the losses shown here are those of a single gear and not a pair, where the additional influences of rotation and the swelling effect need to be taken into account. In addition, the experimental equilibrium temperature would be higher for higher rotational speeds, as a result of increased power loss. Since the exact temperatures were not quoted, the small discrepancy observed is due to the temperature not being allowed to change according to the rotational speed. Finally, since the temperature significantly affects the rotational speed where the transition occurs, the model is very temperature-sensitive. Regardless of the above, the comparison shows very little difference between the published values and the model results.

Figure 3.12 shows the additional churning power loss due to the "swell effect" for two gear pairs, one with a module of 1.5 (mm) and one with a module of 3 (mm). The results correspond to a relative immersion depth of 0.5 and the lubricant used is oil no.1 from Table 2, as in most of the comparisons. Since the equilibrium temperatures for this test were not quoted, the temperature was set at 27 °C, a value which gave the best fit.

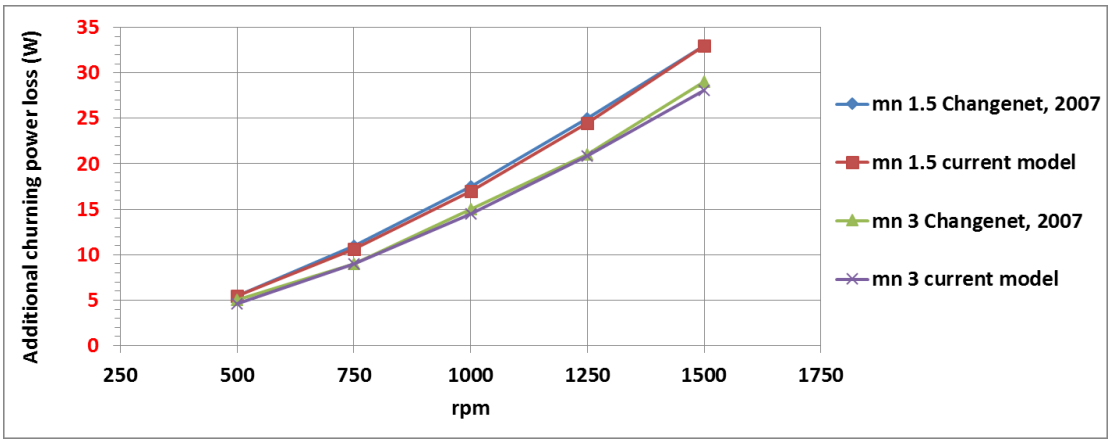



**Figure 3.12: The additional churning power loss due to "counter-clockwise" rotation (h/Rp=0.5, oil no. 1)**

Figure 3.13 compares the published experimental results to the output of the model for a gear pair of normal module equal to 1.5 (mm) – gears 1 and 2 from Table 2. The output takes into account the "counterclockwise" rotation which results in much higher losses compared to adding the individual contributions of each gear. The equilibrium temperature that matches the results was found to be 30 °C.

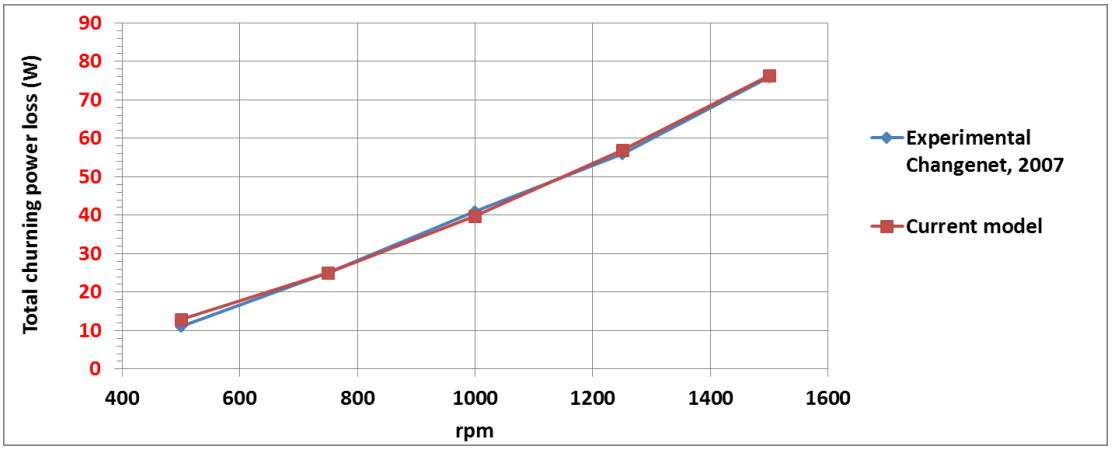



**Figure 3.13: Total churning power loss for a pinion-gear pair of mn = 1.5 (mm), (h/Rp=0.5, oil no. 1)**

Figure 3.14 shows how the different oils affect the equilibrium temperature in the sump and as expected the higher viscosity lubricants no. 2 and no. 3 give higher churning power losses and subsequently result in increased equilibrium temperatures. The ability of the model to take into account the lubricant properties as well as most aspects of the gear geometry was the reason it was incorporated to predict churning losses in this thesis.

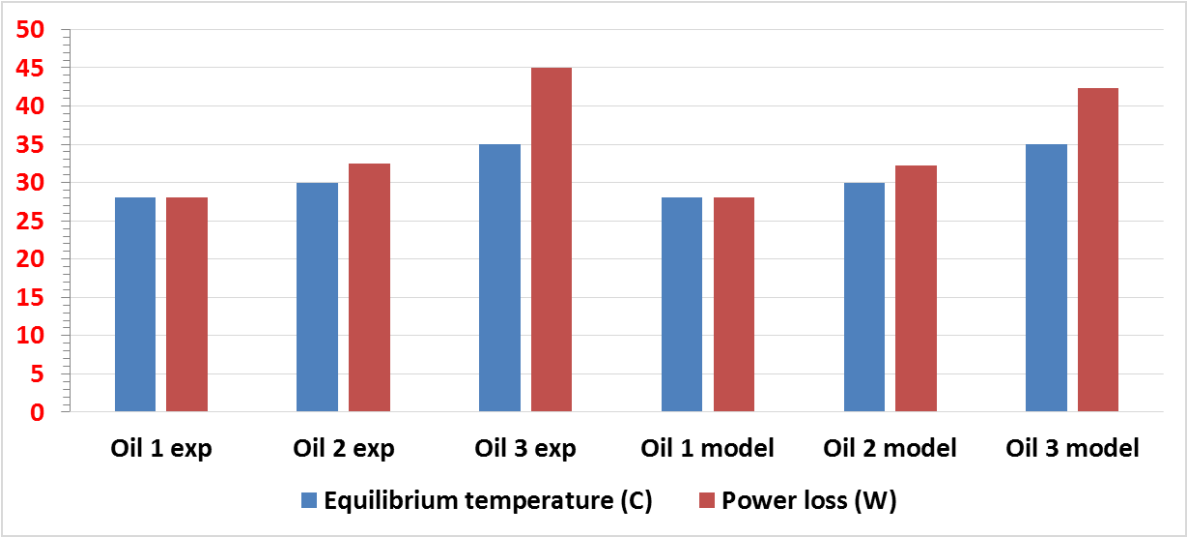



**Figure 3.14: The influence of oil properties on churning power losses and equilibrium sump temperatures (Gear 7, h/Rp=0.55, N=1000 rpm)**

### 3.4 Bearing loss prediction

#### 3.4.1 Model description

The model used to predict bearing losses is that of Morales-Espejel[115] as was described in section 2.4.3 of this thesis. The complete model is able to predict losses for any type of bearing given the designation, geometry, lubrication method and lubricant properties. The four sources of frictional moment in a rolling bearing are due to rolling friction, sliding friction, seal friction and drag. Each of these frictional moments has to be evaluated individually and added in order to calculate the total frictional moment. Equation (33), is used to predict the total frictional moment in the bearing;

$$M_{total} = \varphi_{ish}\varphi_{rs}M_{rr} + M_{sl} + M_{seal} + M_{drag}$$

Where $\varphi_{ish}$ is the rolling friction factor, $\varphi_{rs}$ is the multiplication factor, $M_{rr}$ is the total rolling frictional moment, $M_{sl}$ is the total sliding frictional moment, $M_{seal}$ is the frictional moment of the seals and $M_{drag}$ is the frictional moment due to lubricant drag.

The rolling friction component includes the energy that is spent to channel the lubricant into the EHL contact while rejecting the excess as well as the hysteresis losses in the steel and adhesion between the surfaces. The process of introducing the lubricant into the EHL contact causes a reverse lubricant flow at the inlet which in turn causes inlet shear heating and reduces friction; this is taken into account in the model with the $\varphi_{ish}$ factor. In addition, starvation or kinematic replenishment due to high speeds or high lubricant viscosities is taken into account by means of the $\varphi_{rs}$ factor.

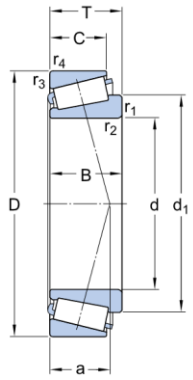
The sliding friction component consists of macro-sliding and micro-sliding; the first is caused by conformal macro-geometry features such as the contact between the raceway and the ball while the second is caused as the surface geometry is distorted from elastic deformation. Both the effects of lubricant shearing and asperity contact have similar thermal consequences to a gear EHL contact and are taken into account for the calculation of the sliding frictional moment. Finally, the component of seal frictional moment takes into account the sliding between the bearing seal (where present) and the steel counterface, while the loss due to oil drag is accounted for in the drag frictional moment. Once the total frictional moment is known, the bearing power loss can be found by multiplying the total moment by the rotational speed of the inner ring[113];

$$P_{brng} = 1.05^{-4}M_{total}\Omega \quad (75)$$

### 3.4.2 Bearing model validation

For the purpose of verification and validation of the current implementation of the bearing loss model, a sample curve of bearing frictional moment vs rotational speed has been compared to the results obtained for the same bearing using the online calculator tools available on skf.com, which implement the same method of Morales-Espejel[115] that is used here.

The selected bearing is one of the bearings comprising the commercial automotive gearbox described later in the thesis. The bearing designation is 32210 which corresponds to a tapered roller bearing with principal dimensions shown in Figure 3.15. The lubrication method was selected to be dip lubrication, since the system of interest in the present work is a dip lubricated automotive gearbox. The oil properties of the first of two 75W90 gear oils that will be characterised in the next chapter have been used. The selected immersion depth was 20 (mm).




| | | | |
|---|---|---|---|
| d | | 50 | mm |
| D | | 90 | mm |
| T | | 24.75 | mm |
| $d_1$ | ≈ | 68.6 | mm |
| B | | 23 | mm |
| C | | 19 | mm |
| $r_{1,2}$ | min. | 1.5 | mm |
| $r_{3,4}$ | min. | 1.5 | mm |
| a | | 21 | mm |

**Figure 3.15: The basic geometry and principal dimensions of the 32210 J2/Q bearing (SKF)**

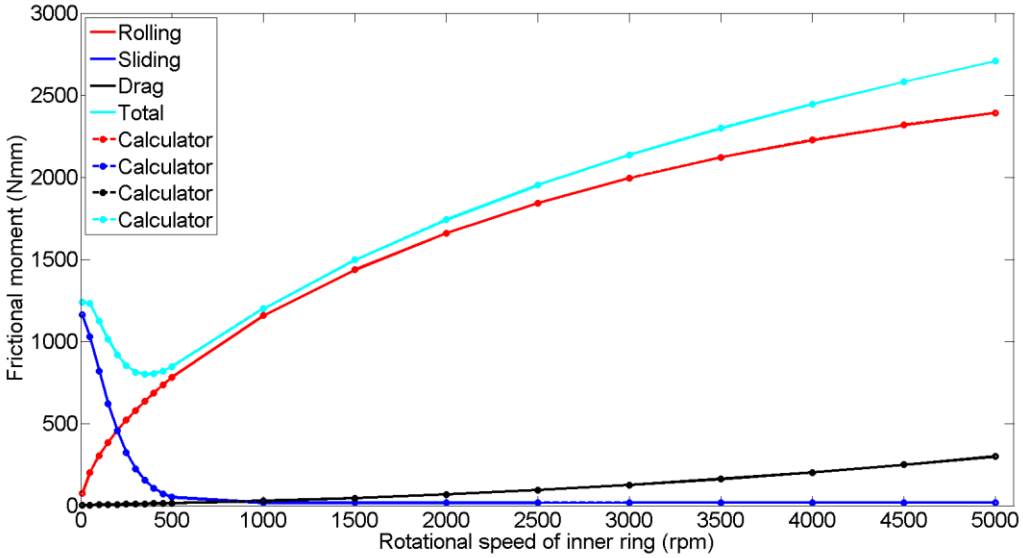



**Figure 3.16: The components of the frictional moment for the 32210 bearing (inputs: radial load, Fr = 5 kN, axial load, Fa = 3 kN, T = 50 °C) using online calculator tools based on the Morales-Espejel model[115115] (calculator) and the current implementation of the model (rolling/sliding/drag/total)**

As can be seen in Figure 3.16, the 'rolling' frictional moment (and subsequently the rolling frictional loss) is dominant for all rotational speeds exceeding 300 rpm which means that in the actual gearbox the bearing will operate mainly in that region where rolling moment is the most significant. It has to be noted that different bearing designs have different geometric characteristics which change the breakdown of observed losses/moments and the ranking of their importance. The ranking seen here is characteristic of the current bearing and the selected operating conditions. For example, in a spherical roller bearing the sliding to rolling frictional moment ratio, according to the definitions given in the model, is higher compared to the tapered roller bearing shown here. This is why the curves shown in Figure 3.16 are slightly different than those seen in Figure 2.13.

### 3.5 Summary

In this chapter, the calculation method which was used to evaluate the film thickness, traction and contact temperatures in the EHL contact has been described. The application of this method to a set of meshing spur gear has been discussed and the associated numerical calculation scheme which was used to extend the friction calculations to cover the path of contact of a gear pair has been presented. Furthermore, the existing models that have been adapted from

literature and used in this study to predict bearing and churning losses have been presented and their implementation in the current study has been validated against published results. In the next chapter, the two lubricants that have been used in this study will be experimentally characterised.

# 4. CHARACTERISATION OF LUBRICANTS

## 4.1 Introduction

One of the primary objectives of this research is to assess the influence of lubricant properties on automotive gearbox efficiency by means of a predictive numerical model of gearbox power losses. Unlike the existing gearbox efficiency model, the aim of the current study is to be able to distinguish between nominally the same lubricants, according to their SAE grade, in terms of their effect on gearbox power losses. Such a predictive tool would be of obvious value to a gearbox or lubricant manufacturer, as it would allow them to select or formulate the most appropriate oil for a given transmission application, automotive or otherwise, in terms of achieving the optimum efficiency. However, this level of predictive accuracy can only be achieved if the tribological properties of the lubricant under consideration are well characterised so that they can be used as input to the predictive power loss model. With this in mind, an experimental procedure to obtain the required lubricant properties was devised. The procedure relies on proven techniques using friction measurements on a ball-on-disc tribometer to extract the relevant rheological parameters by fitting of the stress-strain relationship to the measured data. The adopted experimental procedure and the obtained results are presented in this chapter. First, the oils studied in this work are described, then the experimental equipment is described and finally the procedure for extracting the required rheological parameters from the measured friction and film thickness values is outlined.

## 4.2 Studied lubricants

Two fully formulated gear oils of nominally the same specification, SAE 75W90, are studied. Although they both satisfy the same specifications, the lubricants are based on different chemistries, both in terms of the base oil and additive packages, which in theory should result in some differences between them in terms of gearbox frictional losses. The first lubricant is a commercial gearbox oil and the second is an experimental model oil. The two lubricants will be denoted in this thesis as oil A and oil B respectively. Both were supplied by Valvoline, USA. The basic properties of the two oils at atmospheric pressure were measured and are shown in Table 3.

**Table 3: The basic properties of the lubricants measured at atmospheric pressure**

| | **Oil A** | **Oil B** |
|---|---|---|
| Type | 75W90 gear oil | 75W90 gear oil |
| Base Oil | Group 3/Group 5 | Group 4 |
| Viscosity @ 40 $^0$C, $p_{atm}$ (Pa s) | 0.0751 | 0.0926 |
| Viscosity @ 100 $^0$C, $p_{atm}$ (Pa s) | 0.013 | 0.0135 |
| Pressure viscosity coefficient 40 $^0$C | 22.26 | 21.58 |
| Pressure viscosity coefficient 100 $^0$C | 15.86 | 15.59 |
| Density @ 15 $^0$C (kg/m$^3$) | 858.32 | 888.64 |

Both oils are described as 'synthetic'. It can be seen that the density of the lubricants is slightly different and that oil A has a higher VI compared to oil B. No further details of the composition of the two oils were available from the manufacturer.

### 4.3 Ball-on-disc tests

#### 4.3.1 Test apparatus

The basic variable that defines EHL traction is the shear rate calculated from the Eyring equation (42). This includes two crucial parameters that are unique characteristics of each lubricant and cannot be accurately predicted by analytical equations. The first of these parameters, the Eyring stress $\tau_o$, represents the point where the lubricant enters the shear thinning regime while the second, z parameter in Roelands equation (43), shows how the viscosity is affected by pressure. Both these parameters had to be experimentally evaluated

using an MTM2 (Mini Traction Machine 2) ball-on-disc tribometer test rig which was used to measure friction under varying contact conditions.

The basic details of the MTM2 rig are illustrated in Figure 4.1[153]. The rig uses a steel ball loaded against a steel disc and is able to accurately measure friction over a very wide range of contact pressures, temperatures, entrainment speeds and slide roll ratios. The rig is able to impose all lubrication regimes in the ball on disc contact, from boundary to full film EHL. The test lubricant is contained in the pot so that the disc surface is covered by the lubricant and starvation is prevented. Two electric motors are used to regulate the speed of the ball and the disc and allow for a combination of sliding and rolling in the contact making the rig capable of simulating rolling-sliding contacts encountered in gears. The friction force is measured by a force transducer attached to the ball shaft and a load sensor is employed to regulate the applied load. The temperatures of the pot and the lubricant that is contained within the pot are measured by means of appropriately located resistance temperature detectors (RTD's). The standard specimens used in the MTM rig comprise a steel ball with a dimeter of 19.05 mm (3/4") and a steel disc with a diameter of 46 mm; both specimens are made of AISI 52100 steel (760 HV). The error for friction coefficient measurements depends on the test conditions and more on the ability of the electric motors to precisely regulate and maintain the selected speeds than on the force transducer or the load cell which are very accurate, however it is usually less than 3%.

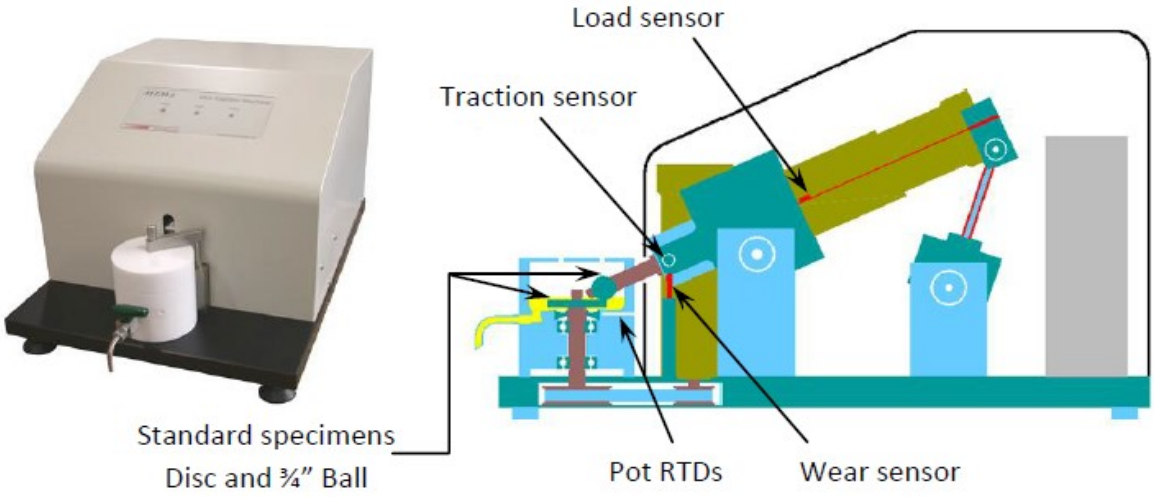



**Figure 4.1: The MTM2 rig used to measure friction with the studied gearbox oils and subsequently obtain the shear stress-strain rate relationships of for the oils**

The MTM rig can be used in different ways to provide measurements in lubricated contacts. For example, it is able to produce a traction curve by keeping the entrainment speed constant

and varying the slide roll ratio (SRR); or it can be used to produce a Stribeck curve, by keeping the SRR constant and varying the entrainment speed. In addition, the rig incorporates the spacer layer imaging (SLIM)[154] technique which can be used to study boundary film formation. In this study, the Stribeck curves were obtained for the two oils at the varying SRRs, pressures and temperatures, as this data is required for the fitting of the rheological parameters which will be outlined later in this chapter.

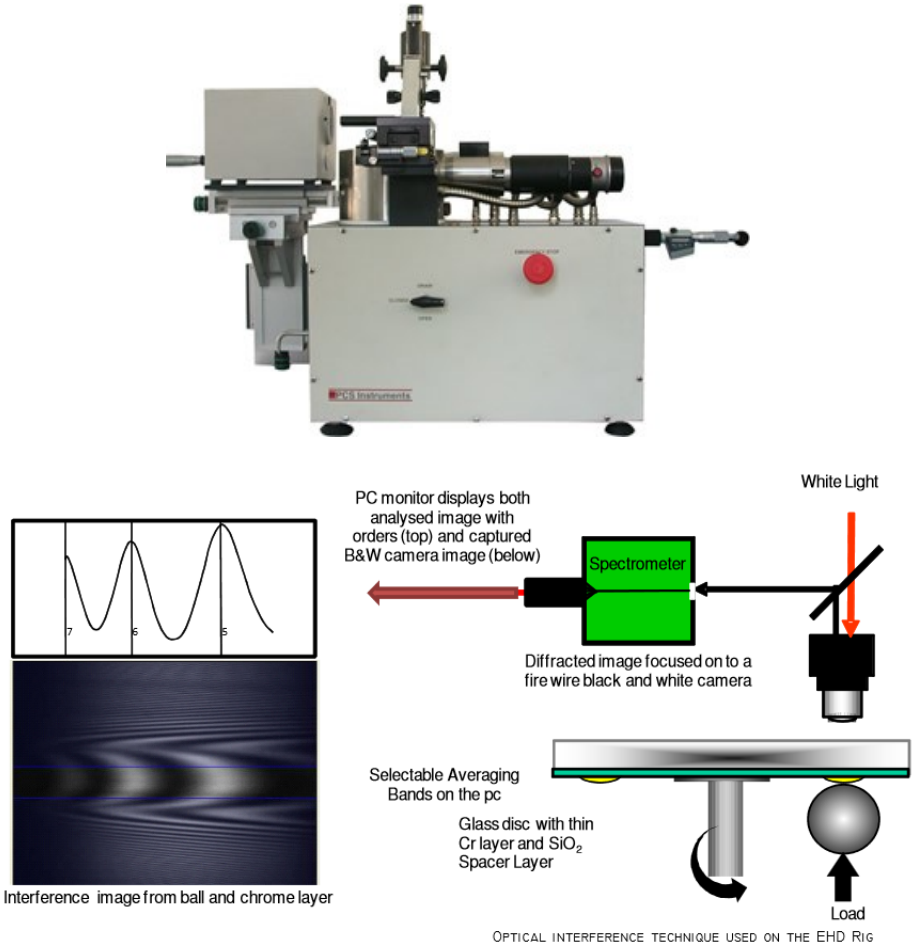



**Figure 4.2: The EHD2 rig used to measure lubricant film thickness**

In addition to measuring traction coefficients under a range of conditions, in order to obtain the shear stress - shear rate relationship for the oils, it is also necessary to know the oil film thickness over the same range of conditions. This can be calculated by means of EHL regression equations and using the known oil viscosity values and contact conditions, but these equations only provide estimates; to obtain more accurate values, this study instead measures the required film thickness of the two oils using another ball-disk rig, referred to as the EHD rig[155]. Figure 4.2 shows the schematics and operating principle of the EHD rig. The instrument uses the same 19.05 mm steel ball which is loaded against a rotating glass disc, covered by a

semi reflective coating, and uses the optical interferometry technique[156] to measure the film thickness in the EHL contact. A white light source illuminates the contact through the glass disc and part of the light penetrates the glass disc and is reflected by the steel ball while another part is reflected by the glass disc. An interference image is formed from combining the light paths which is sent through a spectrometer to a black and white CCD camera. Finally, a video frame grabber captures the image and software is used to analyse it so that the film thickness can be determined. The pot which contains the lubricant is temperature controlled in a way similar to the MTM rig. The error in film thickness measurements is very low, at 5 nm or less[154].

### 4.3.2 Friction coefficient and film thickness results and their treatment to obtain rheological constants for oils A and B

#### 4.3.2.1 Experimental procedure for friction coefficient measurements

In order to be able to extract the rheology coefficients from traction data, a broad range of measurements was undertaken. The conditions under which the measurements were performed are summarised in Table 4;

**Table 4: Range of conditions for MTM traction measurements**

| **Test Conditions** | |
|---|---|
| Loads (N) | 20, 37, 50, 75 (± 0.1) |
| Corresponding max contact pressures (GPa) | 0.7, 0.86, 0.95, 1.1 |
| Entrainment speed ($ms^{-1}$) | 2.75 (± 0.005) |
| Slide/Roll Ratios range (%) | 1/2/3/4/5 %<br>6/8/10/12/14/16/18/20 %<br>25/30/35/40/45/50/55/60/65/70/75/80/85 % |
| Temperatures (°C) | 40,55,70,85,100,115,130,145 (± 1) |

The range of contact pressures was limited by the maximum loading and the standard steel on steel specimen configuration of the MTM machine; higher pressures are possible by using tungsten carbide MTM specimens. However, in this work, the range of pressures quoted above is sufficient as it covers the operating conditions of a typical gear tooth contact. For each of the combinations of the above range of conditions, the friction coefficient was measured. The total number of MTM tests for each oil was 24.

Once the above measurements were performed, the data was used to extract the necessary rheological parameters of the two oils. One approach for this, according to LaFountain et al.[157] is to convert the obtained Stribeck curves to shear stress vs shear rate curves, using the EHD film thickness data, and then extract the rheological parameters by performing the shear stress – shear rate curve fitting over the region where the entrainment velocity is sufficiently high to ensure full film conditions. To achieve this, a Stribeck curve needs to be measured by varying the entrainment velocity at each SRR. The approach is described in Figures 4.3 and 4.4[158]. However, this approach requires the contact to operate in the mixed lubrication regimes in order to produce the "tails" of the Stribeck curve, seen in figure 4.4 below, resulting in excessive wear of the specimens during the test procedure and as a result more tests are needed with frequent specimen replacement.

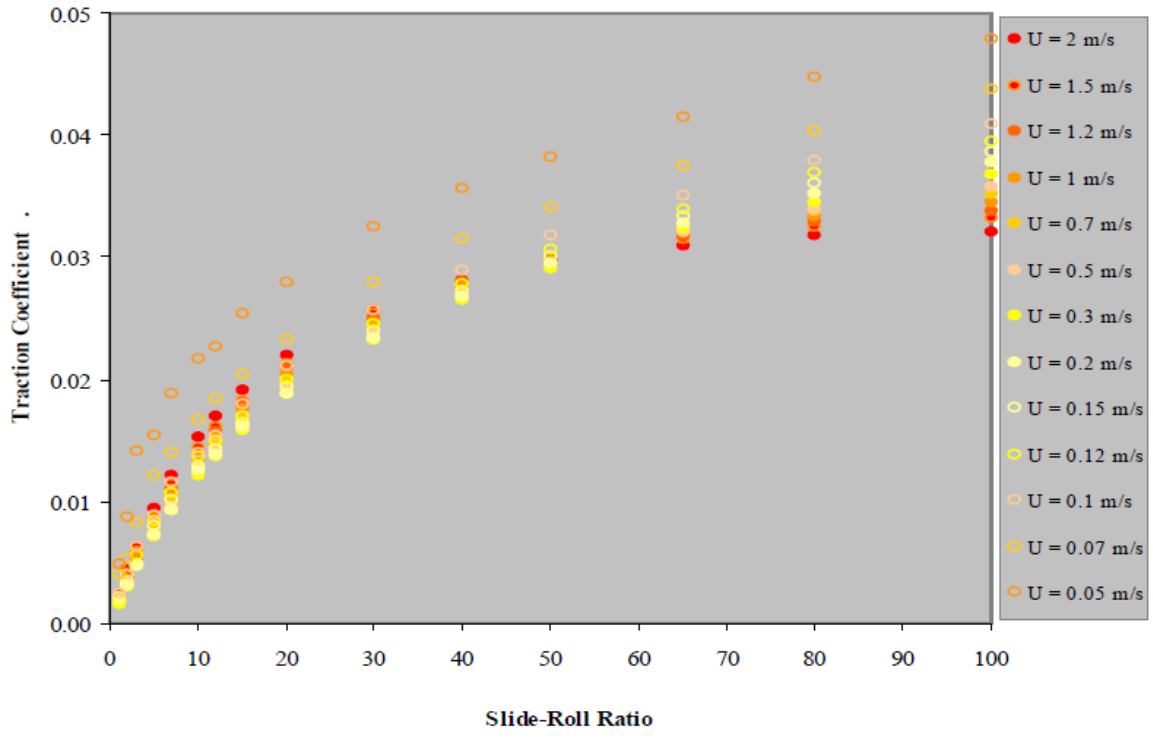



**Figure 4.3: The traction coefficient vs SRR**

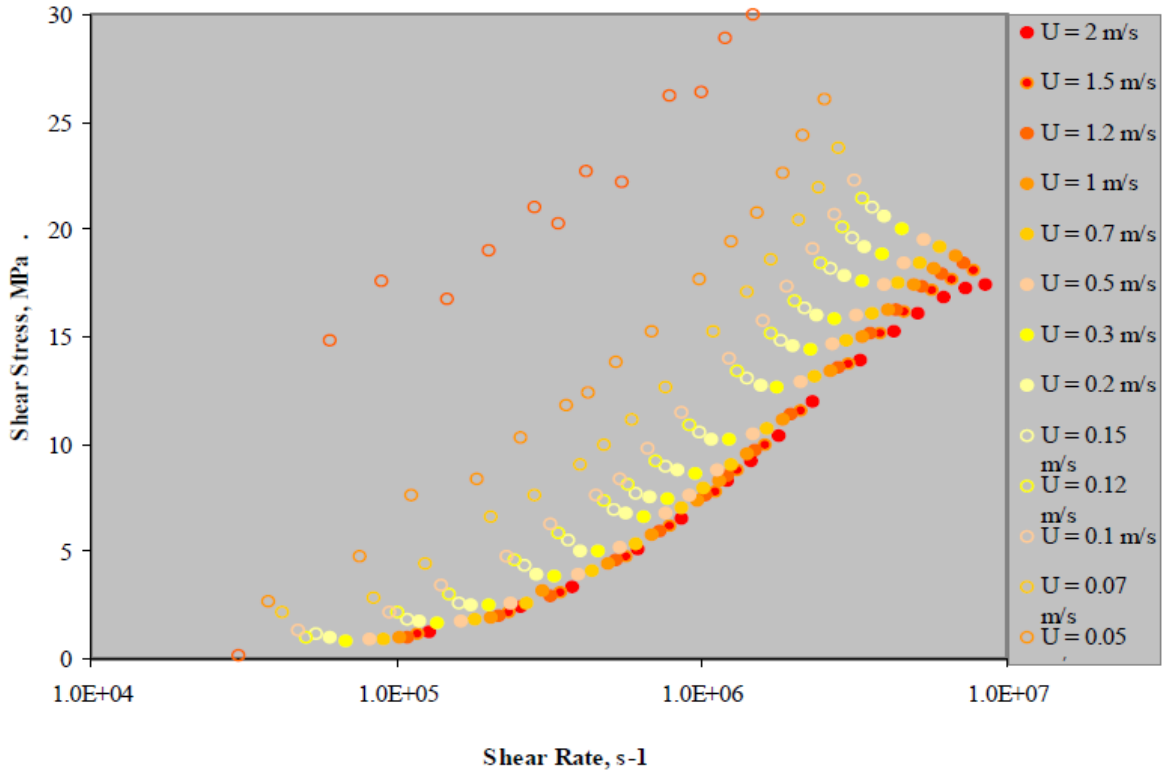



**Figure 4.4: The shear stress vs shear rate curves**

Spikes and Zhang[159] adapt La Fountain et al original approach, to utilise more reference data points and using the entrainment velocity that is sufficiently high to ensure the contact operates in fully flooded conditions, negating the need for the "tails" of the Stribeck curves and reducing the frequency of specimen change. In this approach, the tests are performed at a single entrainment speed and the SRR is varied instead. The present study employs this modified approach at the entrainment speed of 2.75 $ms^{-1}$. An example curve and the converted shear stress vs shear rate curve for oil A obtained using the above procedure is shown in Figures 4.5 and 4.6 respectively where the conditions were 70 $^{0}C$ and 0.50 SRR.

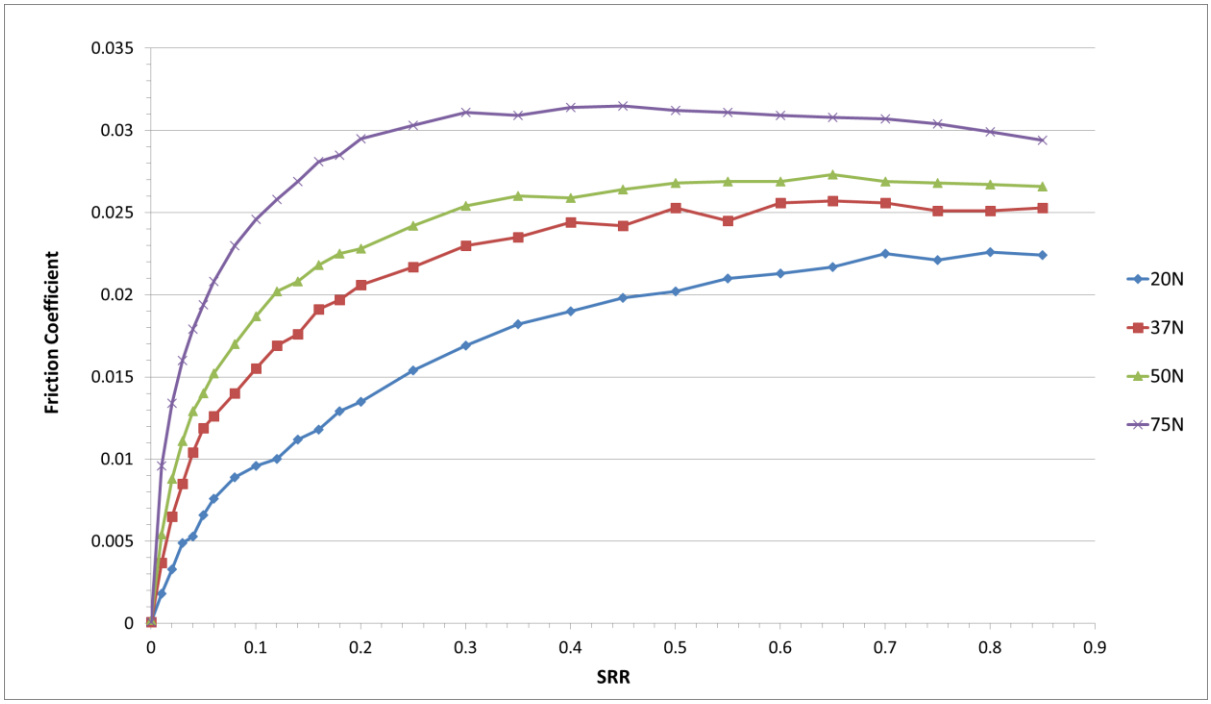



**Figure 4.5: The measured friction coefficient vs SRR at constant entrainment speed of 2.75 m/s over a range of loads**

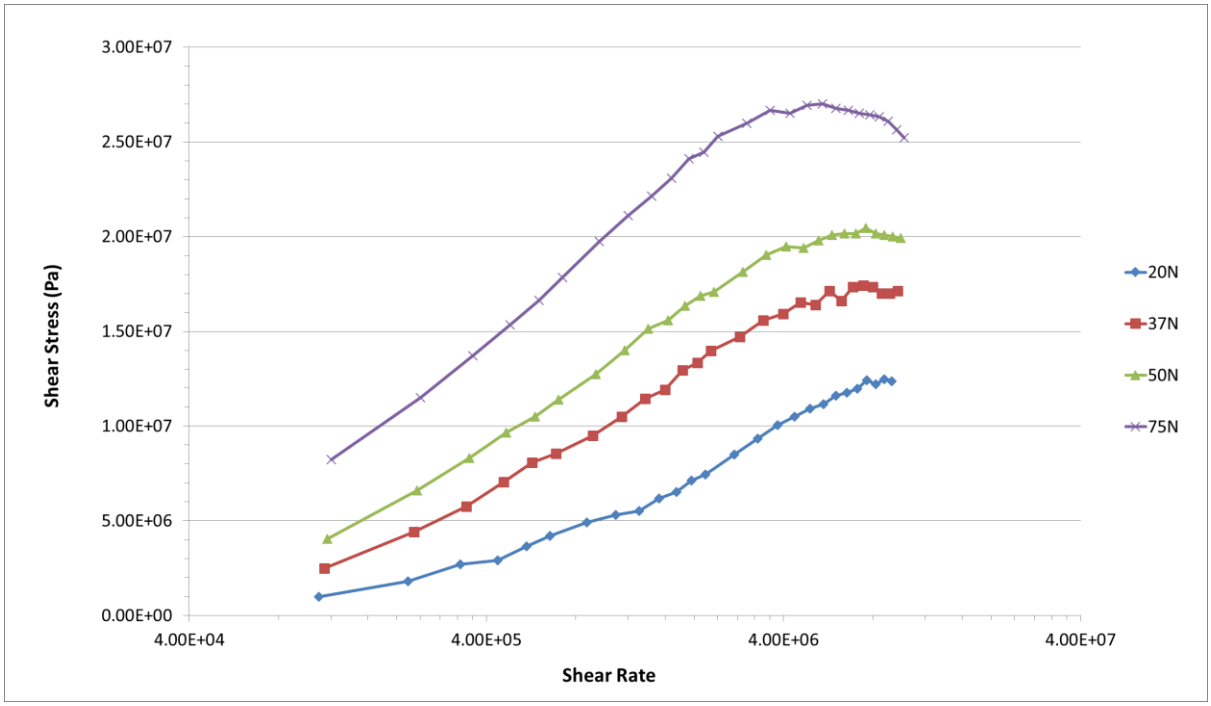



**Figure 4.6: The shear stress vs shear rate curves at constant entrainment speed of 2.75 m/s for oil A over a range of loads obtained using the measured data shown in Figure 4.5 above.**

To ensure valid and repeatable results, all specimens, relevant components and the MTM pot were cleaned with toluene and isopropanol and the specimens were treated in an ultrasonic bath before tests. Furthermore, in order to verify the repeatability of the tests an additional test was performed under identical conditions after the end of each test and the friction measurements were compared to the initial results. Three repeat tests were performed at each condition and the quoted friction coefficients are the average of the three values. Because the contact was operating under fully flooded conditions due to the high entrainment speed, the wear of the specimen was kept to a minimum. For this reason, it was possible to run a test profile consisting of the full range of slide roll ratios at all four loads, using the standard polished MTM specimens. This profile, which constitutes one "set" of measurements or one "test" was run continuously with no lubricant or specimen change. Both the lubricant and the specimens were replaced after each set and before the temperature was increased for the next. As a result, the repeatability of the tests was very good as can be seen in Figure 4.7;

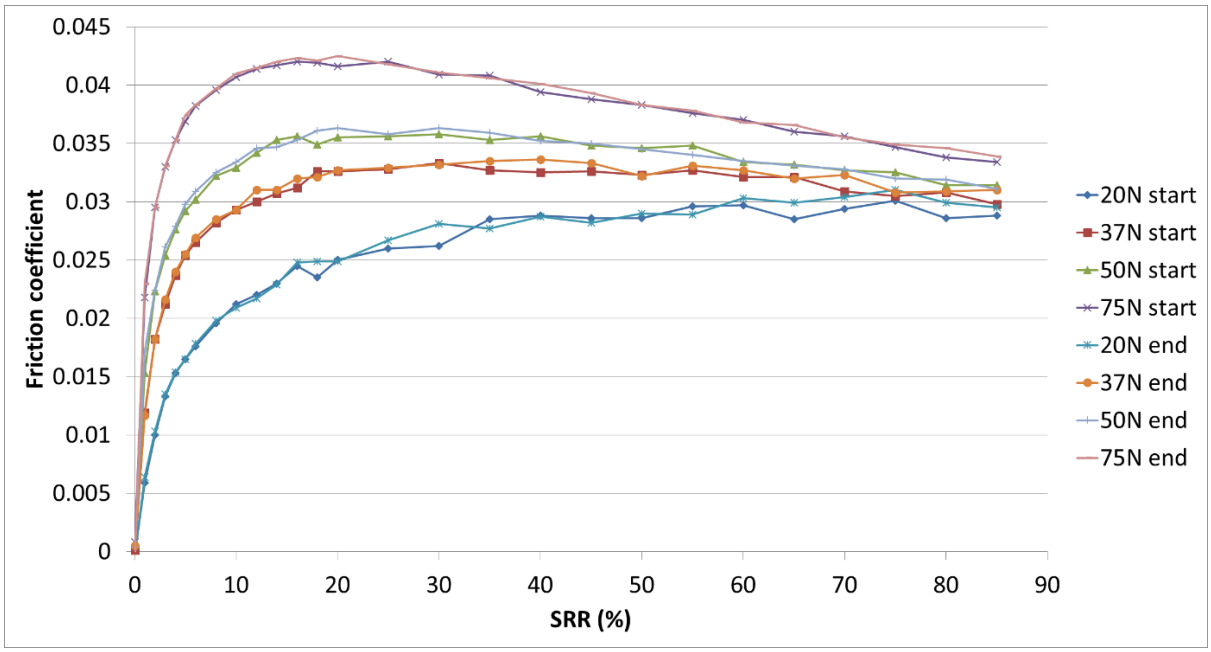



**Figure 4.7: The repeatability of the friction measurements at 40 °C**

### 4.3.2.2 Experimental procedure for EHD film thickness measurements

The SRR was kept constant at 50% which provides an accurate reference point of measurement for the EHD rig, however all SRR's were compared with a deviation of less than 2%. A procedure similar to the one described before was employed to ensure repeatability while the tests were repeated three times and an average value was used. Furthermore, as the film thickness was obtained using a glass disc rather than a steel disc the results needed to be

adjusted to correspond to the Young's modulus of steel on steel. In order to do this, the ratio of the Young's modulus for steel to the Young's modulus for the glass disc had to be calculated – this is about 10%. The film thickness measurements for a range of SRR's and oil A at 40 $^0$C are shown in Figure 4.8;

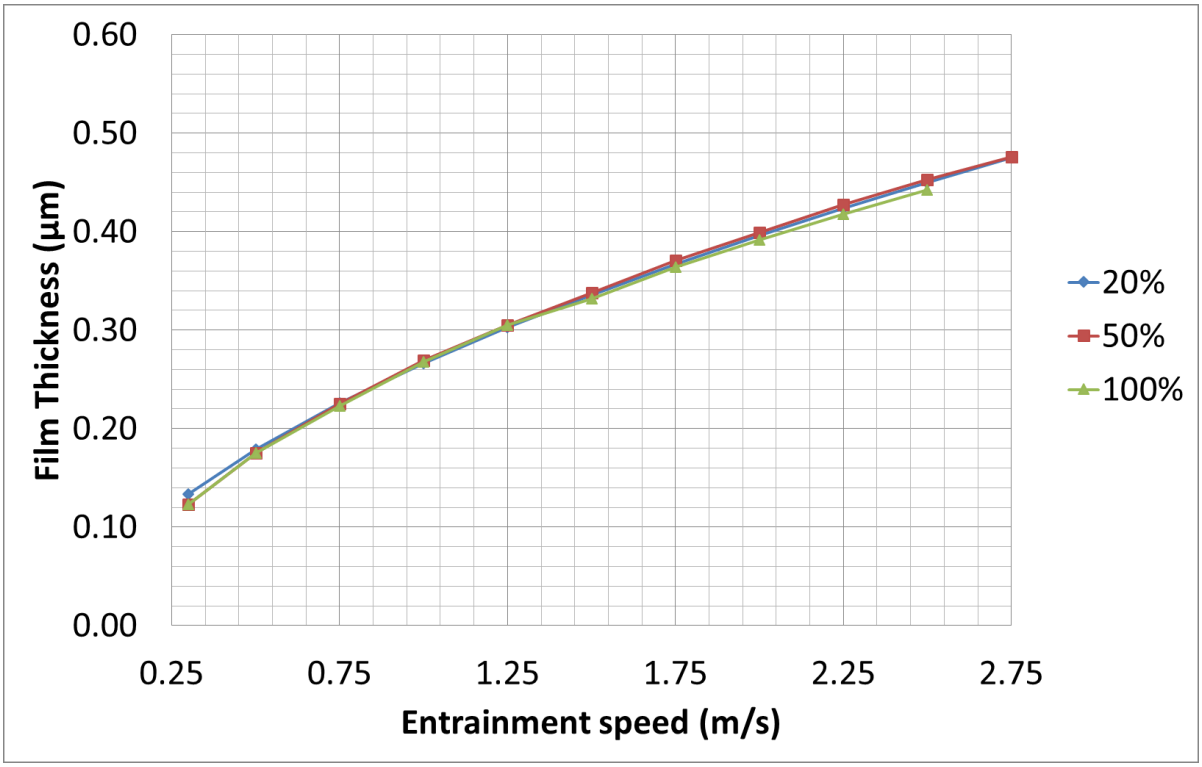



**Figure 4.8: The film thickness variation with SRR at 40 °C**

The actual film thickness measurements at every temperature and entrainment speed, 50% SRR and modified for a steel on steel contact are plotted in Figure 4.9. Using the measured values at 2.75 m/s it can be seen that the EHL contact is indeed operating in full film conditions as the lambda ratio using the standard MTM specimens and the lowest film thickness at 145 $^0$C has the value of about 6 nm. Once the film thickness is measured the shear rate can be calculated and the friction coefficient vs SRR curves are converted to shear stress vs shear rate curves; the rheological coefficients can be extracted through curve fitting following the procedure described below.

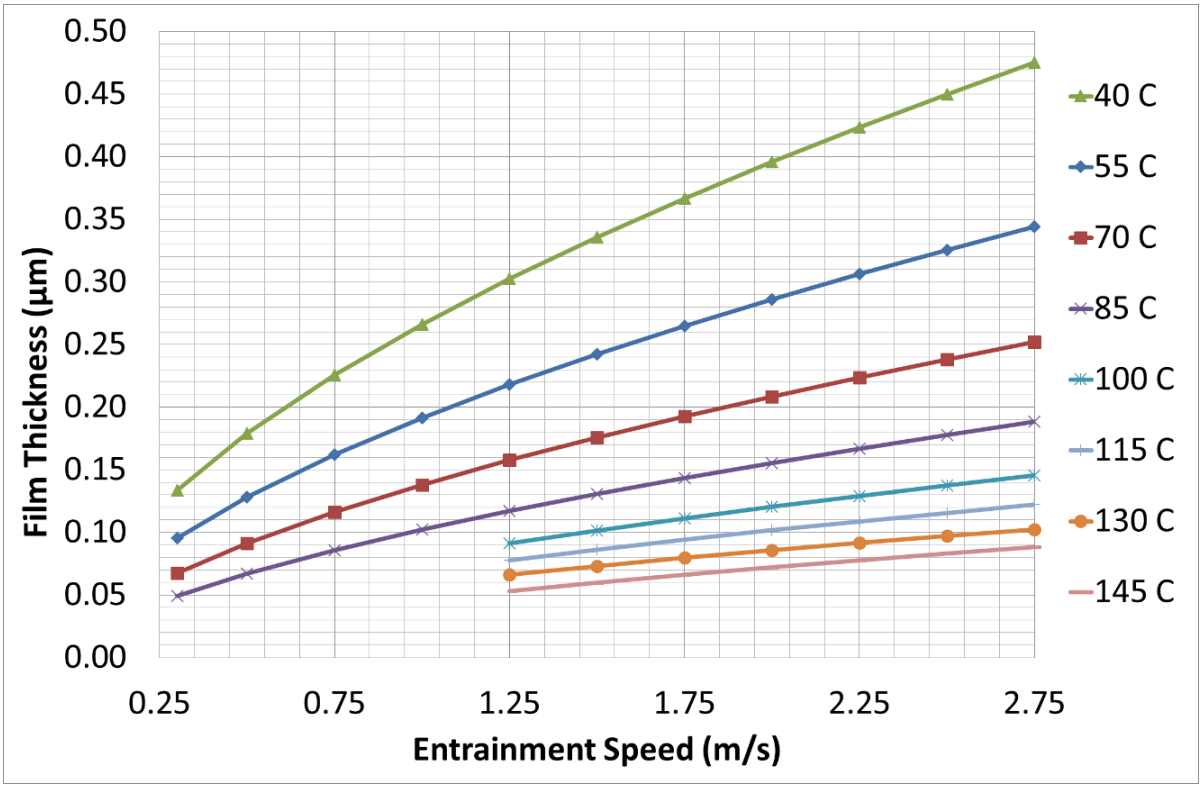



**Figure 4.9: The measured film thickness for oil A at 50% SRR**

#### 4.3.2.3 Extraction of rheological coefficients

In order to extract the required rheological parameters it is possible to fit any of the existing shear stress – shear rate relationships to the measured MTM and EHD data, as demonstrated by Spikes and Zhang[72]. In this study the Eyring model was chosen as appropriate. In parallel, the high shear rate viscosity is calculated using the temperature and pressure corrected Roelands equation. The resulting equation is the Eyring equation with the Roelands pressure and temperature influence on viscosity and can be written as:

$$\tau = \tau_0 \sinh^{-1}\left(\frac{\dot{\gamma}}{\tau_0}\eta_\infty e^{\left(log_e\left(\frac{\eta_r}{\eta_\infty}\right)\left(1+\frac{p}{p_r}\right)^z\left(\frac{T_r+135}{T+135}\right)^{S_0}\right)}\right) \quad (76)$$

Therefore, there are two parameters in this equation that need to be extracted from the fit to the measured data; the Eyring stress, $\tau_0$, and the Roelands parameter, z. The former directly affects the value of the friction coefficient while the latter should remain approximately constant for each lubricant as it is a lubricant characteristic.

It has to be noted that normally a thermal correction is applied to the shear stress versus shear rate curves, such as the ones shown in Figure 4.6, in order to account for the thermal effects

due to which result in the end portion of the curve creating a "tail". This is further explained in Spikes and Zhang[72]. In this case however, there was no need to apply a thermal correction, as there were enough points on the experimental results to obtain a good fit just from the straight portion of the shear stress versus shear rate curves. An example of the fit obtained using the aforementioned approach and the friction and film thickness experimental data for oil A at 145 °C and 20N load can be seen in Figure 4.10.

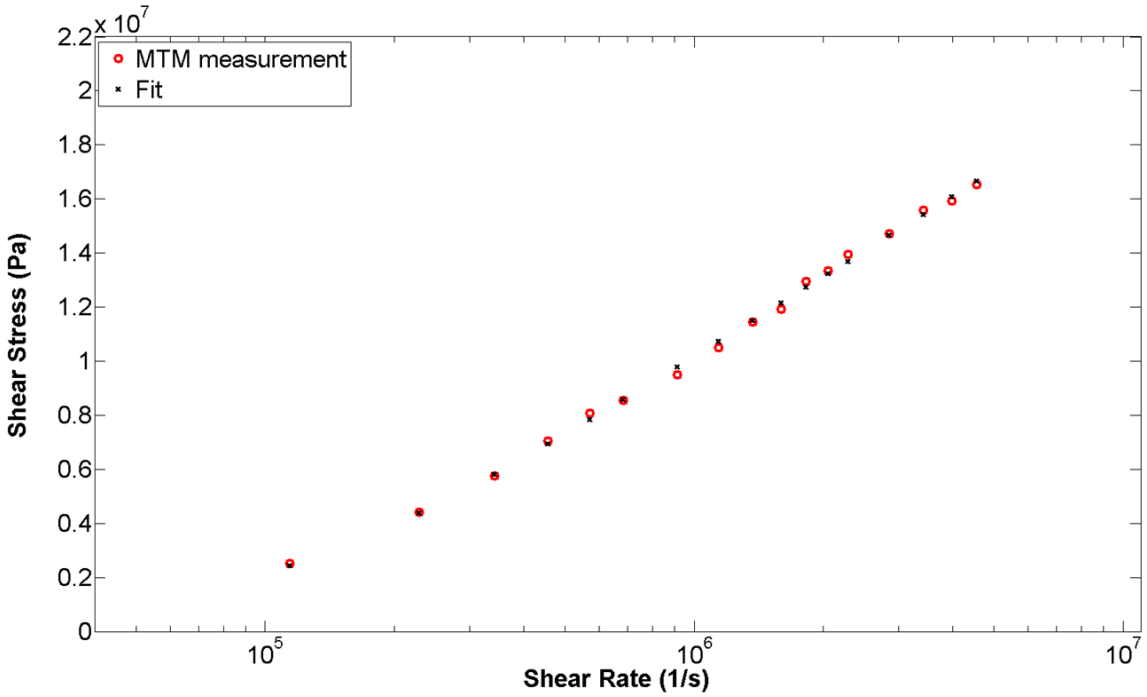



**Figure 4.10: The fit of the Eyring equation to the measured traction data for oil A at 145 °C and 20 N**

The variation of the Eyring stress with temperature and pressure for both lubricants can be seen in Figure 4.11-4.14;

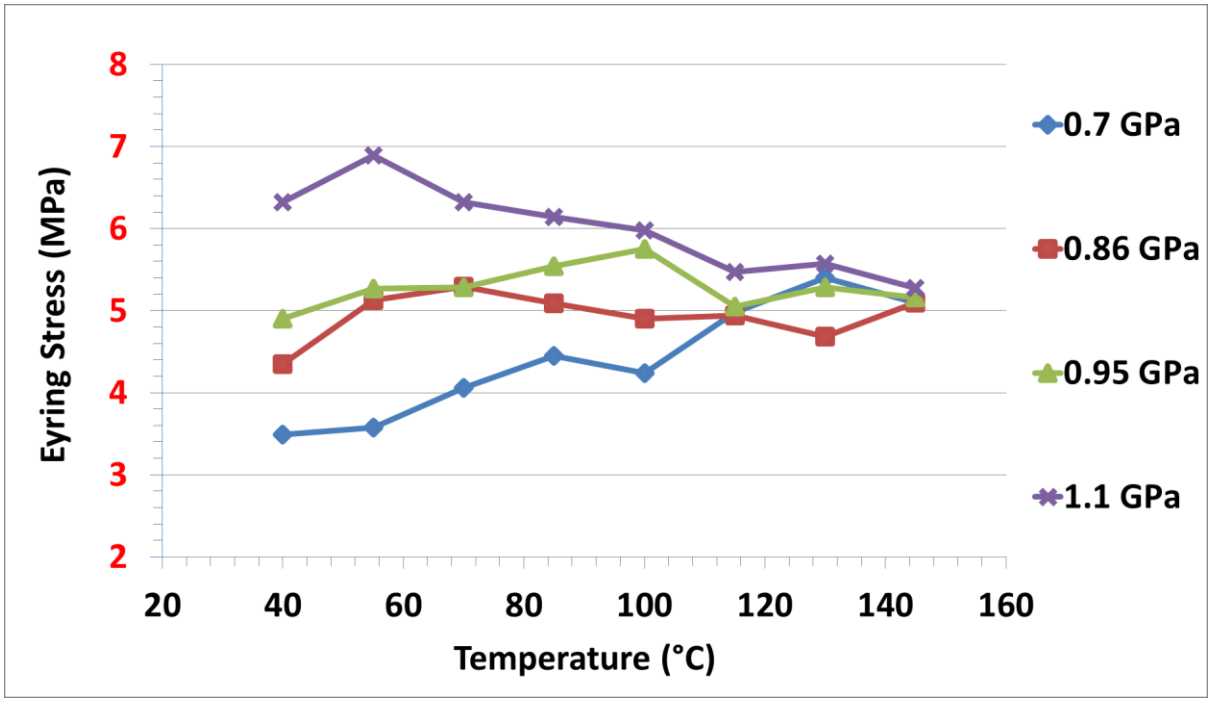



**Figure 4.11: Variation of Eyring stress with temperature (Oil A)**

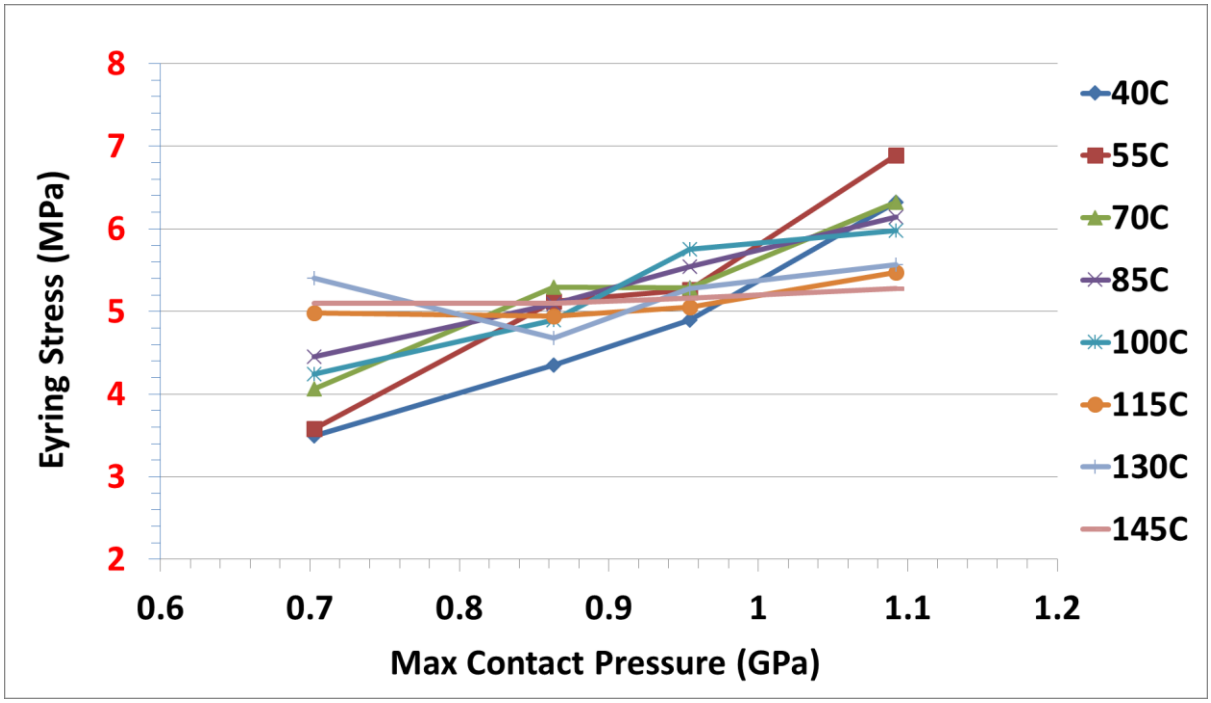



**Figure 4.12: Variation of Eyring stress with pressure (Oil A)**

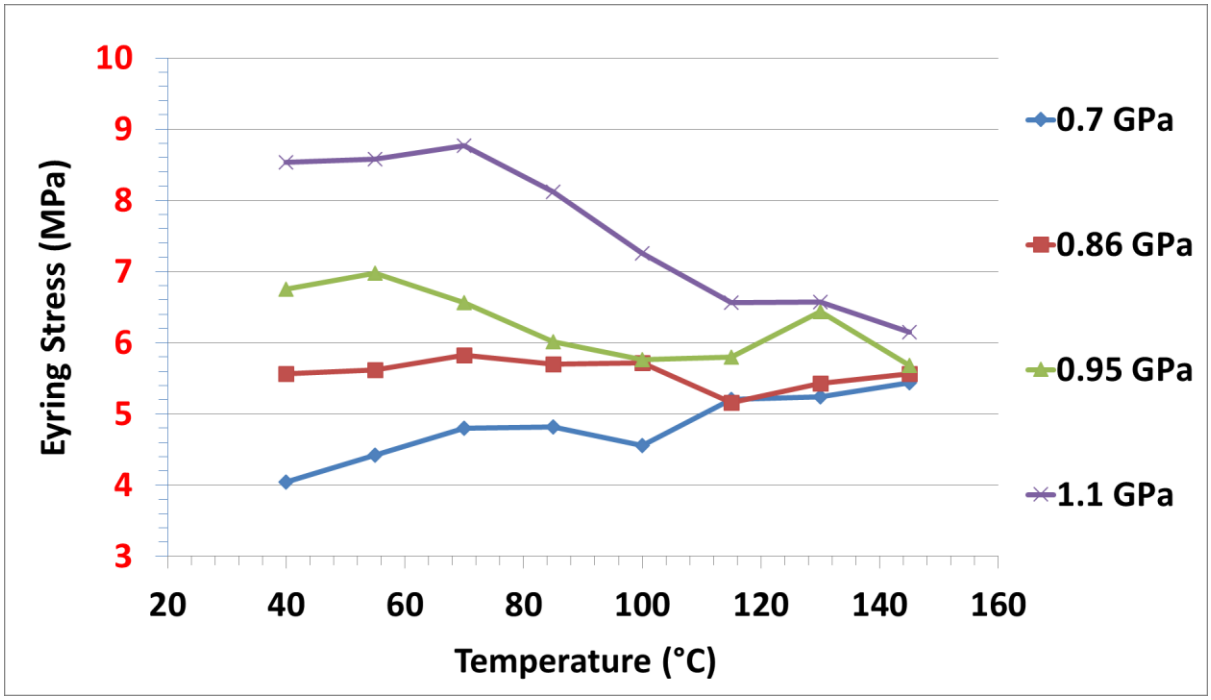



**Figure 4.13: Variation of Eyring stress with temperature (Oil B)**

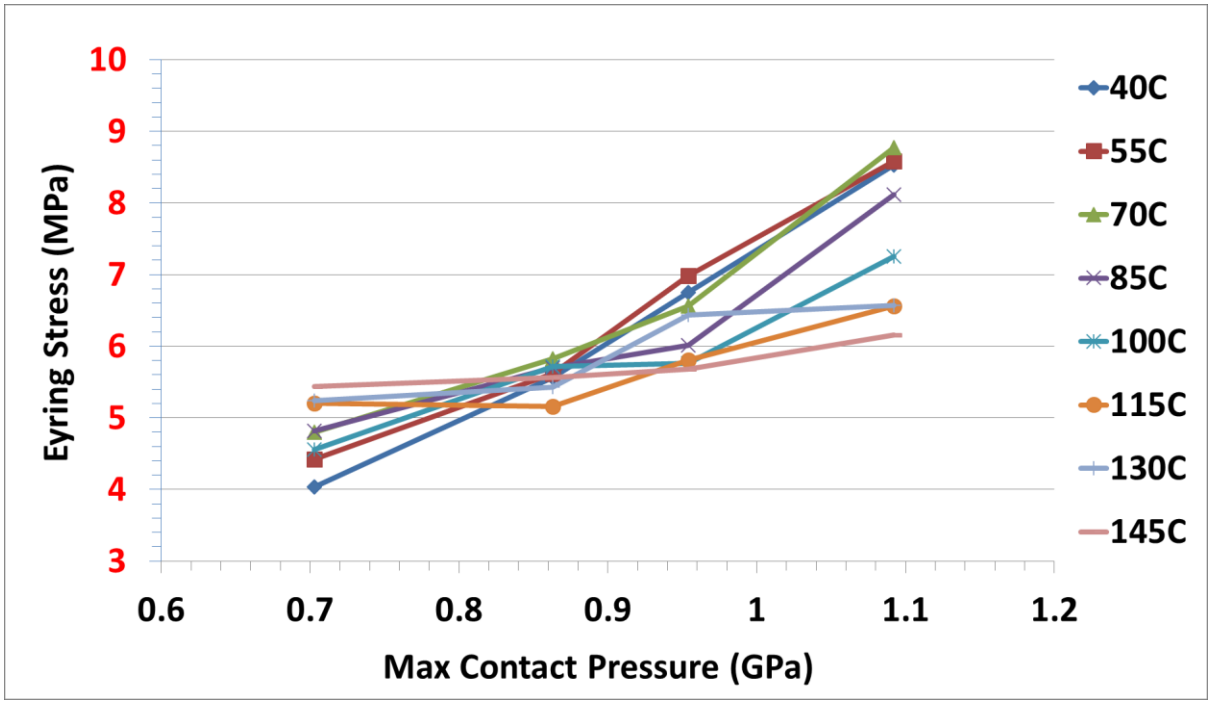



Figure 4.14: Variation of Eyring stress with pressure (Oil B)

The trend obtained for the pressure and temperature variation was roughly similar for both oils. However the absolute values of the Eyring stress obtained for Oil B was on average significantly higher than that of Oil A. The ascending linear dependency of Eyring stress on contact pressure showcased for some lubricants in previous studies ceases to exist at very high

temperatures where the value of the Eyring stress remains nearly constant. These trends and the difference between the two lubricants is the result of formulation differences between the two oils. Since details of lubricant formulation were not available from the manufacturer, further study of the formulation and separate assessment of the additives' effect on the shape of the obtained curves, which was outside of the scope of this study, is needed to explain these trends. Nevertheless, these results prove the importance of oil characterisation for any lubricant comparison study as depending on their formulation, lubricants can behave in completely different ways which are difficult if not impossible to predict solely based on analytical equations.

Representative values of the extracted coefficients for both oils over a range of temperatures and at the maximum contact pressure of 1.1 GPa can be seen in the Table 5. As would be expected, the z parameter is approximately constant with temperature while the downward trend for the Eyring stress with temperature is slightly more pronounced for lubricant B. The value for the Roelands z shown in the table is an average of the values obtained over the range of test temperatures; the deviation in obtained values was less than 5% at all conditions. Given the very small deviations of the value of z for a given oil, a value of 0.5 for oil A and a value of 0.54 for oil B will be used for all simulations in the current work.

**Table 5: Extracted rheological coefficients for Oils A and B at 1.1 GPa**

| Extracted Parameter | Oil A | | Oil B | |
|---|---|---|---|---|
| | 55 $^0$C | 145 $^0$C | 55 $^0$C | 145 $^0$C |
| Eyring stress | 6.9 | 5.3 | 8.6 | 6.2 |
| Roelands z | 0.50 | 0.49 | 0.54 | 0.54 |

It is worth noting that the observed Eyring stress trends where different for the two oils studied here, even though the oils are of the same SAE specification. Previous studies have also observed that Eyring stress values and trends are highly dependent on specific lubricant composition. The existence of this characteristic behaviour of each lubricant, combined with a plethora of gearbox oils available on the market, highlights the importance of accurate characterisation of lubricant frictional behaviour prior to any numerical predictions of gearbox efficiency that is envisaged to be able to differentiate between different lubricants. The work

presented here adopts this approach and should hence able to provide improved efficiency predictions compared to existing models.

### 4.3.3 Boundary friction measurements and its role in predicting the gear teeth contact friction

Most gear pairs operate under mixed to boundary lubrication conditions, due to the high values of surface roughness, resulting from common manufacturing processes, in relation to prevailing film thickness. Consequently, any prediction of friction coefficient along the contact path, must account for the metal-to-metal contact that occurs in mixed and boundary lubrication, rather than just the full film EHL friction, as considered above. To achieve this in the present model, an empirical formula suggested by Olver and Spikes[96] is used. This predicts the effective friction coefficient by introducing the boundary friction coefficient for the boundary regime on the one extreme, and the fluid friciton coefficient for the full film regime on the other extreme, and uses an interpolation between these two values, dependent on the prevailing lambda ratio, to predict the friciton in the mixed regime. The relationship is:

$$\mu = \mu_f + \frac{\mu_b - \mu_f}{(1+\lambda)^m}$$

Where $\mu_b$ is the boundary friction coefficient which is the highest value that the friction coefficient obtains when all the load is carried by the material's asperities, $\mu_f$ is the fluid friction coefficient which is the value when all the load is carried by the lubricant itself and $\lambda$ is the ratio of the minimum film thickness, $h_0$, to the compound surface roughness of the materials, $R_{qc}$.

The validity of this relationship was recenlty confirmed by Guegan et al who measured friction coefficient in EHL contact for a range of rough surfaces covering all three lubrication regimes.

To represent gear teeth contacts as accurately as possible, the current study utilises this expression for the efective friciton coefficient. Instead of a common assumption that the boundary friction is about 0.1 to 0.15 as used in other studies, the boundary frcition for the lubricants cosidered here is measured using the MTM rig. These measured values are then used together with the fluid film friction, predicted as described above, to provide friction prediction anywhere along the path of contact for any imposed operating conditions and surface finishes. Since one of the aims of this study is to be able to differentiate between different oils of the same SAE grade in terms of their influence on gearbox power losses, knowledge of the

boundary friction for each lubricant is obviously important, since oils of the same SAE grade may have very different additive pacakges and hence very different boudary friction values. The MTM rig is capable of measuring friction in boundary conditions by operating at low speeds and/or by using relatively rough disc specimens. The standard ball and disc specimens have a very low combined roughness with the steel ball measuring a maximum roughness value Ra of 20 nm and the disc a maximum Ra of 10 nm. Therefore, the combined roughness of the MTM specimens was increased so that the boundary friction regime is extended to higher speeds and is clearly visible on the Stribeck curve. This was achieved by roughening the surface of the MTM discs to obtain a combined roughness ($R_{qc}$) of around 180 nm. The roughness of the discs was measured at 4 different locations on the discs using a Wyko white light interferometer and an average value of 180 nm obtained.

Using the rough discs, MTM friction Stribeck curves were obtained for the two lubricants over a range of SRR ratios. The obtained friction values were very close, within 6% of each other. Nevertheless, the mean value for the boundary friction coefficient was used in further calculations. Representative measurements can be seen in Figure 4.15 for conditions of 40 $^0$C, 0.86 GPa and 50% SRR. The use of a rough disc effectively shifted the boundary and mixed friction regimes to higher rolling speeds and it was therefore possible to obtain a relatively accurate mean boundary friction coefficient for lubricants A and B, which was 0.116 and 0.125 respectively. As is evident in the figure the measured friction coefficient was practically constant at lambda values below 0.2 and the mean value for the boundary friction coefficient was obtained from the last 6 points. These values were integrated into the EHL code providing an important additional differentiating factor between the two oils considered here. If other oils are to be used in the model, these measruemts would have to be repeated, together with those for extraction of rheological constants described above.

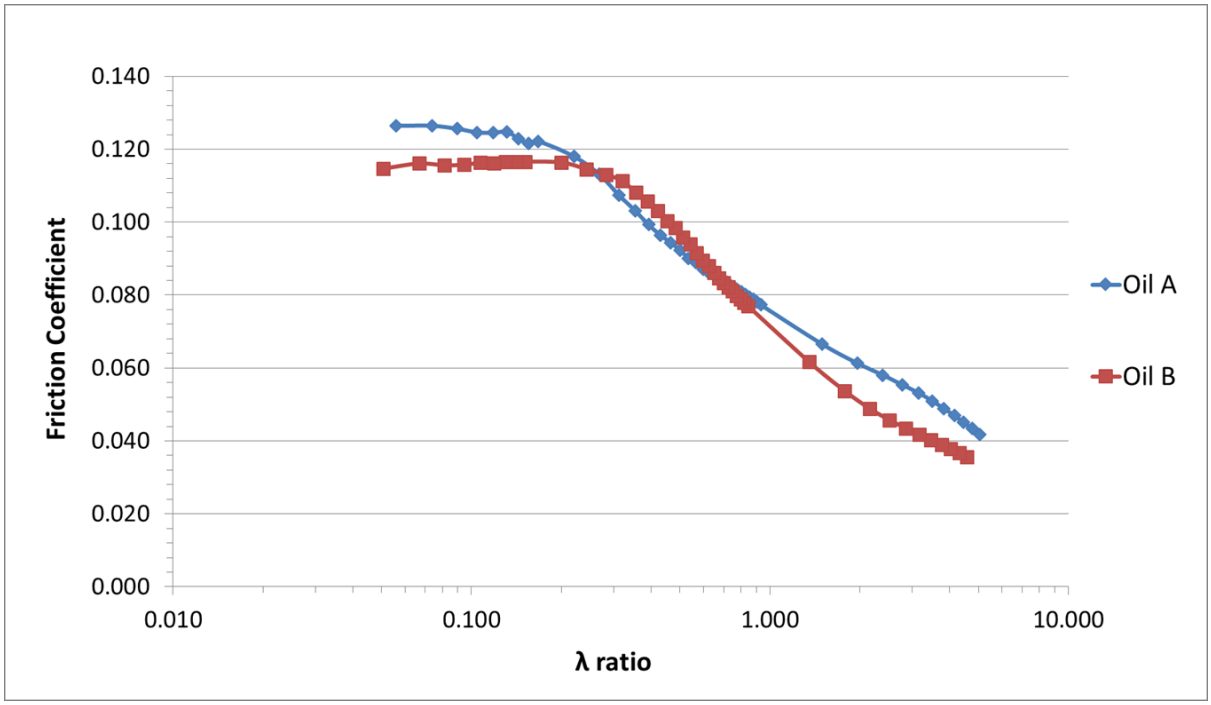



**Figure 4.15: Stribeck curves of the two lubricants using rough specimens at 40 °C, 0.86 GPa, 50% SRR**

Once the coefficients are extracted, a database of the values of the Eyring stress can be constructed and then any value within the range can be interpolated; the pressures were also extrapolated to 1.5 GPa. The matrix of values can then be fed back into the EHD traction model to improve the accuracy of the calculations.

### 4.4 Summary

In this chapter, the experimental procedure for the characterisation of the test lubricants has been outlined. Experimental equipment and associated experimental procedures used for this purpose were first described. The procedure used to extract the necessary rheological parameters needed for the implemented Eyring model, namely the Eyring shear stress and the Roelands z coefficient, is then described and applied to the obtained experimental data. Finally, the procedure for measuring the boundary friction coefficient for the two lubricants was presented and the way in which this was combined with the full film EHL traction predictions to obtain the effective friction coefficient for all conditions and gear surface finishes is described. The introduction of these lubricant properties on the loss prediction model shown in this study is of crucial importance, as it allows for the model to differentiate between the same grade gearbox oils in terms of their influence on gearbox efficiency, which is one of the

important improvements offered by the present model over other approaches for predicting gearbox losses.

# 5. MODELLING RESULTS: SINGLE STAGE GEARBOX

## 5.1 Introduction

In this chapter, the results from the modelling of the EHL contact in a gear pair are presented. The EHL model described in Chapter 3 is combined with the results of the lubricant characterisation tests and used to predict efficiency and temperatures along the contact path of the gear teeth. The model will also be used to study the effect of roughness on the power losses and study the effect of specific lubricant properties on gear friction losses over a range of operating conditions. The additional losses due to lubricant churning, bearings and seals are incorporated in the model and a comparison of the two lubricants in terms of overall gearbox efficiency is shown. Further comparisons to illustrate the relative contribution of different loss sources at different operating conditions are also presented. Finally, a parametric study to show the effect of bearing selection, lubricant rheology (viscosity, Eyring stress, Roelands coefficient and boundary friction coefficient) as well as multiple aspects of gear geometry will be undertaken.

## 5.2 Modelling of gear teeth contact losses in an example spur gear pair

The geometry of a set of gears is readily derived following design procedures provided by international gear standard bodies such as British Gear association (BGA)[160] or American Gear Manufacturers Association (AGMA). Such a design procedure ensures that the gear sizes, for the selected material, are sufficient to carry the tooth contact stresses and bending stresses imposed by the transmitted torque. The resulting gear parameters are the module, gear diameters, facewidth (and hence facewidth ratio), tooth numbers, profile shifts of pinion and wheel, helix angle (if helical gears are chosen) and any profile reliefs needed to minimize transmission error. Such procedure was initially performed in this study to obtain a set of gears that are able to carry maximum torque from a specific internal combustion engine, given that an automotive gearbox is of interest in this study.

However, given that the current efficiency model is designed to be applicable to arbitrary geometry spur gears, it was decided to use a gear geometry for which published experimental power loss results exist, so that comparison of model predictions and those experimental results can be made, at least in terms of general trends (since different oils and lubrication systems are used in published data, no direct comparison is possible). Hence, the set of spur gears for the study presented in this chapter were selected to be of identical geometry to the gear pair used in the experimental study of Petry Johnson[127]. Similarly, the centre distance, the gear ratio of

1:1 and the surface finishes are those used in the same experimental study. The characteristics of the selected gear pair are shown in Table 6.

As can be seen, the facewidth ratio is just over 0.2, which quite narrow, though not untypical in automotive gearing. The bearings and shafts were designed considering the lifecycle of a light commercial vehicle which is equivalent to 10 years of average use or around 11000 hours. The resulting simple 1:1 gearbox consists of two spur gears, four sealed bearings and two similar shafts enclosed in a rectangular casing. The casing dimensions were selected so that the gears can have a radial clearance of two times the normal module which is considered adequate to exclude any enclosure effects regarding churning losses, while the axial clearance was set to be equal to the module of the gears, a value that has been experimentally proven to reduce churning losses[83].

**Table 6: The basic geometric characteristics of the gear pair**

| Parameter | Value |
|---|---|
| Normal module (mm) | 3.95 |
| Number of teeth | 23 |
| Gear Ratio | 1:1 |
| Reference Diameter (mm) | 90.9 |
| Profile shift, $x_1$ and $x_2$ | 0 |
| Base Diameter (mm) | 82.3 |
| Root Diameter (mm) | 81.0 |
| Tip Diameter (mm) | 98.8 |
| Start of active profile (mm) | 85.9 |
| Face width (mm) | 19.5 |
| Centre distance (mm) | 91.4 |
| Pressure Angle (deg.) | 25 |
| Tooth Roughness Rq (compound), nm | 430 (ground) |

The gearbox includes two bearings per shaft, selected to be deep groove ball bearings sealed at one side and lubricated by the splashing of the lubricant inside the gearbox as is typical for these applications. As mentioned above, the operational life was chosen to be 11000 hours, considered adequate for a light commercial vehicle, which corresponds to a 3 hour use per day over the course of 10 years. The bearing design load was selected to be 60% of the maximum load with the bearings continuously operating at 1700 rpm and at a maximum temperature of 80 $^{0}$C. The bearings were then sized according to the standard bearing life equations to give $L_{10}$ life above the lifetime quoted above. Following these procedures, 6307 RS1 single sealed deep groove ball bearings (DGBB) were selected for this example study. The choice of two DGBBs for each shaft is somewhat arbitrary here, and gearboxes more commonly employ one DGBB and one floating cylindrical roller bearing (CRB). The present model can incorporate any bearing type, provided that Morales' bearing friction model[115] can be applied to it, and the use of two DGBB bearings was considered desirable for simplicity and is perfectly appropriate for this example study. The shafts were designed for the maximum load using Von Misses criteria and their diameter has been set at 35 mm which corresponds to the bearing inner ring diameter and is well above the minimum shaft diameter given the shaft loads. A schematic of the simulated gearbox is shown in Figure 5.1.

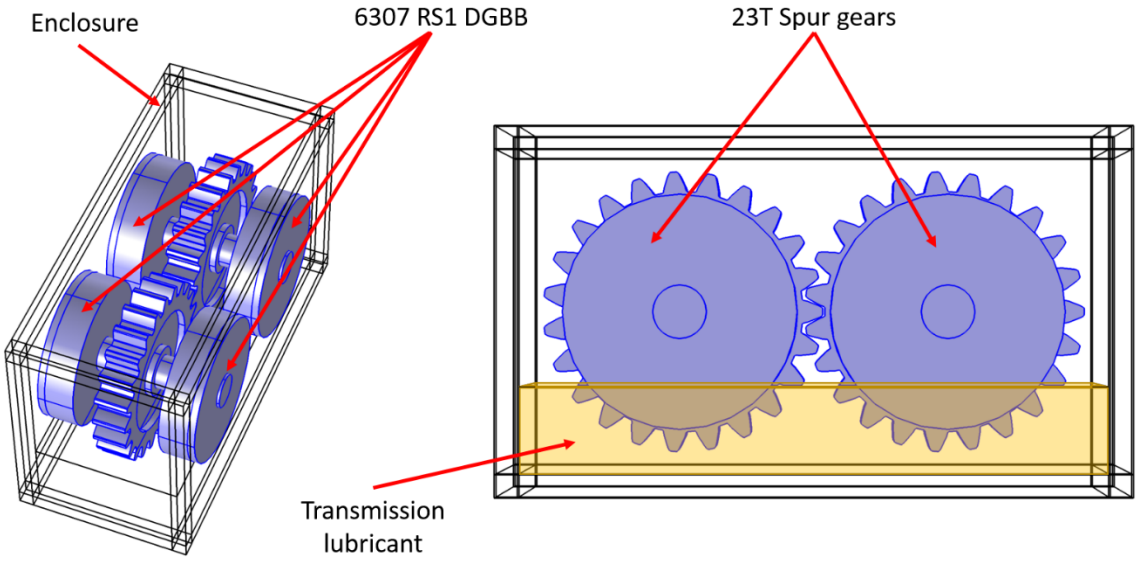



**Figure 5.1: The components and layout of the simulated single stage gearbox**

### 5.3 Gear teeth contact calculations

Using the above inputs, the efficiency and contact temperatures were calculated along the contact path of the gear pair for lubricant A at an input torque of 640 Nm, an average oil sump

temperature of 65 $^0$C and a rotational speed of 1250 rpm. Figure 5.2 shows the load profile, contact pressure and slide roll ratio of the gear pair along the contact path. The total load shared by the two gearbox shafts is in the region of 15 kN, which results in a peak contact pressure of around 1.7 GPa, a typical value for a loaded gear pair made of case carburised steel. The slide roll ratio varies from 0.75 at the first point of the contact path to 0 at the pitch point where teeth operate in pure rolling conditions. At the same time, the profile of the slide roll ratio is symmetric given the gear pair geometry and of 1:1 gear ratio.

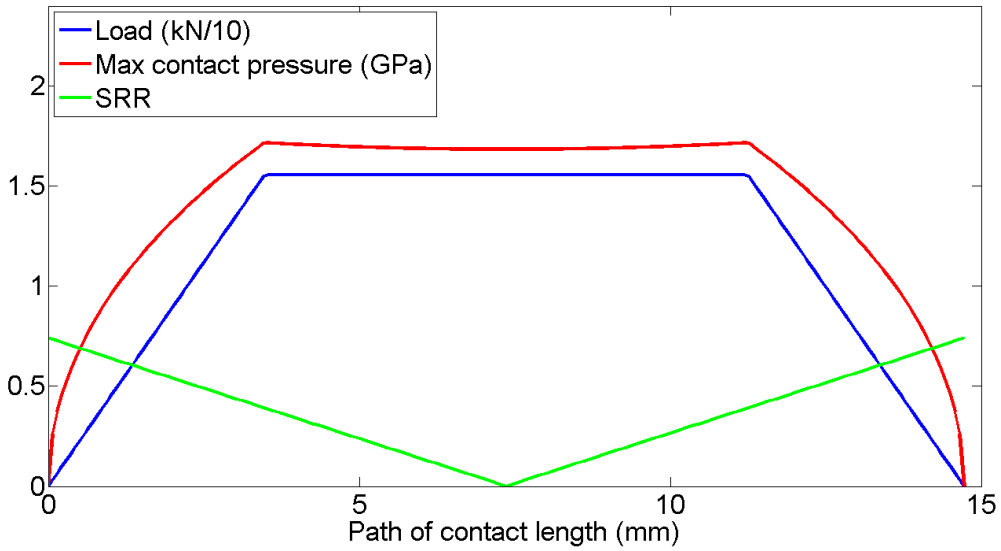



**Figure 5.2: The load and calculated Hertzian maximum contact pressure and slide roll ratio along the path of contact for the specified gear pair and loading**

Figure 5.3 shows the predicted friction coefficient, the evolution of the mean EHL film temperature as well as the lambda ratio. The friction coefficient rises to a maximum value of 0.0593 at 6.95 mm along the contact path while the peak mean film temperature rises to a maximum of over 120 $^0$C. The lambda ratio is 0.6 on average and the minimum film thickness is very low at less than 0.3 μm. As the friction coefficient incorporates the surface roughness, it rises very rapidly because of the high amount of sliding and the very low film thickness while, as expected, it becomes zero at the pitch point because of the pure rolling condition. The average value is around 0.06 which is considered typical of gear teeth contacts. The mean film temperature inside the EHL contact also exhibits a rapid rise as the contact progresses from the first point of contact further into the contact path, and reaches the maximum near the lowest and highest points of single pair contact (LPSPC and HPSPC respectively). The film thickness varies less as it is calculated at the temperature of the contact inlet (bulk tooth temperature) and

the assumption of the average bulk temperature which does not change during contacts progression along the contact path has been adopted as explained in Chapter 3.

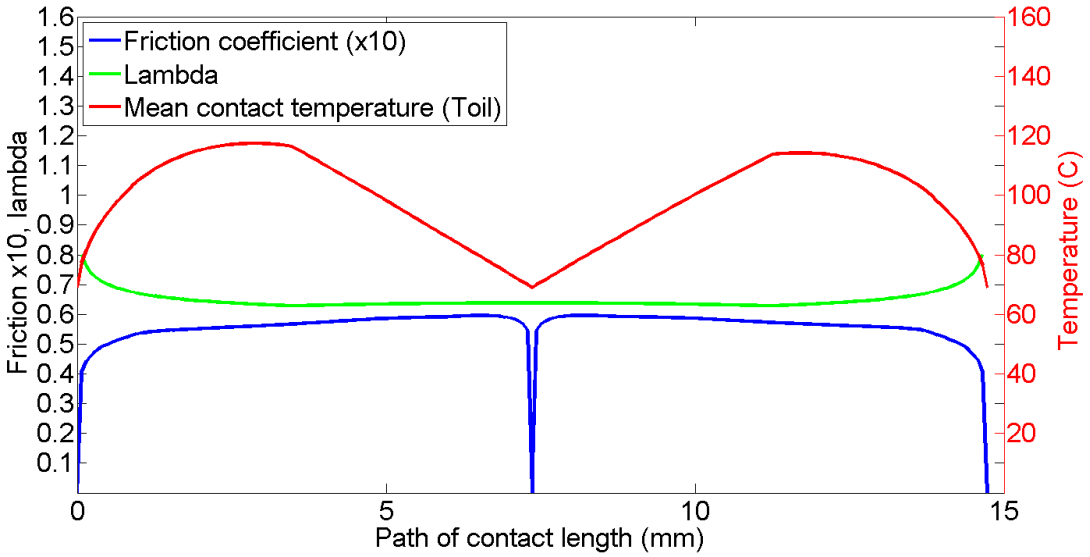



**Figure 5.3: The coefficient of friction, lambda ratio and mean film temperature along the path of contact**

Finally, the dissipated power is calculated and consequently, the efficiency of the gear pair can be evaluated at every point along the path of contact, as is shown in Figure 5.4. The average efficiency over the path of contact is calculated to be 99%, a value that may be expected for a spur gear pair. The minimum efficiency is just under 98.5 % and efficiency is 100% at the pitch point due to pure rolling conditions.

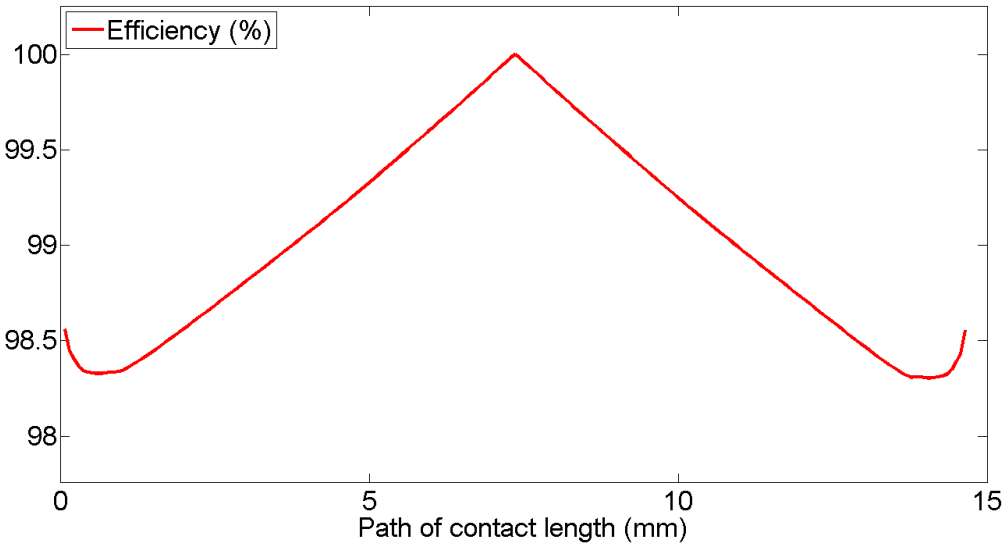



**Figure 5.4: The efficiency of the gear pair along the contact path**

### 5.4 Effect of roughness on gear contact losses

In a very broad range of applications, not least high volume automotive applications, it is usually not economically viable to have gears manufactured to a high quality, low roughness surface finish. Since the current model incorporates the effects of surface finish on gear EHL losses, it is worth investigating its effect on overall mesh efficiency. In order to achieve this, the model was run for two surface finishes and over a range of torque inputs while keeping the rotational speed constant and for a range of speeds while keeping the torque input constant. The roughness values that were used were chosen to correspond approximately to the ground gear finish as well as a finish that may be achieved by means of chemical polishing of the gears. The combined Rq roughness of 430 nm for the ground gears and 113 nm for chemical polishing were used. The employed Rq values are those used in Petry Johnson et al.[127]. A range of gear speeds, from 1250 rpm to 8000 rpm, was used while the input torque was varied between 140 Nm and 640 Nm. Figures 5.5 and 5.6 show how the gear EHL losses vary in both cases.

It can be observed that the losses increase roughly linearly with speed and torque, which means that the actual efficiency (losses divided by the product of torque and speed) remains relatively unchanged over this range of conditions. However, there is a clear difference between the two roughness values with the chemical polishing resulting in a very significant relative reduction of losses of more than 30% across the torque and speed range. The trend is very similar both for speed and torque and the results are in very good agreement with the experimental results of Petry Johnson et al. using the same inputs. This improvement offered by the super finished gears indicates that the studied gears operated with relatively low lambda ratios, as is the case for most gearing applications, which in turn means that a lubricant able to either increase the film thickness (higher viscosity) or provide low boundary and mixed lubrication friction coefficient (better additive package) would result in improved gearbox efficiency.

It has to be noted that since gears are ground and they routinely operate in the mixed lubrication regime, their actual surface roughness will change during their operational life, especially so after the initial wear in. Effectively, this means that the surface roughness is expected to reduce, something that would in turn have an effect on the power losses.

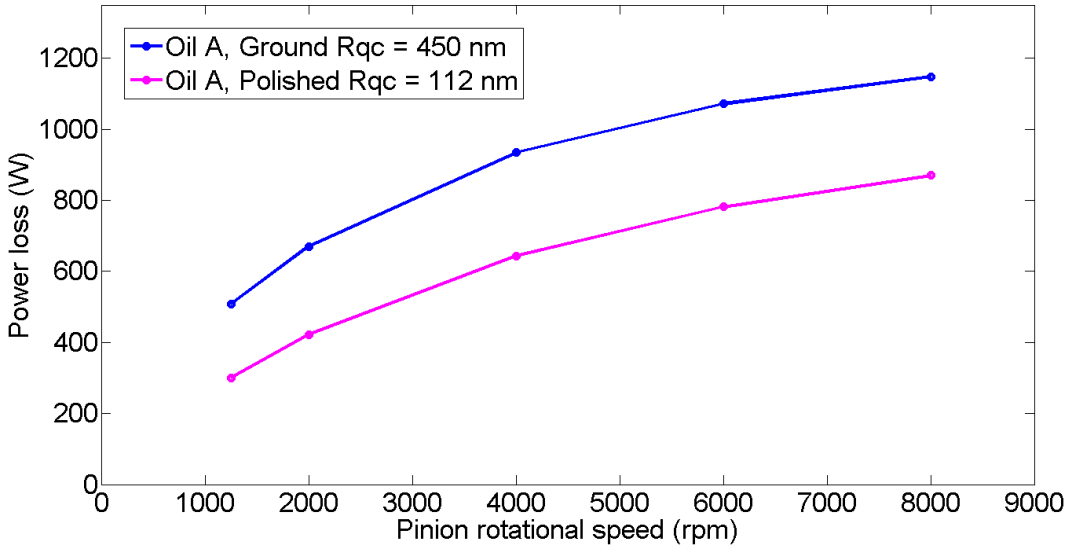



**Figure 5.5: Predicted gear friction losses variation with rotational speed for ground and polished surface finishing at 65 °C and 640 Nm**

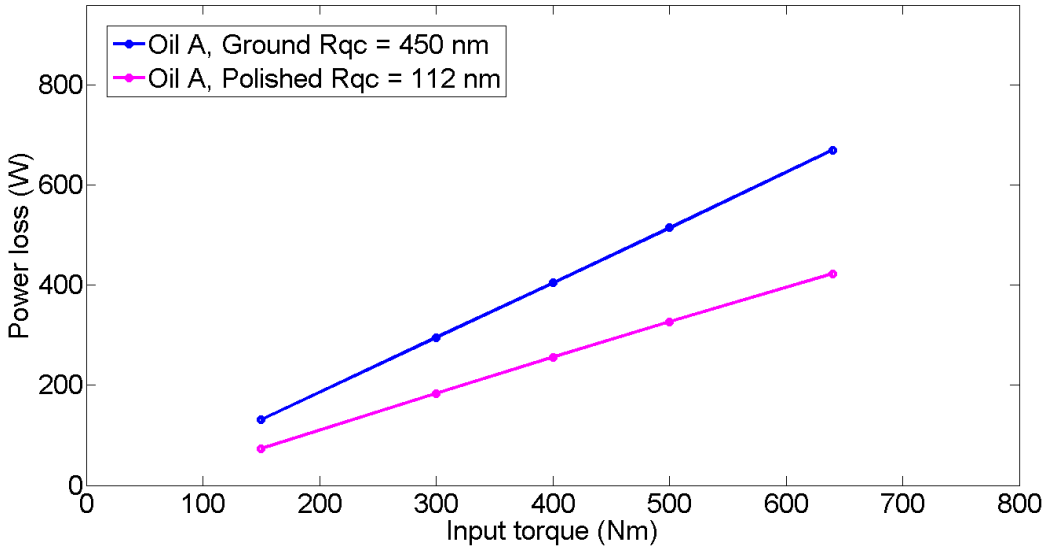


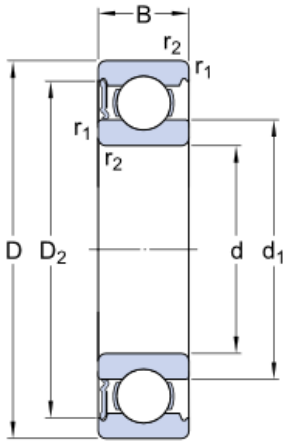

**Figure 5.6: Predicted gear frictional losses variation with input torque for ground and polished surface finishing at 65 °C and 2000 rpm**

## 5.5 Modelling of additional losses

### 5.5.1 Bearing and seal losses

The losses in the bearings and seals as well as those due to churning are now considered and their contribution to the overall losses relative to the EHL gear losses, studied above, is considered over a range of conditions. Regarding bearing and seal losses, the model which has

been used is according to Morales[115] as described in detail earlier in the thesis. The selected 6307 RS1 single row DGBB's were modelled under the same torques, speeds and sump temperatures as the gear EHL losses above. The basic geometric characteristics of the bearings can be seen in Figure 5.7[161]. The basic dynamic load rating is 35.1 kN, the basic static load rating is 19 kN, while the limiting speed is 6000 rpm, well above the currently imposed conditions.




| | | | |
|---|---|---|---|
| d | | 35 | mm |
| D | | 80 | mm |
| B | | 21 | mm |
| $d_1$ | ≈ | 49.56 | mm |
| $D_2$ | ≈ | 69.2 | mm |

**Figure 5.7: The basic geometry of the 6307 RS1 bearing (SKF)**

The losses of the bearings were calculated at 65 $^0$C and assuming that the bearings are dip lubricated, with an oil immersion depth of 20 mm. This higher than usual immersion depth was chosen with the assumption of the gears operating at an immersion depth of 6mn; in that case and given the dimensions of the bearings, their corresponding immersion depth would be 20 mm.

The selected bearings are lubricated by the oil bath in the gearbox and they are sealed on one side. Seal-shaft contacts can contribute significantly to the overall losses, Although the seal losses are generally included into the overall bearing losses in the predictive tools provided by the bearing manufacturers, in this study the individual contribution of seal losses, separate from bearing losses, was calculated. The seal losses were deduced by comparison of predicted bearing losses for a sealed and non-sealed open bearing of the same designation (6307), again using Morales bearing loss model[115] as implemented by SKF, major bearing manufacturer. The radial load on each shaft bearing is easily calculated from the tooth load and geometric considerations (gears are centrally straddle-mounted so the 15 kN tooth load is shared equally by the two shaft bearings). It should be noted that because of the type of bearing selected and

the use of spur gears, no axial pre-load was applied to the bearings in this study. Presence of any axial pre-load would increase the total bearing losses substantially. Bearing losses have been calculated for a set of torque and speed conditions and both oils A and B, as shown in table 7 below. The same conditions are used later to compare individual loss contributions in the whole gearbox. As is evident in the table, the combined losses of the bearings and seals at 65 °C for the lubricants were almost identical and ranged from 14 W in low load condition 1, to 95 W in high load condition 5; the insignificant difference which is less than 2% is mostly due to the variation in the viscosity index of the lubricants. Table 6 below shows the losses for the selected bearings with the seal losses isolated.

**Table 7: The predicted bearing and seal losses**

| Condition | Load (kN) | Bearing loss per bearing (excluding seal loss) (W) | | Seal loss per bearing (W) | |
|---|---|---|---|---|---|
| | | Oil A | Oil B | Oil A | Oil B |
| 1 | 4.85 | 9 | 9 | 5 | 5 |
| 2 | 7.76 | 31 | 31 | 9 | 9 |
| 3 | 9.7 | 54 | 55 | 11 | 11 |
| 4 | 8.97 | 76 | 76 | 16 | 17 |
| 5 | 7.76 | 82 | 83 | 13 | 13 |

### 5.5.2 Gear churning losses

As described in the previous chapters, churning losses have been calculated using an experimentally derived model of Changenet and Velex[110], which uses two formulae to calculate the churning torque. This model was already described in section 3.3, so only the results will be presented here. Figure 5.8 below shows predicted churning losses for 2 immersion depths (equal to 3 x module and 12 x module) and oils A and B, over a range of gear speeds. Immersion depth of 12 x module is a hypothetical case as in practical applications the immersion depth would not exceed 6 x module. The transition in churning loss trends is clearly visible between 2500 rpm and 4000 rpm which corresponds to a critical Reynolds number of 6000 and 9000 respectively. Changenet and Velex provide different empirical formulae for the two ranges of

the Reynolds number and hence the observed transition is expected. Regarding the two oils, it is clear that the higher viscosity of oil B gives higher churning losses compared to oil A. The effect of rotational speed is the most significant and if this is coupled with higher immersion depths it can lead to the churning losses comprising upwards of 30% of the total power losses, while the reverse is true for lower speeds and/or shallow immersion depths.

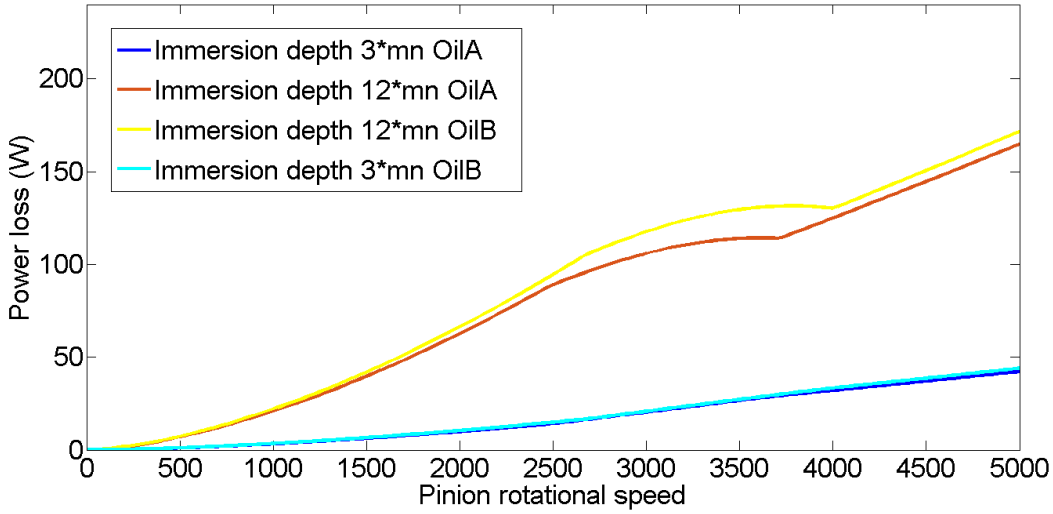



**Figure 5.8: The predicted churning losses of the modelled gear *pair* (i.e. combined loss for both gears) at 65 $^{0}$C for both lubricants at two different immersion depths.**

## 5.6 Lubricant comparison

### 5.6.1 Comparison of fully formulated oils

In order to investigate the effect of lubricant properties on EHL power loss and therefore on efficiency, the model was run for a set of conditions selected to correspond to various points on the wide open throttle (WOT) torque curve of a sample diesel engine, a 6.7 L Cummins I6 turbo diesel engine which generates a maximum output torque of 900 Nm. Therefore, the torque and rotational speed inputs for the gear pair which were used for the design of the bearings and shafts were based on the above specifications. It should be noted that the choice of this engine is not arbitrary, as it was the engine installed in the vehicle for which the full gearbox efficiency study was performed, as presented later in this thesis. Although not necessary, it was thought wise to use the same range of torques for the study shown in this chapter too, so that the stability of the model over the correct range of loads and speeds can be confirmed.

Lubricants A and B were then compared under the scope of efficiency to highlight potential differences. The chosen set of conditions is summarized in Table 8. In addition, the results presented in this section are with an initial oil sump temperature of 65 °C and a roughness value corresponding to a ground gear finish (Rqc=430 nm) unless otherwise indicated.

**Table 8: Operating conditions for lubricant comparison shown in this section**

| Condition | Input torque (Nm) | Gear rpm |
|---|---|---|
| 1 | 400 | 650 |
| 2 | 640 | 1250 |
| 3 | 800 | 1600 |
| 4 | 740 | 2300 |
| 5 | 640 | 2800 |

Firstly, the lubricants are compared in terms of gear contact friction losses only, i.e. excluding the bearing, seal and churning losses. This comparison is shown in Figure 5.9.

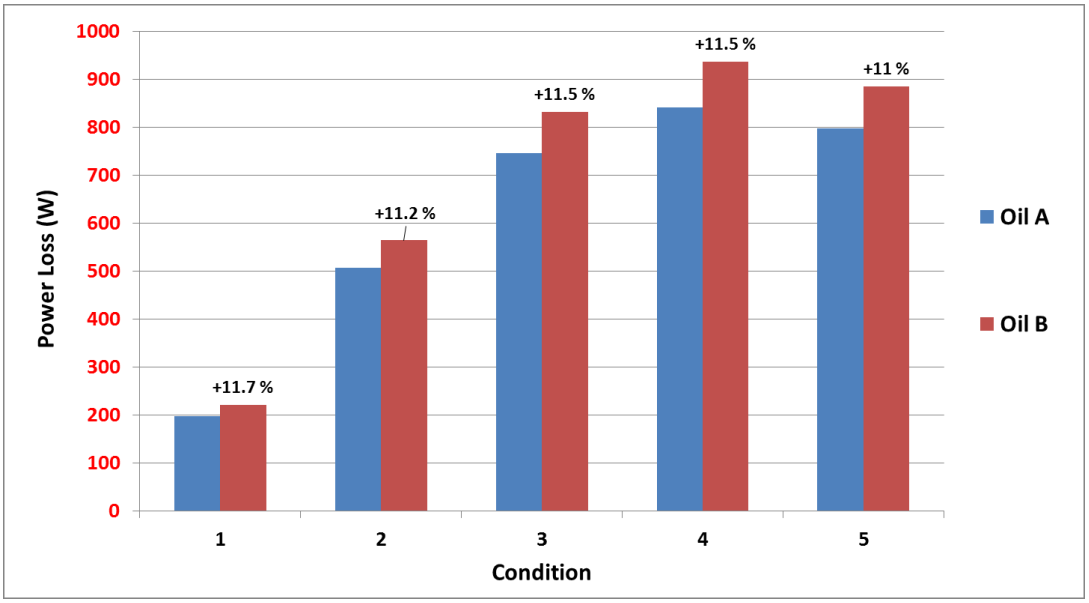



**Figure 5.9: The power loss of the gear pair for lubricants A and B when only gear friction is considered (the quoted percentages indicate the increase in losses with oil B relative to oil A) for a sump temperature of 65 °C and ground surface roughness (430 nm)**

The results highlight that there is a pronounced difference in generated power loss between the two lubricants even though they both have the same nominal SAE grade. The percentage increase in power loss with oil B relative to loss with oil A ranged from 11% to 11.7% in all conditions. The difference in the two oils in terms of overall efficiency of this single gear mesh, is shown in Figure 5.10. The overall efficiency difference ranges from 0.05% to 0.09%. While this may appear small, it is nevertheless significant especially considering the fact that this is only a single gear pair and that in a multi-gear, multi-stage transmission system such as an automotive or heavy duty gearbox, these numbers would be multiplied for each stage and gear pair making the difference between the two lubricants much more important in terms of power loss and efficiency. As far as absolute numbers are concerned, the range of efficiency, just over 99%, seen here is very much in agreement with what would be expected from a typical spur gear pair.

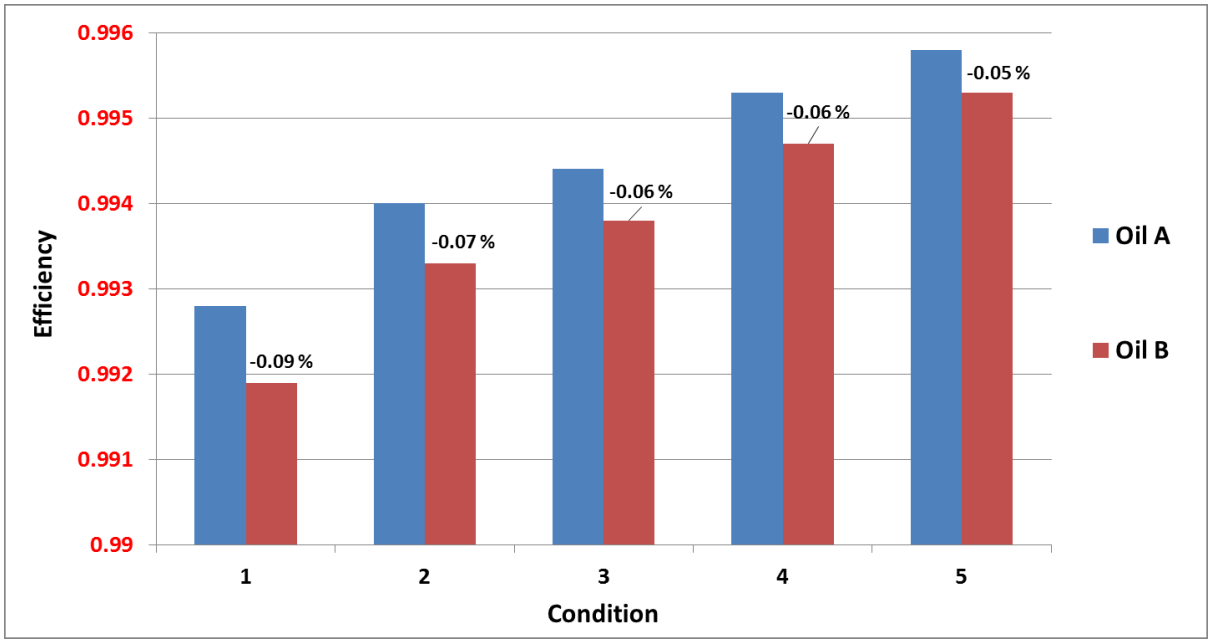



**Figure 5.10: The efficiency of the gear pair for lubricants A and B when only gear friction is considered (the quoted percentages indicate the drop in efficiency with oil B relative to oil A) for a sump temperature of 65 °C and ground surface roughness (430 nm)**

This initial comparison above was created to highlight the differences that arise from the inclusion of the extracted rheology coefficients namely the Eyring stress, the Roelands coefficient, and the effect this has on high pressure viscosity, as well as the boundary friction coefficient. These results however do not include the additional losses due to bearings and churning and compare just gear friction. When churning, bearing and seal losses are included,

the difference between the lubricants will change as will be shown next. The full gearbox efficiency model is obtained by combining the individual gear EHL, bearing, seal and churning predictions outlined in this thesis. The model is now used to study the effects of lubricant on gearbox efficiency. The aim is to establish whether or not it is able to differentiate between the two lubricants and also to assess the relative contribution of the individual losses at different gearbox operating conditions. Figures 5.11 and 5.12 show the same comparison with churning loss included at an immersion depth of 6mn and bearing and seal losses included for the selected 6307 RS1 DGBB.

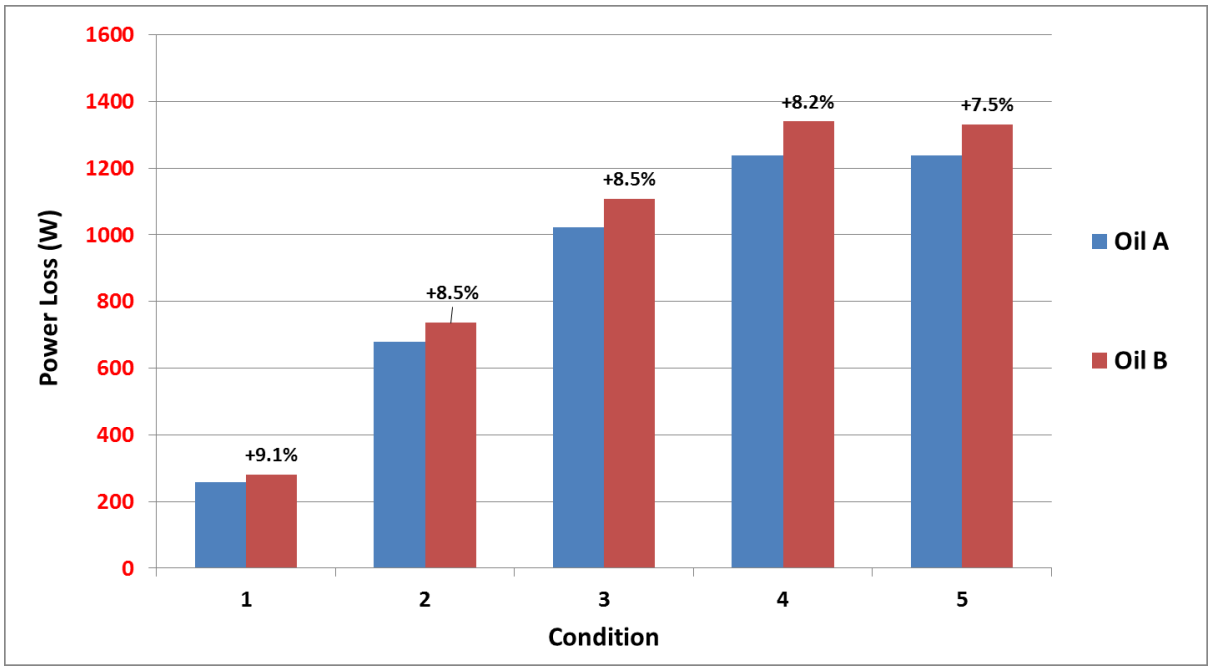



**Figure 5.11: The power loss of the gear pair for lubricants A and B when gear friction, bearing, seal and churning losses are included (the quoted percentages indicate the increase in losses with oil B relative to oil A) for a sump temperature of 65 °C and ground surface roughness (430 nm)**

Compared to the previous figures, where only gear losses were included, the same ranking, with lubricant A being more efficient than B remains, but the difference is now somewhat narrower. The reason for this is that both bearing and churning losses only take into account the viscosity difference between the two oils which, at 65 °C, is not pronounced (38.32 cSt for Oil A vs 41.26 cSt for Oil B). In terms of overall gearbox efficiency, the predicted values are of course lower since more power losses are now included. These results highlight the importance of accurately modelling lubricant rheology and including crucial parameters which determine traction. In the following section, the relative contribution of gear friction, bearing

and churning will be examined further and the influence of viscosity, gear geometry and bearing selection on the losses will be analysed.

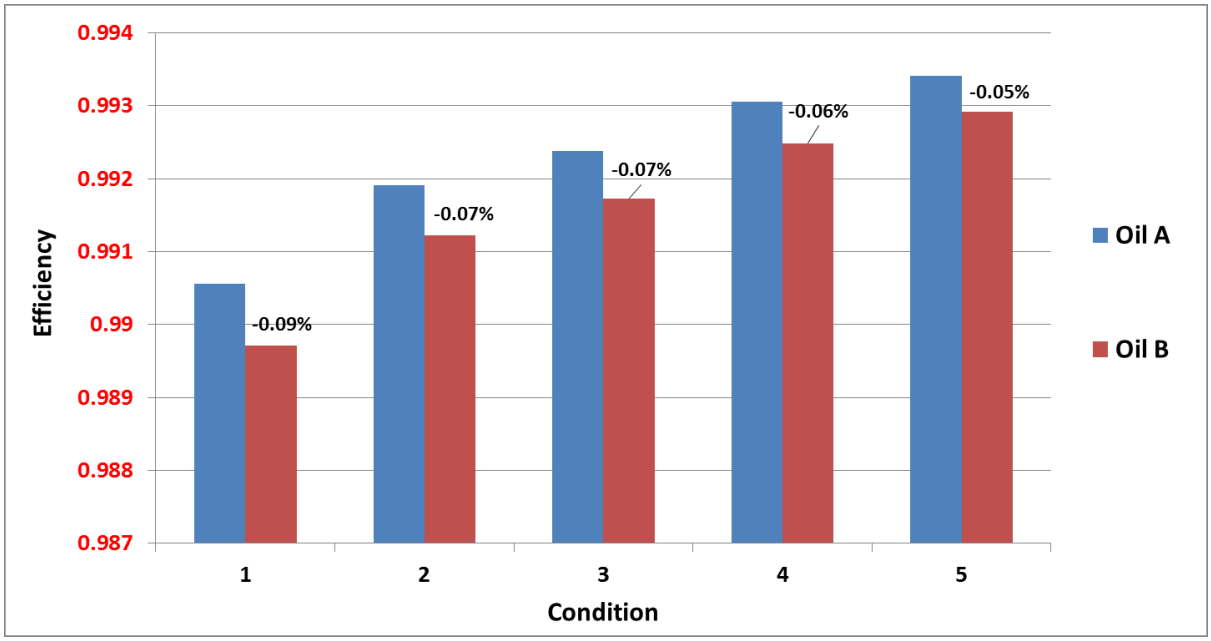



**Figure 5.12: The efficiency of the gear pair for lubricants A and B when gear friction, bearing, seal and churning losses are included (the quoted percentages indicate the drop in efficiency with oil B relative to oil A) for a sump temperature of 65 °C and ground surface roughness (430 nm)**

### 5.6.2 Parametric study on the influence of lubricant properties on gear friction

In this section, the effect of lubricant rheological parameters on gear friction loss and efficiency is investigated. The characterisation of the lubricants described in chapter 5 of this thesis revealed significant differences in specific lubricant parameters, most importantly the Eyring stress, the Roelands parameter z, and the boundary friction coefficient, $\mu_b$. These three parameters are not taken into account by existing bearing and churning models and for this reason, the following comparisons will focus on the losses predicted by the gear friction module only to illustrate the capabilities of the present model in terms of informing the lubricant selection for a particular application.

For the purpose of comparison, three different hypothetical lubricants have been simulated, based on lubricant A as a reference point. For the first lubricant, named A1, the Eyring stress has been reduced by 30% for all temperature and pressure values. The second simulated lubricant, A2, has a different boundary friction coefficient, reduced to 0.08 from 0.1128. This

effect could replicate the use of a boundary friction modifier. The third lubricant, A3, has a Roelands z parameter of 0.4, down from 0.5 which was the average value for oil A as extracted from the rheological characterisation. In all cases, the other parameters, including atmospheric viscosity, VI, density, pressure-viscosity coefficient and shear modulus have remained identical to lubricant A for the purpose of comparison.

Results of predicted power loss due to gear friction with these three lubricants are shown in Figure 5.13, followed by efficiency in Figure 5.14. As far as Oil A1 is concerned, the reduction of Eyring stress down to 70% of the original value led to a significant reduction in gear friction losses, which becomes more important as the conditions get more severe. Even in the mildest condition (1), a 4.1 % reduction in power loss which translates to a 0.03% increase in efficiency has been observed. For the most severe condition (5), the power loss decreased by 7% and the efficiency of the gear was up by 0.02%. Overall, although the efficiency increase is not massive, it is definitely noteworthy and it would have an important effect where gear friction comprises a large proportion of the overall loss i.e. in high torque and heavy sliding applications.

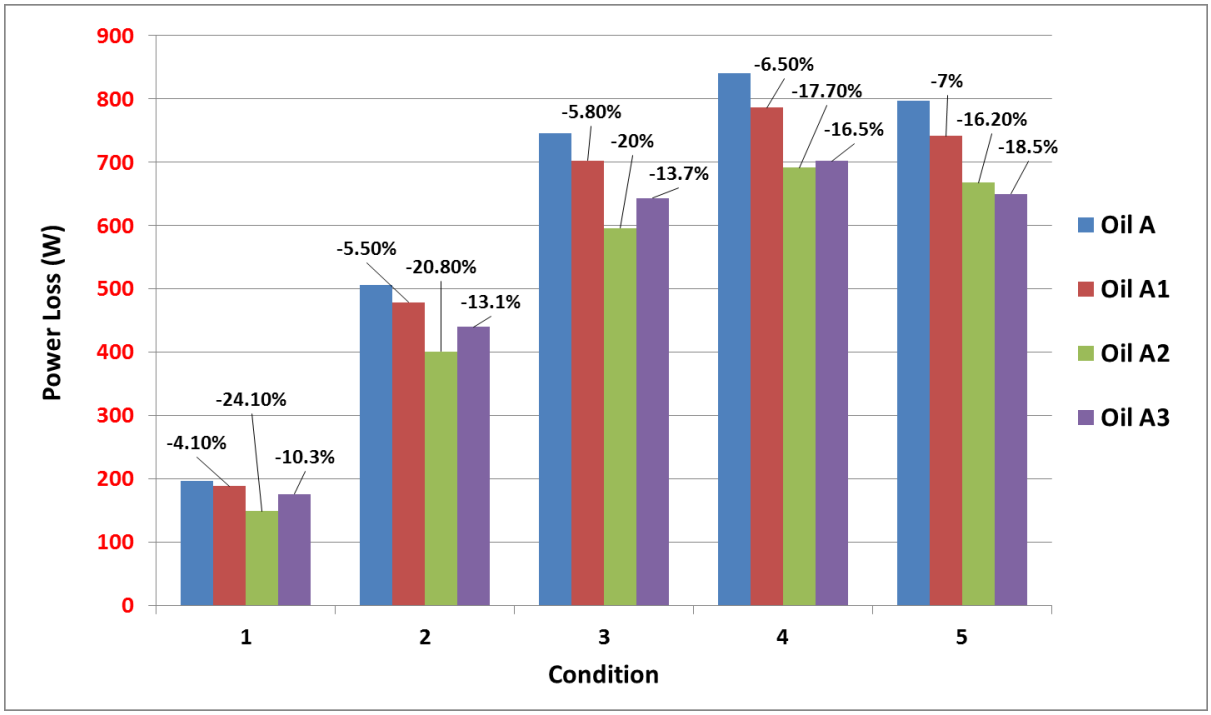



**Figure 5.13: The power loss of the gear pair for lubricants A, A1, A2 and A3 when only gear friction is considered for a sump temperature of 65 °C and ground surface roughness (430 nm)**

Lubricant A2 is simulated to have a boundary friction coefficient capped to 0.08. In practice, this simulates the effect of introducing a friction modifier that is able to reduce boundary friction. As expected, this modification would have a significant effect when asperity contact is more prominent (i.e. at low lambda ratios). Indeed, a massive 24.1% reduction of gear friction loss, which translates to a 0.17% increase in efficiency is observed for the low load, low rotational speed condition 1 where the minimum lambda value is 0.438 and the average value for the effective friction coefficient is 0.0649 for oil A. Using a boundary friction coefficient of 0.08 reduces the average friction coefficient to 0.049 explaining the differences. As the speed gets higher, and the fluid film thickens, the effect of the reduced boundary friction is less pronounced. In the highest rotational speed condition 5, where the lambda value does not drop below 1.08, oil A2 is just 0.06% more efficient than oil A, suggesting that the boundary friction reduction though an improved friction modifier would only be worthwhile in very severe conditions and very low lambda ratios (<0.9).

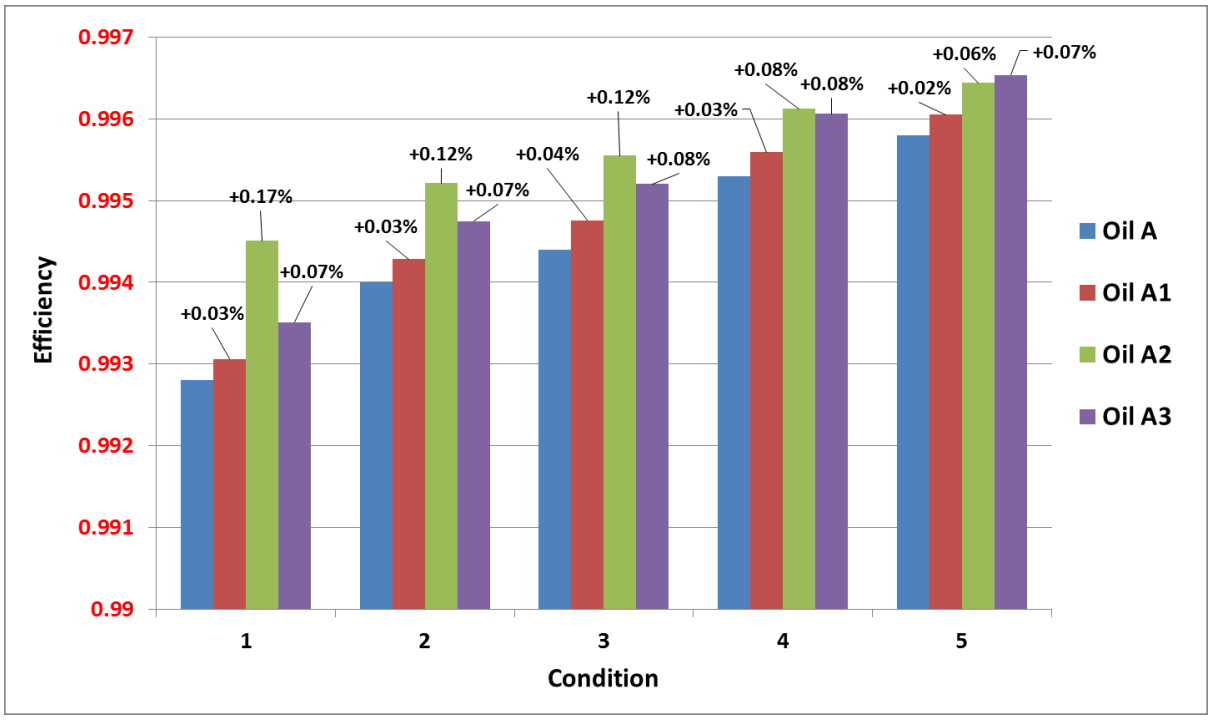



**Figure 5.14: The efficiency of the gear pair for lubricants A, A1, A2 and A3 when only gear friction is considered for a sump temperature of 65 °C and ground surface roughness (430 nm)**

As far as the third simulated lubricant is concerned, z is reduced from 0.5 to 0.4. This is the parameter that defines how the viscosity is affected by pressure in the Roelands temperature and pressure corrected in-contact viscosity equation (section 3.2). This parameter affects losses

in a different way compared to oils A1 and A2 as it changes the viscosity which is calculated at the in-contact temperature and pressure. Oil A3 results in reduced losses due to a lower friction coefficient under all conditions. As the lubricant enters the contact and pressure increases, the in-contact viscosity for the same in-contact pressure will be lower, resulting in a comparatively thinner lubricant and therefore reduced shear heating. As a result, the mean contact temperature will be reduced, and as long as the lambda values are not very low and excessive asperity contact which would increase the flash temperature rise is avoided, the predicted friction coefficient and power loss will be lower. Indeed, the average value for the friction coefficient is reduced from 0.0649 to 0.0583 while the lambda ratio remains relatively unaffected. It has to be noted that the film thickness is calculated using properties at the pressure and temperature of the contact inlet. Since this is a hypothetical study to specifically assess the influence of the Roelands parameter z, the pressure viscosity coefficient, $a$, was not changed hence the influence on film thickness itself was limited to just thermal effects. The efficiency has increased by about 0.07 % under all conditions. This parameter is dependent on the chemistry of the lubricant base oil and formulations with a lower z value would theoretically reduce the overall loss and increase efficiency.

Finally, the efficiency with the three lubricants was studied over a range of torques for a fixed speed and a range of speeds for a fixed torque, similar to the study in the influence of roughness presented in section 5.4. Figure 5.16 shows the power loss of the pair when the rotational speed is constant at 2000 rpm while the input torque was varied from a low of 150 Nm to a high of 640 Nm. For Figure 5.15, the input torque was kept constant at 640 Nm and the rotational speed was increased from 1250 to 8000 rpm. In the former case, the ranking order of lubricants did not change, with oil A being less efficient under all conditions and A2 and A3 being the most efficient. The difference between A2 and A3 was very small. The predicted power loss was almost identical at medium torque values, with oil A2 being slightly more efficient at the lowest and highest torques.

The result is different when the torque is constant and the rotational speed increases. Lubricants A and A1 are still the least efficient with the gap between the lubricants getting wider as rotational speed increases - lower Eyring stress results in lower in-contact temperatures and lower friction. For lubricant A2, the reduction in boundary friction will only make a difference if the lambda ratios are low, which is true for the lowest speed (1250 rpm) where lubricant A2 is the most efficient. As the speed increases, so does the film thickness and in contact

temperatures become much higher. This has an immediate effect on losses with lubricant A3 being much more efficient at those high speeds and the reduced boundary friction of A2 having less of an effect.

In summary, the ranking order of lubricants depends on input conditions with low boundary friction (heavily additivised oils) reducing overall loss at very high contact pressures or very low rotational speeds when the fluid film thickness is low. A reduction in Eyring stress leads to an overall drop in loss under all conditions, while reducing the in-contact viscosity's dependence on pressure by means of altering the Roelands parameter results in lower losses at severe conditions, especially so at very high rotational speeds. Nevertheless, these effects would be different in a full size gearbox, where gear friction is only a part of the overall gearbox losses.

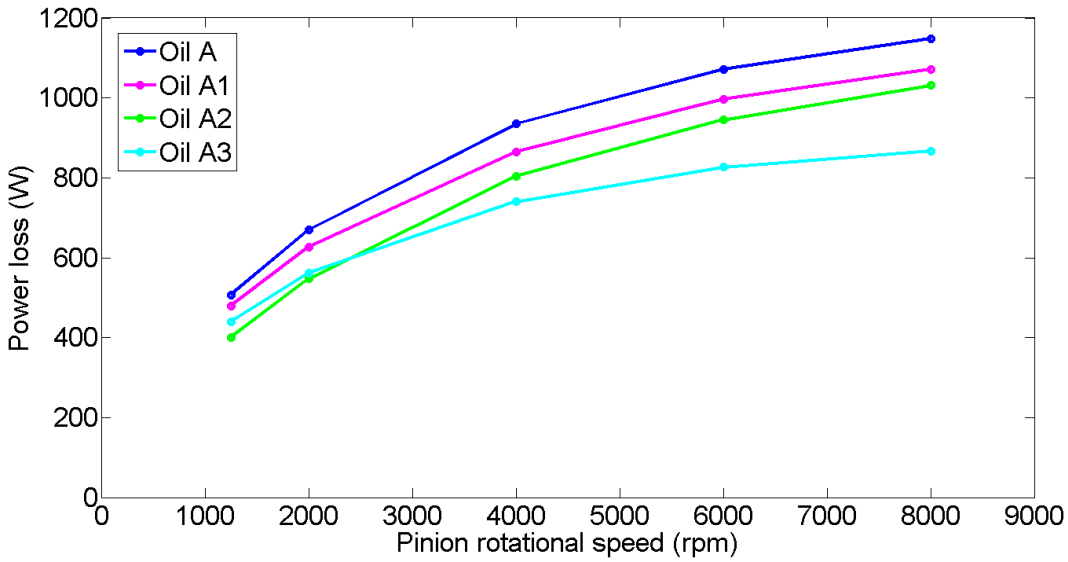



**Figure 5.15: The gear friction losses variation with rotational speed for lubricants A, A1, A2 and A3 (Input torque = 640 Nm)**

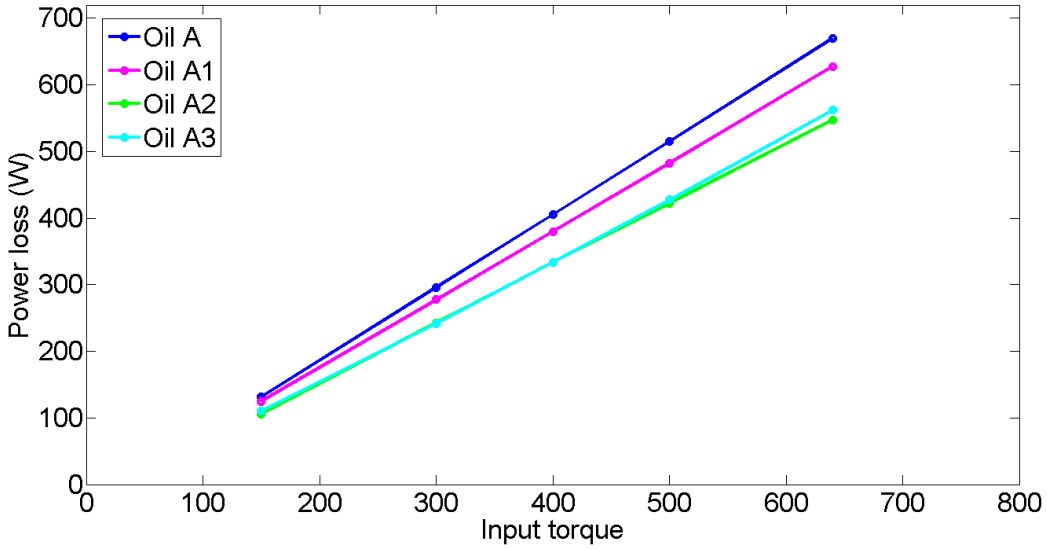



**Figure 5.16: The gear friction losses variation with input torque for lubricants A, A1, A2 and A3 (Input speed = 2000 rpm)**

### 5.6.3 The influence of lubricant viscosity on losses breakdown

In this section, the influence of lubricant viscosity on the breakdown of losses has been investigated. The base viscosity of lubricant A at 40 °C and 100 °C has been varied keeping the viscosity index constant, resulting in a wide range of viscosities from 0.25 times the base viscosity to 7.5 times the base viscosity. The simulation was run for a 1:1 gear ratio, an input torque of 300 Nm and 640 Nm, a rotational speed of 1250 rpm and an input sump temperature of 65 °C. An additional rotational speed of 3000 rpm was also simulated to show how different components react to increased rotational speed.

Like in the previous section, this study is mainly a hypothetical study to establish trends in losses as viscosity is changing. At no point it is suggested that gearbox lubricants *should* have the viscosities shown in the chart as optimum. In a real automotive gearbox, there will be other considerations and further complications such as additional stages, different immersion depths as well as more shafts and bearings. For this reason, the ranking of viscosities suggested here would not be directly applicable.

For the lower rotational speed and low torque condition (Figure 5.17), the most efficient value for viscosity is between 2 and 2.5 times the base viscosity whereas this shifts to higher viscosities when the input torque is high (Figure 5.18). The gears benefit from higher viscosity oil because they are rough and the more viscous oil results in thicker films, reducing the overall

loss. Bearings on the other hand are very smooth and a higher viscosity oil serves to increase losses due to added churning of oil within the bearing; this is more evident for the higher rotational speeds shown below. In turn, this means that in order to select a lubricant for a specific application, one must take into account these differences and find the balance between keeping the gear surfaces sufficiently separated and preventing excessive bearing loss. Gear churning losses are slightly higher as viscosity increases as may be expected but the relatively shallow immersion depth and the small size of the gear is keeping the overall contribution low in all cases at this relatively low speed of 1250 rpm.

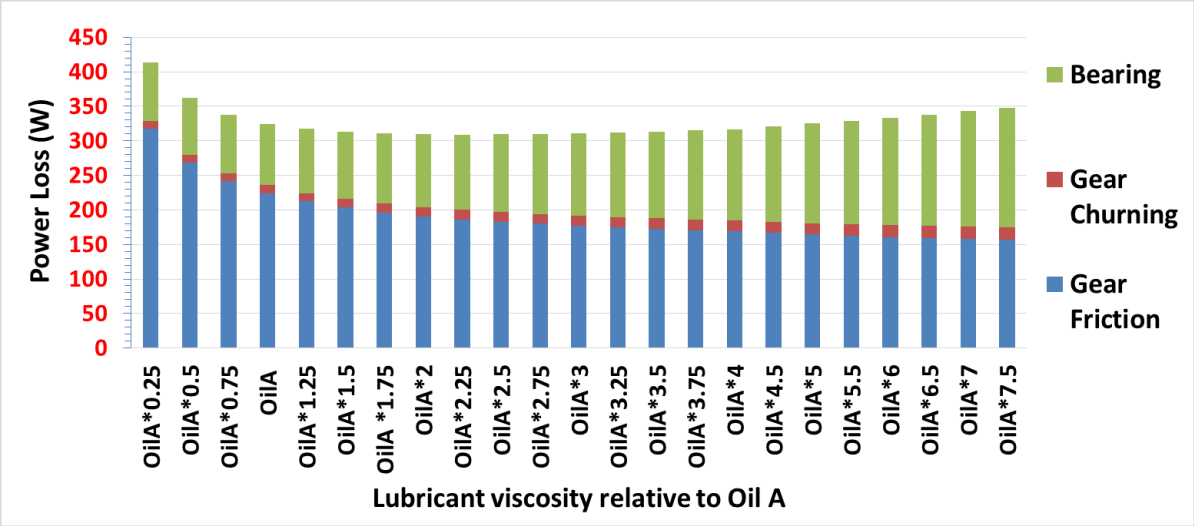



**Figure 5.17: The effect of lubricant viscosity on the losses breakdown for an input torque of 300 Nm (1250 rpm, 65 C°, 1:1, fixed module, immersion depth 6mn)**

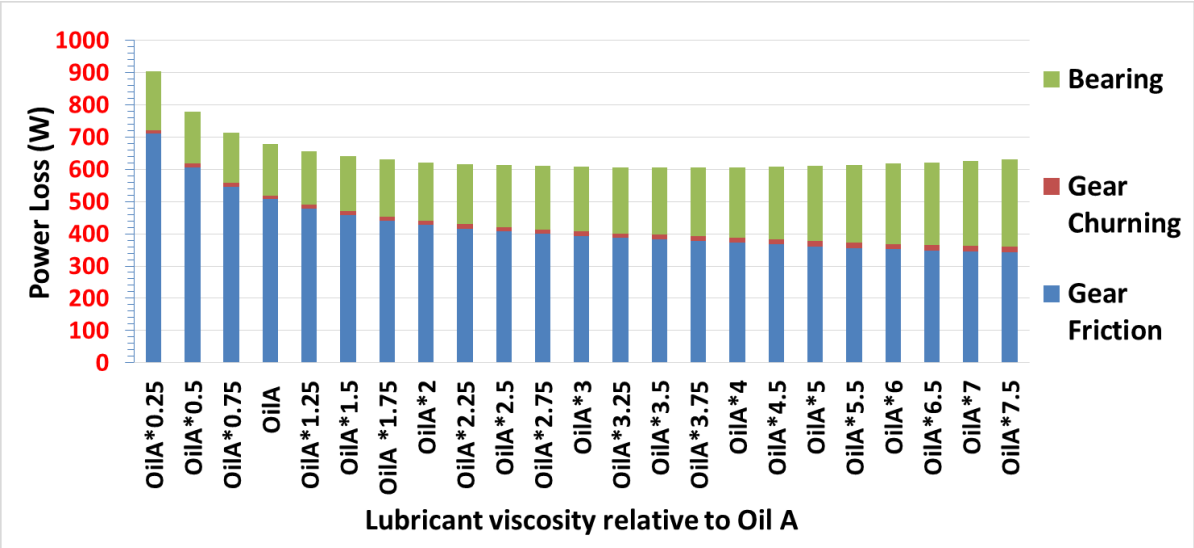



**Figure 5.18: The effect of lubricant viscosity on the losses breakdown for an input torque of 640 Nm (1250 rpm, 65 C°, 1:1, fixed module, immersion depth 6mn)**

When the rotational speed is increased to 3000 rpm, illustrated in Figures 5.19 and 5.20, the contribution of gear churning and especially bearings becomes more significant and the point at which bearing losses are high enough to make the overall system less efficient comes earlier between 1 and 1.5 times the base viscosity. This is not the case when the torque is high, as the more pronounced gear friction losses move the most efficient point to around 2 to 2.75 times the base viscosity.

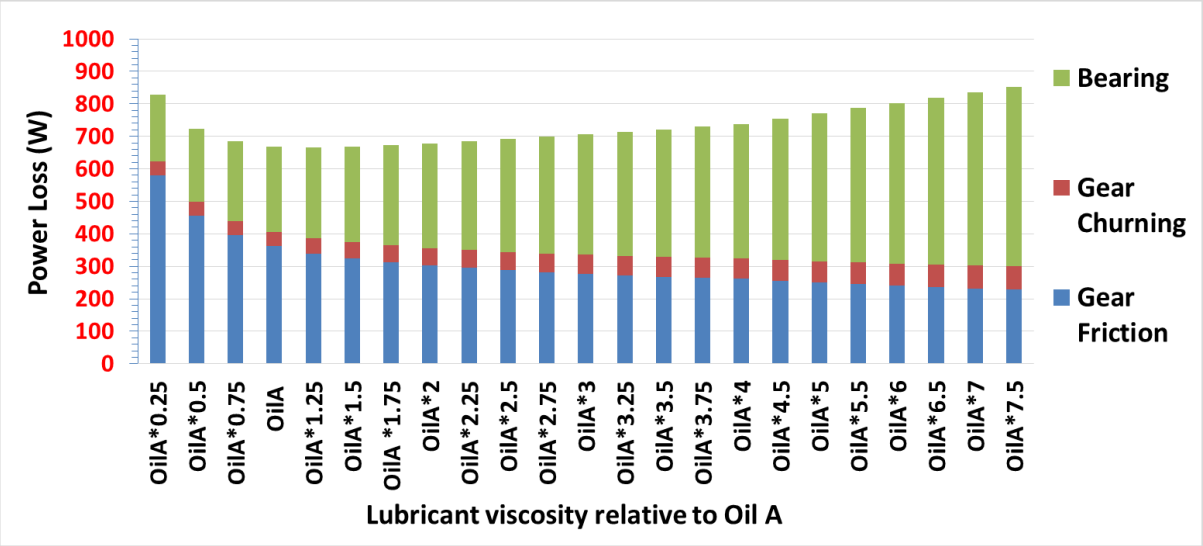



**Figure 5.19: The effect of lubricant viscosity on the losses breakdown for an input torque of 300 Nm (3000 rpm, 65 C°, 1:1, fixed module, immersion depth 6mn)**

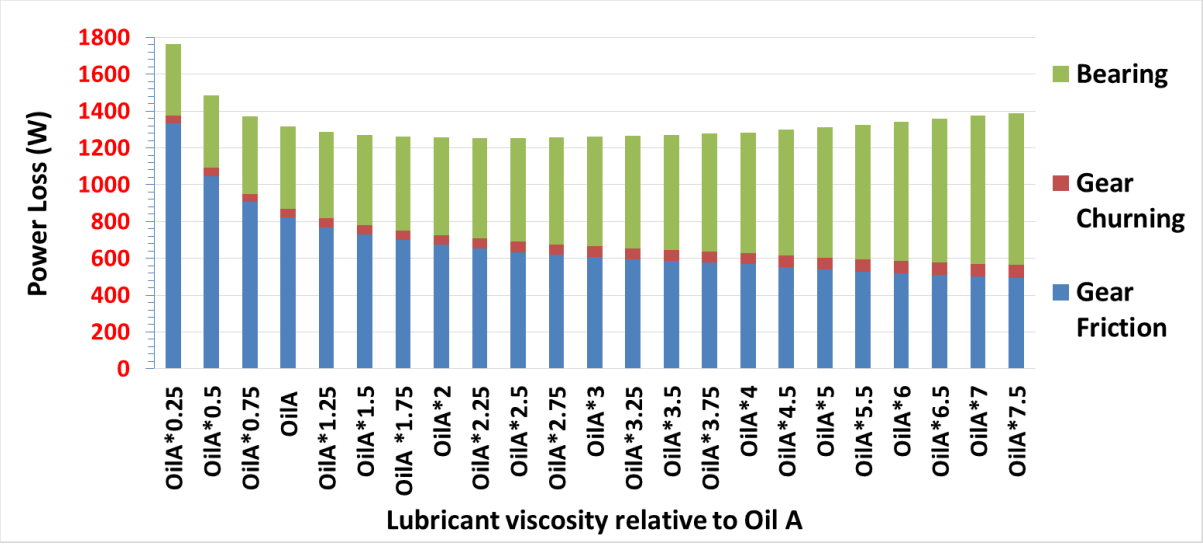



**Figure 5.20: The effect of lubricant viscosity on the losses breakdown for an input torque of 640 Nm (3000 rpm, 65 C°, 1:1, fixed module, immersion depth 6mn)**

## 5.7 Parametric studies on the influence of selected parameters on gearbox power losses

This sub-section presents a series of parametric studies with the main objective of establishing trends in the influence of selected parameters on gearbox losses. The studies will be carried out in a single stage set-up since these trends are much easier to establish than in a full multi-speed gearbox studied later. It should be noted that the comparisons in this section often use hypothetical gear geometry in order to study the effects of specific parameters (lubricant properties, number of teeth, face width etc.) on efficiency. The geometry is not necessarily the one that would be arrived at through application of gear design rules and hence should not be taken as appropriate for the given loading. The section is not meant to provide gear design rules, but a systematic study of parameters of interest on overall gearbox efficiency.

### 5.7.1 Losses breakdown and the influence of bearing selection

The relative proportion of the losses in the gearbox is an important factor which highlights the potential for efficiency improvement. The individual gear contact friction, bearing, seal and churning losses and their contribution to the overall gearbox loss was studied for the same set of 5 conditions outlined above in Table 8. The resulting losses from the above procedure were plotted so that the relative proportion can be visualised and they are shown in Figure 5.21; the numbers on the graph represent percentages of total power loss for each individual loss component. At the low speed and low torque condition 1, the bearing and seal losses comprise 21.8% of the total while churning accounts for 1.5%. As the rotational speed increases these losses increase and at condition 5, bearing and seal accounts for 32.3% of the total while churning is 3.2%. The bearing loss increase is mainly due to bearing oil churning and therefore the rotational speed has a pronounced effect on both bearing and gear churning losses. Churning losses are not significant in relative terms, but since they are highly dependent on the immersion depth as explained above, an increase in the immersion depth would make them more prominent.

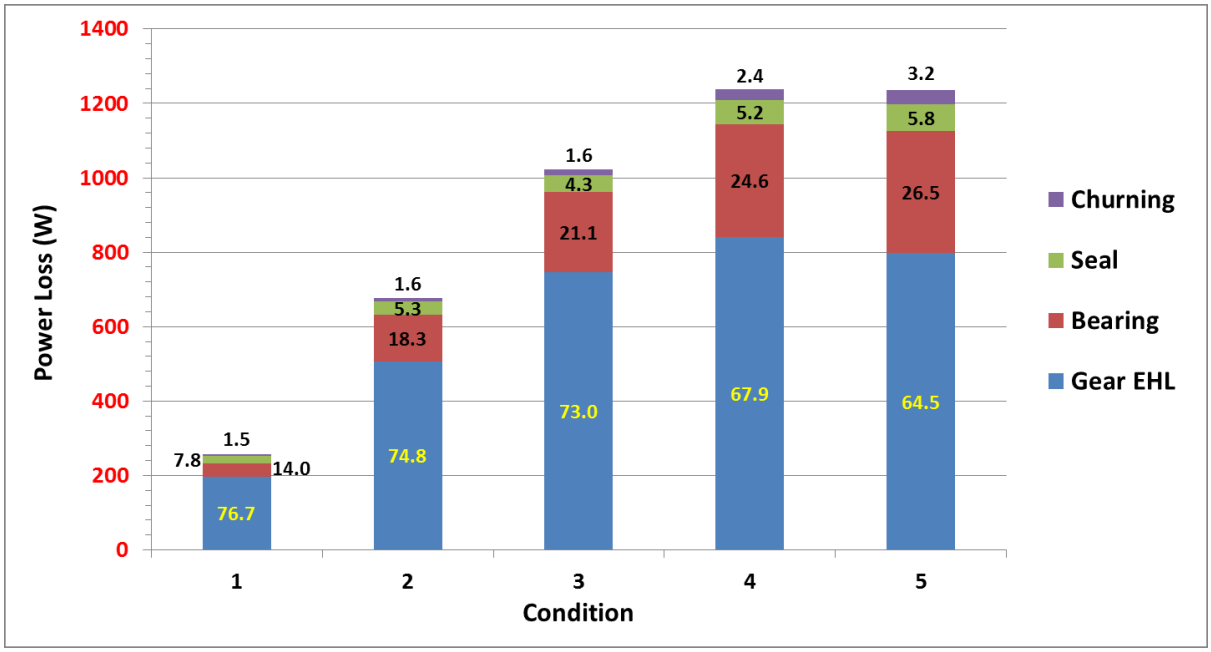



**Figure 5.21: The cumulative losses in the gearbox when the 6307 RS1 DGBB is used**

The role of temperature is crucial in these calculations, however they were all done at a constant initial sump temperature of 65 $^{0}$C. It has to be noted that, since the model calculates the losses at the inlet temperature, when convergence is achieved, the actual temperatures where all the losses (including bearing and churning) are calculated are higher, ranging from 67 °C to 71 °C. The difference in converged temperature between the two lubricants ranges from 0.3 °C to 0.7 °C however this has little impact on the observed differences.

The use of DGBBs, which are a relatively efficient bearing type, means that the bearing loss contribution in this gearbox set-up is invariably small. Since the studied gearbox uses spur gears, there is no need to support axial loads hence a deep groove ball bearing is a viable option. This results in very low bearing losses compared to an automotive gearbox which commonly uses tapered roller bearings in order to support axial forces generated by helical gears. If a tapered roller bearing is used then the bearing losses will become much more important, especially so for low load conditions. To show the effect of bearing selection, a version of the gearbox which uses a 32210 J2/Q TRB was simulated using the same input conditions 1-5.

It has to be noted that this bearing is much larger than the 6307 bearing previously used and a smaller version could accommodate the loads however the focus of this section is mainly to provide a hypothetical study on bearing influence. Bearing losses can be drastically different if larger bearings are chosen for increased operational life or specific bearing types (such as TRBs) are chosen to accommodate axial loads in addition to radial loads. For this reason, no

direct comparisons between the two arrangements should be made. In addition, the selection of a 32210 bearing is of interest because this size of bearing is used in the commercial gearbox detailed in the next chapter.

For the purposes of evaluating the breakdown of losses in conditions other than WOT, a 6$^{th}$ condition was run, using the average values extracted from an experimental low-load drive cycle which will be presented in detail in the following chapter. The 6$^{th}$ condition has an average input torque of 144 Nm, a rotational speed of 1750 rpm, an average input (sump) temperature of 56.23 °C and an immersion depth for the gears equal to the pitch radius. Two cases were run for the bearings; one with no axial load and one including an axial load equal to one third of the radial load - this analogy corresponds to the observed ratio of axial to radial loads observed for the same bearings used in the commercial gearbox presented in the next chapter. The power loss and efficiency results for these conditions are shown in Figures 5.22 and 5.23.

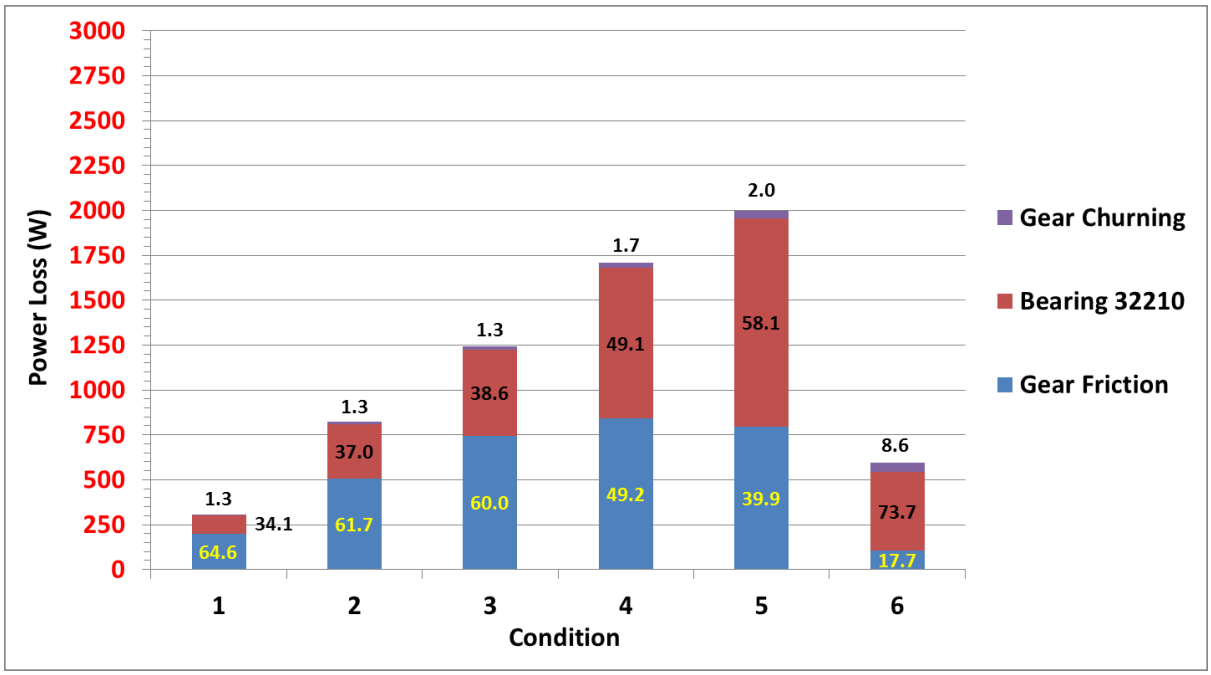



**Figure 5.22: The cumulative losses in the gearbox when the 32210 J2/Q TRB is used (no axial load)**

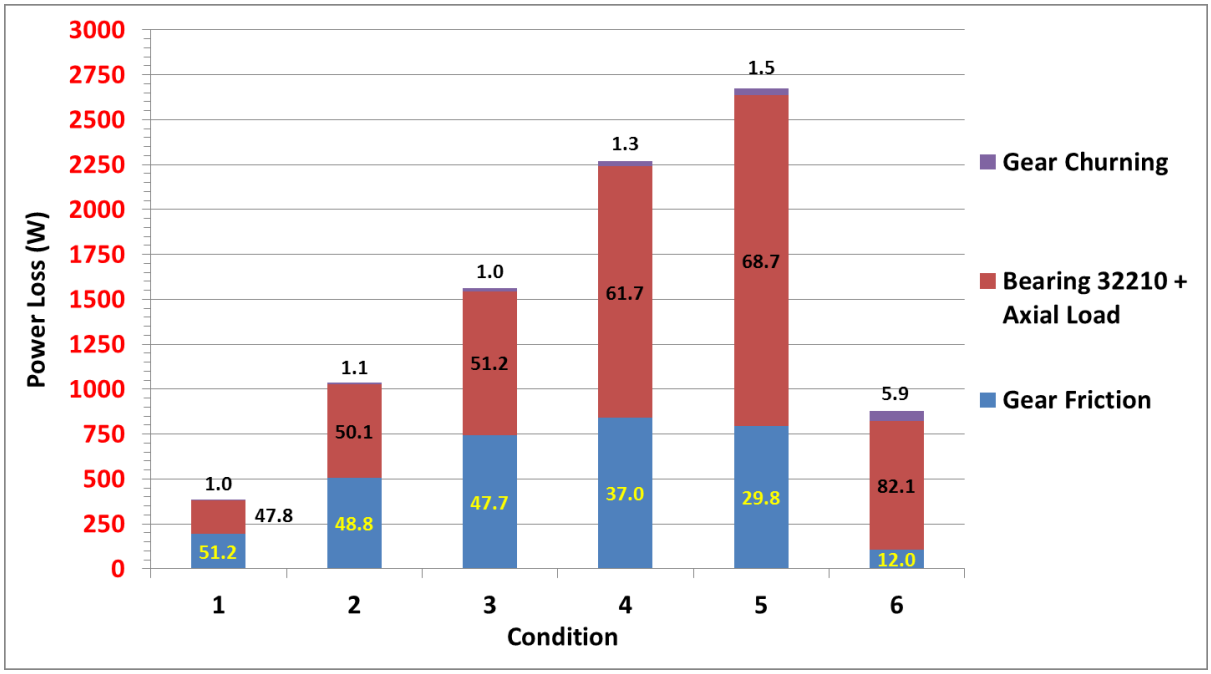



**Figure 5.23: The cumulative losses in the gearbox when the 32210 J2/Q TRB is used (axial load/radial load = 1/3)**

Comparing these figures to their equivalents when the 6307 RS1 DGBB was used shows a dramatic change in the losses breakdown; the bearing losses, rather than gear tooth friction, are now dominant under a wide range of conditions, especially so when the axial load is incorporated. Using oil A with TRBs and no axial load, bearing losses comprise 34.1% of the overall losses in condition 1 but this contribution rises to 73.7% for the newly introduced condition 6 which is more representative of a real-world automotive gearbox operating condition. The figures for oil B are higher still. This is in stark contrast with the numbers when the DGBBs were used, where the maximum contribution of the combined bearing and seal losses, encountered at condition 5 was 32.3%. As far as the bearings themselves are concerned, results are mostly due to the fact that the losses for the TRBs are much higher compared to DGBBs due to different geometry and bearing efficiency, particularly the presence of sliding at the TRB roller – flange contact and associated increase in friction in combination with an increase in bearing size.

Regarding churning losses, the relative contribution is very low for conditions 1-5, where the immersion depth was not changed, while increasing the depth to cover half of the gears (condition 6) results in an increased contribution of 8.6% for no axial load on the TRBs. This is much higher than the maximum contribution when DGBBs at shallow immersion depths were used (3.2%). Nevertheless, the contribution of churning is still quite low in absolute terms,

partly because of the massive bearing loss but mainly due to the fact that only one, relatively small, gear pair is used. In an automotive gearbox where multiple gear pairs are used, churning contribution will significantly increase and, depending on the conditions, it could even be the dominant loss source, as will be demonstrated in the following chapter.

When the newly introduced condition 6 is examined, the relatively high rpm and very low input torque, combined with the larger bearing, increase the relative bearing loss contribution even more. The bearing losses are dominant comprising between 73.7% and 82.1 % of the overall loss, whereas gear friction loss is now relatively low. This condition is representative of a low load highway drive cycle for automotive gearboxes where there is no need for high input torques; it has to be noted that conditions 1-5 were based on a wide open throttle (WOT) engine map which is rarely the case when it comes to real life driving conditions. It can be said that generally the higher the input torque, the more significant the contribution of gear friction becomes.

Figures 5.24 and 5.25 below show a comparison of the two lubricants when the TRBs are used and condition 6 is included.

For the reasons explained above (bearing and churning losses are only affected by viscosity), the percentile difference between the two lubricants is smaller compared to when DGBB's were used; the same is true for the efficiency. When one analyses condition 6 however, the efficiency is much lower although the power loss is also lower. Most importantly, the gap between the two lubricants in terms of efficiency is the highest observed at 0.26% in favour of oil A. This is due to the lower temperature of 56.23 °C, where the viscosity difference between the two oils is much more significant (50.15 cSt for Oil A vs 58.66 cSt for Oil B).

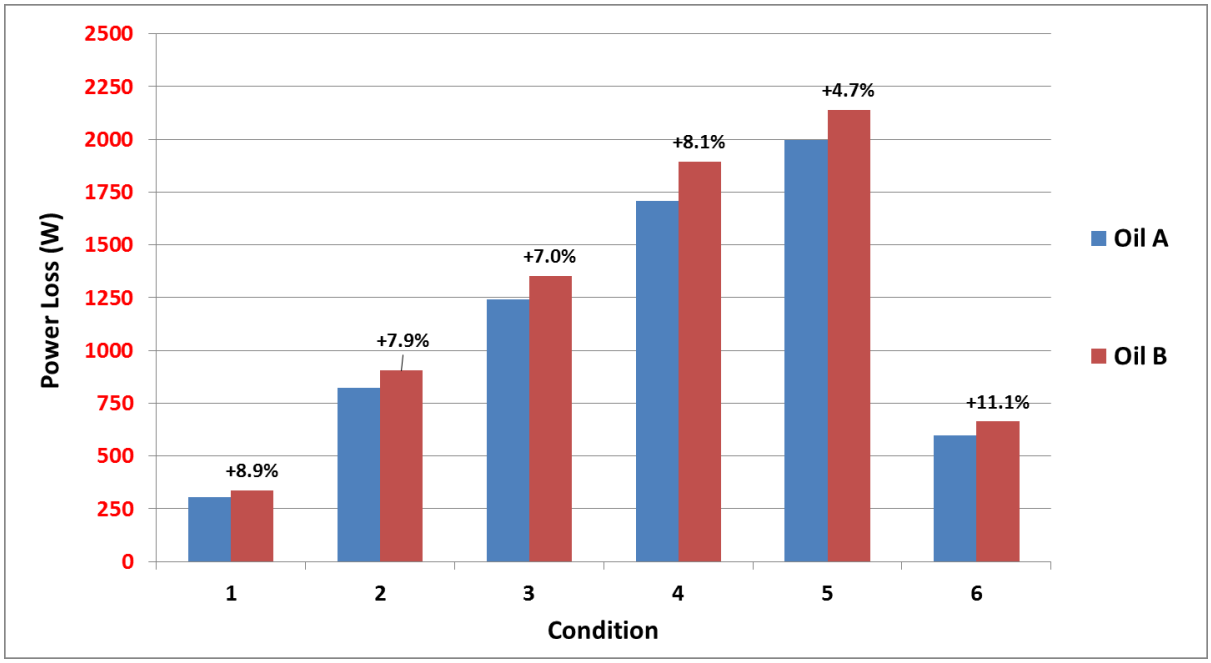



**Figure 5.24: The power loss of the gear pair for lubricants A and B when TRBs are used (no axial load)**

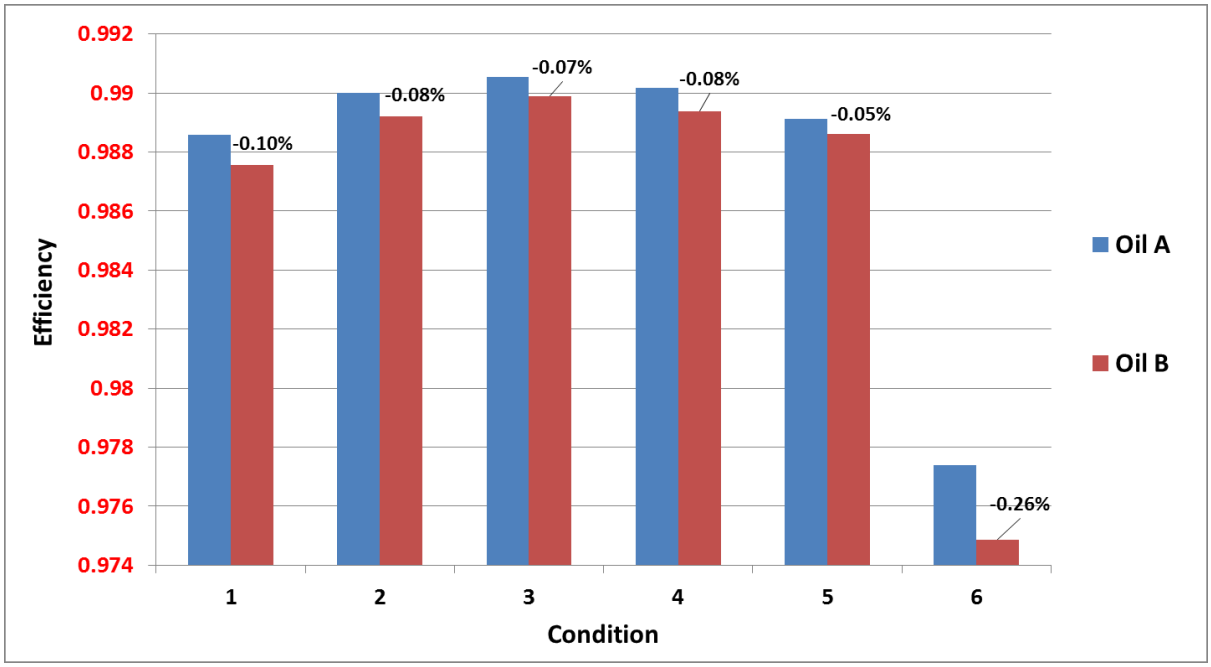



**Figure 5.25: The efficiency of the gear pair for lubricants A and B when TRBs are used (no axial load)**

### 5.7.2 The influence of face-width ratio on losses breakdown

An important parameter when it comes to gear design is the face-width ratio which is the ratio of the face width over the reference diameter of the gear. Simulations were run for several face-

width ratios ranging from 0.2 to 1.3. The input conditions were the same as in the previous sections, with a rotational speed of 1250 rpm, a 1:1 ratio and an input temperature of 65 °C. As the gear became wider, the square of the diameter was reduced by the same factor in order for the gear volume, $V=b\pi d^2/2$, to remain unchanged. Since the torque carrying capability of a gear is roughly proportional to the volume, based on both the bending and contact stress considerations, this means that all gear shapes considered here could be used in the same application to provide a fair comparison. Results are shown in Figures 5.26 and 5.27 for an input torque of 300 Nm and 640 Nm.

Gear friction and bearing losses increase as the face-width ratio increases. For the lower input torque of 300 Nm, the losses breakdown remains relatively constant, with gear friction losses comprising between 65.6% and 69.8% of the overall with bearings generating 27.4%-32.7% of the heat and churning accounting for the remaining 1.2%-3.6%. For the higher torque, the overall trend is similar. As far as gear friction losses are concerned, smaller reference diameters lead to reduced peripheral speed of the gears. This results in lower film thickness and therefore lower lambda ratios which in turn increase the effective friction coefficient. Contact temperatures are higher and the losses due to gear friction increase. When it comes to bearings the losses are also higher as the gears get smaller and wider; this is due to the increased total bearing load. Churning losses on the other hand reduce slightly as a result of the gears becoming smaller however this is not enough to compensate for the increase in bearing and gear friction losses. The end result is that narrower face widths and larger reference diameters are indeed more efficient than smaller, wider gears and are also likely to last longer given the improved lubrication conditions at the gear teeth contacts. For this reason narrow gears are used whenever the space restrictions of the application allow.

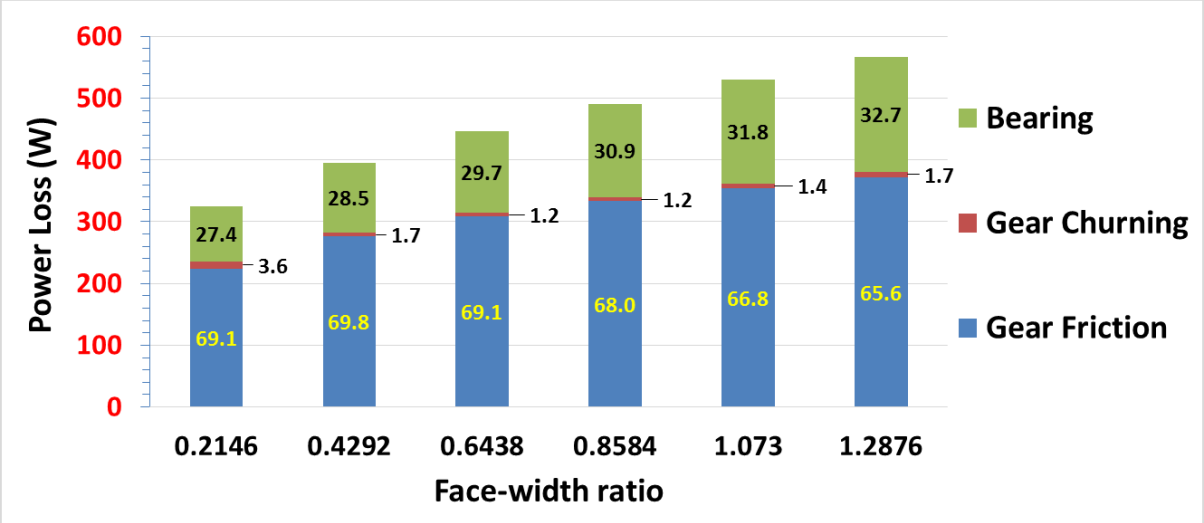



**Figure 5.26: The losses breakdown for the gear pair as the face-width ratio of the pair is increased at an input torque of 300 Nm (1250 rpm, 65 C°, 1:1, immersion depth 6mn, variable module, variable dref)**

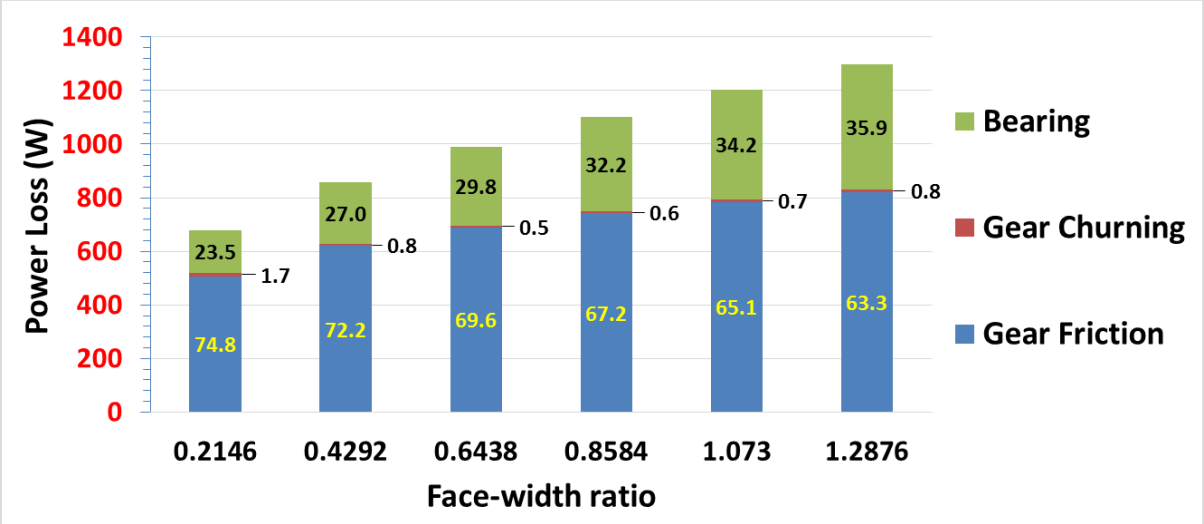



**Figure 5.27: The losses breakdown for the gear pair as the face-width ratio of the pair is increased at an input torque of 640 Nm (1250 rpm, 65 C°, 1:1, immersion depth 6mn, variable module, variable dref)**

### 5.7.3 The influence of the tooth number on losses breakdown

Here the number of teeth on both gear and pinion was increased for a 1:1 ratio while the module was kept constant at 3.95 mm. All other conditions were the same as in the previous section, with the rotational speed being 1250 rpm. As can be seen in figures 5.28 and 5.29, the contribution of gear friction becomes negligible as more teeth are added and the reference

diameter increases, comprising just 0.1 % of the overall losses for a gear with 138 teeth (reference diameter is 545 mm). The reason for this is that the slide-roll ratio in gear teeth contacts as well as the contact pressures are reduced with the increase in tooth number (and associated increase in gear diameter) since the input torque was kept the same. On the other hand, the churning loss is increased massively and takes up 97.4 % of the overall as the large gears rotate in the sump at 1250 rpm. Finally, bearings are not significantly affected as they were kept the same - they can support the load. The same observations stand for the increased torque of 640 Nm.

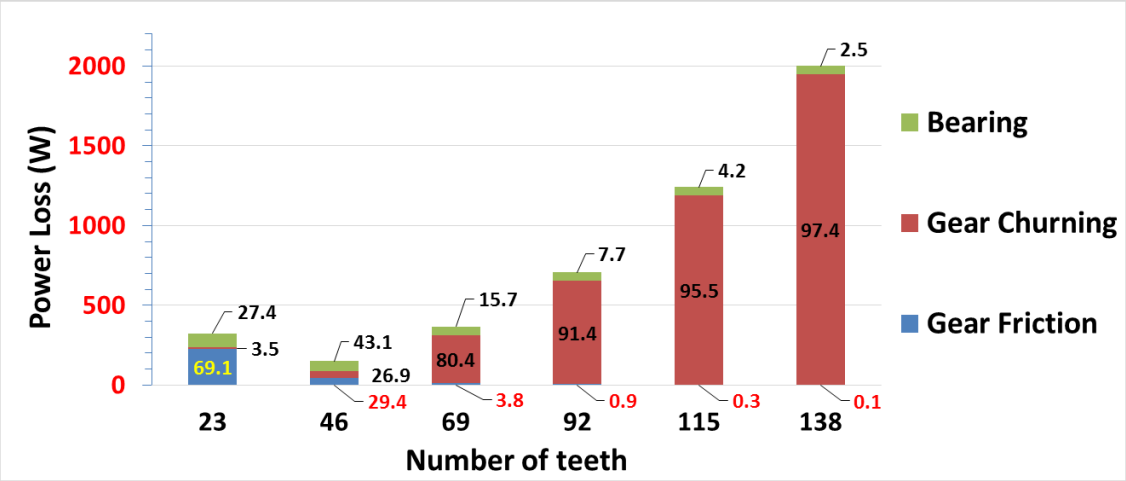



**Figure 5.28: The losses breakdown for the gear pair as the number of teeth is increased at an input torque of 300 Nm (1250 rpm, 65 C°, 1:1, immersion depth 6mn, fixed module, variable dref)**

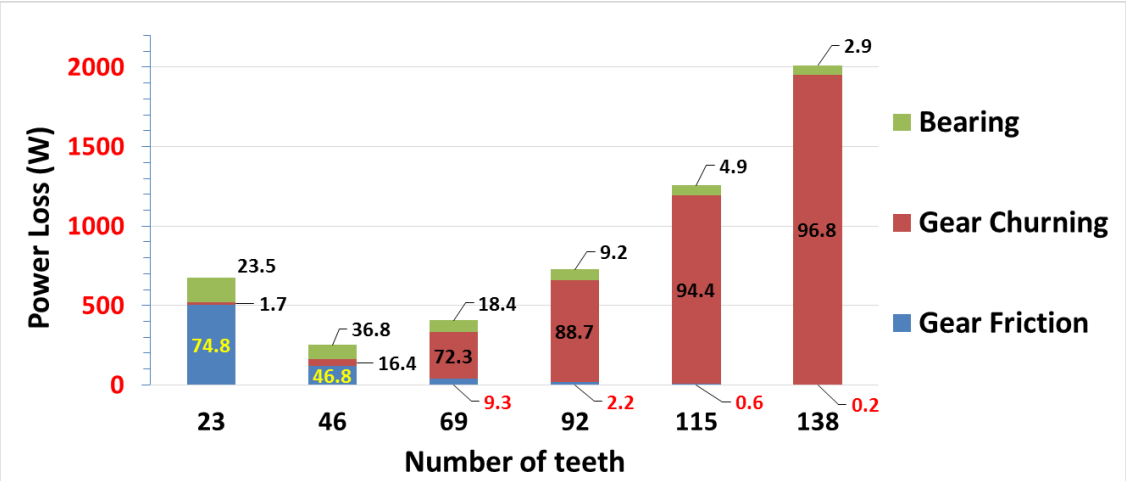



**Figure 5.29: The losses breakdown for the gear pair as the number of teeth is increased at an input torque of 640 Nm (1250 rpm, 65 C°, 1:1, immersion depth 6mn, variable module, variable dref)**

### 5.7.4 The influence of gear ratio on losses breakdown

In this section, the influence of gear ratio on the breakdown of losses has been investigated. Simulations were run for six different gear ratios to study the relative contribution of the individual sources. Results are shown in the following figures for two values of input torque; 300 Nm and 640 Nm. This comparison was made for lubricant A, at a sump temperature of 65 °C, and rotational speed of 1250 rpm and a constant module of 3.95 mm. The immersion depth is fixed at 6mn and it follows the changes of size of the gear i.e. as the gear gets larger, its immersion depth stays the same.

As can be seen in Figure 5.30, gear friction losses go down when the gear ratio is increased, as a result of lower contact pressures and SRRs while the reduced rotational speed of the wheel shaft results in lower bearing losses. In addition, the larger gears provide better cooling resulting in lower contact temperatures. The churning losses on the other hand are not significantly affected, which is expected as the immersion depth remains relatively shallow. The same is true for bearing losses, assuming that the bearing size will remain the same. The above results in higher gear ratios being significantly more efficient. The same trend is true for the increased torque, shown in Figure 5.31 with the only difference being an expected increase in the contribution of gear friction.

As will be shown when the commercial automotive gearbox will be examined in the following chapter, the immersion depth is selected for the larger gears in an attempt to minimise churning loss and the smaller gears are either partly immersed or not immersed at all, lubricated by splashing and the swell effects. Moreover, automotive gearboxes often feature different levels and are not flat-bottomed so that all the gears are adequately lubricated. The difference in churning and overall losses between the cases when immersion depth follows the wheel size as opposed to pinion size is very large, with churning being minimised and comprising just 5.4% of the overall losses even in the extreme case of a 10:1 ratio. The reduced churning, coupled to the fact that gear friction losses continue to drop, results in higher ratios being consistently more efficient. Again, the most important thing to note is that the 1:1 ratio is never more efficient and a 2:1 to 4:1 ratio is preferable until size begins to make very high ratios impractical and uneconomical.

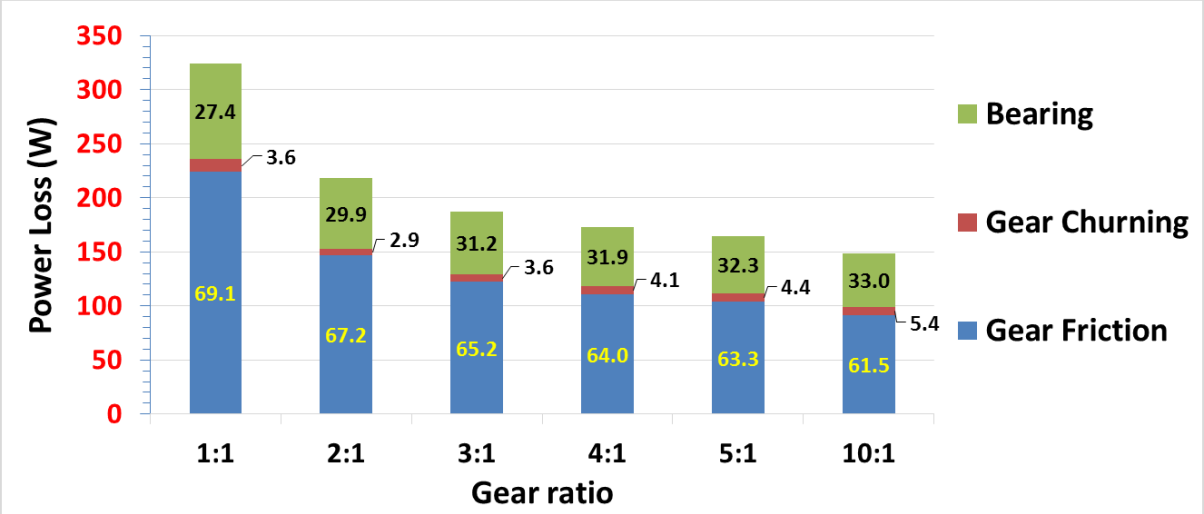



**Figure 5.30: The losses breakdown of the gear pair for six different gear ratios and an input torque of 300 Nm (1250 rpm, 65 C°, gear immersion depth 6mn, fixed module, variable gear dref)**

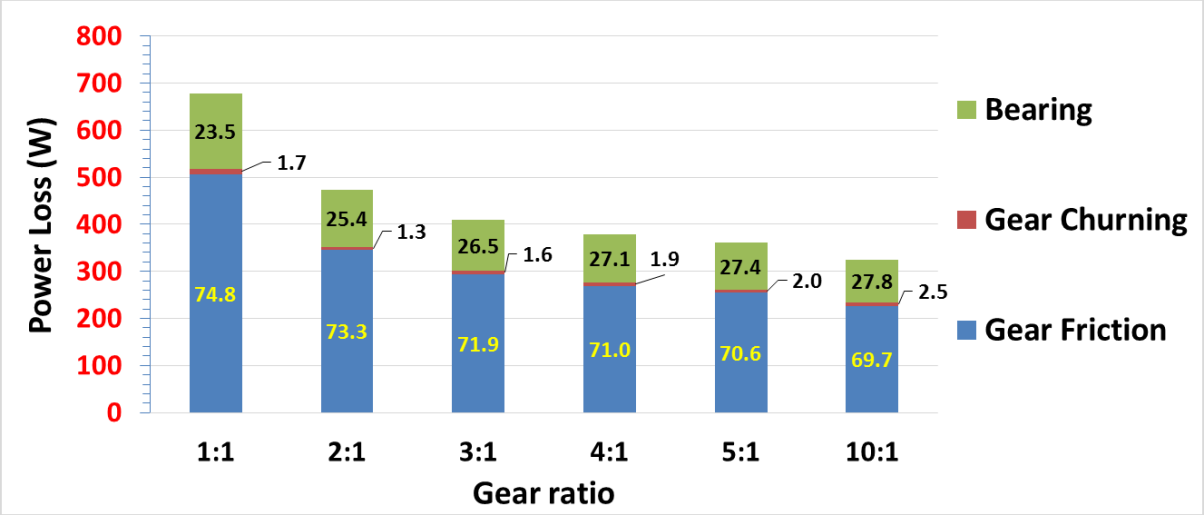



**Figure 5.31: The losses breakdown of the gear pair for six different gear ratios and an input torque of 640 Nm (1250 rpm, 65 C°, gear immersion depth 6mn, fixed module, variable gear dref)**

### 5.8 Summary

In this chapter, the results from the application of the model to a simple single stage spur gearbox were presented. The main objective of the presented parametric studies was to establish trends in the influence of various parameters on gearbox losses, since these trends are much easier to establish in a simple single stage set-up than a full multi-speed gearbox.

The presented results included contact path calculations for the selected spur gear pair to illustrate the evolution of film thickness, temperatures and friction along the contact path. The resulting gear mesh efficiency is studied. The effect of roughness on gear power losses was then investigated. The two test lubricants, characterised in chapter 5, were compared in terms of gearbox power losses. To further study the influence of oil parameters on gearbox efficiency, three further, hypothetical lubricants were simulated, using oil A as a reference, to study the effect of specific lubricant properties on gear friction losses. Finally, the relative contribution of different losses was examined and the influence of selected design parameters, such as bearing type, gear facewidth ratio, gear ratio and gear tooth number, on the overall losses and the breakdown between the individual losses were investigated. The significance of the results and the main trends established here will be discussed in the Discussion chapter later in this thesis. The next chapter will present the results of the model applied to a commercial automotive gearbox.

# 6. PREDICTING LOSSES UNDER REAL ROAD CONDITIONS IN A 6 SPEED AUTOMOTIVE GEARBOX

## 6.1 Introduction

In this chapter, the model that was previously detailed will be applied to predict power losses in a 6-speed commercial manual automotive gearbox installed in a vehicle and subjected to real road driving conditions. The gearbox is fitted on a full size US-spec pickup truck. The truck and the gearbox were instrumented with multiple sensors and the vehicle was then driven on a real road under varying duty cycles. The data gathered during the vehicle operation is then used to compare the predictions of the current gearbox efficiency model with the actual gearbox temperatures (and hence indirectly efficiency) recorded during the vehicle operation. In order to achieve this comparison, the core gearbox power loss model described previously is extended to include a thermal model of the gearbox, in order to predict temperatures in the lubricant sump. The losses breakdown in the gearbox are analysed and the temperature predictions are compared to experimental values. In addition, two standardised drive cycles will be simulated by the present model, to highlight the importance of lubricant selection and the effect of severity of the chosen drive cycle on the losses.

## 6.2 Simulation

### 6.2.1 Experimental drive cycle, vehicle details and model inputs

A drive cycle can be defined as a fixed vehicle operation schedule which allows experiments such as emission tests, engine and drivetrain durability tests to be conducted under repeatable conditions. It comprises a series of data points, most commonly vehicle speed and/or gear selection vs time[162].

Drive cycles can be classified as steady state or transient depending on how the velocity changes with time. A steady state drive cycle usually comprises a sequence of constant load and engine speed combinations, whereas in a transient drive cycle the engine load and the vehicle speed are almost constantly changing. For the purpose of this study, three experimental drive cycles under real road operating conditions will be used together with two of the most popular drive cycles used today, the New European Driving Cycle (NEDC) and the Artemis URM 150 which is more severe and representative of real world driving.

The gearbox is mounted on a 2006 Dodge Ram 3500. It is a typical full size US pickup truck powered by a 6.7L Cummins turbo diesel engine. The power is transferred to the back twin wheels through a six speed manual gearbox. The gearbox under examination is a full synchromesh automotive gearbox made by Mercedes Benz (G56 AE). This study was granted

access to this vehicle and the gearbox through research collaborators, Valvoline US. This meant that it was possible to dismantle the gearbox, inspect and measure internal components as well as instrument the vehicle with the desired sensors. Further information on the vehicle and the gearbox, including basic dimensions, gear ratios and bearing details, is shown in Table 9.

**Table 9: The basic vehicle and gearbox parameters used as inputs for the model**

| | | | |
|---|---|---|---|
| Vehicle mass, M | 3000 kg | Final drive ratio | 3.73 |
| Wheel size | 235/80/R17 | 1st gear ratio (total) | 5.94 |
| Vehicle Frontal area ($m^2$) | 3.75 | 2st gear ratio (total) | 3.28 |
| Drag coefficient, Cd | 0.46 | 3st gear ratio (total) | 1.98 |
| Gearbox mass (gears + synchros) (kg) | 53 | 4st gear ratio (total) | 1.31 |
| Gearbox mass (casing) | 27.7 | 5st gear ratio (total) | 1 (direct drive) |
| Gearbox mass (oil) (kg) | 5 | 6st gear ratio (total) | 0.742 |
| Gearbox surface area (approx.) ($m^2$) | 0.5 | Normal modules 1st - 6th (mm) | 4.14/3.75/4/3.81/3.25 |
| Input shaft bearing | 32210 (TRB) | Main shaft bearing | 32210 (TRB) |
| Countershaft bearing (input side) | 30307 (TRB) | Countershaft bearing (output side) | 32208 (TRB) |

In order to obtain the required data enabling the comparisons between the model predictions and real life data, the vehicle was instrumented with thermocouples to measure the temperature in the oil sump and around the gearbox, as well as pitot tubes on the bottom, top and sides to measure air velocity. The rotational speed of the crankshaft and the engine load was logged by the ECU and the required torque was calculated according to industry standards[163] as a percentage of the maximum torque at Wide Open Throttle. The maximum torque at any given rotational speed was taken from a WOT map of the engine (Figure 6.1) which was extracted from a rolling road dynamometer run by Valvoline and supplied to this study. The selected gear was also back calculated from the rotational speed and engine load data. The input

shaft/main shaft/countershaft assembly and some details of the gears can be seen in Figures 6.2 and 6.3.

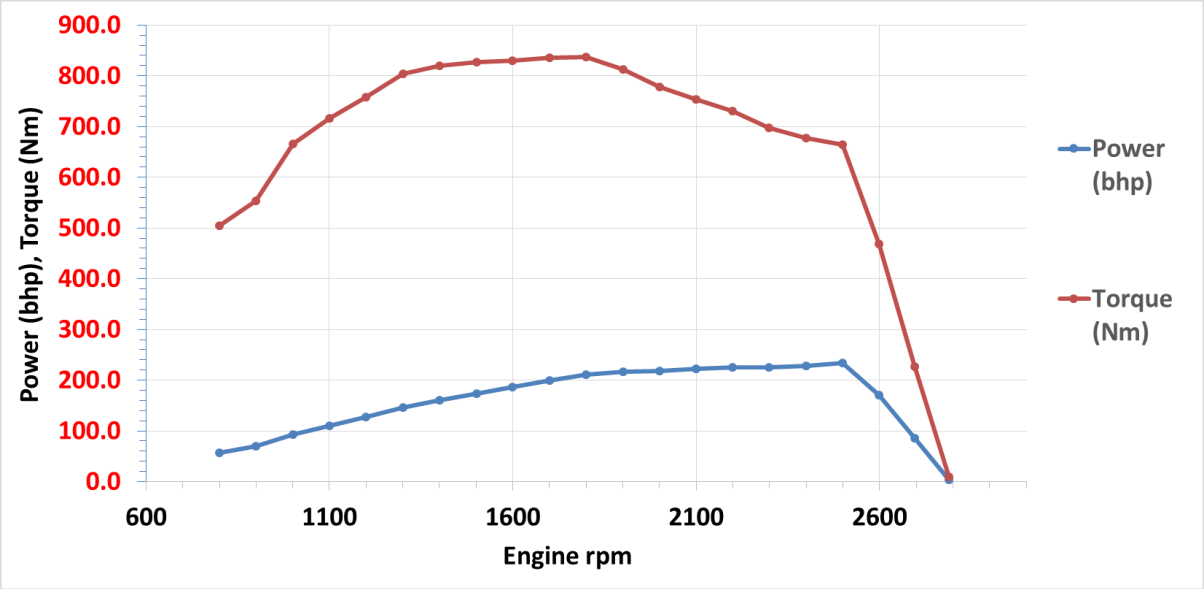



**Figure 6.1: Engine power and torque curves at wide open throttle for the 6.7L Cummins turbodiesel engine installed in the vehicle considered (data supplied by Valvoline)**

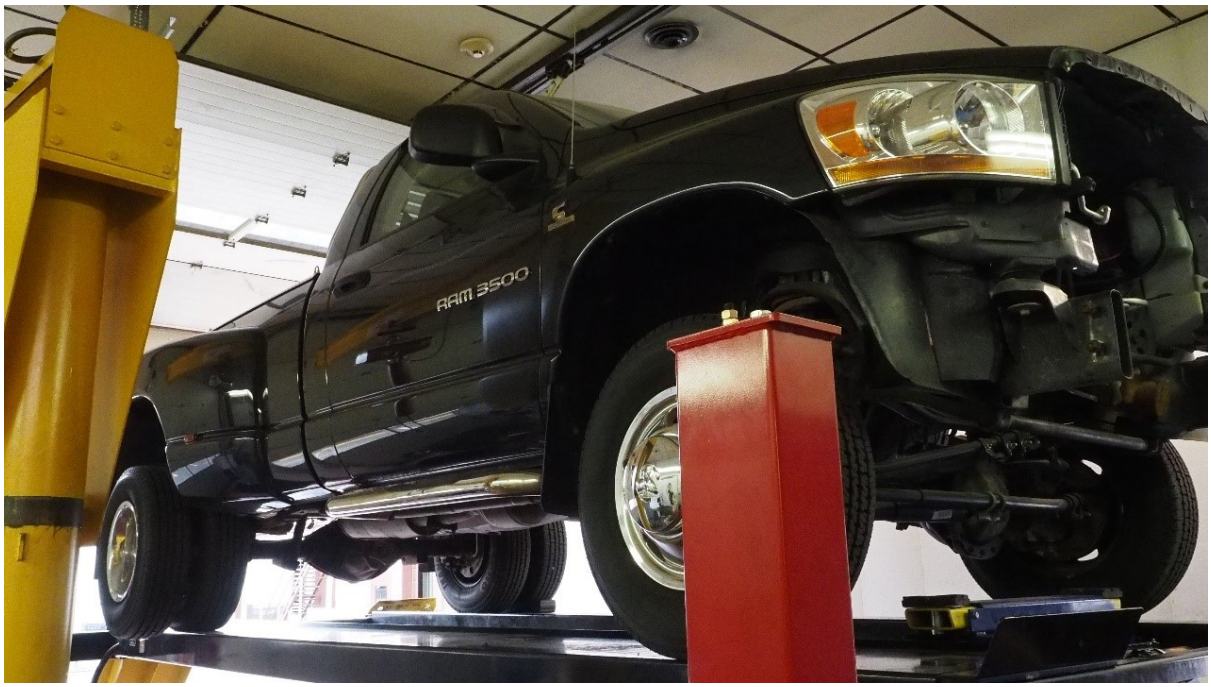



**Figure 6.2: The vehicle that was used for the experimental drive cycle**

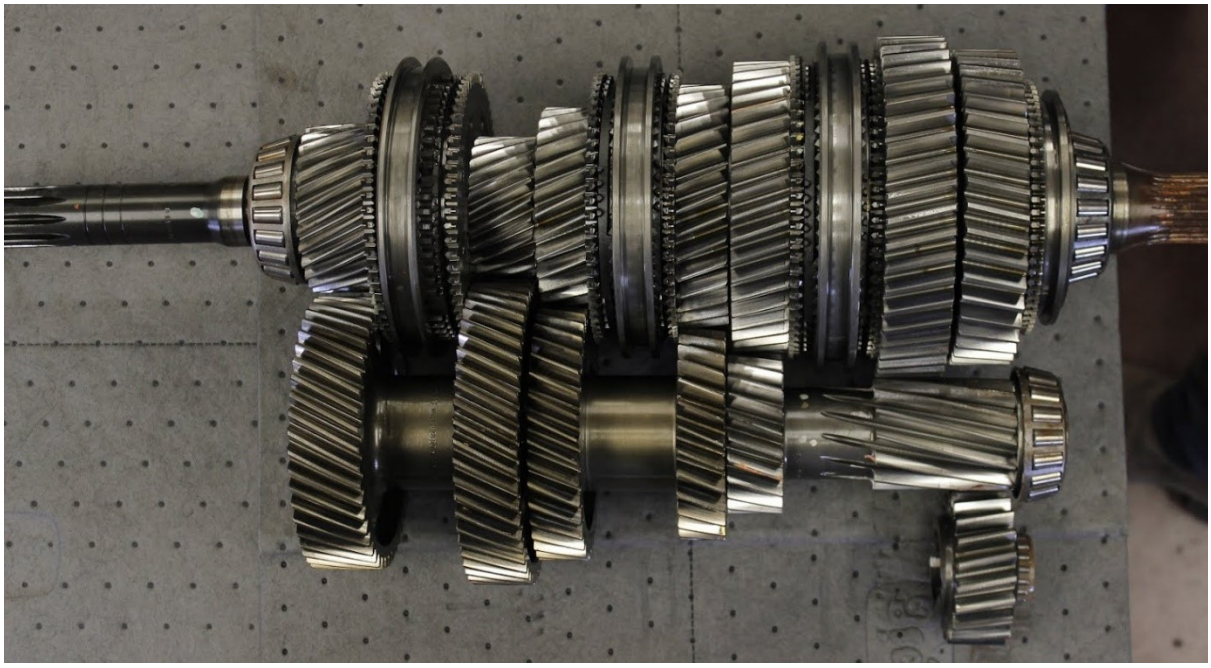


**Figure 6.3: The G56 six speed full synchromesh automotive gearbox**

After the vehicle was instrumented, it was driven multiple times with varying real road conditions in order to achieve different speed profiles and duty cycles. The lubricant used for the experiments was oil A. The instrumentation and the drive itself was conducted by Valvoline staff in Kentucky, USA, while the details of the desired data acquisition and duty cycles were supplied by the present author. The resulting speed profiles for three drives are shown in Figures 6.4, 6.5 and 6.6. It is evident that the drive cycles consist mostly of open road driving rather than start and stop city-style driving. The experimental drive cycles had three variations; the first one was low load, the second one was similar to the first but high load and the third one was more transient incorporating many stop-and-go type parts and was also high load. In the first and second case, the drive cycle was repeated driving i.e. forwards and back on the same road and so the second part is a mirror image of the first part. In the third case, a different uphill route was chosen as it was desired to have higher gearbox torques. There were some periods during the second part of the run (experimental cycle 1) or the initial part (experimental cycle 2) when the data logger was not logging properly hence there are a few straight lines and constant gradients on the profile, evident in the figures, as these areas were interpolated for the sake of temperature continuity. This does not effect the data significantly as the road conditions were relatively steady during this period anyway.

As far as the driving style is concerned, there was no particular shift strategy employed in the first and third case and most upshifts happened at around 2000 rpm. In the second case, a lower

rpm shift strategy was employed in order to highlight the effect of the driving style on the losses breakdown. The employed drive cycles were carefully designed to test the capabilities and usefulness of the model under different driving conditions. In cycle 1, the speeds were relatively high and the torque demand was relatively low which should result in relatively lower gear losses and increased bearing losses, whereas in the second and third cycles, a 3.5 tonne trailer was attached to the vehicle resulting in a much higher engine load and subsequently higher torque demand, which should in turn result friction losses. More information on the experimental drive cycles and a comparison to the two standardised drive cycles which will be modelled in the next section can be found in Table 10.

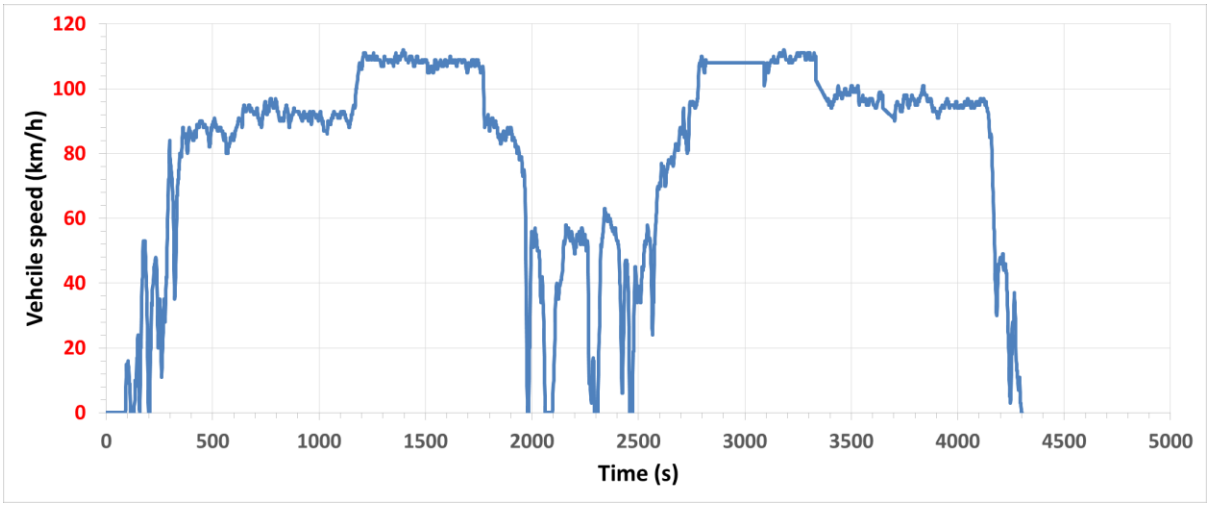



**Figure 6.4: The speed profile for the experimental drive cycle 1**

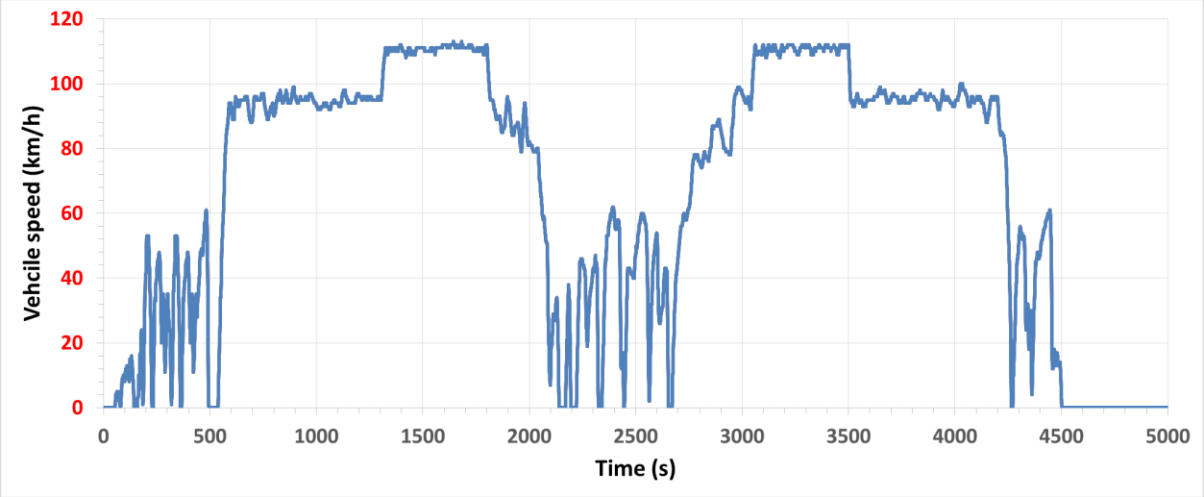



**Figure 6.5: The speed profile for the experimental drive cycle 2**

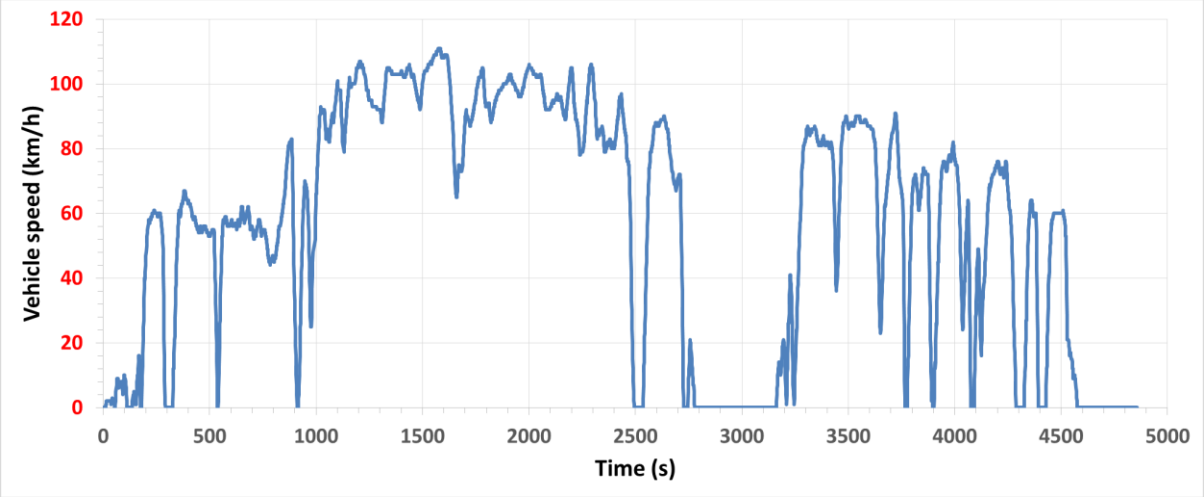



**Figure 6.6: The speed profile for the experimental drive cycle 3**

**Table 10: A comparison between the devised real road experimental drive cycles and the standardised drive cycles**

| Parameter | Experimental 1 | Experimental 2 | Experimental 3 | NEDC | Artemis URM 150 |
|---|---|---|---|---|---|
| Duration (s) | 4303 | 5133 | 4967 | 1220 | 3143 |
| Avg speed (km/h) | 80.85 | 65.54 | 54.4 | 32.47 | 59.18 |
| Max speed (km/h) | 112 | 113 | 111 | 120 | 150.4 |
| Avg torque demand (shift1/shift2) | 144.32 | 286.43 | 243.4 | 48.64/32.95 | 96.78/77.11 |
| Avg engine rpm (shift1/shift2) | 1748 | 1570 | 1377 | 1131/1649 | 1443.2/1877 |

In the G56 gearbox considered here, there are three shafts, seven sets of gear pairs, four synchronisers, four main bearings and several smaller needle bearings and couplings. As far as loss predictions are concerned, all major sources were taken into account, namely the gear

friction, the churning due to gear rotation and the bearing losses. Synchronisers were excluded as they are only partially moving, all needle bearings used to support the gears were not modelled and the casing seal losses were excluded as well. The main assumptions that were made for the modelling of the gearbox are as follows:

1. The gearbox was modelled using spur gears. The kinematics of helical gears would require a recalculation of forces and kinematics (and the resulting film thickness) at each point as the vectors are constantly changing. This could in turn be modelled by splitting the helical gear into many "slices" and doing the calculations for each slice. Although feasible, the drawback of such an approach is the significantly increased computational demand, and therefore for the purposes of this study it was considered adequate to model spur gears. In any case, the most important reason that manufacturers use helical gears in commercial automotive gearboxes is to reduce the noise emitted by the meshing gears however the difference in terms of efficiency between spurs and helicals is expected to be negligible. Helical gears have constant mesh stiffness resulting in lower internal dynamic loads and lower noise at higher speeds; for example BGA recommends use of helical gears at peripheral speeds over 10 m/s[160].
2. In this gearbox, the 5$^{th}$ gear is direct drive therefore when no gear is engaged (N) or when 5$^{th}$ gear is engaged, there is no bearing or gear friction loss. When no gear is engaged, the bearings are only supporting the weight of the components and the gears do not transmit any torque. The weight of the gears and shafts is insignificant compared to the load on the gear contacts when torque is transmitted.
3. There is no preload on any of the bearings – this was confirmed by the service manual of the gearbox.
4. The surface roughness of all the gears was fixed to 250 nm, an average value measured for the input shaft/5$^{th}$ gear pair and the 6$^{th}$ gear pair using a Talysurf roughness measurement rig (Figure 6.7). This value might vary slightly among the different gear pairs, however it was considered adequate to use the same value throughout for simplicity.
5. Only a portion of the surface area of the gearbox was used in the lump mass heat transfer calculations. The reasoning behind this assumption is that only the bottom part of the gearbox is actually exposed to the free stream of air measured at the front grille, since the gearbox only slightly protrudes under the vehicle. The main body of the gearbox is surrounded by the clutch assembly and other underbody panels and protectors, which

effectively block or severely restrict the flow of air. This was confirmed by the readings from the installed pitot tubes; the tubes mounted on the top and side surfaces of the gearbox were showing very small air velocity values. Therefore, at least half of the gearbox was not exposed to the airflow. As will be shown in the next section, the convective heat transfer coefficient between the gearbox surface and the surrounding air is strongly dependent on the value of the air velocity, with free convection making little difference in terms of heat transfer in comparison to forced convection. Therefore, assuming that the entire surface area of the gearbox is surrounded by air moving at the free stream velocity would give unrealistic heat dissipation rates. Since this was an experimental measurement and the exact value of the surface area exposed to the free stream could not be known unless a full velocity profile was available, different values for the "active" surface area, ranging from 20% to 50% of the total, were simulated for all three experimental drive cycles which will be described in the next section. The value found to match the experimental results more closely for all three cycles at the same time was two fifths (40%) of the actual surface area. Therefore this value was used in the lump mass calculations. Given the existing multiple pitot tube locations and measurements, this figure is realistic, but further measurements can be made to refine it.

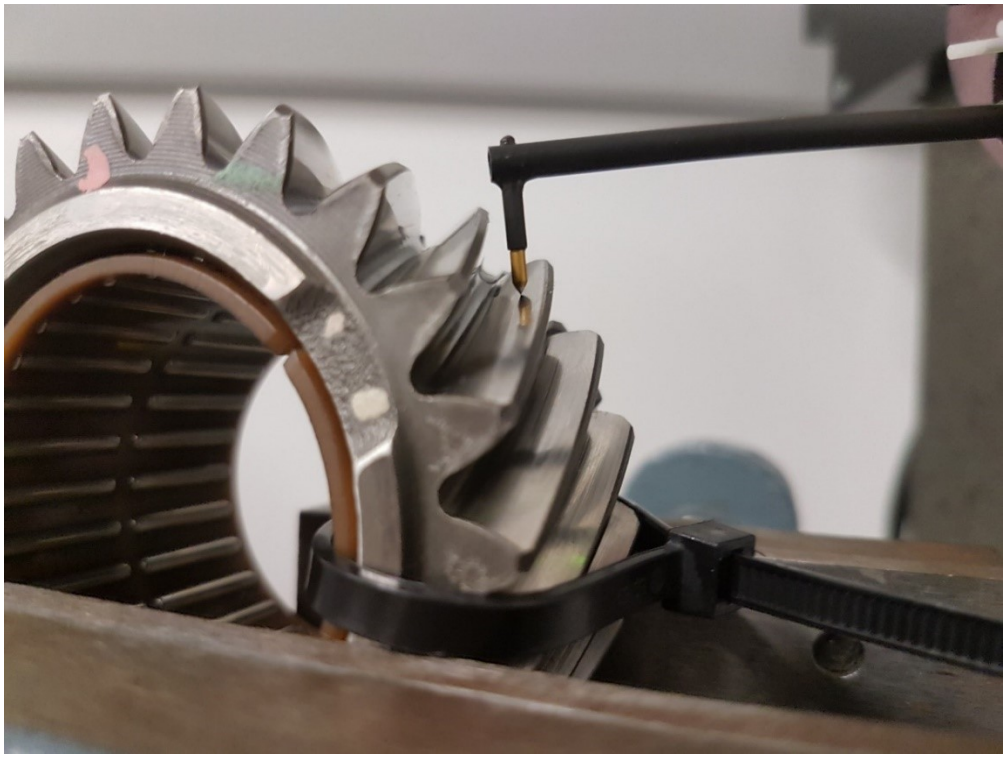


**Figure 6.7: Surface roughness measurement of the 6th gear**

### 6.2.2 Thermal model of the full gearbox

Once the drive cycle demand, the geometry and vehicle inputs are known, the last step to complete this model is to thermally couple it to the environment. In order to predict the temperature of the oil sump, heat transfer between the gearbox and the surroundings during vehicle movement needs to be calculated. For this reason the gearbox was instrumented with multiple thermocouples mounted both outside and inside the casing and their readings for the experimental drive cycle can be seen in Figure 6.8. All the thermocouples inside the oil sump (channels 4, 6 and 1) are basically showing the same temperature while the top and bottom of the gearbox (channels 3 and 7) show roughly 5 °C – 8 °C lower. The thermocouple that was mounted on the bell housing showed a higher temperature however this is due to the proximity to the engine, the clutch assembly and, perhaps most importantly, the exhaust pipes. The thermocouple readings for the other two experimental drive cycles were very similar in terms of observed trends and are not shown here. All experimental readings in the following sections are taken from the thermocouple on channel 5 which was mounted on the centre of the sump.

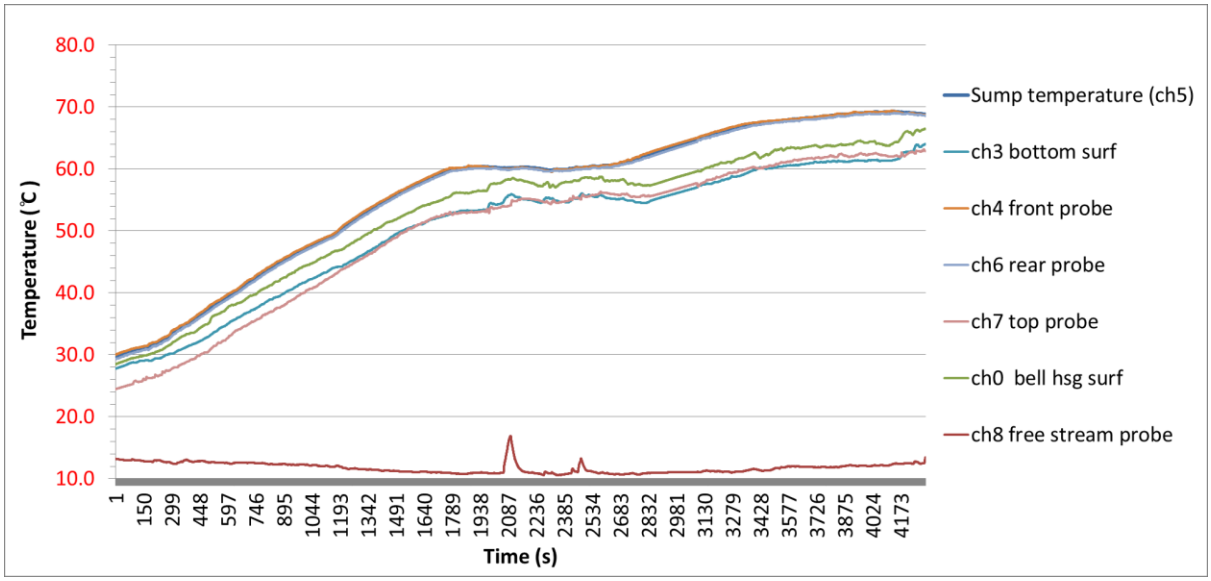



**Figure 6.8: The temperature readings from the thermocouples mounted inside and around the gearbox as well as the ambient temperature reading (ch8) for the first experimental drive cycle shown in Figure 6.4**

Given the minimum variations in temperature between different locations of the gearbox, as shown by the thermocouple readings, a lump mass approach for heat transfer between the gearbox and the surroundings was considered appropriate. The mass of the various parts of the gearbox was known and the surface area of the gearbox was approximated using measured

dimensions. By making these simplifications it is possible to calculate the temperature at each time step in a drive cycle relatively quickly so that the whole drive cycle can be modelled within an acceptable time and on a standard personal computer. In this approach, the lumped mass of gearbox components will absorb the heat resulting from gearbox power losses and will lose some of this heat through the gearbox casing walls to the surroundings because a free stream of air is flowing around part of the casing. Balancing the heat input and the heat lost to the surroundings, it is possible to calculate the temperature of the lubricant sump after one time step:

$$T_t = \Delta t * (P_{total} - htc * A_{gbox} * (T_{t-1} - T_{amb}) + mcp * T_{t-1})/mcp \quad (77)$$

Where $T_t$ and $T_{t-1}$ is the temperature of the sump at the current and at the previous time step, $\Delta t$ is the duration of the time step, $T_{amb}$ is the ambient temperature, $htc$ is the heat transfer coefficient due to forced convection between the surface of the gearbox and the surrounding air, $A_{gbox}$ is the surface area of the gearbox over which the external heat transfer occurs, $P_{total}$ is the overall gearbox power loss due to gear friction, bearings and churning and $mcp$ is the sum of each component's mass (steel parts, aluminium parts and lubricant), multiplied by the specific heat capacity of the material. In order to evaluate the equation, the convective heat transfer coefficient for the gearbox casing needs to be known.

If the fluid conductivity, $k$, the Nusselt number, $Nu$ and the characteristic dimension/length, $L$ (or D) is known then the heat transfer coefficient can be calculated, using standard heat transfer solutions, as follows:

$$htc = \frac{kNu}{L} \quad (78)$$

The characteristic length was selected to be the length of the gearbox in the direction of the air flow and the Nusselt number can then be calculated using the Churchill Bernstein equation[164].

$$Nu = 0.3 + \frac{0.6Re^{\frac{1}{2}}\,Pr^{1/3}}{\left[1 + \left(\frac{0.4}{\mathrm{Pr}}\right)^{\frac{2}{3}}\right]^{\frac{1}{4}}}\left[1 + \left(\frac{Re}{282000}\right)^{\frac{5}{8}}\right]^{\frac{4}{5}} \quad when\ PrRe \geq 0.2 \quad (79)$$

Where

$$Re = \frac{vL}{\nu}\ and\ Pr = \frac{\nu}{\chi} \quad (80)$$

are the Reynolds and Prandtl numbers respectively and $v$ is the fluid velocity, $\nu$ the kinematic viscosity and $\chi$ the thermal diffusivity.

### 6.2.3 Comparison of model predictions to measurements

In this section, the model was run using the inputs from the experimental drive cycles. The input torque was calculated from the engine load and the heat transfer coefficient was calculated using the method described above. The full power loss model described earlier was run for each time interval for the gear selected during that time. The sump temperature changes at each time interval were then predicted using the lump mass approach described above. The predictions were then compared to the experimental results.

In this two-stage, multi gear model, two gear pairs are engaged and transferring torque at any time, except when the 5$^{th}$ gear is selected, in which case the gear friction losses are assumed to be zero. Therefore, the frictional power loss of the gears has to be calculated twice per time step. This in turn results in increased calculation times compared to the single stage gearbox. A cycle consisting of 4000 time steps and with the contact path split into 125 points takes between 2.5 and 4 hours to solve, depending on the conditions and selected gears. Simulating a gearbox with more stages would proportionally increase this time by requiring more iterations of the calculation scheme. On the other hand, the increased number of bearings and the additional churning sources are all accounted for using simple equations which are much faster to solve. As a result, the most important factor to determine simulation time for this particular gearbox is the number of time steps in the drive cycle.

Simulations were run for both lubricants, A and B described previously, and the results were compared. In all cases, lubricant A was more efficient compared to lubricant B, a difference that was reflected both on the lower predicted sump temperatures and the lower power loss. Figures 6.9, 6.10 and 6.11 compare the predicted sump temperature for the two oils when the experimental drive cycles 1-3 were simulated.

For the first cycle, the predictions are very close to the experimental values up until the 3000 s mark. At this point the experimental value plateaus whereas the predicted temperature still rises very slowly for a short period of time until it also plateaus. This delay, which is also observed at the beginning of the test, is likely due to the components that either surround (exhaust) or are directly connected to the gearbox (clutch/flywheel assembly). These are expected to heat up much quicker than the gearbox itself as a result of engine and clutch operation and exhaust

gases. If this was taken into account an additional heat input from the exhaust and the engine would have to be added. The maximum difference between the two lubricants in terms of temperature is 2 °C and Oil B is constantly giving higher losses than Oil A, as will be seen in the losses breakdown figures that follow.

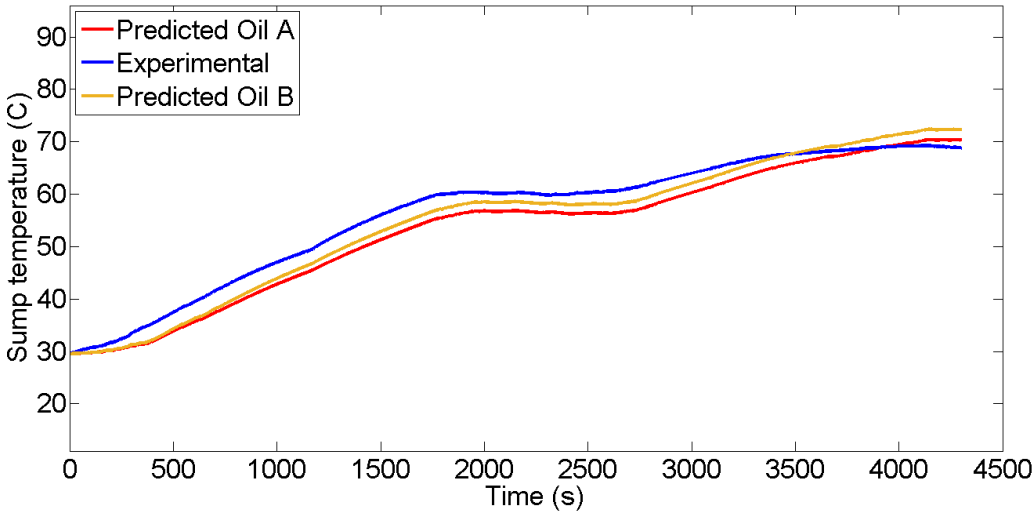



**Figure 6.9: Predicted vs experimental sump temperature for lubricants A and B (experimental drive cycle 1)**

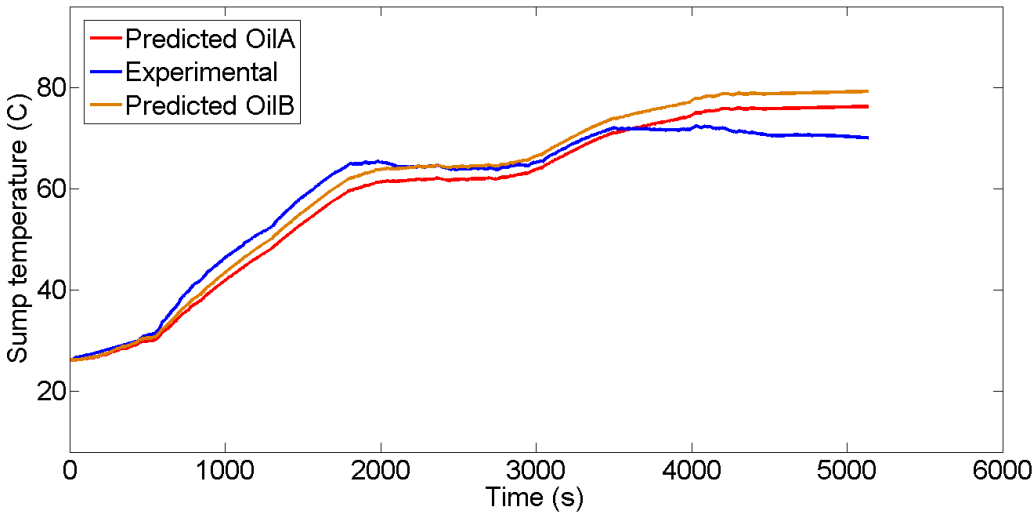



**Figure 6.10: Predicted vs experimental sump temperature for lubricants A and B (experimental drive cycle 2)**

As far as the second cycle is concerned, the predicted temperature again follows the experimental data closely and the same discrepancy is observed towards the end where the predicted temperature rises to a maximum of 5 °C higher than the experimental value. Again,

this is due to the thermal model excluding the engine and other surrounding components which reach a thermal equilibrium before the model does. Nevertheless, taking the latter observation into account the prediction is considered satisfactory and the trend followed is very close to the measured temperatures, particularly given that the experimental data is for real road driving conditions. In the third case, where the drive cycle was more transient compared to the first two, the temperature predictions are also very close to the measurements proving that the model offers a robust way of estimating transient temperatures in the oil sump as long as the gearbox characteristics are modelled correctly.

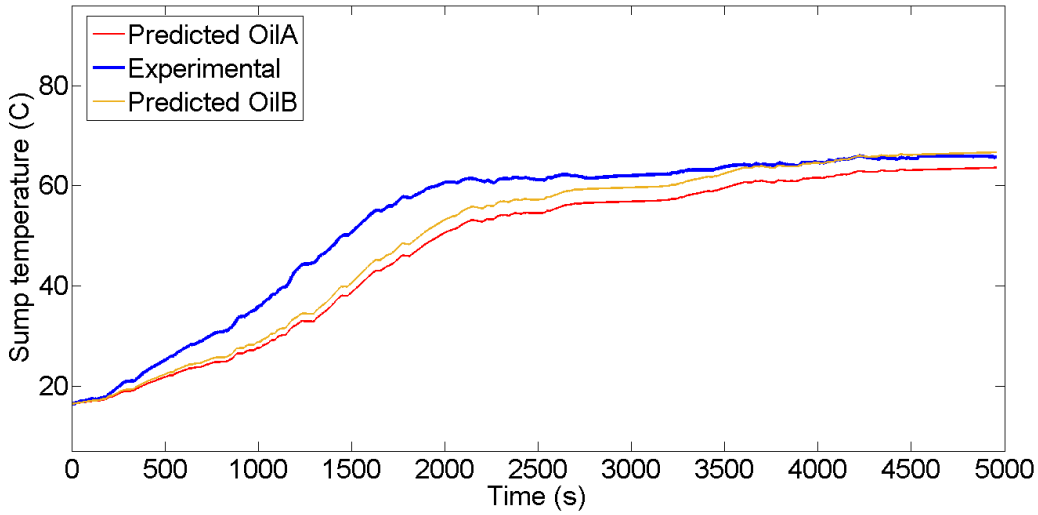



**Figure 6.11: Predicted vs experimental sump temperature for lubricants A and B (experimental drive cycle 3)**

Considering the breakdown of losses inside the gearbox, it can be seen in figures 6.12, 6.13 and 6.14 that, in all cases, bearing losses are dominant, with churning losses being more prominent whenever the vehicle speed is high. Gear friction losses on the other hand are almost always the smallest component except during the high power section between 250 and 400 s where they are equal to the bearing losses (1$^{st}$ cycle). A drive cycle with a high torque input is expected to generate significantly higher gear friction losses, as can be seen in the experimental drive cycle 2 where the average gear friction loss is 19.6 % of the overall with bearings at 52.4 % and churning at 27.9 % (7.9 %, 57.2 % and 35 % respectively for the first drive cycle with a very similar profile). This is in line with the results presented in the previous chapter for a simple single stage gearbox where higher torques increased the relative importance of losses due to gear friction.

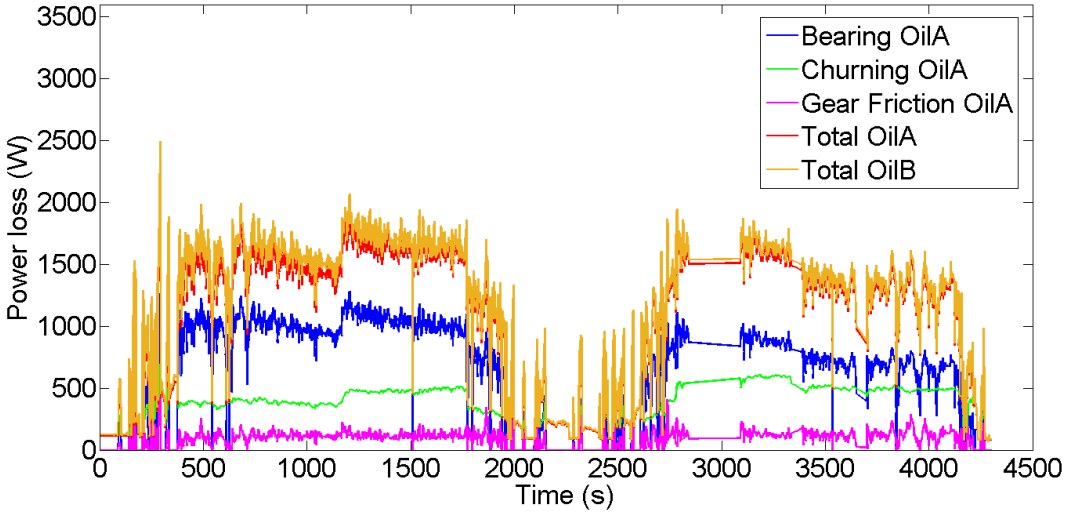



**Figure 6.12: The losses breakdown in the G56 gearbox (experimental cycle 1)**

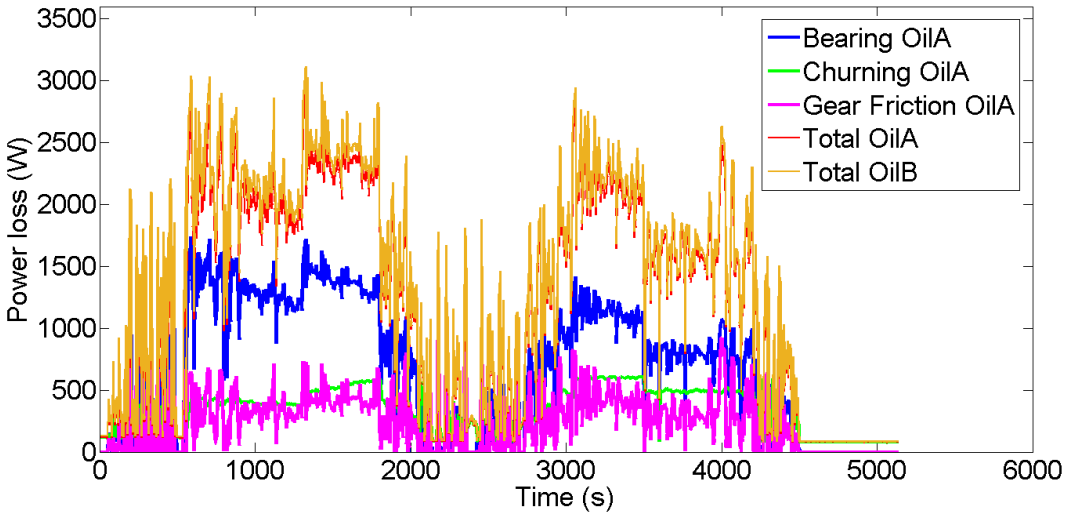



**Figure 6.13: The losses breakdown in the G56 gearbox (experimental cycle 2)**

The reason that the loss distribution is skewed in favour of bearing losses (particularly for the first drive cycle) is that the load is low and that the bearing design (TRB) is relatively inefficient. Compared to the single gear pair studied in the previous chapter, the breakdown trend is similar to condition 6 (see section 6.7.1) except for churning losses which are inevitably high in this automotive gearbox due to a deep immersion depth and multiple gear pairs rotating in the oil sump at all times (the gearbox is full synchromesh). Nevertheless, these results suggest that the earlier studies performed on the simple single stage gearbox can indeed identify important trends that are applicable in real multi-stage gearboxes, and hence can be useful in informing basic design decisions at early stage of gearbox design and oil selection.

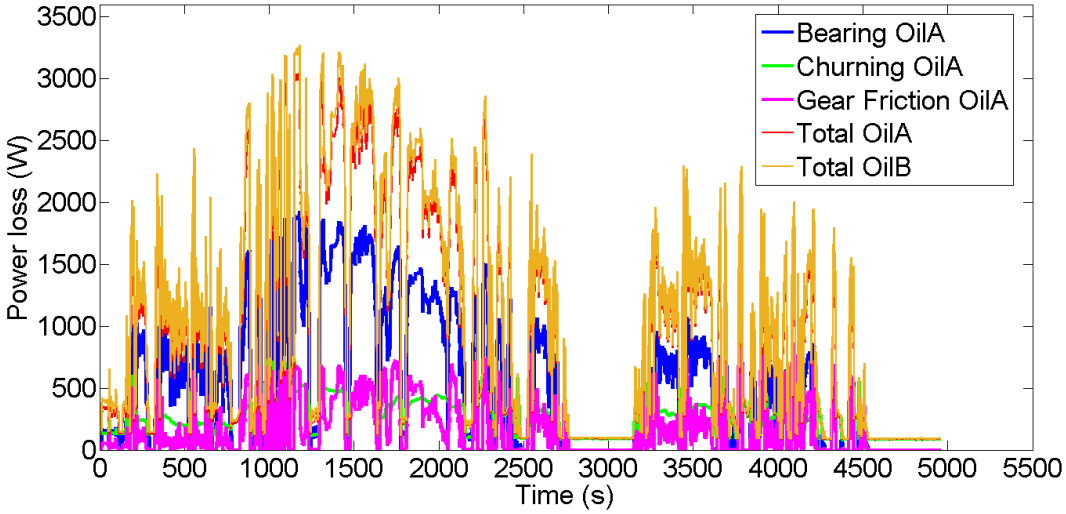



**Figure 6.14: The losses breakdown in the G56 gearbox (experimental cycle 3)**

A further analysis of the bearing losses, shown in Figure 6.15, reveals that the main shaft bearing is responsible for the highest percentage of bearing losses. The main reason for this is that this bearing is carrying relatively high loads, both axial and radial, compared to other bearings. In addition, it operates under relatively high rotational speeds for most of the time because of the extended periods that these drive cycles run in 6$^{th}$ gear (gear ratio 0.742). The input shaft bearing rotates at high speeds at all times (engine speed) and is relatively highly loaded compared to the countershaft bearings, thus producing higher loads than the countershaft bearings, which exhibit the lowest losses of the three bearing locations. The bearings losses breakdown is very similar for the other two experimental drive cycles with the main shaft bearing being the main contributor. These results are significant as they pinpoint the critical components in terms of efficiency and hence can enable the gearbox manufacturers to improve the design at minimum cost by targeting the appropriate components.

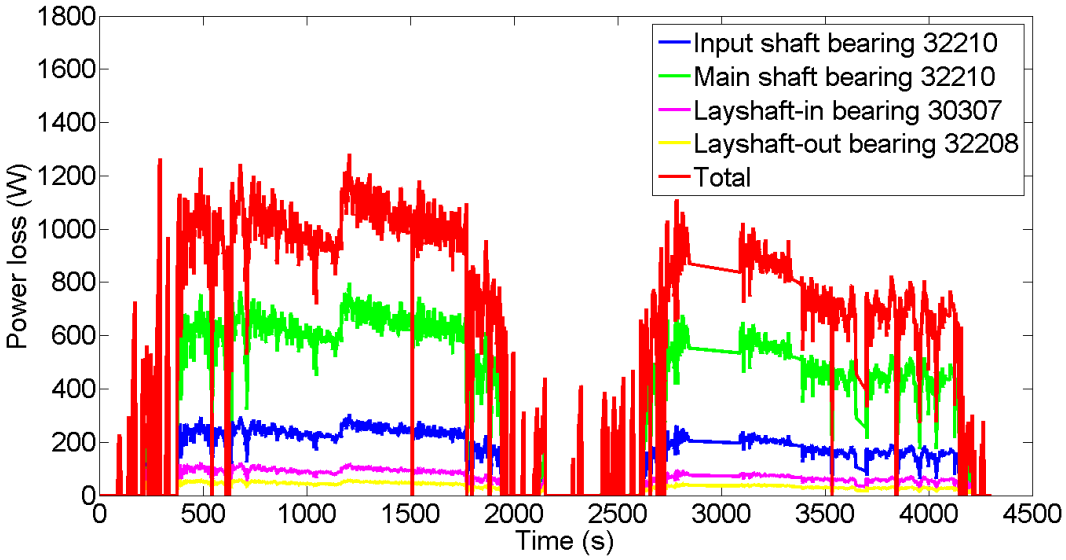



**Figure 6.15: The losses breakdown per bearing in the G56 gearbox for Oil A (experimental cycle 1)**

### 6.2.4 Model predictions in standardised drive cycles

#### 6.2.4.1 Drive cycle profiles and estimation of required inputs

In this section, the model was used to simulate two popular standardised drive cycles namely the legislative NEDC and the Artemis URM 150. The first is used for type approval of cars, vans and other light duty vehicles in the European Union and is closer to a steady state drive cycle than a transient one as it includes lengthy constant velocity periods as well as very gradual acceleration and deceleration phases. The version of the cycle used here includes a 40 second idle period at the start and consists of 4 repeated ECE 15 (city) and one EUDC (highway) drive cycle. The second was developed as part of the European 5$^{th}$ Framework project and is more representative of real road driving conditions, however many manufacturers are still using the NEDC for type approval (and advertising) purposes as it gives far lower emissions. The Artemis URM150 comprises many parts, from city driving (urban) to suburban and highway sections. The two drive cycles are shown in figures 6.16 and 6.17 respectively. To simulate the two drive cycles, the torque at the gearbox input, the rotational speed of the gears and the selected gear had to be known. In order to find the required or demanded torque, the WTO efficiency map of the engine, shown previously was used. The torque demand was calculated from the required tractive effort of the vehicle.

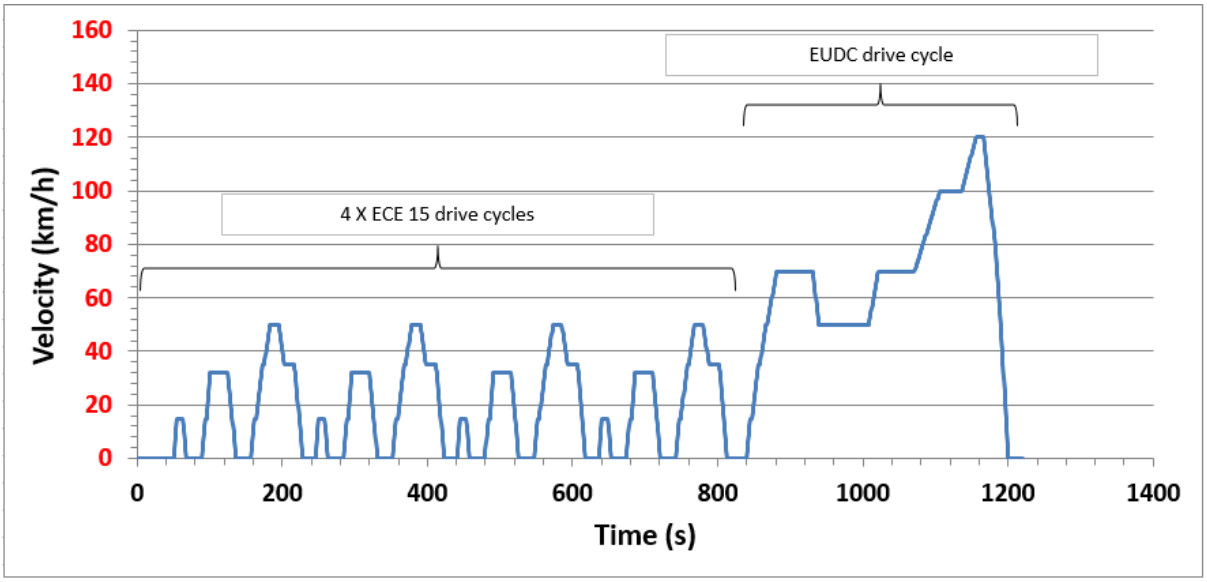



**Figure 6.16: The New European Drive Cycle (NEDC) including an initial 40 s idle period**

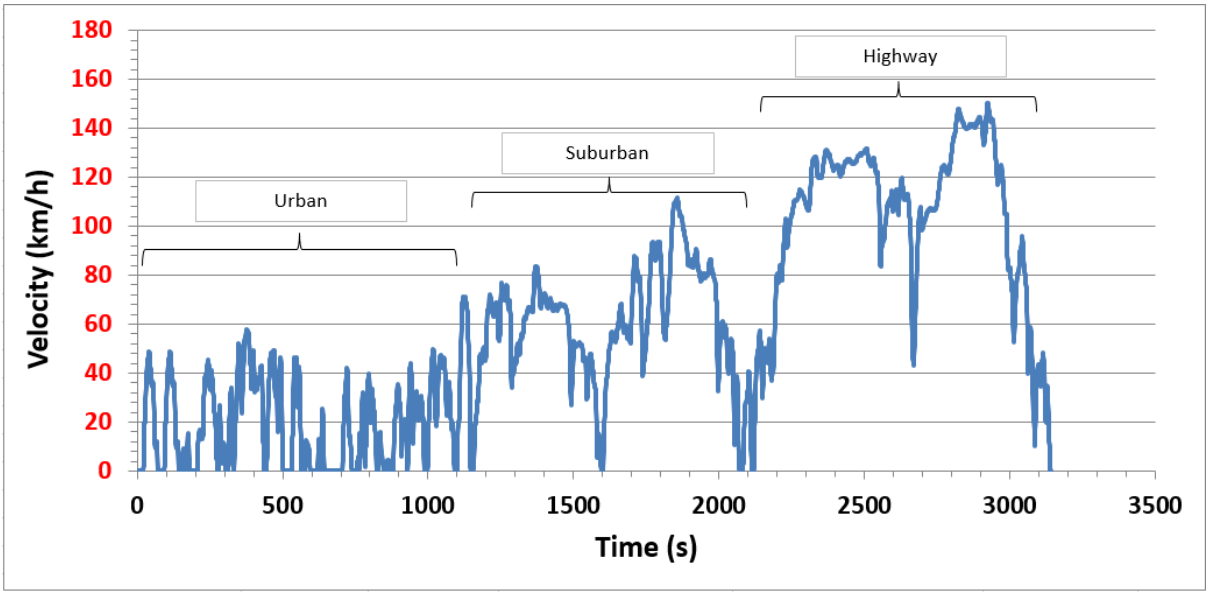



**Figure 6.17: The Artemis URM150 drive cycle**

When a vehicle is travelling at a constant speed or accelerating, the required tractive effort is the force needed to overcome the resistance forces as well as the friction in the various parts of the vehicle (engine, drivetrain). The tractive effort is the sum of these resistances. Excluding internal friction losses, the tractive effort comprises three terms namely aerodynamic, gradient and rolling resistance[165]. Aerodynamic resistance, $R_a$, mostly depends on the shape and size of the vehicle and is proportional to the square of the vehicle's speed. Gradient resistance,$R_g$, depends on the slope of the road and the vehicle's weight whereas rolling resistance, $R_r$,

depends on the rolling resistance of the tyres and hence the tyre and road surface and material, as well as the vehicle's weight.

When the vehicle is accelerating, the sum of all forces acting upon it can be found by Newton's second law:

$$\Sigma F = ma \ (81)$$

Substituting the three resistances and the force provided by the vehicle at the wheels we get:

$$F = R_a + R_g + R_r + ma \ (82)$$

Aerodynamic resistance[166] is mostly due to the turbulent air flow around the body of the vehicle (85%), the friction between the body and the air (12%) as well as the resistance of vehicle components, for example air vents and radiators (3%). It can be expressed as:

$$R_a = \frac{1}{2}\rho v^2 A C_d \ (83)$$

Where $\rho$ is the air density, $v$ is the relative velocity between the air and the moving vehicle, $A$ is the vehicle's frontal area and $C_d$ is the overall vehicle drag coefficient. The frontal area is simply approximated by multiplying the width by the height and subtracting the area between the ground and the lower end of the bumper. The drag coefficient for this particular truck could not be confirmed by the manufacturer but various online sources[167][168][169] put it between 0.44 and 0.48 for a 2006 model therefore an average value of 0.46 was used.

The gradient resistance is simply the component of gravitational force acting on the vehicle when it is travelling at a slope of angle $\theta$.

$$R_g = mgsin\theta \ (84)$$

Finally, the rolling resistance[166] is the sum of resistances due to tyre deformation (90%), surface compression and tyre penetration (4%), tyre slippage and the circulation of the air through and around the wheels (6%). It can be approximated as:

$$R_r = C_r mgcos\theta \ (85)$$

Where $C_r$ is the coefficient of rolling resistance for pneumatic tyres. This coefficient varies greatly from tyre to tyre and generally, the higher the traction a tyre provides, the higher the resistance. A specific value for the tyre fitted on the vehicle was not provided by the manufacturer. For this reason, an average value of 0.1 was used that matches the average given by three major tyre manufacturers for a group test[170].

By substituting the above terms into the basic equation we can calculate the total tractive effort.

$$F = \frac{1}{2}\rho v^2 A C_d + mgsin\theta + C_r mgcos\theta + m\frac{dv}{dt} \quad (86)$$

To calculate the required torque at the wheels one simply needs to multiply the calculated tractive force by the radius of the wheel.

$$T = Fr_w \quad (87)$$

The required rpm of the wheels can be back-calculated from the required velocity of the current step in the drive cycle. Then to calculate the required rpm of the crankshaft (gearbox input), the rotational speed of the wheels has to be multiplied by the ratio of every transmission component between the wheel and the crankshaft namely the differential (final drive) and the gear pairs engaged in the gearbox. For example, when 6$^{th}$ gear is engaged the rotational speed at the gearbox input would be

$$rpm = \left(\frac{30}{\pi r_w} v\right) u(diff)\, u(6)\, u(5) \quad (88)$$

Where $\frac{30}{\pi r_w} v$ is the rpm of the wheels, $u(diff)$ is the final drive ratio, $u(6)$ is the gear ratio between the main shaft and the countershaft for 6$^{th}$ gear and $u(5)$ is the gear ratio between the input shaft and the countershaft. Similarly, the input torque can be found from the required torque at the wheels.

When the gearbox input torque and rotational speed is known, the model can be used to predict the losses in the gearbox if the selected gear pair is known. For this reason, a shift strategy needs to be implemented. For the selected application and based on the WOT power curve of the engine two different shift strategies were modelled. The first shifts gear at 1500 rpm which is the point at the start of the maximum torque region of the curve and the second shifts gear at 2500 rpm which is where maximum power occurs. This comparison was implemented in order to find the most efficient shift strategy when a full efficiency map is not available.

#### 6.2.4.2 Results and lubricant comparison

The two drive cycles were simulated using three sets of conditions - changing the oil, the shift strategy and finally adding a gradient to introduce extra resistance and therefore increase the torque demand and the resulting power loss. Figure 6.18 shows the predicted sump temperature

for the NEDC drive cycle and the two shift strategies with or without the added gradient resistance.

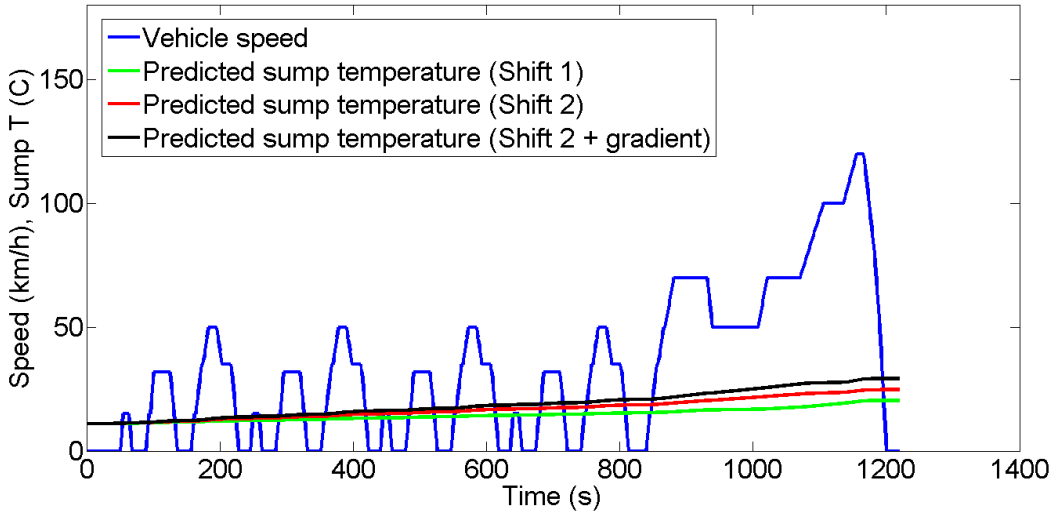



**Figure 6.18: A comparison between the two shift strategies and the effect of gradient resistance on the NEDC drive cycle (Oil A)**

It can be seen that the second shift strategy results in higher predicted temperatures due to higher churning losses in bearings and gears. The added gradient takes the average torque demand under the high power shift strategy from 32.95 Nm to 132.5 Nm therefore appreciably increasing the gear power loss and the predicted temperatures. The maximum predicted temperature is 20.43 °C for the maximum torque shift strategy, 24.8 °C for the maximum power shift strategy and 29.31 °C for the maximum power shift strategy when the gradient resistance is added.

As far as oil comparison is concerned, a 2 °C difference was observed between the two oils when the medium torque and high rpm experimental drive cycle 1 was run (Figure 6.9). On the NEDC which averages 32.95 Nm and 1131 rpm (compared to 144 Nm and 1748 rpm for the experimental cycle 1), it is expected that the difference between the two oils will be minimal. The sump temperature prediction for the NEDC drive cycle and both oils can be seen in Figure 6.19, followed by the losses breakdown (Figure 6.20), all run for the first (maximum torque) shift strategy. As expected, the gear friction losses which are the primary cause of separation between the two oils are very low, confirming that no significant difference should be expected between the two oils.

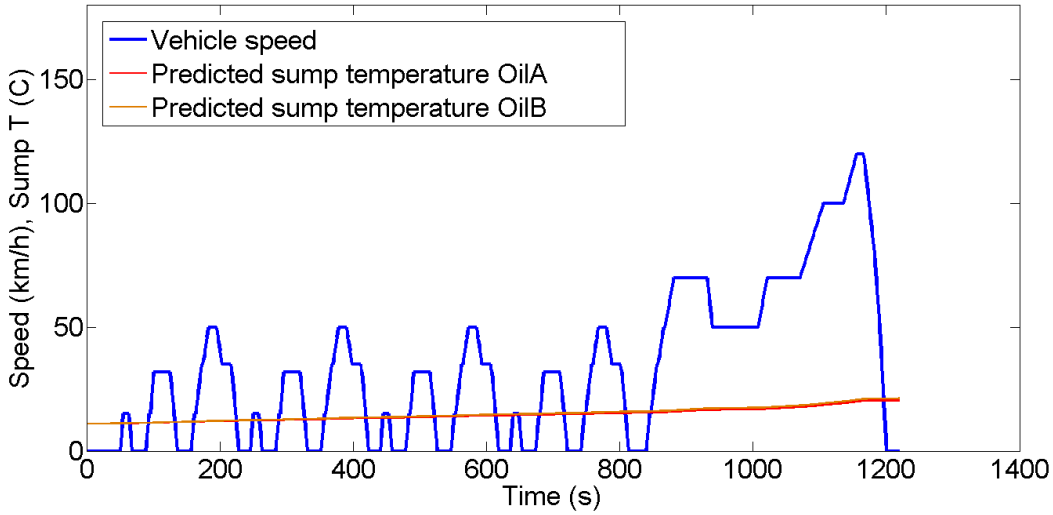



**Figure 6.19: The predicted sump temperatures for oils A and B for the NEDC drive cycle (Shift 1)**

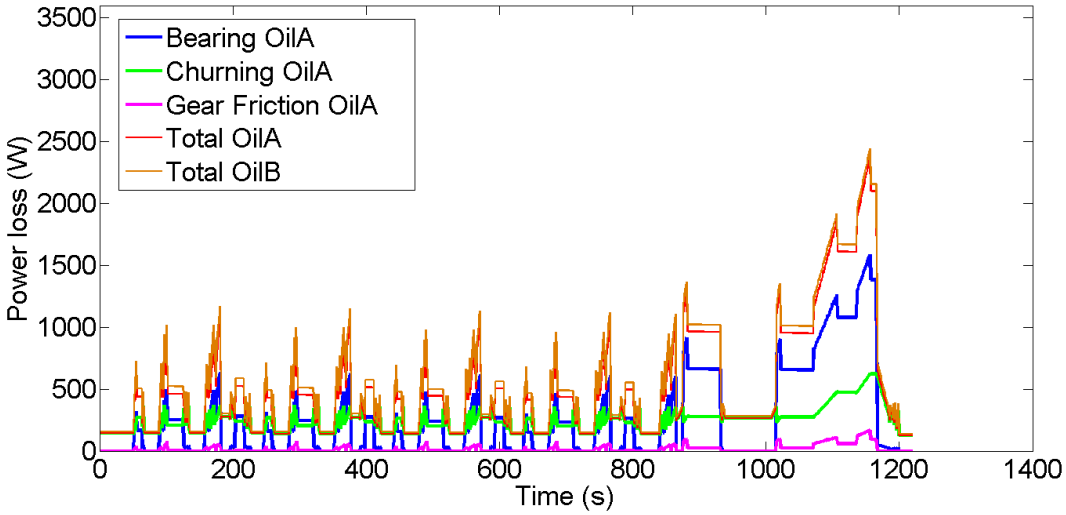



**Figure 6.20: The losses breakdown in the gearbox for the NEDC drive cycle (Shift 1). For clarity, only total losses are shown for oil B.**

Figure 6.19 indeed shows that there is no significant difference in terms of predicted sump temperature as at the end of the drive cycle for the two oils, the difference being only 0.8 °C apart. The same can be said about the losses as it is the total loss that primarily determines the sump temperature. Regarding the breakdown of losses one can observe that bearing and churning losses are roughly equal during the slow "city driving" parts with gear friction losses being very low in comparison, the reason for the latter being the low required input torque

throughout the entire cycle. When the drive cycle shifts to high speeds where rotational speeds of the components are higher, bearing losses overtake churning to become dominant.

The results can be compared to the NEDC drive cycle with the maximum power shift strategy (shift strategy 2) and an added gradient of 6.5 degrees, shown in Figures 6.21 and 6.22 below Under these higher load conditions the difference between the oils becomes more prominent and the maximum observed temperature for oil A is 29.31 °C compared to 31.04 °C for oil B. The loss breakdown is different compared to the low torque cycle shown above. While bearings still dominate, the gear friction losses are now a significant proportion of the overall, especially so during the last part of the drive cycle (EUDC) where they are higher than churning and comprise roughly a quarter of the overall losses, with churning taking up another quarter and bearing loss being almost half.

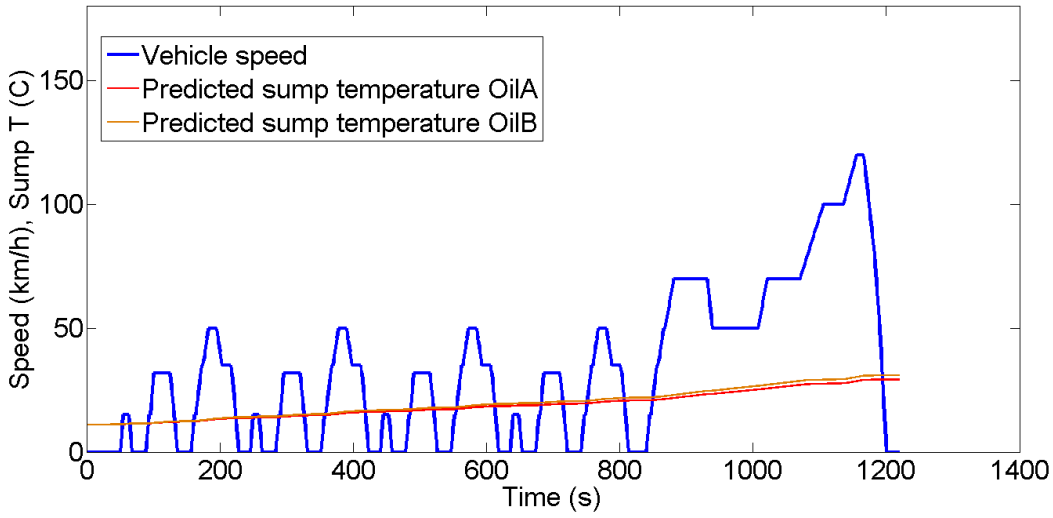



**Figure 6.21: The predicted sump temperatures for oils A and B for the NEDC drive cycle (Shift 2 + gradient)**

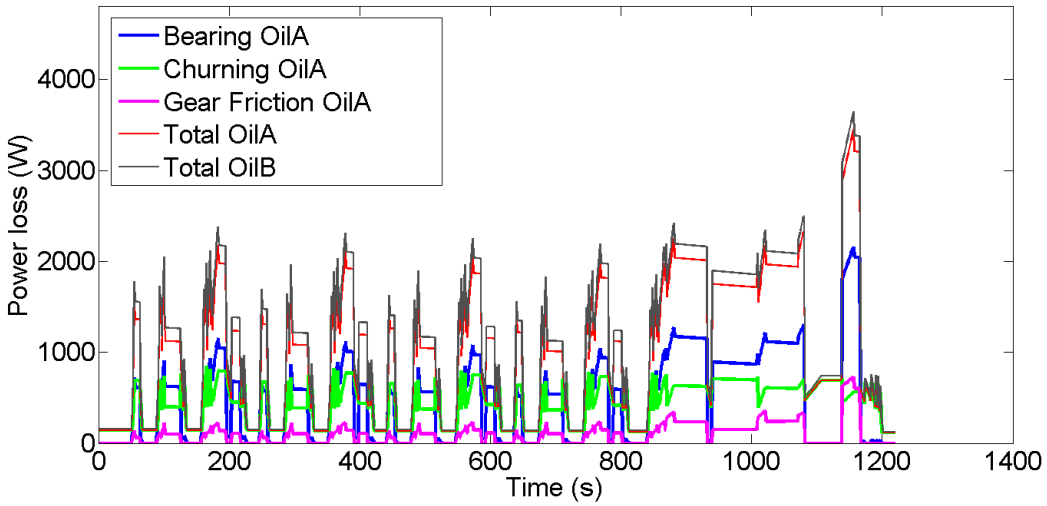



**Figure 6.22: The losses breakdown in the gearbox for the NEDC drive cycle (Shift 2 + gradient). For clarity, only total losses are shown for oil B.**

Therefore a vehicle run on the NEDC drive cycle would be more efficient when oil A is used however the difference is not large. This is mainly because the NEDC is relatively low load and extremely smooth in terms of speed variation, but also because the duration of the drive cycle does not allow for greater differences to develop. Moving on to the more demanding and transient Artemis URM150 drive cycle, the same comparisons reveal a significantly more pronounced difference between the two oils, as shown in Figures 6.23 and 6.24 below. The maximum sump temperature is 42.92 °C for oil A compared to 46.96 °C for oil B, as a result of higher losses from all sources.

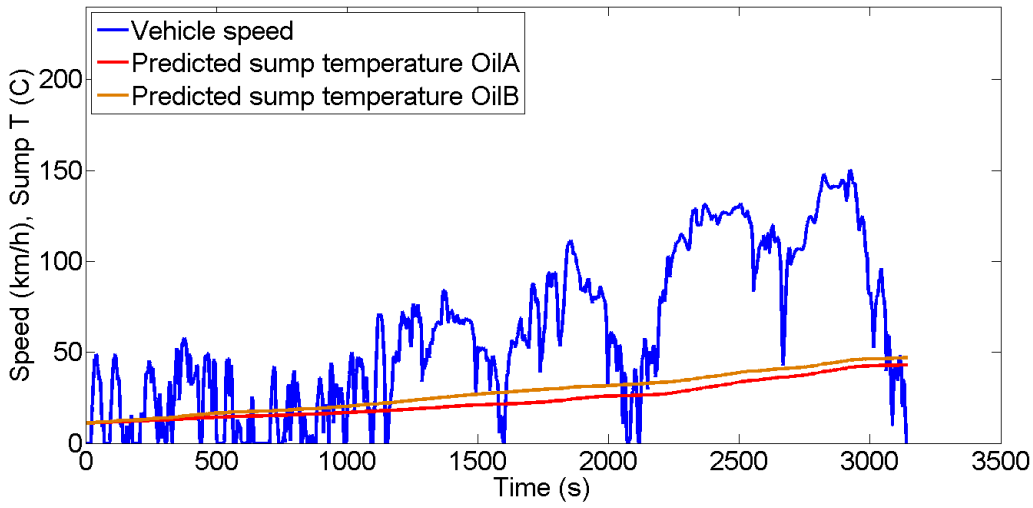



**Figure 6.23: The predicted sump temperatures for oils A and B for the Artemis URM 150 drive cycle (Shift 1)**

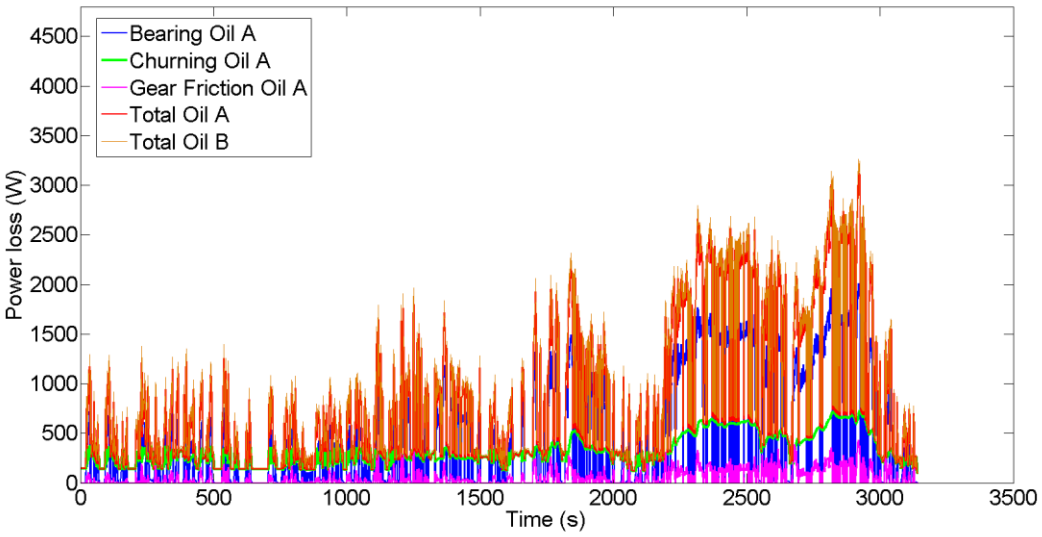



**Figure 6.24: The losses breakdown in the gearbox for the Artemis URM 150 drive cycle (Shift 1)**

As explained in the previous chapters, most of the difference between the oils is expected to occur either because of lower operating temperatures (due to viscosity difference) or at high loads where the regime shifts towards mixed and the difference in boundary friction coefficient becomes more important. To investigate the effect of a boundary friction coefficient further, the same high power run was simulated but with the boundary friction coefficient capped to 0.06 (measured value for oil A is 0.116, and for oil B it is 0.125). This did not make a significant difference as the lambda ratio for these runs was high enough and the gears spent the majority of the time outside of the boundary regime. The effect of the boundary friction (via a different friction modifier for example) would be expected to be more significant in high load drive cycles, potentially narrowing down the gap between the two lubricants significantly. To further illustrate the effect of oil selection on gearbox efficiency, two cumulative graphs showing the losses breakdown for all the drive cycles can be seen in Figure 6.25 below, followed by the difference in the maximum predicted temperature between the two oils in Figure 6.26.

It can be seen that generally, the breakdown of losses compares well to the results obtained with the simple single stage gearbox of chapter 5 when the large bearings were used, except churning losses which are much higher in a full gearbox due to the number of gears rotating in the sump at all times. The only case where gear friction losses are higher in comparison is when the experimental drive cycle was driven with the truck heavily loaded. The much larger torque demand resulted both in higher predicted temperatures and higher gear friction losses.

Although bearing losses always dominate, there is a large variation between different drive cycles and the gear friction losses range from a minimum of 1.6 % for the very low load NEDC S2 drive cycle to a maximum of 19.6 % for the severe experimental drive cycle 2. As far as bearing losses are concerned, the lowest losses (26.7 %) were observed for the experimental drive cycle 3 and the highest (57.2 %) for the low load experimental drive cycle 1. Churning was highest (60.2 %) for the NEDC S2 drive cycle as a result of high rotational speeds and low torque, and lowest (27.3%) for the high load, low rpm experimental drive cycle 3.

An examination of the temperature difference between the two oils reveals that oil A always results in lower predicted temperatures compared to oil B and this difference is maximised when the gear friction losses are higher (due to rheological differences explained above), as is the case with experimental drive cycles 2 and 3, or when the operating temperatures are lower, as a result of bearing losses and churning where viscosity is most important.

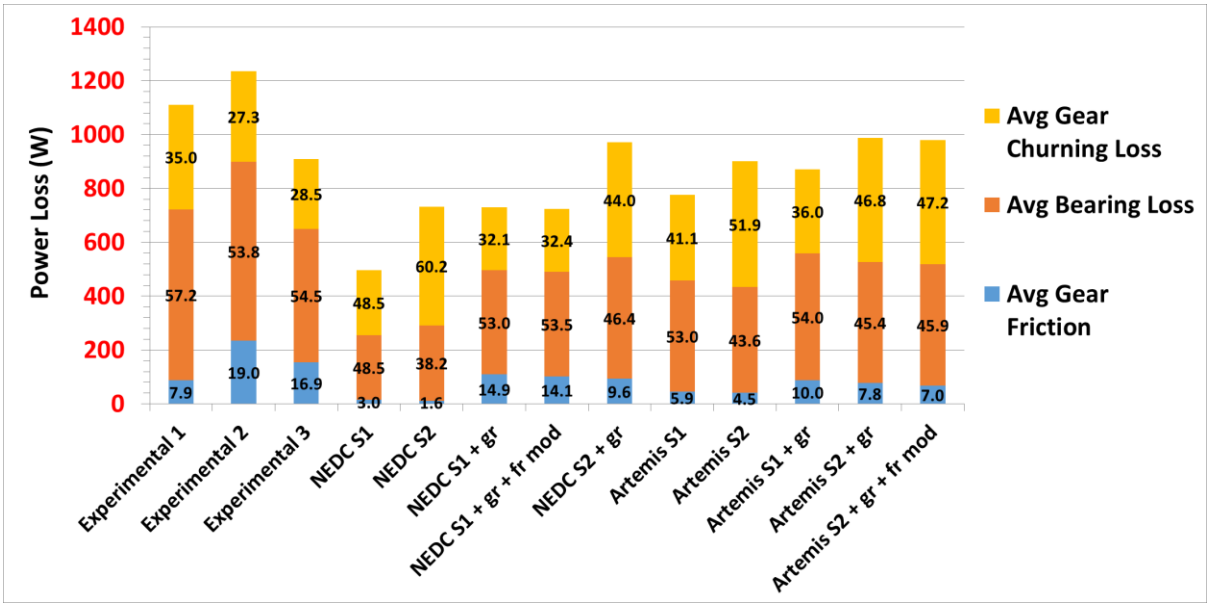



**Figure 6.25: The losses breakdown for the experimental and standardised drive cycles (Oil A)**

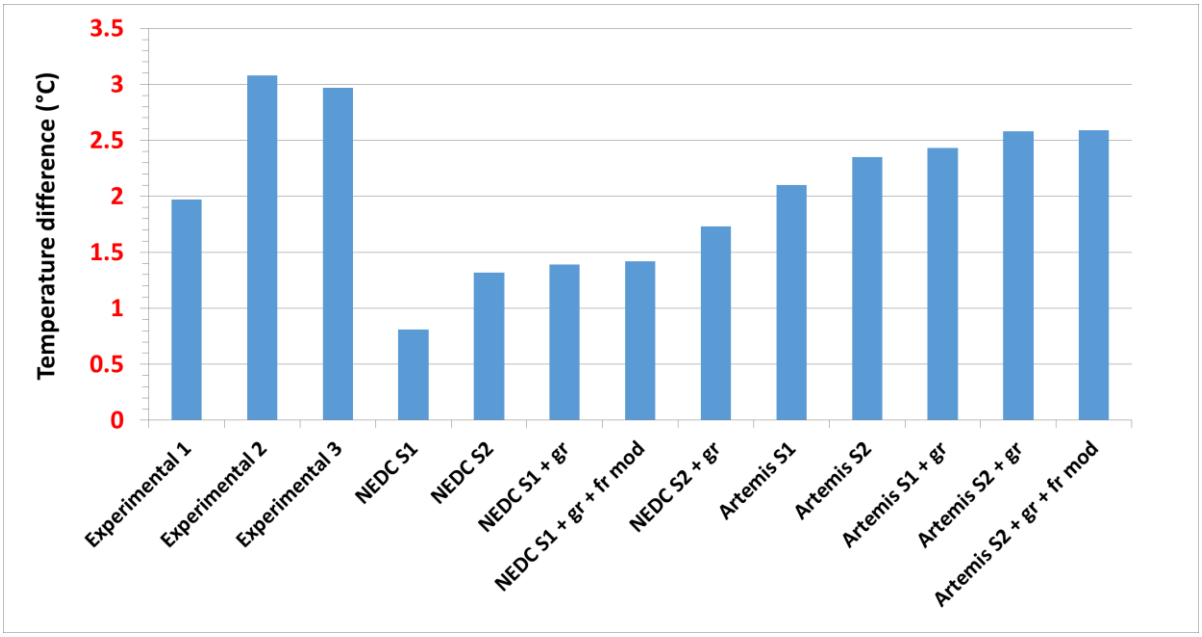



**Figure 6.26: The difference in maximum predicted temperature between oils A and B for each of the simulated drive cycles (predicted temperature for oil B is always higher)**

Finally, the overall efficiency of the gearbox is examined and the two lubricants are compared in terms of efficiency. Figure 6.27 below shows the calculated average efficiency values for both the experimental and the standardised drive cycles. In terms of absolute values, the overall efficiency ranges from 87.1 % to 97.5 % for oil A and falls between 85.9 % and 97.2 % for oil B. This wide range of values shows that the lowest load NEDC drive cycle also gives the lowest efficiency, whereas the experimental drive cycles which exhibit the highest overall losses are also the most efficient. The same trend was observed in the single stage gearbox of chapter 5.

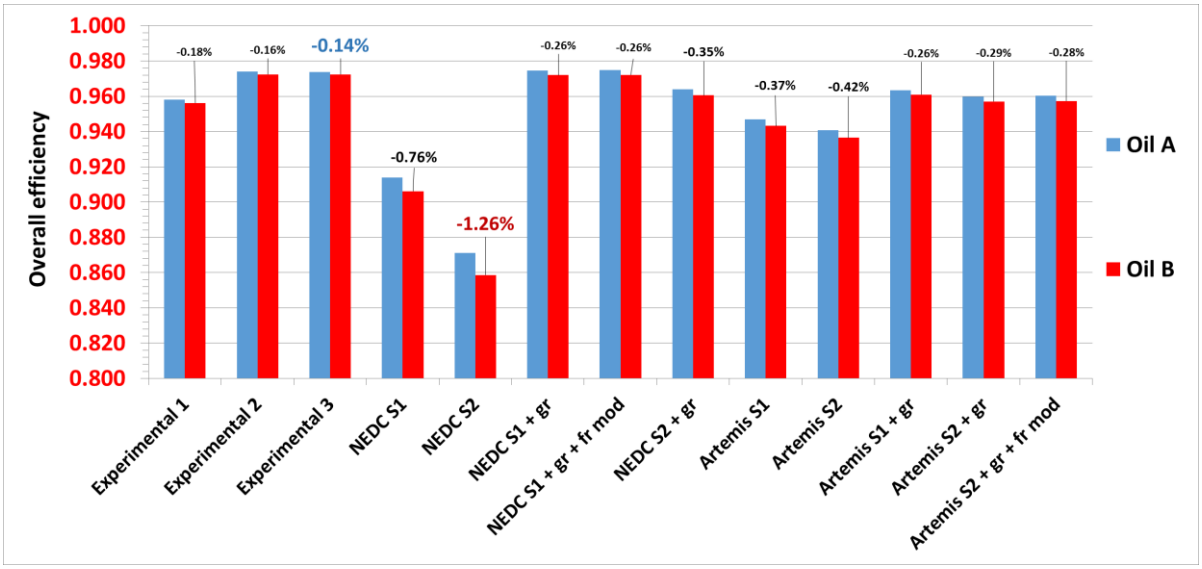



**Figure 6.27: The difference in overall efficiency between oils A and B**

As expected from previous results, oil B is consistently less efficient compared to oil A with percentile values ranging from -0.14 % (experimental drive cycle 3) to -1.26 % (NEDC S2). The difference was low for all experimental drive cycles and higher for the standardised drive cycles. This observation, which is in contrast to the results from the temperature comparison above, is explained by the fact that the predicted temperatures are low in the low load cycles which brings the viscosity difference into effect and surpasses the effect of the experimentally derived lubricant properties.

These results illustrate the value of the present model in helping to select the most appropriate lubricant for the expected duty cycle of the vehicle and hence improve the overall efficiency of the vehicle at a minimum cost. By accounting for the influence of lubricant properties on various loss sources in a full gearbox, the model informs this lubricant selection process or alternatively, its results can be used to help formulate new lubricants intended to reduce losses in a specific application, automotive or otherwise.

## 6.3 SUMMARY

In this chapter, the model was used to simulate a commercial automotive gearbox mounted on a US-specification full size truck. Several experimental drive cycles were run in conjunction with the NEDC and Artemis URM150 standardised drive cycles. Model predictions were compared to measurements in terms of sump temperatures (and therefore power losses indirectly) made during real road test drives and the results generally compare very well, with small differences being explainable in terms of the effects of nearby components and gearbox mounting on gearbox heat transfer. For the latter, effects such as gradient resistance and a boundary friction modifier were explored and the comparative results were presented. The two transmission lubricants were compared in terms of power loss and predicted sump temperatures for these drive cycles, and the results indicate that the model can differentiate between different lubricants in terms of overall gearbox efficiency for specific driving conditions and can therefore be used for lubricant selection. In the next chapter, the main findings of this work will be analysed and discussed.

# 7. DISCUSSION

## 7.1 Introduction

In this section, the most important findings and the main results of this work will be discussed. First the main advantages and limitations of the proposed gearbox efficiency model are discussed. Then the main results both from the single stage and the commercial gearbox will be analysed and compared, the losses breakdown will be examined and the lubricants will be assessed in terms of overall efficiency. Finally, the main trends from the two gearboxes will be qualitatively compared to the results of similar studies.

## 7.2 Advantages and limitations of the proposed gearbox efficiency model

The methodology for prediction of gearbox losses devised here offers a number of improvements over existing predictive tools. Most significantly, it provides a means of including the effects of lubricant properties in terms of contact friction and hence allows for differentiation of lubricants in terms of resulting gearbox efficiency; it accounts for heat flow during the mesh cycle and predicts the resulting temperatures through an accurate iterative scheme; and it accounts for all the main loss sources in a typical gearbox, namely, friction in gear teeth contacts, bearing losses, seal losses and oil churning.

Perhaps the biggest difficulty in accurately modelling gear lubrication, and gear friction in particular, lies in the complexity of obtaining accurate tooth bulk temperatures and in contact flash temperature rise. In gear teeth contacts, the contact friction produces frictional heating which acts to heat up the bulk material of the gear; this in turn rises the gear bulk temperatures and hence affects the inlet temperature (equal to speed weighted average of the two tooth temperatures) of the oil to the gear tooth contact. There is currently no universally accepted way of predicting gear temperatures and usually relatively crude approximations are used. The model proposed here provides an improved way of predicting the relevant gear temperatures through consideration of gear heat transfer coefficients and lubrication conditions in the gear teeth contacts. The implemented methodology relies on an iterative scheme but converges relatively fast and can therefore be used in practical gear design. One difficulty in predicting heat flows in a gear is the determination of heat transfer coefficient of the gear. The model proposes a new method of estimating the heat transfer coefficients, by assuming that the heat is lost through the gear track by conduction to the oil filling the gaps between the teeth and that this oil absorbs heat during the gear rotation and is thrown away, and hence takes the heat away, once per mesh cycle. The heat lost through gear sides is estimated using standard heat

transfer coefficient expressions for cylinders. However, in reality the gear operates within an environment that is a two phase mixture of oil and air and the resulting fluid flow and heat convection are extremely complex. The proposed heat transfer coefficient method, although an improvement, is invariably only an estimate. One way of producing more accurate heat transfer coefficients, and overall gear heat transfer modelling, would be to use a multiphysics approach where a gear of correct geometry, including teeth, is rotating inside a two phase oil-air mixture. This calls for computation fluid dynamics approach to solve for resulting flows and heat transfer. An attempt to do this was made during this study using a commercial multi-physics software COMSOL, but it was quickly realised that any such model is extremely computationally demanding and complex and does not lend itself well to practical gear design, and prediction of gear efficiency over a whole drive cycle, which was the aim here. Nevertheless, this is worth exploring further, particularly as COMSOL have in the past few months introduced a gear geometry module in their software. For completeness, some details of this attempt at multiphysics modelling of a gearbox are included in the Appendix of this thesis.

The main lubricant properties accounted for in the present model are the Eyring shear stress, the Roelands z coefficient (related to lubricant pressure viscosity coefficient) and boundary friction coefficient, in addition to oil viscosity which is usually the only parameter considered by existing gearbox efficiency models. The inclusion of these parameters is crucial to the benefits offered by the model, as it allows it to differentiate between nominally the same lubricants, in terms of SAE grade for example, in terms of the resulting gearbox efficiency, and therefore, allows the model to be used to inform lubricant selection for the particular gearbox and expected duty during the early design process.

The inclusion of bearing, seal and gear churning losses means that the model can be applied to any multi-stage gearbox, as was illustrated here by applying the model to a commercial 6 speed manual gearbox over a wide range of duty cycles. However, the present model ignores the interaction between the different power losses in the gearbox, which occur due to individual losses heating up different parts of the gearbox, and hence the oil in these areas, to different temperatures. It is rather difficult to address this limitation, a thermal network may provide one very approximate way of achieving this, but perhaps one avenue worth exploring in this regard, is again the use of a multi-physics model but in this case of the whole multi-stage gearbox, as this would account for all heat transfers. Due to complexities involved and the computational

requirements, such a model could only be used in the final stages of gearbox design so it is perhaps not suitable for the current purpose.

As far as the complete model of a multi-stage gearbox utilised here is concerned, the model predictions compared relatively well with the experimental measurements of oil sump temperatures, despite the multiple assumptions needed to model a whole multi-stage gearbox under real road driving conditions. In this regard, the additional limitations of the model in the current form, are the omission of some components in the gearbox, such as seals and the needle bearings which support the gears as well as the assumptions detailed in the previous chapter (particularly modelling of spur gears instead of helical gears). In terms of heat transfer, the modelling of the exhaust and the engine which both alter the temperature inside the gearbox are expected to add an additional degree of detail and accuracy. There is a large amount of heat converted in the engine and transferred through the clutch/flywheel assembly to the main body of the gearbox as well as an equally important amount of heat transferred through the exhaust and mainly via radiation. In the current predictions, this omission was more evident in the initial climb of the drive cycles or when the $5^{th}$ gear was selected (and the heat input was limited), in which cases the predictions deviated from the measurements.

## 7.3 Main results

### 7.3.1 Results of the core gear EHL contact model

As has been shown in the results section of this thesis, the friction coefficient is highly dependent on the friction regime. When gears are operating at lambda ratios lower than about 1, the contribution of boundary friction to the effective friction coefficient is significant. An analysis of the figures in Chapter 5 shows that for these conditions the gear pair operates well within the mixed regime, with the lambda ratio taking a value of around 0.6, which explains the relatively high maximum friction coefficient.

The results show that in general, the film thickness remains relatively constant along the contact path since it is determined by the viscosity of the lubricant at the inlet temperature, equal to tooth bulk temperature, and the time taken for one mesh cycle is too short to change this tooth bulk temperature. In contrast, the temperature inside the EHL contact is of a highly transient nature rising rapidly as the slide roll ratio increases along the path of contact due to shear heating and contact of the material asperities. This in turns affects the in-contact lubricant properties and therefore the friction coefficient changes significantly during one mesh cycle.

### 7.3.2 Lubricant comparison for different conditions

One of the main aims of this work was to develop a methodology to predict friction which would be sensitive enough to be able to pinpoint differences between similar lubricants in terms of power loss and efficiency. The importance of friction modelling and temperature predictions is better examined under the scope of efficiency. The comparison figures in Chapter 5 clearly show an efficiency gap between the two lubricants in all five conditions, with lubricant A being superior overall. This gap however is now the same under all conditions varying between 0.05% and 0.09% when the more efficient DGBB's are used. The gap is more pronounced in the low load condition 1 owing mainly to the low predicted sump temperatures which in turn highlight the viscosity difference of the two lubricants. Oil A has a significantly lower viscosity at the coupled temperature compared to Oil B and this causes bearing and churning losses to increase, ultimately leading to lower efficiency in these conditions. On the other hand, the gap gets narrower in the hotter conditions 2-3 before it stabilises at the higher temperatures of conditions 4-5. A change to the less efficient - and slightly oversized - TRB's results in an impressive 0.19% difference in favour of oil A when the average conditions from the experimental drive cycle 1 are used (section 6.7.1).

When comparing the two lubricants in an actual automotive gearbox, the result is again consistently in favour of oil A. However, the condition where the highest difference is observed is the standardised NEDC with the high rpm shift strategy (NEDC S2). This is the drive cycle with the lowest average torque, at just 32.95 Nm and the lowest average predicted friction losses at just 11.93 watts (or 1.6 % of the overall). This could come as a surprise since the modelled lubricants show the highest differences either close to boundary friction, where the effective friction coefficient is higher for oil B, or at very high contact pressures because of the differences in Eyring stress. The difference in this case however is due to the very low predicted temperatures which highlight the viscosity difference between the two lubricants when the temperature is low.

The effect of lubricant viscosity on the commercial gearbox's losses was not fully examined in this study and the above low temperature observation point to the possibility of it being significant. It would be very easy to modify the model to run different viscosity oils. However, for a full comparison the same rheology characterisation shown in chapter 5 would have to be undertaken. Finally, the effect of friction modifiers did not show a significant difference under

these conditions as has been demonstrated in the past for axles. This will be explained in the next section.

The comparative results between the two oils lead to the conclusion that the thermally coupled model is able to pick up any differences in lubricants of similar rating owing to varying rheological characteristics, chemical composition and selected additives. These differences would be very difficult to predict without appropriate characterisation, as has been demonstrated in chapter 4. Consequently, the effect of these characteristics on the frictional losses and in turn on the efficiency and predicted temperatures within the transmission is not negligible and could be even more pronounced depending on the application. Therefore, the choice of an application-specific lubricant should be considered during the design phase of the component.

### 7.3.3 Results on the breakdown of losses

Examining the results from Chapter 5 one can observe that the losses breakdown is heavily dependent on the torque input, the selection of components and the lubricant properties. In general, high viscosity oils give rise to churning losses at high speeds when the surfaces are relatively smooth but actually reduce gear friction losses at high contact pressures because the gears are much rougher and the higher viscosity lubricants manage to persist with thicker films where a thinner lubricant would allow more asperity contact. If there is only a single gear pair and four bearings involved, the vast majority of losses will likely come from gear friction, especially so for the input conditions corresponding to wide open throttle. This trend will persist to the lower torque inputs if efficient bearing designs (like DGBBs) are chosen for supporting the axles. That said, a jump in bearing loss contribution from around 15% on average to more than 70% depending on the condition was observed when the very efficient DGBBs were replaced by TRBs.

Churning losses on the other hand will be very low, usually less than 5% unless a very deep immersion is chosen or the gears are very large. The rotation of the gears (i.e. clockwise vs counterclockwise) can also significantly affect churning losses by causing a “swell effect” and affecting the steady-state oil level in a way which increases the immersion depth of the pinion. In turn, this creates an additional loss component which is included in the model. Gearbox design is also a significant factor with gear ratio, face-width ratio and number of teeth all affecting the distribution of heat among the components. Out of the options simulated here, a

design which uses narrow gears with as many teeth as designing for stress -or any other design criterion- will allow, in combination with a medium viscosity oil would be the most efficient.

In an actual automotive gearbox, under real driving conditions, the torque input is rarely high enough for the gear friction losses to dominate as has been demonstrated in the previous chapter. This is not to say that there are not experimental cases where gear friction is important as has been demonstrated during the more severe experimental drive cycle 2, where gear friction becomes progressively larger as the average torque was increased (i.e. compared to experimental drive cycle 1). Gear friction would very likely become even more important under more severe conditions such as very high ambient temperatures, a steep gradient in combination with an excessive payload or racing applications where efficiency is important such as endurance races. Nevertheless, bearing losses were the highest even in the most severe drive cycle. The combination of relatively inefficient TRBs with high rotational speeds and axial loads resulted in massive bearing losses for these high speed drive cycles proving that bearing selection in a commercial gearbox is vital for efficiency and energy consumption.

Churning was in contrast much more significant compared to the single stage gearbox, as there was a large number of components rotating in the oil sump at the same time, even when there was no power transmitted (as it is a fully synchronised gearbox). The unusual layout of the shafts, with one placed on top of the other meant that the main shaft was not immersed in the lubricant bath at all, negating the need to include contributions due to a swell effect. Nevertheless, the churning losses were significant, never dropping below 27.3 % pointing out the need to carefully assess the oil level during the design phase. Changing the design of the case for efficiency could include making the bottom of the sump multi-levelled (rather than using a flat bottomed case like in the G56) which could reduce the overall churning loss in a full synchromesh gearbox like the one studied here.

In general these results indicate that it is possible to identify the gearbox component responsible for the largest contribution of losses under any given duty cycle, and that this component may change with the imposed conditions, and hence the model can be used to inform the design process in order to arrive at a most efficient gearbox at minimum cost. It was also revealing that in many cases, the trends obtained with the single stage gearbox, modelling of which is inevitably computationally more efficient, were similar to those in a multi-stage gearbox so that this simplified modelling approach can be used in the first instance when selecting gearbox components.

### 7.3.4 Comparison to experimental studies

Besides direct comparisons to published experimental and analytical results, which were undertaken in chapter 4, there were not many experimental studies the results of the proposed method could be directly compared to. In terms of single gear pair losses, the trends observed in chapter 5 show that the results from the EHL module favourably compare to the results from Petry Johnson et al[127], where mechanical losses rise linearly both with rotational speed and torque. Nevertheless, these comparisons can only be of a qualitative nature as, apart from the lubricants being different, several parameters were not incorporated in the model. The most important of these were the implementation of a jet lubrication system and a temperature controlled oil sump.

Regarding the commercial gearbox, the losses breakdown can be compared to previous experimental results conducted on a commercial differential unit[171]. In the NEDC drive cycle, bearing losses accounted for 77% of the overall with gear friction taking up 17% and churning just 6%. These figures are very close to the results presented in this thesis for the NEDC drive cycle with the added gradient and the discrepancies are mainly because of the multiple gear pairs in the commercial gearbox.

Previous studies[128] have suggested that the ranking order of lubricants may change depending on the input conditions and the specified drive cycle. This could not be confirmed in the current study as for all experimental and standardised drive cycles, oil A was always more efficient compared to oil B. As shown in the previous chapter, the two lubricants were closer for the high load drive cycles compared to the low load drive cycles mostly due to the difference in oil viscosity at lower temperatures. Nevertheless, a discrepancy of at least 0.14%, quite significant in efficiency terms, persists even when the predicted temperatures are high enough that the viscosity difference becomes negligible, which is the case for the three experimental drive cycles. It must be noted that the lubricants studied here have the same rating whereas the previous study reached these conclusions when comparing different viscosity fluids namely gear oil and PAO.

# 8. CONCLUSIONS

## 8.1 Summary

The goal of this study was to develop an easy to implement and cost effective model with the aim of producing reliable efficiency predictions for drivetrain components such as an automotive gearbox. For this purpose a model combining analytical and experimentally derived methods was developed in order to predict power losses, temperatures and efficiency under varying operating conditions.

The conducted work includes an experimental as well as a computational part; the rheology of the fully formulated lubricants used has been characterised using ball-on-disc tribometer tests while the computational part incorporates the test outputs to improve the accuracy of the predictions. The results of the model highlight the difference in the observed behaviour of two fully formulated gear oils of similar specification.

A thermally coupled model of a simple dip lubricated spur gearbox consisting of two spur gears, two shafts, four supporting single-seal bearings and a simple casing has been developed. The model uses an iterative numerical calculation scheme in order to predict EHL friction in spur gear contacts and also accounts for losses in bearings, seals and churning losses due to component rotation.

The same philosophy of the single gear pair model is extrapolated, enhanced and applied to a commercial six speed automotive gearbox. The losses and temperatures predicted by the EHL module are coupled to a lump mass model of the gearbox which uses the inputs of the EHL module and combines them with the gearbox geometry and a calculated heat transfer coefficient to predict the power loss of the individual components, the transient temperature in the lubricant sump and the efficiency for a given drive cycle.

## 8.2 Main achievements

The most significant achievements of this work are summarised below:

- An entire commercial six speed automotive gearbox has been modelled for the first time in a way that uses the inputs from experimental and standardised drive cycles coupled to experimentally derived lubricant properties. The present thermally coupled model brings together individual modules to calculate EHL friction, churning and bearing losses and can be effectively used to predict heat losses, temperatures and the overall efficiency. In addition to modelling a specific commercial gearbox, the model

can also be parameterised to account for different lubricant types as well as adapt to and accommodate practically any given gearbox geometry. The model successfully incorporates all the heat transfers involved i.e. conduction and convection both forced and natural. Temperature results from different simulated drive cycles are very close to experimental predictions suggesting that the modelling approach is robust and satisfactory.

- The model represents an integrated, convenient, flexible and cost effective alternative to an experimental gear rig setup with reasonable sacrifices in terms of accuracy. In the simple form of a single stage, single gear pair setup, it can produce results in minutes and a few hours are required to run a complete commercial gearbox.

- The dependency of the overall gearbox efficiency not only on the operating conditions but also on the specific lubricant rheology was validated. While the broad range of temperatures, torque values and rotational speeds led to changes in both overall losses and the relative contribution of each loss source, the lubricant rheology created a discrepancy between the two lubricants that persisted through this wide range of conditions. Regarding the breakdown of losses, the results of the current study have been qualitatively compared to results from experimental back to back rigs and axle rig tests and the observed trends are in good agreement.

- The lubricant characterisation showed a complex behaviour for both lubricants suggesting that there is no “standard” trend when it comes to elastohydrodynamic properties such as the variation of Eyring stress with pressure and temperature. The experimental part of the study is important when there is a need for increased accuracy and highlights the difference between the lubricants which would only exist in terms of viscosity if just the basic lubricant properties were used. The process is simple enough that a candidate lubricant can be tested in about a week and can produce highly repeatable results.

- Because of its ability to differentiate between lubricants of the same rating (as long as the required rheological characteristics are known), the model provides an efficient lubricant comparison tool which can be used by lubricant manufacturers and OEMS's alike to evaluate the composition of developed lubricants by testing them under simulated conditions, considerably reducing product development time and cost.

### 8.3 Future work

During this study there were areas where further work would possibly contribute to a more detailed or inclusive model and improve predictions. In some cases a more detailed approach was avoided to keep the model as computationally light as possible or due to time constraints. Nevertheless, the predicted results are robust and very close to the experiments while the same principles that were applied to develop the existing method can be applied to improve it.

Further experimental validation of the devised efficiency model would be beneficial. In particular, comparison of the model predictions against measurements made on a laboratory gearbox set-up instrumented to measure efficiency and temperatures would go a long way towards validating the model predictions. Although predictions for a full six speed gearbox have been validated against measurements made on a road driven vehicle, validating the simple single stage model against measurements made under controlled lab conditions would offer increased confidence in the model results and could point to the aspects of the model that need further improvement, particularly the individual loss calculations which can be measured on such a lab rig. This may most easily be achieved by using a back-to-back (four square) gear test rig with appropriate instrumentation. Combining the adaptability of the developed method with the versatility of a back to back rig would enable a wide range of gear and bearing configurations to be tested. Such validation could pave the way towards using the model as a gear design optimisation tool, able to assess the effects of different aspects of design and material selection on gear efficiency.

Regarding oil characterisation, the ball on disc tests could be repeated using tungsten carbide specimens to reveal the behaviour of the lubricant under very high contact pressures and expand upon the current dataset. These contact pressures are commonly encountered in gears, cams and other non-conformal contacts and a series of high pressure tests could further improve the accuracy of the predictions.

The remaining drivetrain and powertrain components could also be modelled and implemented in the thermal calculations. While modelling all the minor bearings and seals in the gearbox is not expected to substantially improve the results, the engine, exhaust and clutch/flywheel assembly are all expected to generate significant heat loss. This is backed by the thermocouple readings for the surface temperature of the gearbox casing, shown in chapter 7. The radiation from the exhaust which was positioned close to the right hand side of the gearbox was enough to generate an increased temperature of around 5 °C compared to the rest of the casing. Furthermore, the heat generated by the friction in the clutch assembly is expected to be particularly important in the case of a transient high-load drive cycle, where there is frequent clutch usage. Last but not least, the largest amount of heat is generated by the engine itself and no matter how disconnected it is from the gearbox, there will be a thermal gradient across the two.

In terms of coupling the gearbox module to the remaining drivetrain components, a complete fuel efficiency map for the engine can be implemented. Since this is not readily available, a series of dynamometer runs at different throttle (and therefore engine load/torque) inputs can be undertaken and the efficiency of the engine can be predicted at any rpm and torque by means of interpolation. This is not particularly difficult to implement and would greatly improve upon the existing WOT map. The efficiency of the gearbox at these conditions can then be coupled to the efficiency of the engine and further connected to previous differential and axle work to create a full vehicle efficiency model.

The thermal gradients inside the gearbox could be further studied by means of a finite element model. This method has some important limitations as a model of the complete gearbox implementing spur gears and oil splashing could prove particularly heavy to run and would require significant computational effort. The basis of such a model has already been created and tested to confirm that the temperature gradient in the oil sump is less than 3 °C as has been proven experimentally. A description of the FEA model and some preliminary results are shown in the appendix. In addition, the convective heat transfer for the outside of the gearbox could be defined more accurately, either using the finite element method or by assessing additional experimental data from multiple runs or a combination of the two so that the gearbox surface area included in the calculations can be fine-tuned. For example, readings from the pitot tubes could be used to create an air velocity map around the gearbox and an FEA model could be employed to model the actual heat loss, using the pitot tubes readings as inputs.

Finally, the experimental database for oil characterisation and road testing could be significantly expanded by testing more lubricants and especially lubricants of different ratings. This could be used to investigate potential correlation between groups of base oils or specific additives (for example friction and extreme pressure modifiers) and the predicted temperatures/lubricant efficiency under widely-used drive cycles and could also generate significant commercial interest.

# 9. APPENDIX: FEA GEARBOX SIMULATION

In this thesis, the importance of heat flows in a gearbox and the resulting interaction between the individual loss components was demonstrated. If, for instance, gears have high friction losses, they will heat up the oil and subsequently reduce the bearing losses. High bearing losses on the other hand can cause an increase in gear friction because the oil viscosity is reduced and pushes the gears to operate at even lower lambda ratios. Even if the flow and heat transfer in a gearbox cannot be totally solved for, a detailed representation of the gears can provide for heat transfer coefficients which can then be used in an analytical approach such as the one presented here.

There is no universally accepted way of predicting heat transfer coefficients and heat flows in the whole gearbox. One avenue worth exploring in this respect is multiphysics modelling. Such an approach offers the possibility to simultaneously model fluid flows, including presence of multiple phases (oil and air) and heat transfers in a gearbox. With advancements in computing power, realistic simulations for some simpler gearboxes such as the single stage one used in this study are possible.

With this in mind, an attempt was made to model heat flows inside a simple gearbox using multiphysics modelling, which can account for fluid flow as well as heat transfer. However, this was always a difficult task, not least due to the complexities in modelling the real gear geometry using finite element analysis (FEA) tools. In addition, a model of a complete gearbox or even a single stage arrangement is computationally very demanding as it has to take into account complex two phase flows and simultaneously solve for the heat transfer. Some progress has been made in that respect however a complete multi-physics simulation of a working gearbox was not part of the present PhD project. This appendix contains details of the progress made in order to inform any future work.

The FEA method could also be used to thermally couple the EHL model to the environment in a similar way the lump mass approach does in the current model. The input conditions, the outputs of the EHL model and the properties of the materials and the lubricants could be incorporated into the model, which would in turn predict the temperature distribution throughout the gearbox. The details of the geometry, the heat sources, the initial and boundary conditions and the mesh density would have to be assessed carefully in order for the model to produce meaningful results. The schematics of such an approach are shown in Figure 9.1.

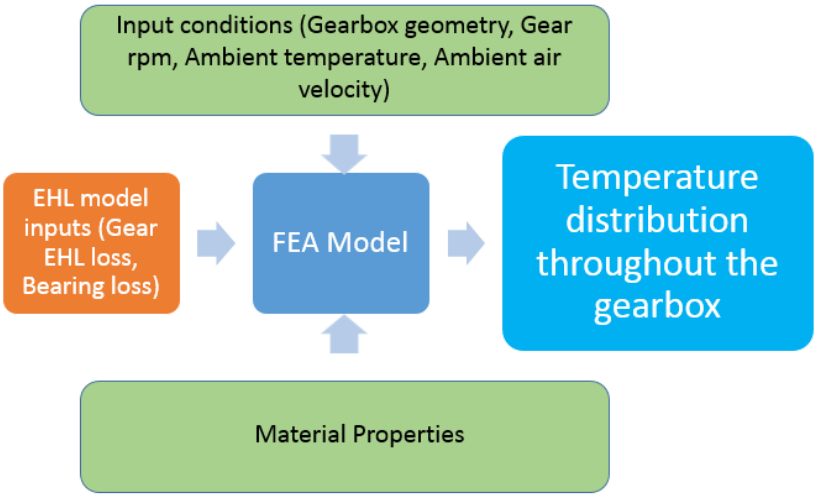



**Figure 9.1: The FEA method flowchart**

A simple gearbox such as the one shown in Figure 9.2 can be modelled using discs instead of gears and discs can also be used to simulate bearings. This approach will not provide an accurate treatment of churning however, it can provide an indication of temperature variation across the gearbox. The EHL contacts in the gear teeth could be modelled as line heat sources or fixed temperature boundaries across the face of the discs or gears and the bearing losses can be incorporated as volume heat sources. Such a model would simultaneously account for conduction through the solid and metal parts, convection in the lubricant sump and the air, heat exchange between the oil and the air inside the gearbox as well as forced convective cooling due to the surrounding airflow.

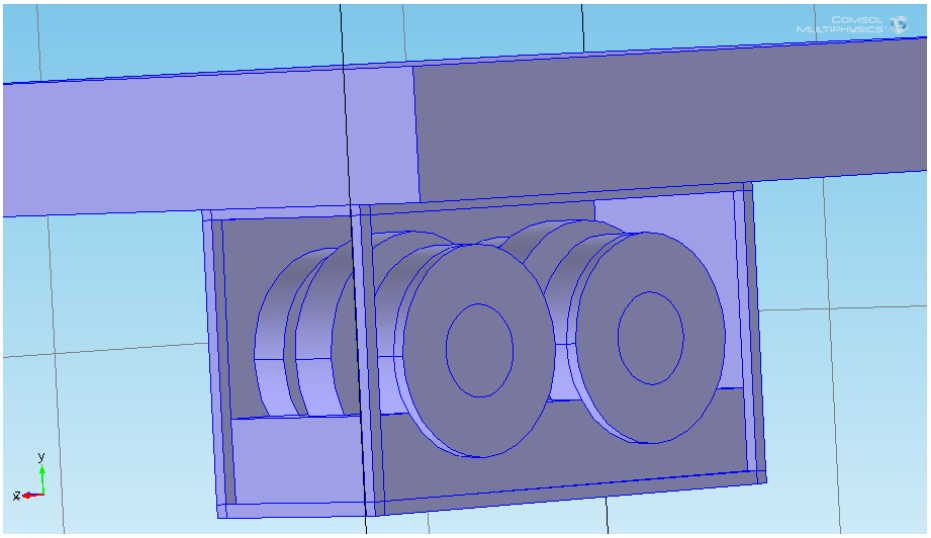


**Figure 9.2: A sample FEA model of a single stage gearbox with a lump mass representing the mass of the vehicle**

In the FEA method, mesh density is crucial and any predictions should be mesh independent. If actual gears are used instead of discs, further local mesh adjustments have to be included, often necessitating the use of very high mesh densities. A comparison of coarse (80000 elements) and fine (800000 elements) mesh densities can be seen in Figure 9.3, while a representation of the surrounding airflow and the velocity profile of the lubricant and air when the discs are rotating in the sump is shown in Figures 9.4 and 9.5 respectively.

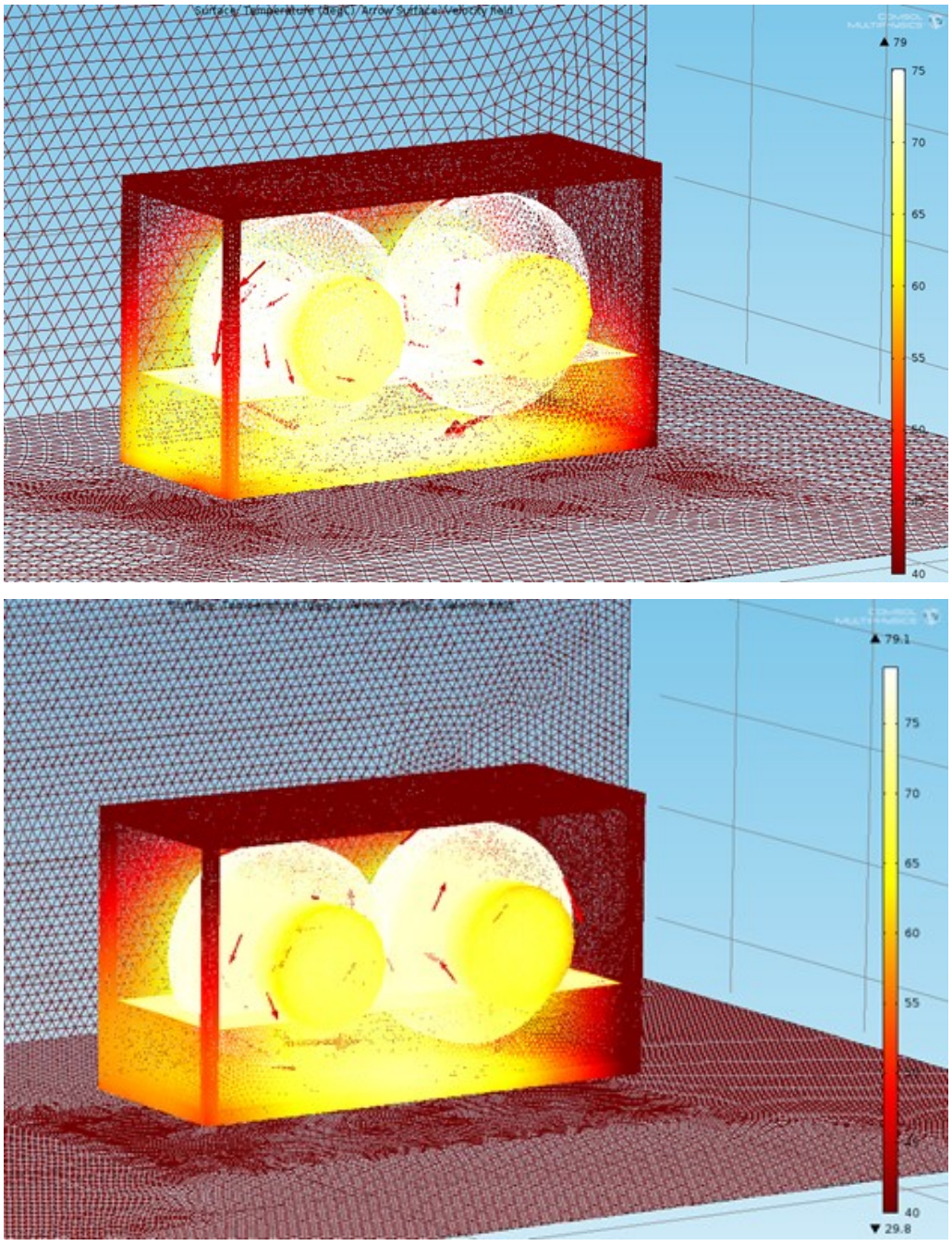



**Figure 9.3: Coarse (80000 elements) vs finest (800000 elements) mesh setting**

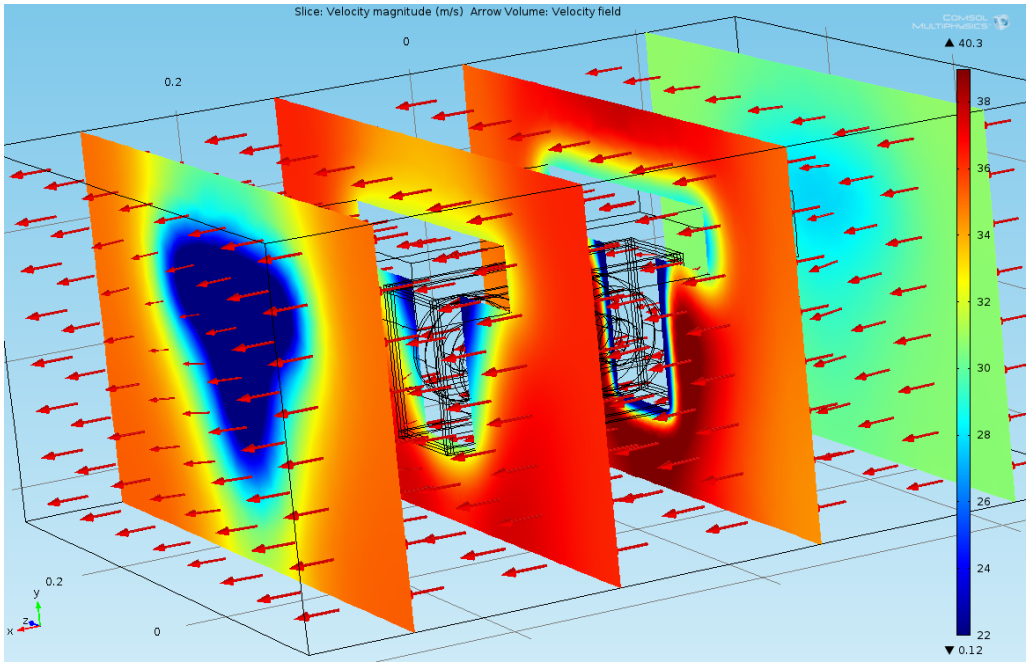



**Figure 9.4: The velocity profile of the airflow around the sample gearbox**

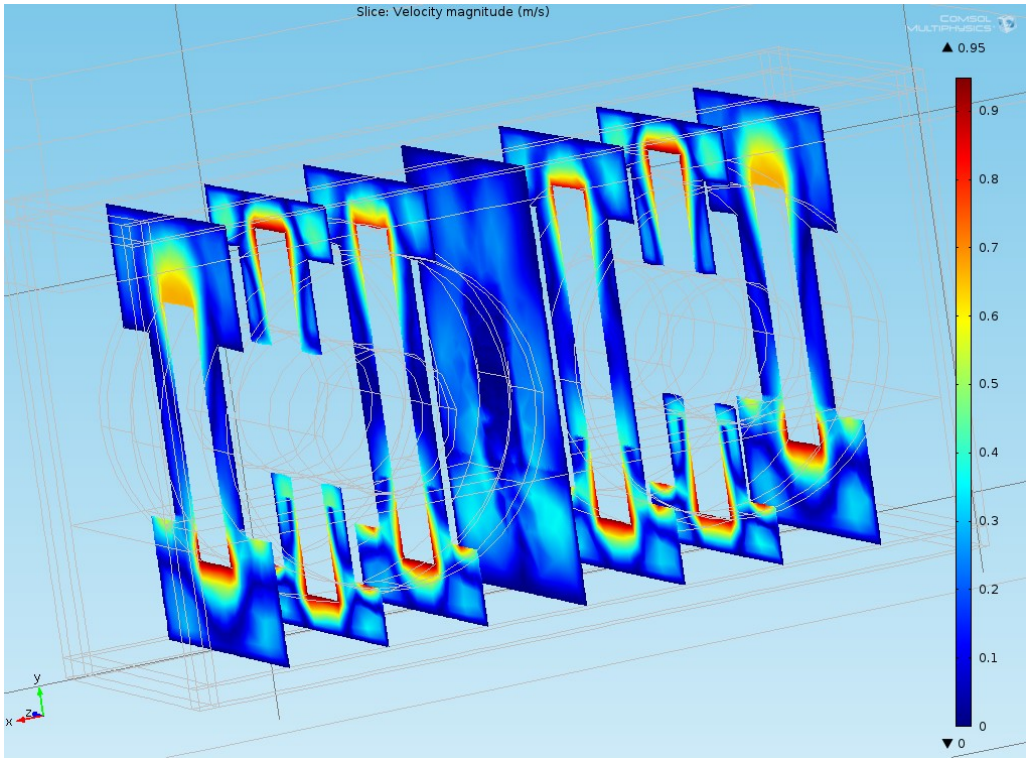



**Figure 9.5: The flow of the oil and air created by the friction due to the rotational motion of the bearings and the discs inside the gearbox. There is constant heat exchange between the air and oil domain however the two fluids are separated by a thin boundary layer as simulation of a two phase flow in 3D was computationally demanding (there is no mixing of the two phases and the CFD model is single phase)**

Nevertheless, an accurate treatment of the surrounding airflow would require a full model of the underbody of a vehicle, unless approximations can be made using an adequate number of experimental air velocity measurements. Perhaps the biggest drawback of the method is the sheer computational demand that is needed in order to get robust predictions, especially when modelling large components of complex geometry which would require high mesh densities. In that respect, any assumptions or simplifications that are made to reduce calculation time must be carefully assessed in order for the results to be trustworthy.

Taking the aforementioned limitations of the method into account, an attempt was made to model the six speed manual gearbox detailed in chapter 6, with the intention to visualise the heat flow and get the thermal gradients across the gearbox. To avoid modelling a two phase flow in three dimensions, a boundary layer was introduced at the lubricant-oil interface, which allowed heat exchange but not mass exchange. The gears and bearings were modelled as discs and according to the measured dimensions. Overall, the simulated geometry was very similar to the actual gearbox with the exception of the simplified rectangular casing. In terms of kinematics, care was taken so that the components would rotate in the same way as their real-life counterparts, including synchroniser rotational motion.

The inputs that were used, including contact temperatures and bearing power loss were taken from the EHL model predictions. The EHL contacts between the discs were modelled as fixed temperature boundaries and the bearings were modelled as volume heat sources. Steady state simulation of this gearbox revealed that the temperature difference between the hottest and coolest parts of the gearbox was less than 3 °C, as can be seen in Figure 9.7, which depicts the simulated gearbox when the $6^{th}$ gear is engaged. This is in line with experimental evidence that suggest an almost uniform temperature distribution in the oil sump under both transient and steady state conditions (Figure 6.8). Therefore, for the purpose of the current study, a lump mass approach was considered adequate. Incorporating gear teeth and introducing a two phase flow in this geometry so that the treatment of churning is accurate, would result in massive computation times and such complex models could take weeks to solve if a complete transient drive cycle consisting of several thousand time steps had to be modelled. Therefore, they should only be employed for simple setups or during the final stages of gearbox design.

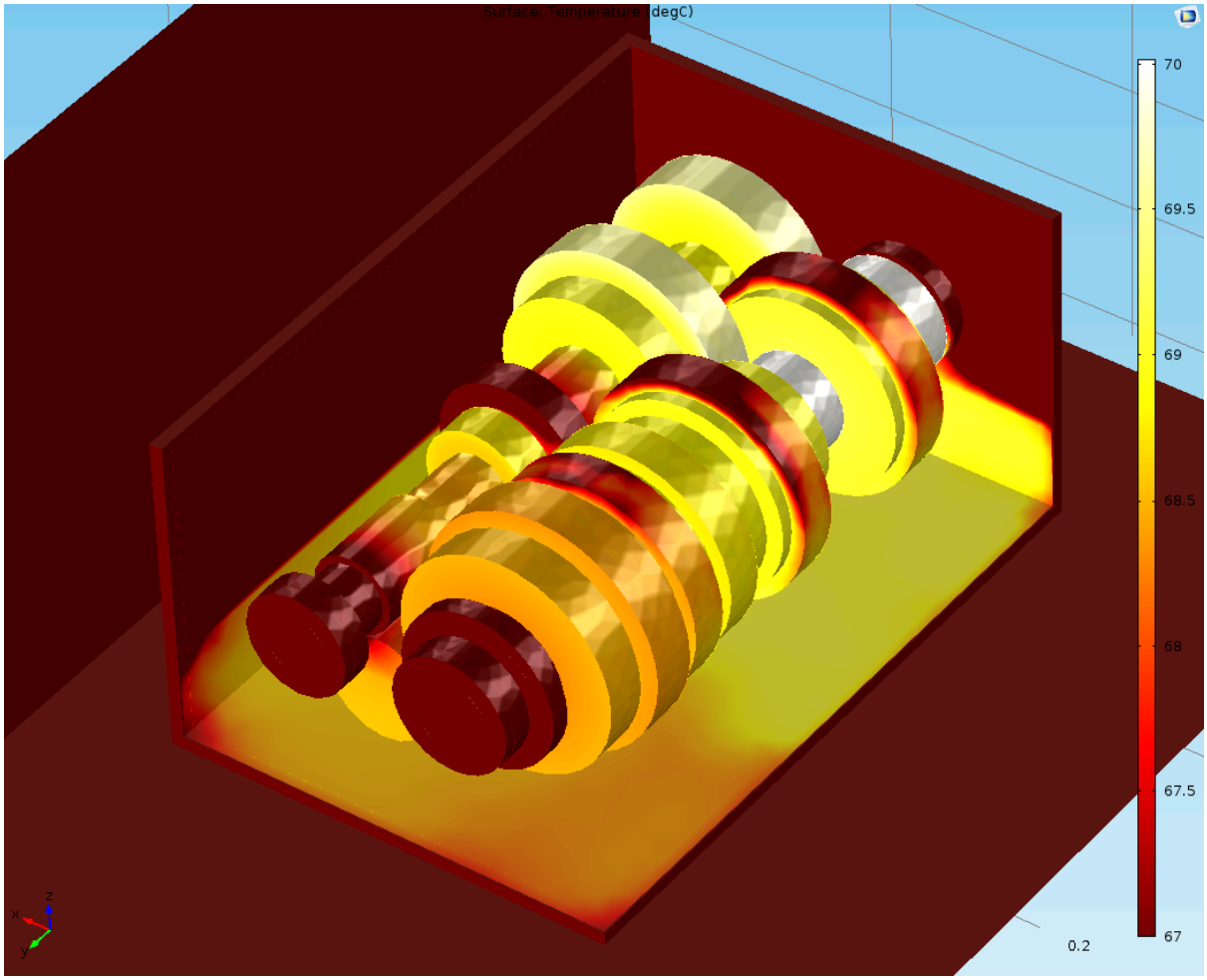



**Figure 9.6: A sample FEA model of the commercial automotive gearbox when 6th gear is engaged**

To summarise, an attempt was made to model heat flows inside a gearbox using multiphysics modelling to simultaneously account for heat transfer and fluid flow. Detailed multiphysics modelling was beyond the scope of this project so only the initial exploratory tests were performed. It soon became clear that in order to simulate a complete gearbox without significant compromises in terms of accuracy, modelling of a two phase flow would be required. Such an approach would make the model extremely computationally demanding and unsuitable for simulating a transient drive cycle consisting of thousands of time steps, such as the experimental drive cycles shown in chapter 6. For this reason, the model was only used to provide additional insight into the temperature gradients across the gearbox and the results supported the use of a lump mass approach.

# REFERENCES

[1] International Energy Agency , http://www.iea.org/textbase/npsum/weo2014sum.pdf

[2] U.S. Energy Information Administration and bureau of labor statistics http://www.eia.gov/

[3]https://www.bloomberg.com/news/articles/2016-09-28/opec-said-to-agree-on-first-oil-output-cut-in-eight-years

[4] http://unfccc.int/kyoto_protocol/items/2830.php

[5] http://unfccc.int/resource/docs/2015/cop21/eng/l09r01.pdf

[6] https://ec.europa.eu/clima/policies/transport/vehicles_en

[7] European Union. Directive 1999/94/ec of the european parliament and of the council of 13 December 1999 relating to the availability of consumer information on fuel economy and co2 emissions in respect of the marketing of new passenger cars. http://eur-lex.europa.eu/en/index.htm.

[8] US Environmental protection agency http://www3.epa.gov/

[9] The international council for clean transportation http://www.theicct.org/blogs/staff/improving-conversions-between-passenger-vehicle-efficiency-standards

[10] Chan, C.C., 2007. The state of the art of electric, hybrid, and fuel cell vehicles. Proceedings of the IEEE, 95(4), pp.704-718.

[11] Holmberg et al, 2012, Global Energy consumption due to friction in passenger cars, Tribology International 47 (2012) pp 221-234

[12] Baglione, M., Duty, M., Pannone, G., Vehicle system energy analysis methodology and tool for determining vehicle subsystem energy supply and demand, SAE Technical Paper 2007-01-0398, 2007, SP-2072, as cited by the website http://www.fueleconomy.gov/feg/atv.shtml (U.S. department of energy).

[13] The national petroleum council, http://www.npc.org/reports/FTF-report-080112/Chapter_10-HD_Engines-Vehicles.pdf

[14] Bernd-Robert Höhn, Klaus Michaelis, Michael Hinterstoißer, Optimization of Gearbox Efficiency, Gear Research Centre FZG, Technische Universität München, Germany, 2009

[15] "Drivetrain". Automotive Handbook (3rd ed.). Bosch. 1993. p. 536. ISBN 0-8376-0330-7.

[16] Martin Servin, Interactive Vehicle simulation, UMIT research lab, 2013, http://www8.cs.umu.se/kurser/5DV058/VT15/lectures/vehicle.pdf

[17] J. J. Uicker; G. R. Pennock; J. E. Shigley (2003). Theory of Machines and Mechanisms (3rd ed.). New York: Oxford University Press. J. J. Uicker; G. R. Pennock; J. E. Shigley (2003). ISBN 9780195155983.

[18] B. Paul (1979). Kinematics and Dynamics of Planar Machinery. Prentice Hall.

[19] G. Lechner, H. Naunheimer, Automotive Transmissions; fundamentals, selection, design and application, Springer Verlag, 2011, ISBN 9783642162138

[20] Alec Stokes, Manual Gearbox design, Society of Automotive Engineers, Butterworth Heinemann Ltd 1992, ISBN 0750604174

[21] BMW M3 Factory manual, BMW AG, http://www.bimmers.com/m3/troubleshooting/BMW%20M3%20Factory%20Manual/23-manual_transmission.pdf

[22] http://www.merriam-webster.com/dictionary/gear

[23] Robert L Mott. Machine elements in mechanical design. Prentice-Hall, 1999.

[24] http://www.me-mechanicalengineering.com/classification-of-gears/

[25] G. Lechner, H. Naunheimer, Automotive Transmissions; fundamentals, selection, design and application, Springer Verlag, 2011, ISBN 9783642162138 p. 55.

[26] Alec Stokes, Manual Gearbox design, Society of Automotive Engineers, Butterworth Heinemann Ltd 1992, ISBN 0750604174

[27] http://www.meadinfo.org/2008/11/gear-efficiency-spur-helical-bevel-worm.html

[28] T. V. Govindaraju, Kinematics of Machines, Chapter 4: Gears, Shirdi Sai Engineering College, http://elearning.vtu.ac.in/P6/enotes/ME44/Unit4-GR.pdf

[29] Michael J Neale. Tribology handbook. Butterworth-Heinemann, 1995.

[30] Michael M Khonsari and E Richard Booser. Applied tribology: bearing design and lubrication, volume 12. John Wiley & Sons, 2008.

[31] Tribology Lecture Notes, Imperial College London, 2011

[32] Harry Ernest Henderson, Peter D MacK, William Mark Steckle, and B Swinney. Higher quality base oils for tomorrow's engine oil performance categories. Technical report, SAE Technical Paper, 1998.

[33] G.P.K. Linkhammer and C.E. Lambert, Preservation of Organic Matter During Salinity Excursions, Nature, Vol. 339, 1989, pp. 271-274.

[34] R L Shubkin. Synthetic Lubricants and High Performance Functional Fluids. Marcel Dekker Inc., NY, 1992.

[35] P. Nagendramma, S Kaul, Development of ecofriendly/biodegradable lubricants: An overview. Renewable and Sustainable Energy Reviews Volume 16, Issue 1, January 2012, Pages 764–774

[36] A T Polishuk, A brief history of lubricating greases. Llewelyn & McKane Inc., PA, 1998.

[37] R M Mortier and S T Orsulik, eds. Chemistry and Technology of Lubricants. Blackie, London, 1997.

[38] H.K Kohler, Teaching pack on gear technology, Module 5 – Gearbox design, British Gear Association

[39] Stanley I. Pinel , Hans R. Signer & Erwin V. Zaretsky (2001) Comparison Between Oil-Mist and Oil-Jet Lubrication of High-Speed, Small-Bore, Angular-Contact Ball Bearings, Tribology Transactions, 44:3, 327-338, DOI: 10.1080/10402000108982465

[40] Zaretsky, E.V., "Rolling Bearing and Gear Lubrication," Tribology for Aerospace Applications, E. V. Zaretsked., STLE SP-37, Society of Tribologists and Lubrication Engineers, Park Ridge, IL, pp. 207-323, (1997).

[41] http://www.merriam-webster.com/dictionary/viscosity

[42] Maxwell, J.C. "On the Viscosity or Internal Friction of Air and the Other Gases." Bakerian Lecture, 1860. Collected Works, ed. W D Niven, U.P. 2, pp. 1-25, (1890).

[43] G W. Stachowiak, A. W. Batchelor, Engineering Tribology 4th edition, Butterworth-Heinemann, 2013, ISBN 9780123970473

[44] Wright, B., van Os, N.M. and Lyons, J.A. "European Activity Concerning Engine Oil Viscosity Classification - Part IV - The Effect of Shear Rate and Temperature on the Viscosity of Multigrade Oils", SAE 830027.

[45] Osborne Reynolds. On the theory of lubrication and its application to mr. beauchamp tower's experiments, including an experimental determination of the viscosity of olive oil. Proceedings of the Royal Society of London, 40(242-245):191– 203, 1886.

[46] H. Vogel, Phys. Z. 22 (1921) 645.

[47] C. Walther, Erdol und Teer, 4, No. 29/33 (1928), 5, No 34 (1929); proceedings of world petroleum congress, London, 2 (1933) p.419

[48] ASTM Method D 341, Standard Viscosity-Temperature Charts for Liquid Petroleum Products, American Society of Testing and Materials, Philadelphia

[49] Roelands C.J. – Correlational aspects of the viscosity-temperature-pressure relationship of lubricating oils, University of Delft, 1966of Lubricating Oils." Druk V.R.B., Kleine der A3-4 Groningen, (1966).

[50] Yang, Y., Pakkanen, T.A. and Rowley, R.L., "NEMD simulations of viscosity and viscosity index for lubricant–sized model molecules." Int. J. of Thermophysics 23, pp. 1441-1454, (2002).

[51] A. V. Olver, Gear Lubrication – A Review, Proceedings of the Institution of Mechanical Engineers Vol. 216, Part J: J Engineering Tribology, 2002

[52] Barus, C. “Isothermals, Isopietics and Isometrics in Relation to Viscosity”, American Journal of Science. 3rd Ser. 45, pp. 87-96, (1893).

[53] Chu, P.S.Y. and Cameron, A. “Pressure-Viscosity Characteristics of Lubricating Oils.” J, Inst. Pet. 48, pp. 147-155, (1962).

[54] D Dowson. Elastohydrodynamic and micro-elastohydrodynamic lubrication. Wear, 190(2):125–138, 1995.

[55] Ramsey Gohar. Elastohydrodynamics. E. Horwood, 1988.

[56] Gohar R Elastohudrodynamics, 2nd Edition Imperial College Press 2001.

[57] Gu¨mbel, L. (1916), “U¨ ber Geschmierte Arbeitsra¨der” (On the Lubrication of Gears) Zeitschrift fur das Gesamte Turbinenwesen, 13, p 357.

[58] Martin, H. M. (1916), “Lubrication of Gear Teeth,” Engineering, 102, pp 119-121.

[59] Meldahl, A. (1941), “Contribution to Theory of Lubrication of Gears and of Stressing of Lubricated Flanks of Gear Teeth,” Brown Boveri Review, 28(11), pp 374-382.

[60] Alexandr Nikolaevich Grubin, I Eo Vinogradova, and Kh F Ketova. Investigation of the contact of machine components. Central Scientific Research Institute for Technology and Mechanical Engineering, 1949.

[61] A Cameron. Righting a 40-year-old wrong: Am ertel—the true author of ‘grubin ehl’solution. Tribology International, 18(2):92, 1985.

[62] D Dowson and GR Higginson. A numerical solution to the elasto-hydrodynamic problem. Journal of Mechanical Engineering Science, 1(1):6–15, 1959.

[63] D Dowson and GR Higginson. New roller bearing lubrication formula. Engineering (London), 192(4972):158–159, 1961.

[64] Duncan Dowson and BJ Hamrock. Numerical evaluation of the surface deforma- tion of elastic solids subjected to a hertzian contact stress. ASLE transactions, 19(4):279–286, 1976.

[65] Bernard J Hamrock and Duncan Dowson. Isothermal elastohydrodynamic lubri- cation of point contacts: Part i—theoretical formulation. Journal of Lubrication Technology, 98(2):223–228, 1976.

[66] BJ Hamrock and Ds Dowson. Isothermal elastohydrodynamic lubrication of point contacts: Part ii—ellipticity parameter results. Journal of Lubrication Technology, 98(3):375–381, 1976.

[67] Bernard J Hamrock and Duncan Dowson. Isothermal elastohydrodynamic lubrication of point contacts: Part iii—fully flooded results. Journal of Lubrication Technology, 99(2):264–275, 1977.

[68] RJ Chittenden, D Dowson, JF Dunn, and CM Taylor. A theoretical analysis of the isothermal elastohydrodynamic lubrication of concentrated contacts. i. direction of lubricant entrainment coincident with the major axis of the Hertzian contact ellipse. Proceedings of the Royal Society of London. A. Mathematical and Physical Sciences, 397(1813):245–269, 1985.

[69] RJ Chittenden, D Dowson, JF Dunn, and CM Taylor. A theoretical analysis of the isothermal elastohydrodynamic lubrication of concentrated contacts. ii. general case, with lubricant entrainment along either principal axis of the hertzian contact ellipse or at some intermediate angle. Proceedings of the Royal Society of London. A. Mathematical and Physical Sciences, 397(1813):271–294, 1985.

[70] John Halling. Principles of tribology. MacMillan, 1975.

[71] Bernard J Hamrock, Steven R Schmid, and Bo O Jacobson. Fundamentals of fluid film lubrication, volume 169. CRC press, 2004.

[72] H. Spikes, J. Zhang, History, Origin and Prediction of Elastohydrodynamic Friction, Tribology Letters 56:1-25, 2014 DOI 10.1007/s11249-014-0396-y

[73] SMB Albahrani, D Philippon P Vergne JM Bluet, A review of in situ methodologies for studying elastohydrodynamic lubrication, Proceedings of the Institution of Mechanical Engineers, Part J_ Journal of Engineering Tribology, 2015

[74] Dowson D. History of Tribology, Second Edition, publ. PEP Ltd. Bury St Edmunds, 1998.

[75] PMEB Cann, E Ioannides, B Jacobson, and AA Lubrecht. The lambda ratio—a critical re-examination. Wear, 175(1):177–188, 1994.

[76] S Bair and WO Winer. Regimes of traction in concentrated contact lubrication. Journal of Tribology, 104(3):382–386, 1982.

[77] Pedrero, J. I., 1999, “Determination of the Efficiency of Cylindrical Gear Sets,” Fourth World Congress on Gearing and Power Transmission, Paris, France.

[78] Denny, C. M., 1998, “Mesh Friction in Gearing,” AGMA Fall Technical Meeting, Paper No. 98FTM2.

[79] Michlin, Y., and Myunster, V., 2002, “Determination of Power Losses in Gear Transmissions With Rolling and Sliding Friction Incorporated,” Mech. Mach. Theory, 37, pp. 167–174.

[80] Höhn, B.-R., Michaelis, K., and Wimmer, A., 2005, “Low Loss Gears,” AGMA Fall Technical Meeting, Paper No. 05FTM11.

[81] Anderson, N. E., and Loewenthal, S. H., 1981, “Effect of Geometry and Operating Conditions on Spur Gear System Power Loss,” ASME J. Mech. Des.,103, pp. 151–159.

[82] Anderson, N. E., and Loewenthal, S. H., 1982, “Design of Spur Gears for Improved Efficiency,” ASME J. Mech. Des., 104, pp. 767–774.

[83] Anderson, N. E., and Loewenthal, S. H., 1986, "Efficiency of Nonstandard and High Contact Ratio Involute Spur Gears," ASME J. Mech., Transm, Autom. Des., 108, pp. 119–126.

[84] Vaishya, M., and Houser, D. R., 1999, "Modeling and Measurement of Sliding Friction for Gear Analysis," AGMA Fall Technical Meeting, Lakewood, CO, Paper No. 99FTMS1.

[85] Heingartner, P., and Mba, D., 2003, "Determining Power Losses in The Helical Gear Mesh: Case Study," Proceedings of DETC'3, ASME 2003 Design Engineering Technical Conferences and Computers and Information in Engineering Conference, Chicago, IL.

[86] Diab, Y., Ville, F., Velex, P., 2006, "Prediction of Power Losses Due to Tooth Friction in Gears," Tribol. Trans 49, pp. 260–270.

[87] HE Merritt. Gears, pitman, 1942.

[88] GH Benedict and BW Kelley. Instantaneous coefficients of gear tooth friction. ASLE TRANSACTIONS, 4(1):59–70, 1961.

[89] JP O'Donoghue and A Cameron. Friction and temperature in rolling sliding con- tacts. ASLE TRANSACTIONS, 9(2):186–194, 1966.

[90] Dowson, D., and Higginson, G. R., 1964, "A Theory of Involute Gear Lubrication," Proceedings of a Symposium Organized by the Mechanical Tests of Lubricants Panel of the Institute, Institute of Petroleum, Gear Lubrication, Elsevier, London, pp. 8–15.

[91] Martin, K. F., 1981, "The Efficiency of Involute Spur Gears," ASME J. Mech. Des., 103, pp. 160–169.

[92] Simon, V., 1981, "Load Capacity and Efficiency of Spur Gears in Regard to Thermo-End Lubrication," International Symposium on Gearing and Power Transmissions, Tokyo, Japan.

[93] Wu, S., and Cheng, H. S., 1991, "A Friction Model of Partial-EHL Contacts and its Application to Power Loss in Spur Gears," Tribol. Trans., 34, pp. 398–407.

[94] Mihalidis, A., Bakolas, V., Panagiotidis, K., and Drivakos, N., 2002, "Prediction of The Friction Coefficient of Spur Gear Pairs," VDI-Ber., 1665, pp. 705–719.

[95] Xu, H., Kahraman, A., Anderson, N. E., and Maddock, D. G., 2007, "Prediction of Mechanical Efficiency of Parallel-Axis Gear Pairs," ASME J. Mech. Des., 129, pp. 58–68.

[96] A. V. Olver and H. A. Spikes Prediction of traction in elastohydrodynamic lubrication Proceedings of the Institution of Mechanical Engineers, Part J: Journal of Engineering Tribology 1998 212: 321

[97] KL Johnson and JL Tevaarwerk. Shear behaviour of elastohydrodynamic oil films. Proceedings of the Royal Society of London. A. Mathematical and Physical Sciences, 356(1685):215–236, 1977.

[98] CR Evans and KL Johnson. The rheological properties of elastohydrodynamic lubricants. Proceedings of the Institution of Mechanical Engineers, Part C: Journal of Mechanical Engineering Science, 200(5):303–312, 1986.

[99] CR Evans and KL Johnson. Regimes of traction in elastohydrodynamic lubrication. Proceedings of the Institution of Mechanical Engineers, Part C: Journal of Mechanical Engineering Science, 200(5):313–324, 1986.

[100] Muraki, M., Matsuoka, T. and Kimura, Y. Influence of temperature rise on non-Newtonian behaviour of fluids in EHD conditions. In Proceedings of the Fifth International Congress on Tribology (EdsK. Holmberg and I. Nieminen), Espoo, Finland, 1989, Vol. 4, pp. 226-231.

[101] Daily, J. W., and Nece, R. E., 1960. "Chamber Dimension Effects on Induced Flow and Frictional Resistance of Enclosed Rotating Disk," ASME J. Basic Eng., 82, pp. 217–232.

[102] Mann, R. W., and Marston, C. H., 1961, "Friction Drag on Bladed Disks in Housings as a Function of Reynolds Number, Axial and Radial Clearance and Blade Aspect Ratio and Solidity,"ASME J. Basic Eng., 83, pp. 719–723.

[103] Soo, S. L., and Princeton, N. J., 1958, "Laminar Flow Over an Enclosed Rotating Disk," Trans. ASME, 80, pp. 287–296.

[104] Terekhov, A. S., 1975, "Hydraulic Losses in Gearboxes With Oil Immersion," Vestnik Mashinostroeniya, 55, pp. 13–17.

[105] Boness, R. J., 1989, "Churning Losses of Discs and Gears Running Partially Submerged in Oil," Proc. ASME Int. Power Trans. Gearing Conf., Chicago, Vol. 1, pp. 355–359.

[106] Lauster, E., and Boos, M., 1983, "Zum Wärmehaushalt mechanischer Schaltgetriebe für Nutzfahrzeuge," VDI-Ber., 488, pp. 45–55.

[107] Bernd-Robert H¨ohn, Klaus Michaelis, and Thomas Vollmer. Thermal rating of gear drives: balance between power loss and heat dissipation. American Gear Man- ufacturers Association, 1996.

[108] P Luke and AV Olver. A study of churning losses in dip-lubricated spur gears. Proceedings of the Institution of Mechanical Engineers, Part G: Journal of Aerospace Engineering, 213(5):337–346, 1999

[109] Anant S Kolekar, Andrew V Olver, Adam E Sworski, and Frances E Lock- wood. Windage and churning effects in dipped lubrication. Journal of Tribology, 136(2):021801, 2014.

[110] Changenet, and Velex, 2007, "A Model for the Prediction of Churning Losses in Geared Transmissions—Preliminary Results," Transactions of the ASME, Journal of Mechanical Design, 129(1), pp. 128–133

[111] Changenet, and Velex, 2008, “Housing Influence on Churning Losses in Geared Transmissions” Transactions of the ASME, Journal of Mechanical Design, Vol 130, pp. 128–133

[112] Wimmer, A., Salzgeber, K.; Haslinger, R.: WP1 – Analysis of Minimum Oil Requirements Considering Friction in Gears and Engines. Final Report Oil-free Powertrain, EU Project Contract No: IPS-2001-CT-98006, June 2003.

[113] SKF group – SKF General Catalogue 2004 Print Information technology Paderborn 2004

[114] Khonsari, M. M., and Booser, E. R., 2001, Applied Tribology, Bearing Design and Lubrication, Wiley, New York.

[115] G. E. Morales, Using a friction model as an engineering tool, tribology & lubrication, SKF engineering Research Centre, 2006

[116] A.W. Wemekamp, A. Doyer, G.E. Morales, friction theory, thermal modelling and validation of industrial gearbox, SKF engineering research centre, 2013

[117] Neil E Anderson and Stuart H Loewenthal. Spur-gear-system efficiency at part and full load, volume 79. National Aeronautics and Space Administration, Scientific and technical Information Office, 1980.

[118] Neil E Anderson and Stuart H Loewenthal. Effect of geometry and operating conditions on spur gear system power loss. Journal of mechanical design, 103(1):151– 159, 1981.

[119] PH Dawson. Windage loss in larger high-speed gears. Proceedings of the Institution of Mechanical Engineers, Part A: Journal of Power and Energy, 198(1):51–59, 1984.

[120] Youssef Diab, Fabrice Ville, Philippe Velex, and Christophe Changenet. Windage losses in high speed gears—preliminary experimental and theoretical results. Journal of Mechanical Design, 126:903, 2004.

[121] Bell, J. C. and Dyson, A. The effects of rolling and sliding speeds on scuffing of lubricated steel discs. Trans. ASLE, 1975, 18, 62

[122] Standard test method for load-carrying of petroleum oil and synthetic fluid gear lubricants. ASTM Designation 01947, 1983 (American Society for Testing and Materials).

[123] Load-carrying capacity tests for oils. FZG gear machine. IP Designation IP334 (CEC L-O7-A-85), 1986 (Institute of Petroleum, London)

[124] Extreme pressure properties. Friction and wear tests for lubricants. Four-ball machine. IP designation IP239, 1985 (Institute of Petroleum, London).

[125] Measurement of extreme pressure properties of lubricating fluids (Timken method). IP Designation IP240, ASTM Designation D2782, 1984 (Institute of Petroleum, London).

[126] Olver, A.V. Testing transmission lubricants: the importance of thermal response. Proc. Institution of Mechanical Engineers, Part G, Journal of Aerospace Engineering, 1991, 206(G1), 35-44

[127] Petry-Johnson, T., Kahraman, A., Anderson, N. E., and Chase, D. (2008), "An Experimental Investigation of Spur Gear Efficiency," Transactions of the ASME, Journal of Mechanical Design, DOI: 10.1115/1.2898876

[128] Kolekar, A, Olver, AV, Sworski, AE and Lockwood, FE, The efficiency of a hypoid axle - a thermally-coupled lubrication model, Tribology International, 19 March 2012.

[129] Neil E. Anderson, Stuart H. Loewenthal, 1980, Spur-Gear Efficiency at Part and Full Load, NASA Technical Paper 1622, AVRADCOM

[130] N. E. Anderson and P. Loss, "Effect of Geometry and Operating Conditions on Spur Gear System," no. 80, 1981.

[131] Sheng Li & Ahmet Kahraman (2010) Prediction of Spur Gear Mechanical Power Losses Using a Transient Elastohydrodynamic Lubrication Model, Tribology Transactions, 53:4, 554-563

[132] L. Chang, Y.R. Jeng, 2013, Modeling and Analysis of the Meshing Losses of Involute Spur Gears in High-Speed and High-Load Conditions, Transactions of the ASME, Journal of Tribology, Vol 135.

[133] Gevigney, J. D., Changenet, C., Ville F., Velex P. "Thermal Modeling of a back to back gearbox test machine: Application to the FZG test rig". Journal of Engineering Tribology, 2011.

[134] Wemekamp A.W., Doyer A., Morales-Espejel, G.E., "Friction theory, thermal modelling and validation for industrial gearbox", VDI Gear Conference Munich, 2013

[135] Long, H. and Lord, A. A. and Gethin, D. T. and Roylance, B. J. (2003) 'Operating temperatures of oil-lubricated medium-speed gears: numerical models and experimental results', Proceedings of the I MECHE part G: journal of aerospace engineering., 217 (2). pp. 87-106.

[136] Murat Taburdagitan, Metin Akkok, 2006, Determination of surface temperature rise with thermo-elastic analysis of spur gears, WEAR 261 pp. 656-665, Elsevier B.V.

[137] C. Changenet, X. Oviedo-Marlot, and P. Velex, "Power Loss Predictions in Geared Transmissions Using Thermal Networks-Applications to a Six-Speed Manual Gearbox," Journal of Mechanical Design, vol. 128, no. 3, p. 618, 2006.

[138] Johnson, K. L. and Roberts, A. D. Observations of viscoelastic behaviour of an elastohydrodynamic lubricant film. Proceedings of the Royal Society (London.), 1974, A337, 217-242.

[139] Hirst, W. and Moore, A. J. Elastohydrodynamic lubrication at high pressures. I. Proc. Roy. Soc. (London), 1978, A360, 403-425.

[140] Bair, S. and Winer, W. A rheological model for elastohydrodynamic contacts based on primary laboratory data. Transactions of the ASME, Journal of Lubrication Technology, 1979, 101, 258-265.

[141] Bair, S. and Winer, W. The high shear stress rheology of liquid lubricants at pressures of 2 to 200 MPa. Trans. ASME, Journal of Tribology, 1990, 112, 246-253.

[142] H Eyring - Viscosity, Plasticity, and Diffusion as Examples of Absolute Reaction Rates, The Journal of Chemical Physics 4, 236

[143] Johnson, K. L. and Tevaarwerk, J. L. Shear behaviour of elastohydrodynamic films. Proceedings of the Royal Society (London), 1972, A356, 215-238.

[144] Evans, C.R., Johnson, K.L., "The rheological properties of Elastohydrodynamic lubricants." Proc. I.Mech.E. C200, pp. 303-312, (1986).

[145] Evans, C. R. and Johnson, K. L. Regimes of traction in elastohydrodynamic lubrication. Proceedings of the Institution of Mechanical Engineers, Part C, Journal of Mechanical Engineering Science, 1986, 200(C5), 313-324.

[146] Bair, S., Winer, W. O. and Qureshi, F. Lubricant rheological properties at high pressure. Lubrication Science 1993, 5(3), 189-203.

[147] Evans, C.R., Johnson, K.L., "Regimes of traction in elastohydrodynamic lubrication" Proc. Instn Mech Engrs, Part C, Journal of Mechanical Engineering Science, 1986, 200(C5), pp 313-324. SAE International Surface Vehicle Standard J1979-DA OCT2011 p 10, Issued 2010-09 Revised 2011-10

[148] Smeeth, M. Spikes, H. A. The influence of slide roll ratio on the film thickness of an EHD contact operating within the mixed lubrication regime. Presented at the Twenty-second Leeds-Lyon Symposium on Tribology, The Third Body Concept, Lyon, France, 5-8 September 1995.

[149] Gueguan J, A. Kadiric, A. Gabelli, Hugh Spikes, The relationship between friction and film thickness in EHD point contacts in the presence of longitudinal roughness, Tribology Letters (2016) 64:33

[150] Olver, A. V. Thermal matching of tribological systems. In Proceedings of the Twentieth Leeds-Lyon Symposium on Tribology, Lyon, France, September 1993, Dissipative Pro- cesses in Tribology, 1994, pp. 100-110 (Elsevier, Amsterdam).

[151] Cameron, A. Basic lubrication theory, 1976, p. 168 (Ellis Horwood).

[152] Chapman, A. J. Heat transfe, 3rd edition, 1974 (Collier Macmillan).

[153] http://pcs-instruments.com/wp-content/uploads/2014/03/MTM2.pdf

[154] P. M. Cann, H. A. Spikes, and J. Hutchinson (1996), The Development of a Spacer Layer Imaging Method (SLIM) for Mapping Elastohydrodynamic Contacts, Tribology Transactions Vol. 39 , Iss. 4,1996

[155] http://pcs-instruments.com/wp-content/uploads/2014/03/EHD2_Brochure.pdf

[156] Johnston, G. J., R. Wayte, and H. A. Spikes. "The measurement and study of very thin lubricant films in concentrated contacts." Tribology Transactions 34.2 (1991): 187-194.

[157] LaFountain AR, Johnston GJ and Spikes HA: The Elastohydrodynamic Traction of Synthetic Base Oil Blends, Tribology Transactions, 44, 648-656 (2001)

[158] Andrew Richard LaFountain, The behaviour of lubricant blends in elastohydrodynamic contacts, PhD thesis, Imperial College of Science, Technology and Medicine, London, 1999

[159] Spikes H, Jie Z, 2014, History, Origins and Prediction of Elastohydrodynamic Friction, TRIBOLOGY LETTERS, Vol: 56, Pages: 1-25, ISSN: 1023-8883

[160] D.A. Hoffman, Teaching pack on gear technology, Module 4 – Design and stress analysis of spur and helical gears, British Gear Association

[161]SKF Group,
http://www.skf.com/group/products/bearings-units-housings/ball-bearings/deep-groove-ball-bearings/single-row-deep-groove-ball-bearings/single-row/index.html?prodid=1050250307&imperial=false

[162] Barlow TJ, Latham S, McRae IS and Boulter PG: A Reference Book of Driving Cycles for Use in the Measurement of Road Vehicle Emissions, TRL Ltd unpublished report, UPR/IE/054/06, (2006)

[163] Society of Automotive Engineers SAE J1979-DA Revised OCT2011

[164] SW Churchill and M Bernstein. A correlating equation for forced convection from gases and liquids to a circular cylinder in crossflow. *Journal of Heat Transfer*, 99(2):300–306, 1977.

[165] Mannering FL, Kilareski WP & Washburn SS: Principles of Highway Engineering and Traffic Analysis, Third Edition, John Wiley (2005)

[166] Lane DD and Stukel JJ: Dispersion of pollutants in automobile wakes, Journal of the environmental engineering division, EE3 (1976)

[167] http://ecomodder.com/wiki/index.php/Vehicle_Coefficient_of_Drag_List

[168] http://www.allpar.com/model/ram/1994-ram.html

[169] http://www.pickuptrucks.com/html/ram_specs.html

[170] Transportation and Research Board, Tires and Passenger Vehicle Fuel Economy: Informing Consumers, Improving Performance -- Special Report 286 (2006) http://onlinepubs.trb.org/onlinepubs/sr/SR286Rolling_Resistance_Data.pdf

[171] I. Kakavas, A.V. Olver, D. Dini, Hypoid gear vehicle axle efficiency, Tribology International 101 (2016) 314–323